

Optimization of Propellant Tanks Supported by Optimized Laminated Tubular Struts

David Bushnell

775 Northampton Dr., Palo Alto, CA, 94303, Ph.D, AIAA Fellow, email: bush@sonic.net

Michael S. Jacoby

Senior Staff Engineer, Lockheed Martin Missiles and Space, Palo Alto, California 94304, AIAA Member

Charles C. Rankin

Rhombus Consultants Group, Inc., 1121 San Antonio Rd., Palo Alto, CA 94303, Ph.D, AIAA Associate Fellow

The propellant tank is a shell of revolution completely filled with liquid hydrogen (LH₂). This propellant tank is to be launched into space. During launch it is subjected to high axial and lateral accelerations. The tank is supported by a system of struts that consist mainly of tubes with laminated composite walls. This strut-supported tank system is optimized via GENOPT/BIGBOSOR4 in the presence of two loading cases: (1) 10 g axial acceleration and 0 g lateral acceleration and (2) 0 g axial acceleration and 10 g lateral acceleration. In addition to the g-loading the tank has 25 psi internal ullage pressure and the tank wall is 200 degrees cooler than the wall of the launch vehicle from which it is supported by the struts. In the BIGBOSOR4 modal vibration model the mass of the propellant is "lumped" into the tank wall, a conservative model. The tank/strut system is optimized in the presence of the following constraints: (1) the minimum modal vibration frequency must be greater than a given value; (2) five stress components in each ply of the laminated composite wall of the strut tubes shall not exceed five specified allowables; (3) no strut tube shall buckle as a column; (4) no strut tube shall buckle as a thin cylindrical shell; (5) the maximum effective (vonMises) stress in the tank wall shall not exceed a specified value; (6) the tank wall shall not buckle; (8) the maximum force in a strut during the launch-hold phase of a mission shall not exceed a specified value. The objective to be minimized is in general a weighted combination of the normalized mass of the empty tank plus the normalized conductance of the support system: Objective = $W \times (\text{normalized empty tank mass}) + (1-W) \times (\text{normalized strut conductance})$, in which W is a user-selected weight between 0.0 and 1.0. Two propellant tank/strut systems are optimized: (1) a long tank with two "rings" of struts, an aft ring and a forward ring, and (2) a short tank with only one "ring" of struts. It is emphasized that the tank/strut combination is optimized as a single system. The flexibility of the propellant tank is accounted for and found to be significant for optimized tank/strut systems. The flexibility of the launch vehicle to which the tank/strut system is attached is neglected: the ends of the supporting struts attached to the launch vehicle are assumed to be attached to rigid "ground". Parameter studies are conducted in which optimum designs are obtained as a function of the number of strut pairs attached to the tank. During optimization linear theory is used throughout. Predictions for certain of the optimized tank/strut designs obtained here are compared with those from the general-purpose finite element code, STAGS. The agreement between the predictions of GENOPT/BIGBOSOR4 and STAGS qualifies the use of GENOPT/BIGBOSOR4 for preliminary design in the particular cases studied here.

Section 1. INTRODUCTION

This paper is an updated and shortened version of the full unpublished report in [20].

A computer program system called "GENOPT/BIGBOSOR4" is used to obtain the optimum designs. GENOPT is a system of programs that can optimize anything [1] and BIGBOSOR4 [2], the successor to BOSOR4 [3], can analyze shells of revolution supported to ground by an arbitrary arrangement of springs [14]. The gradient-based optimizer used in GENOPT is called "ADS" [4,5]. ADS was created by Vanderplaats and his colleagues in the 1980s.

BIGBOSOR4 [2] is so named because it will handle complex shells of revolution with far more segments than will the original BOSOR4 program [3] from which it is derived. Also, BIGBOSOR4 permits the introduction of springs that connect any shell segment to rigid ground [14]. BOSOR4 does not have that capability. In addition, BIGBOSOR4 will handle prismatic shells, not just shells of revolution.

The work reported here may be thought of as a more general approach to the solution of a strut-supported "dewar" payload described in [6]. In certain respects the model presented in [6] is more general than that presented here and in other respects the model in [6] is less general than that presented here:

- (1) In [6] the launch vehicle is flexible and in the present model the launch vehicle is rigid and considered to be "ground". However, the approximate models of payload shell and launch vehicle shell flexibilities used in [6] are not suitable for thin tanks filled with propellant.
- (2) In [6] much attention is paid to an advanced type of strut with a thermal disconnect system (a strut called "PODS" in [6]), and the support system is optimized for both launch and orbital conditions. The "PODS" concept is not introduced here, and the "in orbit" condition is not considered here.
- (3) In [6] clearance constraints are introduced that prevent supporting struts from passing through the dewar and that prevent supporting struts from passing through each other. Here it is up to the user of GENOPT/BIGBOSOR4 to provide upper and lower bounds of strut positions and angles so that most clearance constraints will automatically be satisfied or come close to being satisfied.
- (4) The model used in [6] is more "primitive" (approximate) than that presented here. For example, the flexibilities of the dewar and launch vehicle from which the dewar is supported are obtained from a model that is greatly simplified and that is much too conservative for heavy payloads.
- (5) The model used in [6] only permits three pairs of struts at each of two axial locations, whereas the model presented here permits any number of pairs of struts around the tank circumference at each axial location.

Note that the "DEWAR" program [6] cannot be used for large payloads because its model in which the flexibility of the payload shell is accounted for is far too conservative to be practical. This unacceptable conservativeness of the "DEWAR" model leads to payload shell support rings the cross sections of which are unnecessarily large, especially for heavy payloads.

In GENOPT the optimizer, ADS [4,5], is "hard-wired" in a so-called "1-5-7" mode: the "modified method of steepest descent". Constraint gradients are computed by finite differences of the behaviors of the "perturbed" design and the behaviors at the "current" design, in which the word, "behaviors", means modal vibration or stress or buckling, etc. A "perturbed" design is a design in which the value of one decision variable has been increased by a small amount (usually five per cent) from its "current" value. A constraint-gradient matrix is automatically generated by computation of the change in each behavior caused by the perturbation of each decision variable. The values of the "behavioral" constraints and the constraint-gradient matrix are inputs to the

ADS optimizer by means of which a new "current" design is obtained by the modified method of steepest descent. The interaction of the BIGBOSOR4 computer program with the ADS optimizer is entirely automated. The program user need specify only the number of design iterations for short computer runs and does not even have to specify that for longer computer runs that involve automated multiple optimization processes starting from different points in design space.

The GENOPT/BIGBOSOR4 system of computer programs has previously been used to obtain optimum designs of several structures that are comprised mainly of shells of revolution [2 and 7 - 10] or prismatic shells [11 - 13].

In the GENOPT system [1] there are two types of cases: **generic** and **specific**. In this work the generic case is called "**tank**", and the specific cases have names such as "test", "test1", "test2", "test3", etc. The specific cases are all members of the generic class, "**tank**". There are two types of user: the **GENOPT user** and the **END user**. The GENOPT user creates the software by means of which specific problems in the generic class (such as "tank") can be solved. The END user sets up and runs specific cases such as "test", "test1", "test2", etc. In the work reported here the GENOPT user and the END user are the same person: the first author of this paper.

Section 2. INFORMATION ABOUT GENOPT

Information about GENOPT is provided in the papers cited in the Introduction. Also, there are several files provided on the "shellbuckling.com" website cited in [20]. The files listed next are contained in the compressed "tar" file, general.info.tar.gz, which is contained in the bigger compressed "tar" file, .../genopt/case/tank/tanktank2.tar.gz, that is part of the very big compressed "tar" file that can be downloaded from the "Downloads" page of the "shellbuckling.com" website [20]. The individual files contained in the "general.info.tar.gz" file are as follows:

 FILES GIVING GENERAL INFORMATION ABOUT GENOPT AND ABOUT THE INTRODUCTION OF SPRINGS INTO BIGBOSOR4. (Struts are a kind of spring support).

```

-rw-r--r--  1 bush bush  94295 Nov  24  2012 bigbosor4.springs
-rw-r--r--  1 bush bush   5720 Nov  24  2012 genopt.abstract
-rw-rw-r--  1 bush bush   2024 Nov  24  2012 genopt.commands
-rw-rw-r--  1 bush bush   3234 Nov  24  2012 genopt.files
-rw-r--r--  1 bush bush  93262 Nov  24  2012 genopt.getting.started
-rw-rw-r--  1 bush bush   8909 Nov  24  2012 genopt.information
-rw-rw-r--  1 bush bush    987 Nov  24  2012 genopt.information.files
-rw-rw-r--  1 bush bush   2507 Nov  24  2012 genopt.programs
-rw-r--r--  1 bush bush 251587 Nov  24  2012 genopt.runstream
-rw-rw-r--  1 bush bush  11183 Nov  24  2012 genopt.summary
-rw-rw-r--  1 bush bush   1077 Nov  24  2012 genopt.variable.roles
  
```

See Appendix 3 for an abstract of the bigbosor4.springs file.

Section 3. AN EXAMPLE OF A GENOPT/BIGBOSOR4 RUN STREAM

A rather detailed example of a GENOPT/BIGBOSOR4 run stream executed during the present work is contained in Table 1 of [20] and in the file called “genopt.runstream” that is one of the files contained in the compressed “tar” file, general.info.tar.gz, as just listed. The run stream involves execution of the various GENOPT processors, which are listed near the beginning of Table 1 of [20] and repeated here for convenience:

gentext The GENOPT user and the GENOPT process, gentext, generate a prompt file, tank.PRO (Table 2 of [20]) and an information file, tank.DEF, that contains a glossary: Table 1 of this paper. (Input data for “gentext” are stored in a file called “tank.INP”.) Skeletal libraries, behavior.new and struct.new, are automatically created by gentext. These skeletal libraries are to be “fleshed out” by the GENOPT user. (See the files, behavior.tank and struct.tank that are contained in the compressed tar file, tank.tar.gz [20].) Before the next GENOPT command, “**genprograms**”, is given by the GENOPT user, the GENOPT user must, for the generic case called “**tank**” that is the subject of this particular paper, type the following:

cd ../<working directory>
cp ../genopt/case/tank/tanktank2.tar.gz <working directory>
gunzip tanktank2.tar.gz
tar xvf tanktank2.tar
gunzip tank.tar.gz
tar xvf tank.tar
cp behavior.tank ../genoptcase/behavior.new
cp struct.tank ../genoptcase/struct.new
cp addbosor4.density.var ../bosdec/sources/addbosor4.src
cp bosdec.density.var ../bosdec/sources/bosdec.src
cd ../genoptcase

genprograms The GENOPT user (via the GENOPT system) generates (makes) executables: begin, decide, mainsetup, optimize, change, chooseplot, and diplot that pertain to the generic case called “**tank**”.

begin The End user provides starting data: the file called “test.BEG” (Table 2 in this paper).

decide The End user chooses decision variables, bounds, linked variables, and inequality constraints: the file called “test.DEC” (Table 5 of [20])

mainsetup The End user sets up strategy parameters: the file called “test.OPT” (Table 6 of [20] or Table 7 of [20]).

optimize The End user performs optimization (Figs. 14 and 15) or analyzes a fixed design (Figs. 4 – 6 and the output file, test.OPM, listed in Table 8 of [20]) or performs design sensitivity (Figs. 17 – 19 here, Figs 32 – 54 of [20])

change The End user changes/archives variables: the file called “test.CHG” (Table 9 of [20]).

autochange New values for decision variables are randomly computed by GENOPT: (See the "spikes" in the plot in Fig. 14 here and in Fig. 29 of [20])

superopt The End user finds "global" optimum (autochange/optimize): (Figs. 14 and 15 here and the following figures and tables of [20]: Fig. 29, 59, 59b, Table 8, Figs. 57, 58, 86, 88, Table 15)

superduperopt GENOPT automatically executes **superopt** "x" times, in which "x" is provided by the End user

chooseplot The End user chooses which variables/margins to plot vs. design iterations: the file called "test.CPL" (Table 10 of [20])

diplot The End user plots variables vs. design iterations: (Figs. 14 and 15 here; Figs. 29-31, 57, 58 of [20])

insert The GENOPT user adds parameters to the problem.

cleanspec The End user cleans up SPECific case files.

cleangen The GENOPT user cleans up GENeric case files.

Section 4. SOME GEOMETRICAL AND OTHER DETAILS

In this study the propellant tank consists of three sections:

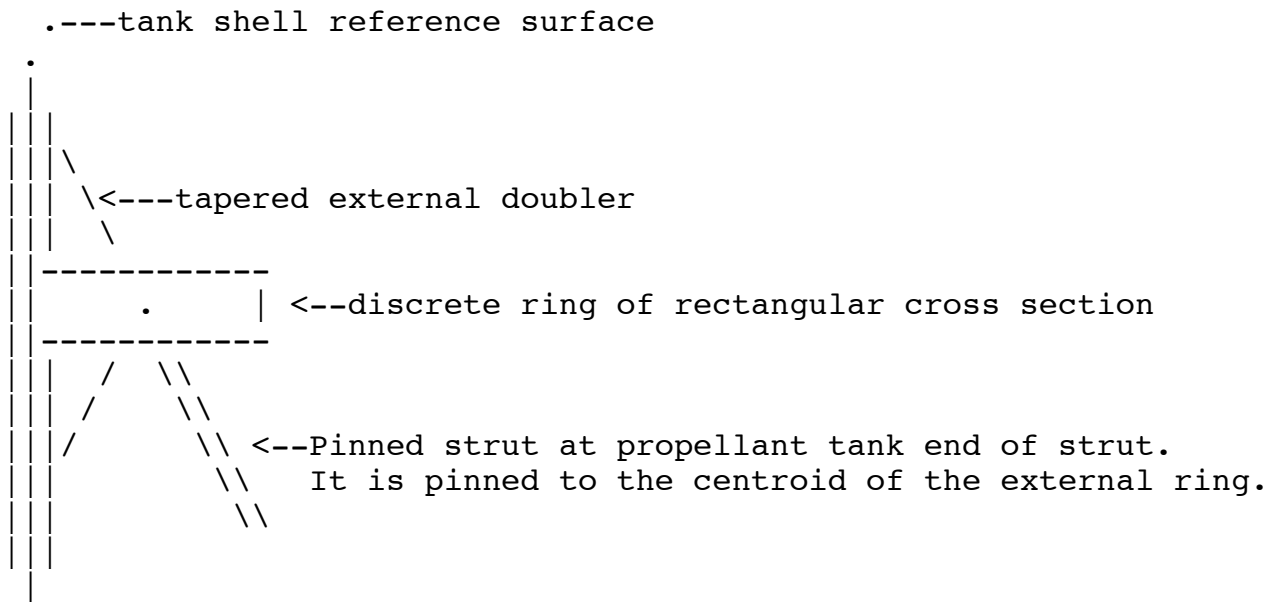
- (1) an aft dome (2:1 ellipsoidal head here. An ellipsoidal head with any ratio of major to minor axis is allowed.)
- (2) a cylindrical portion
- (3) a forward dome (2:1 ellipsoidal head here. An ellipsoidal head with any a/b is allowed.)

An example of this geometry is displayed in Figs. 1a, 1b and 1c.

The ellipsoidal domes are each modeled as multi-segment shells in which the meridional curvature of each segment is constant. Hence, each dome shell segment is a torispherical segment with meridional curvature equal to the average meridional curvature of the ellipsoidal shell in that segment. In [10] this device was found to be necessary in order to avoid partial finite element "locking", to which BIGBOSOR4 is susceptible in shell segments that have meridional curvature that varies along the meridian within any given shell segment. (See Fig. 2 of [10] for a discretized 12-segment model of a different ellipsoidal shell.) In this work, as in [10], twelve shell segments are used in the discretized model of each ellipsoidal dome.

The strut supports are arranged in a manner analogous to that displayed in Fig. 1 of [6]. See Figs. 2 and 3 in this paper. In [6] only three pairs of "forward" and "backward" slanting struts are permitted at each of two axial locations. In the present model any number of pairs of "forward" and "backward" slanting struts are permitted at each axial "ring" of struts, such as at the aft "ring" of struts shown in Fig. 2 and at the forward "ring" of struts shown in Fig 3 and at the aft ring of struts shown in Figs. 11 – 13.

In the models used for the present work the ends of each "ring" of struts attached to the propellant tank are pinned to a reinforced axial section of the tank. This reinforcement consists of a tapered external doubler approximately centered about the axial location of each "ring" of struts plus an external discrete ring of rectangular cross section. The pinned tank-end of each strut in the "ring" of struts is located at the centroid of the external reinforcing ring. The external reinforcing ring is considered to be attached to the reference surface of the tank shell wall, not to the outer surface of the tapered doubler. The material of the shell wall, reinforcing doubler and the external reinforcing ring therefore overlap in the short axial region of the model where the shell wall, external tapered doubler and external ring material occupy the same space. See the sketches in Figs. 1b and 1c and below:



Sketch of the propellant tank wall with a local reinforcement at the axial location where the tank-end of the "ring" of pinned struts is attached to the centroid of the external propellant tank support ring. Note: in this sketch the innermost "layer" of the propellant tank, which consists of an orthogrid with "smeared" stringers and rings, is not shown. (That innermost "layer" is shown in Fig. 1c).

In the BIGBOSOR4 models of the propellant tank, which is a shell of revolution, the tank wall in each shell segment consists of three "layers":

Layer No. 1: The innermost shell wall "layer" represents an orthogrid of rings and stringers with rectangular cross sections. These uniformly spaced stiffeners are "smeared out" in the model. In the GENOPT/TANK/BIGBOSOR4 model the orthogrid "layer" is treated as if it were a ply of composite "cloth" with zero in-plane shear stiffness and zero Poisson ratio. Hence, the "smeared stiffener" data input option in BIGBOSOR4, in which the user is asked to provide the material properties and heights and thicknesses of the stringers and rings, the number of stringers over 360 degrees of the circumference of the shell of revolution and the ring spacing, is not used. The thickness of this innermost shell wall "composite layer" is equal to the constant height of the orthogrid ($STRHI = RNGHI$ in Fig. 1c). The material properties of this layer are equal to the actual properties of the orthogrid material multiplied by the ratio, (constant thickness of orthogrid

stiffeners)/(constant orthogrid stiffener spacing). This innermost “composite layer” exists in all sections of the propellant tank and is of constant properties throughout, that is, the orthogrid height and effective stiffness and density are constant and the same in all three major segments of the propellant tank: aft dome, middle cylindrical portion, and forward dome. The fact that ellipsoidal or hemispherical end domes cannot be manufactured precisely in this way is overlooked in this study, the purpose of which is to create a capability to obtain reasonably good PRELIMINARY tank/strut designs. (The end domes could be fabricated such that “smeared” properties are approximately constant along the meridian by calling for different numbers of stringers over 360 degrees of circumference in each of the 12 meridional shell segments with which the end domes are represented in the GENOPT/TANK/BIGBOSOR4 model. The number of stringers over 360 degrees of circumference would be proportional to the average distance of each shell segment from the axis of revolution of the propellant tank.) Note that in this “composite ply” model of the internal orthogrid “layer” of the shell wall the torsional rigidity of the orthogrid stiffeners is neglected. Therefore, it is a conservative model.

Layer No. 2: The middle layer of the propellant tank shell wall is of constant thickness in each of the three major segments of the propellant tank: aft dome, cylindrical portion, and forward dome. This constant thickness may be different (THKAFT, THKMID, THKFWD defined in Tables 1 and 2) in each of these three major segments, “aft”, “middle”, and “forward” (for example, see Fig. 1c for THKMID and THKFWD). It is this constant-thickness middle layer of the tank wall into which is “lumped” the mass of the propellant in the BIGBOSOR4 modal vibration model. In the BIGBOSOR4 models for buckling and stress the inertial effect of the propellant in the tank is handled as described in Appendix 4, not by lumping the propellant mass into the middle layer of the tank wall as is done in the modal vibration model.

Layer No. 3: The outermost layer is of variable thickness and represents the external tapered doublers (Figs. 1b and 1c). In regions with no doublers the thickness of this outermost layer is zero.

The ends of each “ring” of struts attached to the launch vehicle (represented by the outermost vessel depicted in Fig. 1a) are considered attached to rigid “ground”. In [6] the flexibility of the launch vehicle is included in an approximate way. Here the launch-vehicle-ends of the struts must be connected to rigid “ground” because the BIGBOSOR4 model in which springs exist [14, Appendix 3] only permits springs connected to ground, not to another flexible shell segment.

The flexibility of the propellant tank is included in the model, of course, since the propellant tank is modeled by BIGBOSOR4 as an ordinary flexible, segmented shell of revolution.

Figures 1a - 6 show the arrangement of struts for the starting design (Figs. 1a-3) and for the optimized design (Figs. 4-6) of the long propellant tank/strut system supported by two “rings” of struts, aft and forward, for the specific case called “test”, in which there are four pairs of struts attached to each of the two propellant tank support rings. The ends of the struts at the propellant tank are attached to the centroids of external rings located at the aft and forward dome/cylinder junctions. (See Fig. 1c, for example.)

Figures 7 - 10 show the same for the starting design (Figs. 7, 8) and for the optimized design (Figs. 9, 10) of the short propellant tank/strut system supported by one “ring” of struts (called “aft”) with four strut pairs attached at the centroid of the external ring at the midlength of the short cylindrical part of the propellant tank.

Figures 11 - 13 show plan views of the aft set of struts for the OPTIMIZED designs of the long propellant tank/strut system with aft and forward sets of struts for the specific cases, “test2” (two pairs of struts at each of

the two axial locations), "test3" (three pairs of struts at each of the two axial locations) and "test5" (five pairs of struts at each of the two axial locations). **Note from the caption of Fig. 11 that GENOPT/TANK should not be used for the optimization of propellant tanks supported by less than three pairs of struts at each axial location.**

Section 5. MATERIAL PROPERTIES, OVERALL TANK DIMENSIONS, FACTORS OF SAFETY AND ACCELERATION ARBITRARILY USED IN THIS STUDY

A glossary of variables that play a role in this study is given in Table 1. Typical values of input variables for a starting design of the long propellant tank with aft and forward sets of struts, 4 strut pairs in each set, are listed in Table 2. The names of several of the decision variable candidates are included in Figs. 1a and 1c. (A decision variable candidate is a problem variable that may be chosen by the End user as a decision variable during the interactive execution of the GENOPT processor called "DECIDE" Decision variable candidates are "Role 1" variables, as listed in Table 1 for the generic case called "tank".)

The first sentence in the abstract reads, "The propellant tank is a shell of revolution completely filled with liquid hydrogen (LH2)." However, in the GENOPT/TANK software the tank can be filled with any fluid. The effect of the fluid is introduced by means of its weight density, which is called "DENPRP" in Tables 1 and 2.

In the particular cases explored here the propellant tank is made of aluminum. (In other cases the propellant tank can be made of any isotropic material.) The supporting struts are laminated composite angle-ply tubes with metallic end fittings. In all of the configurations studied in this particular project the thickness of each ply in the laminated composite wall of each aft strut tube (Figs. 1a and 2) is the same as that of all the other plies in that aft strut tube. The thickness of each ply in the laminated composite wall of each forward strut tube (Figs. 1a and 3) is the same as that of all the other plies in that forward strut tube. All strut tubes at a given axial level, aft or forward, are the same. The forward strut tubes are permitted to differ from the aft strut tubes. There are 12 plies in each strut tube.

The ply thicknesses in the laminated composite wall of each **aft** strut tube wall are:
[THICK(1), THICK(2), THICK(3), THICK(4), THICK(5), THICK(6)]symmetric

The thicknesses in each **forward** strut tube wall are:
[THICK(7), THICK(8), THICK(9), THICK(10), THICK(11), THICK(12)]symmetric

In the particular specific cases described here, in the "DECIDE" processor of GENOPT, the variables, THICK(2), THICK(3), THICK(4), THICK(5) and THICK(6), are all linked to THICK(1). Analogously, THICK(8), THICK(9), THICK(10), THICK(11) and THICK(12) are all linked to THICK(7). (See Table 5 of [20].)

Hence, there exist in this specific model called "test" only two independent decision variables for ply thickness in strut tubes: THICK(1) (a ply thickness in all **aft** struts) and THICK(7) (a ply thickness in all **forward** struts). It is emphasized that this restriction is only enforced in the specific cases that happen to be investigated in the work reported here. Different specific cases can be processed in which each of the thicknesses of the six plies, THICK(1), THICK(2), THICK(3), THICK(4), THICK(5), THICK(6), in the wall of the aft strut tube can differ

from each other and in which each of the thicknesses of the six plies, THICK(7), THICK(8), THICK(9), THICK(10), THICK(11), THICK(12), in the wall of the forward strut tube and differ from each other.

The layup angles in the laminated wall of each **aft** strut tube is as follows:

[ANGLE(1), ANGLE(2), ANGLE(3), ANGLE(4), ANGLE(5), ANGLE(6)]symmetric

The layup angles in the laminated wall of each **forward** strut tube is as follows:

[ANGLE(7), ANGLE(8), ANGLE(9), ANGLE(10), ANGLE(11), ANGLE(12)]symmetric

In the particular cases described here, in the "DECIDE" processor of GENOPT, the variables pertaining to each **aft** strut tube, ANGLE(2), ANGLE(4) and ANGLE(6) are constrained (linked) to be equal to the negatives of ANGLE(1), ANGLE(3) and ANGLE(5), respectively. Analogous linking is established for the plies in the wall of each strut tube in the **forward** set of struts. (See Table 5 of [20].)

The material properties used in this study are, in many instances, arbitrary. For example, the thermal conductivity along the fibers of each ply of the laminated composite strut tubes, listed in Table 2, is taken to be COND1(1) = 0.00727 BTU/(in-hr-deg.R) and the thermal conductivity transverse to the fibers is taken to be COND2(1) = 0.00437 BTU/(in-hr-deg.R). These values were simply "lifted" from the end of Table 5 near the top of p.14 of the "dewar" paper [6]. No attempt was made in this work to differentiate these strut tube thermal conductivities at the cold end and at the warm end of a strut tube. The effect of strut tube cool-down is neglected throughout despite the fact that there is an input datum called "DTSUP" (Table 2), which implies inclusion of this phenomenon.

The coefficient of thermal expansion along the ply fibers is taken to be ALPHA1(1) = 0.1000000E-05 and transverse to the ply fibers is taken to be ALPHA2(1) = 0.1000000E-04, although the thermal expansion of the strut tube and its end fittings play no role in this work. The coefficients of thermal expansion of the strut tube end fittings are arbitrarily taken to be ALFITT(1) = ALFITV(1) = 0.1000000E-04. The coefficients of thermal expansion of the isotropic propellant tank material and of the isotropic propellant tank support ring material are arbitrarily taken to be ALTNK = ALRNGT(1) = 0.1000000E-04. (See Table 2 for these input data entries for the specific case called "test".)

In models that include propellant tank external support rings the height of each ring, TRNGHI(1), is arbitrarily constrained to be five times its thickness, TRNGTH(1). In this work the combination of external tapered doubler and propellant tank external support ring (Figs. 1b and 1c) is assigned a "tank reinforcement type index". In the propellant tank models for which results are presented here there exists only a single "tank reinforcement type". Hence, in long tanks with two "rings" of struts, aft and forward, the tapered doubler dimensions, axial length DUBAXL(1) and maximum thickness DUBTHK(1), and propellant tank external support ring cross section dimensions, thickness TRNGTH(1) and height TRNGHI(1), are the same at both aft and forward axial locations. See Fig. 1c for the meanings of these names of decision variable candidates, and see Table 2 for the starting values of these decision variable candidates.

The propellant tank cool-down for Load Case 1 [TNKCOOL(1)] and for Load Case 2 [TNKCOOL(2)] is arbitrarily taken to be -200 degrees and the maximum allowable launch-hold force in a strut is arbitrarily taken to be FORCEA(i,j) = 15000 lb, in which "i" = load case number and "j" = strut ring number. If this maximum allowable force in a strut is set too low relative to the weight of the propellant-filled tank GENOPT cannot find a FEASIBLE or ALMOST FEASIBLE optimum design; the optimization simply does not work because all

designs obtained during optimization cycles are either NOT FEASIBLE or unacceptable to GENOPT on some other grounds, such as “MILDLY UNFEASIBLE”, “MORE UNFEASIBLE”, “MOSTLY UNFEASIBLE”.

The material properties, E1, E2, G12, NU, G13, G23, ALPHA1, ALPHA2, COND1, COND2, DENSTY, of a ply of the laminated composite strut tubes and the five maximum allowable stress components, STRESSiA(j,k), $i =$ material type, $j =$ load case number, $k =$ stress component, were arbitrarily taken from one of the papers related to the PANDA2 computer program for optimization of stiffened laminated composite panels and shells [15]. See Table 2 for the values used in the work reported here. No consideration is given to the dependence of material properties on the temperature.

The curing temperature, TEMTUR, of a laminated composite strut tube is arbitrarily taken to be 170 degrees. Cases reported in [20] were run either with TEMTUR = 0 or TEMTUR = 170 degrees. (See Table 2.)

The overall dimensions of the propellant tank are arbitrarily assigned: tank diameter AFTDIA = FWDDIA = 200 inches, overall long tank length FLTANK = 400 inches, overall short tank length equals 150 inches, end domes are 2:1 ellipsoidal shells. The diameter of the launch vehicle (considered to be rigid "ground" in this study) is arbitrarily taken to be DIAVEH = 300 inches. (See Fig. 1a and Table 2.)

The factor of safety for each stress component in each ply of the laminated composite strut tubes is arbitrarily set to STRESiF(j,k) = 1.5; the factor of safety for effective stress in the propellant tank is arbitrarily set to TNKSTRF(j,k) = 1.0; the factor of safety for modal vibration frequency is arbitrarily set to FREQF(j, L) = 1.2, $L = 1, 2, 3, 4$ corresponding to $n = 0, 1, 2, 3$ or 4 circumferential waves; the factor of safety for buckling of a strut as a column is arbitrarily set to COLBUKF(j,k) = 1.0; the factor of safety for buckling of a strut as a thin cylindrical shell is arbitrarily set to SHLBUKF(j,k) = 2.0 (to compensate for imperfection sensitivity). (See Table 2.)

The minimum allowable frequency is arbitrarily set to FREQA(j,L) = 10 cps (Table 2).

The axial and lateral acceleration components, GAXIAL(j) and GLATRL(j), of the tank are respectively arbitrarily set to 10g in two separate load cases (Table 2) as listed in the short section below entitled “Section 8. TWO LOAD CASES”. The tank is assumed to be oriented with its axis of revolution aligned with the axial component of acceleration of the launch vehicle. (IAXIS = 1 in Table 2.). At present the GENOPT/TANK software only works for the IAXIS = 1 option.

Section 6. BEHAVIORS ACCOUNTED FOR DURING OPTIMIZATION CYCLES

As mentioned above, optimization of the tank/strut system is constrained by "behaviors", such as modal vibration, stress and buckling. The “behaviors” are computed by the subroutines, SUBROUTINE BEHXi, $i = 1, 2, 3, \dots$, that are contained in the “behavior.tank” library stored in the compressed tar file, tank.tar.gz, which is in turn included in the larger compressed tar file, ...genopt/case/tank/tanktank2.tar.gz, which is included in a very large compressed tar file that can be downloaded from the “Downloads” page of the website, shellbuckling.com [20]. The "behaviors" constraining the design in this work are:

BEHAVIOR(1), called “FREQ” in Table 1 and computed in SUBROUTINE BEHX1: Four modal vibration modes corresponding to $n = 0$ (axial/rolling “rigid-body” mode associated with the lowest frequency

corresponding to $n = 0$ circumferential waves), $n = 1$ (lateral/pitching “rigid-body” mode associated with the lowest frequency corresponding to $n = 1$ circumferential wave), and two flexible body “shell” vibration modes associated with the lowest frequency with $n = 2$ circumferential waves and with either $n = 3$ or $n = 4$ circumferential waves, whichever has the lowest frequency. The four vibration modes are computed from a BIGBOSOR4 model of the strut-supported propellant tank. The flexibility of the propellant tank is accounted for by the computation of reduced "effective" spring constants (axial stiffnesses) of the supporting struts in this modal vibration model. The mass of the propellant is "lumped" into the middle layer of the three-layered propellant tank. In a general shell of revolution the amount of propellant mass to be "lumped" into the propellant tank shell wall middle layer at a nodal point in a shell segment depends on the radius from the axis of revolution and on the rate of change of this radius with meridional arc length. Hence, in the aft and forward ellipsoidal domes the effective density of the middle tank layer varies along the meridian of each dome shell segment. However, the “permanent” (stand alone) version of BIGBOSOR4 cannot handle shell segments with meridionally varying material density within a single shell segment. Therefore, "temporary" versions of BIGBOSOR4 and BOSDEC were created that are valid only for the generic case, "**tank**". As reported in [20], optimized designs were evaluated with either the "temporary" or the "permanent" versions of BIGBOSOR4 and BOSDEC. In the work reported in this paper only the “temporary” versions of BIGBOSOR4 and BOSDEC were used for optimization. These “temporary” versions of BIGBOSOR4 and BOSDEC are embodied in the files called “addbosor4.density.var” and “bosdec.density.var”, respectively [20]. The "stand-alone" version of BIGBOSOR4 was not changed in any way. More complete explanations are given in [20].

BEHAVIOR(2), called “STRES1” in Table 1 and computed in SUBROUTINE BEHX2 for material type 1, called “STRES2” in Table 1 and computed in SUBROUTINE BEHX3 for material type 2 and called “STRES3” in Table 1 and computed in SUBROUTINE BEHX4 for material type 3: Maximum of each of five components of stress in the laminated composite walls of the strut tubes. The five stress components in each unidirectional ply of the composite laminates for each material type (1 or 2 or 3) are:

- a. maximum tension along the fibers [STRES $i(j,1)$, i =material type, j = load case number]
- b. maximum compression along the fibers [STRES $i(j,2)$, i =material type, j = load case number]
- c. maximum tension transverse to the fibers [STRES $i(j,3)$, i =material type, j = load case number]
- d. maximum compression transverse to the fibers [STRES $i(j,4)$, i =material type, j = load case number]
- e. maximum in-plane shear stress [STRES $i(j,5)$, i =material type, j = load case number]

These 5 maximum stress components are computed from both a BIGBOSOR4 model and from a PANDA-type model [15] of the most highly loaded laminated composite strut tube at each axial location (aft and forward) of a ring of "n" pairs of struts. Maximum tensile and maximum compressive loading of any strut at each axial location (aft and forward) are both included in the determination of the most critical stress components. In the GENOPT/TANK model the material number, 1 or 2 or 3, is identified with the strut type number. Therefore, in the long propellant tank with aft and forward sets of struts the **aft set of struts has material number 1** (strut type 1) and the **forward set of struts has material number 2** (strut type 2). In the short propellant tank with one set of struts these struts have material number 1 (strut type 1). All struts of a given type are the same: same length, same diameter, same wall construction.

BEHAVIOR(3), called “COLBUK” in Table 1 and computed in SUBROUTINE BEHX5: Buckling of the most highly compressed strut as a column (Euler buckling), computed from both a BIGBOSOR4 model and a simple Euler model of the most highly compressed laminated composite strut at each axial location (aft and forward) of a ring of "n" pairs of struts.

BEHAVIOR(4), called “SHLBUK” in Table 1 and computed in SUBROUTINE BEHX6: Buckling of the strut tube as a thin cylindrical shell computed from both a BIGBOSOR4 model and a PANDA2-type model [15] of the most highly compressed strut at each axial location (aft and forward) of a ring of "n" pairs of struts. The BIGBOSOR4 strut shell buckling model does not account for the effect of transverse shear deformation (t.s.d.) nor for the anisotropic terms in the 6 x 6 integrated constitutive matrix, C(i,j). The approximate PANDA2-type model accounts for t.s.d. and shell wall anisotropy. Therefore, the PANDA2 model generally yields the most critical estimate of shell buckling of a strut in the work reported here.

BEHAVIOR(5), called “TNKSTR” in Table 1 and computed in SUBROUTINE BEHX8: Maximum effective (von Mises) stress in the propellant tank computed from a BIGBOSOR4 model of the propellant tank in which the struts are replaced by concentrated loads applied to the propellant tank along the aft and forward propellant tank support rings to which the "n" pairs of struts are attached.

BEHAVIOR(6), called “TNKBUK” in Table 1 and computed in SUBROUTINE BEHX9: Buckling of the propellant tank computed from a BIGBOSOR4 model of the propellant tank in which the aft and forward rings of "n" pairs of struts are replaced by concentrated loads applied to the propellant tank along the aft and forward propellant tank support rings to which the struts are attached.

BEHAVIOR(7), called “FORCE” in Table 1 and computed in SUBROUTINE BEHX7: Maximum force in a strut generated during the launch-hold phase of a mission computed from a BIGBOSOR4 model of the tank/strut system subjected to a 1-g loading plus internal 25 psi ullage pressure plus 200 degrees propellant tank cool-down. The propellant tank axis is assumed to be aligned with the axial direction of the launch vehicle from which the tank is supported. The purpose of this behavioral constraint is to obtain an optimum design of the tank/strut system in which an advanced strut, such as a strut that includes a thermal disconnect, does not "short circuit" during the launch-hold phase of a mission. NOTE: if the End user sets the allowable maximum force in a strut at too low a level, GENOPT/BIGBOSOR4 cannot find a FEASIBLE or ALMOST FEASIBLE optimum design; the optimization simply does not work properly because there is no feasible region in design space.

Section 7. INFORMATION ABOUT THE GENERIC CASE CALLED "tank"

In the GENOPT universe there are two types of cases:

(1) A **generic** case (called "**tank**" in this paper)

(2) **Specific** cases that fit within the generic set. These specific cases are called "**test**", "test1", "test2", "test3", "test4", "test5", "test6", "test7" and "test8" in the work reported in [20].

Corresponding to each of the two classes of case, **generic** and **specific**, there are possibly different users. The role of the **GENOPT user** is to create the software for setting up the GENERIC environment ("tank"). The **End user** exercises the GENERIC environment, "tank", for SPECIFIC cases, such as the cases called "test", "test1", "test2", "test3", "test4", "test5", "test6", "test7" and "test8" in [20].

The following files pertain to the GENERIC case, "**tank**". The files listed next are contained in the compressed "tar" file, tank.tar.gz, which is contained in the bigger compressed “tar” file, .../genopt/case/tank/tanktank2.tar.gz, which is part of the very big compressed “tar” file that can be downloaded

from the “Downloads” page of the “shellbuckling.com” website [20]. Some of the files contained in the “tank.tar.gz” file are the following:

FILES RELATED TO THE GENOPT USER'S GENERIC CASE = “**tank**” PHASE OF THIS PROJECT

149170	Feb	18	2013	behavior.tank	("fleshed-out" version)
209589	Jun	10	2012	bosdec.tank	("permanent" version)
67909	Feb	18	2013	struct.tank	("fleshed-out" version)
39212	Feb	18	2013	tank.DEF	(general information)
155703	Aug	17	2012	tank.INP	(input for GENTEXT)
63078	Aug	17	2012	tank.PRO (Table 2 in [20])	(prompting file)
10105	Feb	18	2013	tank.glossary (Table 1)	(part of tank.DEF)
679734	May	18	2012	addbosor4.density.var	("temporary" BIGBOSOR4)
679342	Jun	27	2012	addbosor4.regular	("permanent" BIGBOSOR4)
210151	Jun	10	2012	bosdec.density.var	("temporary" version)

Skeletal forms of the files, behavior.tank and struct.tank, are created automatically by GENOPT during the GENOPT user's long interactive session associated with the GENOPT command, GENTEXT. It is the responsibility of the GENOPT user to "flesh out" these skeletal libraries (called behavior.new and struct.new) so that they compute any "behaviors" (vibration, buckling, stress, etc.) that may constrain the design during optimization cycles. The “fleshed out” versions are archived in the files, behavior.tank and struct.tank.

The files, bosdec.tank and bosdec.density.var, are entirely written by the GENOPT user. bosdec.tank and bosdec.density.var, generate valid input files for BIGBOSOR4, which is the shell-of-revolution analyzer that computes the various vibration, buckling, and stress behaviors that constrain the design during optimization cycles. The results presented in this paper are all derived from bosdec.density.var, which produces valid input for the “temporary” version of BIGBOSOR4, represented by the archived file, addbosor4.density.var. If a GENOPT user wants to optimize something that does not involve or use BIGBOSOR4, then the “bosdec” and “addbosor4” files play no role. However, dummy “bosdec” and “addbosor4” libraries should be provided in order that a successful compilation will follow via the GENOPT user’s command, “genprograms”.

The three files, tank.INP, tank.PRO and tank.DEF, are created automatically by the GENOPT processor, GENTEXT. tank.INP contains an image of the GENOPT user's long interactive GENTEXT session; tank.PRO (Table 2 in [20]) is a prompting file created automatically by GENTEXT from the input words, phrases, and paragraphs created by the GENOPT user during his/her long interactive GENTEXT session; tank.DEF is a file created automatically by GENTEXT. It contains general information about GENOPT and a glossary of variable names, definitions and properties established by the GENOPT user during his/her interactive GENTEXT session. The file, tank.glossary (Table 1), is the “glossary” part of the file, tank.DEF.

The two files, addbosor4.density.var and bosdec.density.var, contain the "temporary" versions of bigbosor4 and bosdec in which there is an "exact" representation of the "lumped" propellant mass into the middle layer of the wall of the propellant tank for the purpose of obtaining a reasonably accurate (and conservative) computation of modal vibration frequencies corresponding to tank axial motion, tank lateral/pitching motion, and two “shell” vibration modes, that is, vibration modes with $n = 2$ and $n = 3$ or 4 circumferential waves.

In the "temporary" version of bigbosor4 the density of the middle layer of the wall of the propellant tank varies along the meridian of the aft ellipsoidal dome and along the meridian of the forward ellipsoidal dome. The file, addbosor4.regular, contains the "permanent" version of bigbosor4. In the "permanent" version of bigbosor4 the density of the middle layer of the wall of the propellant tank is constant along the meridians of the aft and forward ellipsoidal domes. Please see the section entitled "TWO BIGBOSOR4/BOSDEC MODELS..." in [20] and APPENDIX 2 in [20] for more details about the "temporary" versions of BIGBOSOR4 and BOSDEC.

Section 8. TWO LOAD CASES

Calculations of each of the types of "behavior" listed above in the section entitled, "Section 6. BEHAVIORS ACCOUNTED FOR DURING OPTIMIZATION CYCLES", are performed for each of the two load cases experienced by the tank/strut system:

(1) Load Case 1:

Load Set A ("eigenvalue" loads):

axial acceleration of the launch vehicle, $GAXIAL(1) = 10 \text{ g}$

lateral acceleration of the launch vehicle, $GLATRL(1) = 0 \text{ g}$

Load Set B ("non-eigenvalue" loads):

internal ullage pressure, $PRESS(1) = 25 \text{ psi}$

propellant tank cool-down, $TNKCOOL(1) = -200 \text{ degrees}$

IMPORTANT CAUTION: The End user must check to see that Load Set B of Load Case 1 does not cause buckling when applied to the propellant tank by itself! For the optimized configuration listed in the section entitled "Section 10. DECISION VARIABLE CANDIDATES" (long propellant tank with two sets of struts, aft and forward) the knuckle region of the forward dome of the propellant tank buckles at a load factor of 4.107 with 40 circumferential waves when Load Set B of Load Case 1 is applied by itself as a Load Set A. Hence, Load Set B of Load Case 1 acting by itself does **not** create a critical situation in the specific case called "test". For the optimized configuration listed in the section entitled "Section 16. OPTIMIZED SHORT PROPELLANT TANK WITH ONE 'RING' OF STRUTS WITH FOUR PAIRS OF STRUTS ATTACHED TO THE ONE TANK SUPPORT RING" the knuckle region of the aft dome of the propellant tank buckles at a load factor of 15.04 with 25 circumferential waves when Load Set B of Load Case 1 is applied by itself as a Load Set A. Hence, Load Set B of Load Case 1 acting by itself does **not** create a critical situation in the specific case called "test2".

(2) Load Case 2:

Load Set A ("eigenvalue" loads):

axial acceleration of the launch vehicle, $GAXIAL(2) = 0 \text{ g}$

lateral acceleration of the launch vehicle, $GLATRL(2) = 10 \text{ g}$

Load Set B ("non-eigenvalue" loads):

internal ullage pressure, $PRESS(2) = 25 \text{ psi}$

propellant tank cool-down, $TNKCOOL(2) = -200 \text{ degrees}$

IMPORTANT CAUTION: The End user must check to see that Load Set B of Load Case 2 does not cause buckling when applied to the propellant tank by itself! In the work reported here Load Set B of Load Case 2 is

always the same as that for Load Case 1. Hence, Load Set B of Load Case 2 acting by itself does **not** create a critical situation in either the “test” or “test2” cases.

Cool-down of the supporting struts is not accounted for.

NOTE: In the analyses of buckling of the struts as columns and as thin shells all the loads are considered to be in Load Set A, both for Load Case 1 and for Load Case 2. For these strut buckling analyses there is no Load Set B. For stress analyses all the loads are considered to be in Load Set A, both for Load Case 1 and for Load Case 2. It was difficult to obtain buckling load factors from STAGS when there exists both Load Set A and Load Set B.

Section 9. FINDING THE OPTIMUM DESIGNS

The following points pertain to optimization of the tank/strut system:

1. The objective function is in general a compound objective as follows:

$$\text{objective} = W \times (\text{empty tank mass}) / (\text{nominal empty tank mass}) \\ (1 - W) \times (\text{total strut conductance}) / (\text{nominal conductance})$$

in which the weighting, W , (nominal empty tank mass) and (nominal conductance) are input variables supplied by the End user during the "BEGIN" interactive session. See the test.BEG file listed in Table 2. In Table 2 "W" is called "WGT"; (nominal empty tank mass) is called "TNKNRM"; and (nominal conductance) is called "CONNRM". If W (that is, WGT in Table 2) equals zero the objective is simply the (total strut conductance), which is called CONDCT in the output. The "total strut conductance" is the conductance of one strut in each strut set times the number of struts in that strut set summed over the number of strut sets [either one strut set or two strut sets (aft and forward) in this work]. **Normalization factors, “TNKNRM” and “CONNRM”, are used so that the normalized “empty tank mass” and normalized “total strut conductance” components of the objective are of approximately the same size.**

2. In this project optimization is carried out with W (that is, WGT) equal to 0.5. The curing temperature, TEMTUR, of a laminated composite strut tube is arbitrarily taken to be 170 degrees. Experience with optimizing tank/strut systems during this effort demonstrated that, for some unknown reason, the use of a non-zero value of TEMTUR seems to lead to a "global" optimum design with a smaller (better) objective than does the use of TEMTUR = 0. Therefore, in future optimizations of tank/strut systems, please always use a significant non-zero value for the variable called TEMTUR. (However, in optimizations of tank/skirt systems always use TEMTUR = 0.0.)

3. The GENOPT processor called SUPEROPT is executed. If there are two sets, aft and forward, of struts one SUPEROPT execution allowed to run to completion (about 470 design iterations) requires somewhat more than 24 hours on the first author's very fast computer. However, SUPEROPT executions may be terminated early in order to save calendar time. However, doing this may well lead to a local minimum objective that is not especially close to a “global” minimum objective. The word, “global”, is enclosed in quotation marks because GENOPT cannot literally determine the global optimum design, but can come close to the objective corresponding to the global optimum design by repeated executions of SUPEROPT or by execution of the

GENOPT processor called "SUPERDUPEROPT", in which SUPEROPT is automatically executed "x" times in succession, in which "x" is specified by the End user.

4. In this study GENOPT often has difficulty finding a "global" optimum design. The SUPEROPT process often converges several times to objectives that are significantly higher than that corresponding to the "best" design, that is, the lowest objective for a design that is either "FEASIBLE" or "ALMOST FEASIBLE". Figures 29, 57, 58, 59, 59b and 86 of [20] and Figs. 14 and 15 in this paper demonstrate this characteristic.

5. The "global" optimum design of the tank/strut system with two sets of struts and with four pairs of struts at each axial location, aft and forward, was determined first (Figs. 4 – 6). In this specific case, called "test", the SUPEROPT execution was allowed to run to a natural completion (470 design iterations, about 24 hours, Figs. 14 and 15). Optimum designs were then determined for other specific cases in a sequence such as the following:

a. The specific case called "test5" (two sets of struts with five pairs of struts at each axial location, Fig. 13). Except for the values of AGRND(1) and AGRND(2), the starting design of "test5" is the optimum design of "test" (two sets of struts with 4 pairs of struts at each axial location). AGRND(1) and AGRND(2), defined in the test.BEG file as 'circ.angle to pinned "ground" end of strut', are each changed from 45 degrees (which is the upper bound required for proper clearance when there are 4 pairs of struts at each axial location) to 36 degrees (which is the upper bound required for proper clearance when there are 5 pairs of struts at each axial location).

b. The specific case called "test3" (two sets of struts with three pairs of struts at each axial location, Fig. 12). Except for the values of AGRND(1) and AGRND(2), the starting design of "test3" is the optimum design of "test" (two sets of struts with 4 pairs of struts at each axial location). AGRND(1) and AGRND(2) are each changed from 45 degrees (which is the upper bound required for proper clearance when there are 4 pairs of struts at each axial location) to 60 degrees (which is the upper bound required for proper clearance when there are 3 pairs of struts at each axial location). [See Fig. 2 for the definition of AGRND(1) and Fig. 3 for the definition of AGRND(2).]

Plots can be obtained of the objective, variables, and design margins versus design iterations during each execution of SUPEROPT. Examples of such plots are given in Figs. 29-31 of [20], for examples. Figures 14 and 15 in this paper demonstrate that during SUPEROPT optimization cycles the tank/strut system may converge to several different local minima of the objective, $WGT^*(\text{normalized empty tank mass}) + (1-WGT)^*(\text{normalized conductance})$. This property often makes it especially difficult to find a "global" optimum design.

In the previous paragraph "global" is in quotes because the strategy used in GENOPT cannot rigorously determine a true global optimum design. Instead GENOPT attempts to find a design for which the objective is likely to be near that of a true global optimum by starting from many different points in design space during a single execution of SUPEROPT. Each new "starting" point is established randomly in a manner consistent with equality and inequality constraints. The GENOPT processor called "AUTOCHANGE" determines each new "starting" point in design space. In Figs. 14 and 15 each new "starting" point corresponds to a "spike" in the plot of objective versus design iterations.

Section 10. DECISION VARIABLE CANDIDATES FOR THE OPTIMIZED SPECIFIC CASE CALLED "test": THE LONG PROPELLANT TANK WITH TWO SETS OF STRUTS, AFT AND FORWARD, 4 PAIRS OF STRUTS IN EACH SET

Here is an example of decision variable candidates, that is, problem variables associated with Role 1 in Table 1, used during the optimization of the long tank/strut system with two "rings" of struts with 4 strut pairs at each "ring" (the specific case called "test"; see Figs. 4 - 6 for the optimized design listed here).

The following lists of optimum design, behaviors, margins and objective are part of the complete and rather long file called "test.OPM". The test.OPM file is included in the compressed file, tank.tar.gz [20], that contains many other files that document the generic case called "tank" and the specific cases called "test", "test2", etc. There it is called "test.4pair.stagsmodel.opm" or "test.4pair.feb2013.opm" rather than "test.OPM", which is the name of the output file generated from an execution of the GENOPT processor called "optimize".

Optimized Design Found With The Temporary Version Of BIGBOSOR4/BOSDEC And With Curing Temperature, TEMTUR=170 Degrees For The Long Propellant Tank With Two Rings Of Struts With 4 Pairs Of Struts In Each Ring Of Struts (Dimensions are in inches).

NOTE: The optimum design listed here was obtained **before** certain updates made in August 2012 and February 2013 were incorporated into the "tank" FORTRAN source libraries called "struct" (struct.tank) and "behavior" (behavior.tank). However, the corresponding behaviors and design margins listed here were computed with the use of the latest versions of "struct" and "behavior", those existing after the August 2012 and February 2013 updates. The predictions from STAGS [16] - [19] are from a model with the dimensions listed here. The re-optimized design, behaviors, margins and objective obtained after the August 2012 and February 2013 updates to "struct" and "behavior" are listed in Appendix 1. The final versions of the FORTRAN source code libraries, "struct" and "behavior", are part of [20].

VALUES OF DESIGN VARIABLES CORRESPONDING TO BEST FEASIBLE DESIGN

VAR. NO.	CURRENT VALUE	DEFINITION
1	7.150E-02	thickness of the tank aft dome skin: THKAFT
2	5.802E-02	thickness of the tank cylinder skin: THKMID
3	5.775E-02	thickness of the forward tank dome skin: THKFWD
4	3.426E+00	spacing of the tank orthogrid stringers: STRSPC
5	4.042E+00	spacing of the tank orthogrid rings: RNGSPC
6	1.370E-01	thickness of the tank orthogrid stringers: STRTHK
7	4.250E-01	height of the tank orthogrid stringers: STRHI
8	3.431E-01	thickness of the tank orthogrid rings: RNGTHK
9	4.250E-01	height of the tank orthogrid rings: RNGHI
10	1.500E+02	global axial coordinate of tank support ring: ZTANK(1)
11	4.500E+02	global axial coordinate of tank support ring: ZTANK(2)
12	9.008E+01	global axial coordinate of "ground": ZGRND(1)
13	5.152E+02	global axial coordinate of "ground": ZGRND(2)
14	6.002E+00	circ.angle (deg.) to pinned tank end of strut: ATANK(1)
15	6.000E+00	circ.angle (deg.) to pinned tank end of strut: ATANK(2)
16	4.500E+01	circ.angle to pinned "ground" end of strut: AGRND(1)
17	4.500E+01	circ.angle to pinned "ground" end of strut: AGRND(2)
18	7.071E+00	inner diam. of support tube active at launch: IDTUBE(1)

```

19 7.369E+00 inner diam. of support tube active at launch: IDTUBE(2 )
20 1.000E-06 height of mid-tank T-ring web: WEBHI
21 1.000E-06 thickness of mid-tank T-ring web: WEBTHK
22 1.000E-06 width (height) of mid-tank T-ring flange: FLGHI
23 1.000E-06 thickness of mid-tank T-ring flange: FLGTHK
24 3.000E+01 axial length of the propellant tank doubler: DUBAXL(1 )
25 8.860E-01 max.thickness of the propellant tank doubler: DUBTHK(1 )
26 3.397E-01 thickness of the tank reinforcement ring: TRNGTH(1 )
27 1.699E+00 height of the tank reinforcement ring: TRNGHI(1 )
28 6.456E-03 thickness of a lamina: THICK(1 )
29 6.456E-03 thickness of a lamina: THICK(2 )
30 6.456E-03 thickness of a lamina: THICK(3 )
31 6.456E-03 thickness of a lamina: THICK(4 )
32 6.456E-03 thickness of a lamina: THICK(5 )
33 6.456E-03 thickness of a lamina: THICK(6 )
34 6.819E-03 thickness of a lamina: THICK(7 )
35 6.819E-03 thickness of a lamina: THICK(8 )
36 6.819E-03 thickness of a lamina: THICK(9 )
37 6.819E-03 thickness of a lamina: THICK(10)
38 6.819E-03 thickness of a lamina: THICK(11)
39 6.819E-03 thickness of a lamina: THICK(12)
40 1.958E+01 layup angle: ANGLE(1 )
41 -1.958E+01 layup angle: ANGLE(2 )
42 5.400E+01 layup angle: ANGLE(3 )
43 -5.400E+01 layup angle: ANGLE(4 )
44 1.000E+01 layup angle: ANGLE(5 )
45 -1.000E+01 layup angle: ANGLE(6 )
46 1.696E+01 layup angle: ANGLE(7 )
47 -1.696E+01 layup angle: ANGLE(8 )
48 6.089E+01 layup angle: ANGLE(9 )
49 -6.089E+01 layup angle: ANGLE(10)
50 1.312E+01 layup angle: ANGLE(11)
51 -1.312E+01 layup angle: ANGLE(12)

```

Section 11. VALUES OF “BEHAVIORS”, CORRESPONDING DESIGN MARGINS AND OBJECTIVE FOR THE OPTIMIZED SPECIFIC CASE CALLED “test” (frequency in Hz, stress in psi, force in lb)

During optimization, “behaviors” (tank/strut vibration frequencies, maximum strut stresses, strut buckling load factors, maximum launch-hold force in a strut, maximum propellant tank stress, propellant tank buckling load factors) and the corresponding design margins are computed for each of the two load cases for each optimization cycle. In the work reported here “behaviors” and design margins are computed for each of the two load cases identified above in the short section entitled "Section 8. TWO LOAD CASES".

The “behaviors” and corresponding design margins computed for the optimized tank/strut system (the configuration listed above in the section called “Section 10. DECISION VARIABLE CANDIDATES...”) for the long tank with two "rings" of struts, an aft "ring" of struts and a "forward" ring of struts, are as follows for

the specific case called "test" (4 pairs of struts in each "ring" of struts). The critical and almost critical design margins are listed in bold face.

 *** RESULTS FOR **LOAD CASE NO. 1** (axial acceleration of 10g, etc.) ***
 PARAMETERS WHICH DESCRIBE **BEHAVIOR** (e.g. modal vibration, stress, buckling load, strut force)

BEH. NO.	CURRENT VALUE	DEFINITION
1	1.207E+01	modal vibration frequency (cps): FREQ(1 ,1)
2	1.216E+01	modal vibration frequency (cps): FREQ(1 ,2)
3	1.324E+01	modal vibration frequency (cps): FREQ(1 ,3)
4	1.333E+01	modal vibration frequency (cps): FREQ(1 ,4)
5	4.724E+03	maximum stress in material 1: STRES1(1 ,1)
6	2.206E+04	maximum stress in material 1: STRES1(1 ,2)
7	4.240E+03	maximum stress in material 1: STRES1(1 ,3)
8	9.140E+02	maximum stress in material 1: STRES1(1 ,5)
9	5.262E+04	maximum stress in material 2: STRES2(1 ,1)
10	1.416E+04	maximum stress in material 2: STRES2(1 ,2)
11	6.671E+03	maximum stress in material 2: STRES2(1 ,3)
12	2.328E+03	maximum stress in material 2: STRES2(1 ,5)
13	4.163E+00	buckling of a strut as a column: COLBUK(1 ,1)
14	1.781E+04	buckling of a strut as a column: COLBUK(1 ,2)
15	5.408E+00	buckling of strut as a shell: SHLBUK(1 ,1)
16	2.382E+02	buckling of strut as a shell: SHLBUK(1 ,2)
17	7.703E+03	launch-hold force in a strut: FORCE(1 ,1)
18	1.475E+04	launch-hold force in a strut: FORCE(1 ,2)
19	5.000E+04	maximum stress in the propellant tank: TNKSTR(1 ,1)
20	5.000E+04	maximum stress in the propellant tank: TNKSTR(1 ,2)
21	1.100E+01	propellant tank buckling load factor: TNKBUK(1 ,1)
22	1.100E+01	propellant tank buckling load factor: TNKBUK(1 ,2)

*** RESULTS FOR **LOAD CASE NO. 1** (axial acceleration of 10g, etc.) ***
MARGINS CORRESPONDING TO CURRENT DESIGN (F.S.= FACTOR OF SAFETY)

MARGIN NO.	CURRENT VALUE	DEFINITION
1	5.763E-03	(FREQ(1,1)/FREQA(1,1))/FREQF(1,1)-1; F.S.= 1.20
2	1.340E-02	(FREQ(1,2)/FREQA(1,2))/FREQF(1,2)-1; F.S.= 1.20
3	1.031E-01	(FREQ(1,3)/FREQA(1,3))/FREQF(1,3)-1; F.S.= 1.20
4	1.106E-01	(FREQ(1,4)/FREQA(1,4))/FREQF(1,4)-1; F.S.= 1.20
5	1.884E+01	(STRES1A(1,1)/STRES1(1,1))/STRES1F(1,1)-1; F.S.= 1.50
6	2.164E+00	(STRES1A(1,2)/STRES1(1,2))/STRES1F(1,2)-1; F.S.= 1.50
7	6.597E-01	(STRES1A(1,3)/STRES1(1,3))/STRES1F(1,3)-1; F.S.= 1.50
8	3.588E+00	(STRES1A(1,5)/STRES1(1,5))/STRES1F(1,5)-1; F.S.= 1.50
9	7.808E-01	(STRES2A(1,1)/STRES2(1,1))/STRES2F(1,1)-1; F.S.= 1.50
10	3.931E+00	(STRES2A(1,2)/STRES2(1,2))/STRES2F(1,2)-1; F.S.= 1.50
11	5.509E-02	(STRES2A(1,3)/STRES2(1,3))/STRES2F(1,3)-1; F.S.= 1.50
12	8.014E-01	(STRES2A(1,5)/STRES2(1,5))/STRES2F(1,5)-1; F.S.= 1.50
13	3.163E+00	(COLBUK(1,1)/COLBUKA(1,1))/COLBUKF(1,1)-1; F.S.= 1.00

14	1.781E+04	(COLBUK(1,2)/COLBUKA(1,2))/COLBUKF(1,2)-1; F.S.= 1.00
15	1.704E+00	(SHLBUK(1,1)/SHLBUKA(1,1))/SHLBUKF(1,1)-1; F.S.= 2.00
16	1.181E+02	(SHLBUK(1,2)/SHLBUKA(1,2))/SHLBUKF(1,2)-1; F.S.= 2.00
17	9.474E-01	(FORCEA(1,1)/FORCE(1,1))/FORCEF(1,1)-1; F.S.= 1.00
18	1.663E-02	(FORCEA(1,2)/FORCE(1,2))/FORCEF(1,2)-1; F.S.= 1.00
19	-3.278E-05	(TNKSTRA(1,1)/TNKSTR(1,1))/TNKSTRF(1,1)-1; F.S.= 1.00
20	-2.497E-05	(TNKSTRA(1,2)/TNKSTR(1,2))/TNKSTRF(1,2)-1; F.S.= 1.00
21	9.999E+00	(TNKBUK(1,1)/TNKBUKA(1,1))/TNKBUKF(1,1)-1; F.S.= 1.00
22	9.999E+00	(TNKBUK(1,2)/TNKBUKA(1,2))/TNKBUKF(1,2)-1; F.S.= 1.00

*** RESULTS FOR **LOAD CASE NO. 2** (lateral acceleration of 10g, etc.) ***
PARAMETERS WHICH DESCRIBE **BEHAVIOR** (e.g. modal vibration, stress, buckling load, strut force)

BEH. NO.	CURRENT VALUE	DEFINITION
1	1.199E+01	modal vibration frequency (cps): FREQ(2 ,1)
2	1.228E+01	modal vibration frequency (cps): FREQ(2 ,2)
3	1.323E+01	modal vibration frequency (cps): FREQ(2 ,3)
4	1.333E+01	modal vibration frequency (cps): FREQ(2 ,4)
5	6.398E+04	maximum stress in material 1: STRES1(2 ,1)
6	3.711E+04	maximum stress in material 1: STRES1(2 ,2)
7	7.016E+03	maximum stress in material 1: STRES1(2 ,3)
8	3.659E+03	maximum stress in material 1: STRES1(2 ,5)
9	5.888E+04	maximum stress in material 2: STRES2(2 ,1)
10	3.438E+04	maximum stress in material 2: STRES2(2 ,2)
11	7.035E+03	maximum stress in material 2: STRES2(2 ,3)
12	2.584E+03	maximum stress in material 2: STRES2(2 ,5)
13	2.398E+00	buckling of a strut as a column: COLBUK(2 ,1)
14	2.645E+00	buckling of a strut as a column: COLBUK(2 ,2)
15	3.115E+00	buckling of strut as a shell: SHLBUK(2 ,1)
16	3.299E+00	buckling of strut as a shell: SHLBUK(2 ,2)
17	7.317E+03	launch-hold force in a strut: FORCE(2 ,1)
18	1.439E+04	launch-hold force in a strut: FORCE(2 ,2)
19	4.994E+04	maximum stress in the propellant tank: TNKSTR(2 ,1)
20	4.994E+04	maximum stress in the propellant tank: TNKSTR(2 ,2)
21	9.359E+00	propellant tank buckling load factor: TNKBUK(2 ,1)
22	9.361E+00	propellant tank buckling load factor: TNKBUK(2 ,2)

*** RESULTS FOR **LOAD CASE NO. 2** (lateral acceleration of 10g, etc.) ***
MARGINS CORRESPONDING TO CURRENT DESIGN (F.S.= FACTOR OF SAFETY)

MARGIN NO.	CURRENT VALUE	DEFINITION
1	-8.823E-04	(FREQ(2,1)/FREQA(2,1))/FREQF(2,1)-1; F.S.= 1.20
2	2.326E-02	(FREQ(2,2)/FREQA(2,2))/FREQF(2,2)-1; F.S.= 1.20
3	1.026E-01	(FREQ(2,3)/FREQA(2,3))/FREQF(2,3)-1; F.S.= 1.20
4	1.104E-01	(FREQ(2,4)/FREQA(2,4))/FREQF(2,4)-1; F.S.= 1.20
5	4.646E-01	(STRES1A(2,1)/STRES1(2,1))/STRES1F(2,1)-1; F.S.= 1.50

6	8.811E-01	(STRES1A(2,2)/STRES1(2,2))/STRES1F(2,2)-1; F.S.= 1.50
7	3.091E-03	(STRES1A(2,3)/STRES1(2,3))/STRES1F(2,3)-1; F.S.= 1.50
8	1.461E-01	(STRES1A(2,5)/STRES1(2,5))/STRES1F(2,5)-1; F.S.= 1.50
9	5.916E-01	(STRES2A(2,1)/STRES2(2,1))/STRES2F(2,1)-1; F.S.= 1.50
10	1.030E+00	(STRES2A(2,2)/STRES2(2,2))/STRES2F(2,2)-1; F.S.= 1.50
11	4.510E-04	(STRES2A(2,3)/STRES2(2,3))/STRES2F(2,3)-1; F.S.= 1.50
12	6.230E-01	(STRES2A(2,5)/STRES2(2,5))/STRES2F(2,5)-1; F.S.= 1.50
13	1.398E+00	(COLBUK(2,1)/COLBUKA(2,1))/COLBUKF(2,1)-1; F.S.= 1.00
14	1.645E+00	(COLBUK(2,2)/COLBUKA(2,2))/COLBUKF(2,2)-1; F.S.= 1.00
15	5.576E-01	(SHLBUK(2,1)/SHLBUKA(2,1))/SHLBUKF(2,1)-1; F.S.= 2.00
16	6.493E-01	(SHLBUK(2,2)/SHLBUKA(2,2))/SHLBUKF(2,2)-1; F.S.= 2.00
17	1.050E+00	(FORCEA(2,1)/FORCE(2,1))/FORCEF(2,1)-1; F.S.= 1.00
18	4.235E-02	(FORCEA(2,2)/FORCE(2,2))/FORCEF(2,2)-1; F.S.= 1.00
19	1.234E-03	(TNKSTRA(2,1)/TNKSTR(2,1))/TNKSTRF(2,1)-1; F.S.= 1.00
20	1.264E-02	(TNKSTRA(2,2)/TNKSTR(2,2))/TNKSTRF(2,2)-1; F.S.= 1.00
21	8.359E+00	(TNKBUK(2,1)/TNKBUKA(2,1))/TNKBUKF(2,1)-1; F.S.= 1.00
22	8.361E+00	(TNKBUK(2,2)/TNKBUKA(2,2))/TNKBUKF(2,2)-1; F.S.= 1.00

In the lists of "behavior" and "margins" the following conventions apply:

Behavioral variable names (edited from Table 1):

FREQ means modal vibration frequency

STRES means stress component in a ply of a composite strut tube

COLBUK means buckling of a strut as a column

SHLBUK means buckling of a strut as a thin shell

FORCE means force in a strut tube during launch-hold

TNKSTR means stress in the propellant tank wall

TNKBUK means buckling of the propellant tank

"A", "F", and "F.S.":

An "A" added to a behavioral variable name means "allowable"

An "F" added to a behavioral variable name means "factor of safety"

"F.S." means "factor of safety"

Indices, i,j,k:

FREQ(i,j) = modal vibration frequency: i = load case; j = vibration mode

j = 1 means first eigenvalue for n = 0 waves (usually the mode with significant axial motion of the tank)

j = 2 means first eigenvalue for n = 1 waves (a mode with significant lateral-pitch motion of the tank)

j = 3 means first eigenvalue for n = 2 waves (a mode in which the tank wall deforms with 2 circ. waves)

j = 4 means first eigenvalue for n = 3 or 4 waves (a mode in which the tank wall deforms)

STRES_i(j,k) = stress component in strut: i = material no., j=load case, k = stress component

i = 1 means "material no. 1" which also means "strut type no. 1" (aft ring of struts)

i = 2 means "material no. 2" which also means "strut type no. 2" (forward ring of struts)

j = 1 means "Load Case 1" (See the section above entitled "Section 8. TWO LOAD CASES")

j = 2 means "Load Case 2" (See the section above entitled "Section 8. TWO LOAD CASES")

k = 1 means tension along the fibers of a ply

k = 2 means compression along the fibers of a ply

k = 3 means tension transverse to the fibers of a ply

k = 4 means compression transverse to the fibers of a ply

k = 5 means in-plane shear in a ply

COLBUK(i,j) = buckling of the strut as a column: i = load case; j = strut type

j = 1 means the type of strut attached to the aft propellant tank support ring. All these struts are the same.

j = 2 means the type of strut attached to the forward propellant tank support ring. All these struts are the same.

SHLBUK(i,j) = buckling of the strut as a thin shell: i = load case; j = strut type

j = 1 means the type of strut attached to the aft propellant tank support ring.

j = 2 means the type of strut attached to the forward propellant tank support ring.

FORCE(i,j) = maximum force in a strut: i = load case; j = strut type

j = 1 means the type of strut attached to the aft propellant tank support ring.

j = 2 means the type of strut attached to the forward propellant tank support ring.

TNKSTR(i,j) = maximum effective stress: i = load case; j = meridian number

j = 1 = effective stress in the tank is the maximum from the distribution along meridian no. 1

j = 2 = effective stress in the tank is the maximum from the distribution along meridian no. 2

TNKBUK(i,j) = buckling load factor: i = load case; j = meridian number

j = 1 means buckling load factor of the tank from the stress distribution along meridian no. 1

j = 2 means buckling load factor of the tank from the stress distribution along meridian no. 2

Corresponding to the optimized "test" design the design objective is:

```

***** DESIGN OBJECTIVE *****
CURRENT VALUE OF THE OBJECTIVE FUNCTION:
VAR.    CURRENT
NO.     VALUE          DEFINITION
1       1.004E+00    WGTxTOTMAS/TNKNRM +(1-WGT)xCONDCT/CONNRM

```

in which:

```

WGT, TOTMAS, TNKNRM, CONDCT, CONNRM=
5.0000E-01  1.1050E+01  1.0000E+01  1.8061E-03  2.0000E-03

```

Section 12. EFFECT OF THE FLEXIBILITY OF THE PROPELLANT TANK ON THE STRUT "SPRING" STIFFNESS USED FOR THE COMPUTATION OF MODAL VIBRATION FREQUENCIES

In the case of an ordinary shell of revolution, such as the propellant tank without strut (spring) supports, vibration modes with different numbers of circumferential waves, "n", are decoupled. Therefore a relatively small number of simultaneous equations with narrowly banded stiffness and mass matrices are required to determine vibration modes and frequencies, buckling modes and buckling load factors, and stresses in non-axisymmetrically loaded shells. The behavior for each value of "n" can be computed independently of other values of "n". If struts (springs) are introduced this orthogonality with respect to "n" no longer holds; all the modes of deformation with different values of "n" are coupled. Therefore, large, full stiffness and mass matrices govern the problem. The approximate GENOPT/TANK/BIGBOSOR4 analysis on which the results reported here are based maintains the orthogonality of the tank/strut system with respect to the number of circumferential waves, "n", by computing reduced "effective" axial stiffnesses of the struts (springs) that account for the flexibility of the propellant tank in an approximate and conservative manner.

Of particular interest is the effect of the flexibility of the propellant tank on the "effective" spring constant (axial stiffness) of the supporting struts. This effect can be ascertained from part of the output listed in Table 8 of [20] (values updated here) for the long propellant tank with aft and forward sets of struts with 4 pairs of struts at each axial location:

For Load Case 1 (PRESS = 25 psi, GAXIAL = 10g, GLATRL = 0g, TNKCOOL=-200 degrees):

Spring constant for compound strut type 1 (**aft strut set**) = SPRCON(1) = 1.6918E+05 lb/in)

Spring constant including tank flexibility: FKTOTL(1) = 0.90485E+05 lb/in)

Spring constant for compound strut type 2 (**forward strut set**) = SPRCON(2) = 1.8157E+05 lb/in)

Spring constant including tank flexibility: FKTOTL(2) = 1.2149E+05 lb/in)

For Load Case 2 (PRESS = 25 psi, GAXIAL = 0g, GLATRL = 10g, TNKCOOL=-200 degrees):

Spring constant for compound strut type 1 (**aft strut set**) = SPRCON(1) = 1.6918E+05 lb/in)

Spring constant including tank flexibility: FKTOTL(1) = 1.0843E+05 lb/in)

Spring constant for compound strut type 2 (**forward strut set**) = SPRCON(2) = 1.8157E+05 lb/in)

Spring constant including tank flexibility: FKTOTL(2) = 1.0227E+05 lb/in)

The "Spring constant for compound strut type..." is the spring constant neglecting flexibility of the propellant tank. This is the spring constant of a three-segment (compound) strut: segment 1 is the end fitting at the propellant-tank end of the strut; segment 2 is the laminated composite strut tube; segment 3 is the end fitting at the launch vehicle ("ground") end of the strut. The "Spring constant for compound strut type..." is called "SPRCON" (SPRing CONstant) in the GENOPT/TANK output file called "test.OPM".

For the optimized design the flexibility of the tank has a significant effect on the "effective" axial stiffness of the struts. Note that the effective axial stiffness of the struts (strut "spring constant", FKTOTL, that includes the effect of flexibility of the propellant tank) depends on the loading. In the models for modal vibration the first four design margins are slightly different for Load Cases 1 and 2 because of this dependence of reduced strut effective stiffness on loading.

Why do we use a strategy in which the flexibility of the propellant tank is represented as a “knockdown factor” to adjust the axial stiffness of the struts? We do this rather than rigorously solve the problem of a spring-supported shell of revolution in order to reduce the computer time required for optimization. In a rigorous analysis of a shell of revolution supported by springs the displacement meridional distributions corresponding to n circumferential waves, $n = 0, 1, 2, 3, \dots, NMAX$, would all couple, leading to a huge number of degrees of freedom, $NDOF = (NMAX+1) \times MDOF$, in which $MDOF$ is the number of degrees of freedom corresponding to discretization of the shell meridian (approximately equal to the number of meridional nodal points times the number of degrees of freedom per nodal point) and $NMAX$ is the maximum number of circumferential waves used in the representation of the displacement field. The stiffness matrix of dimension $NDOF \times NDOF$ would be full. When we approximate the true behavior of the spring-supported axisymmetric tank by using a reduced effective axial spring stiffness we preserve the decoupling of the displacement fields with different numbers of circumferential waves. Therefore, we solve equations with $MDOF$ degrees of freedom $NMAX + 1$ times rather than solve one huge set of equations with $NDOF$ degrees of freedom.

Figures 16a and 16b show vibration modes of the optimized long propellant tank with aft and forward sets of struts, 4 pairs of struts in each set. These plots are generated by BIGBOSOR4. The struts are not shown in the plots because BIGBOSOR4 does not have the capability to include in the plot springs that are attached to a shell of revolution (the propellant tank). The most significant modes are (A), (C) and (D) because these are the modes that are most likely to be excited during launch of the propellant tank into space.

In these modes [and in Mode (B), which is not likely to be excited during launch] the propellant tank is shown as moving approximately as a rigid body. However, as described above, in the GENOPT/BIGBOSOR4 model the flexibility of the propellant tank is accounted for in computations of reduced “effective” axial strut (spring) stiffnesses. As demonstrated above, the flexibility of the propellant tank significantly reduces the effective axial stiffness of a strut, for example almost halving the effective stiffness of an aft strut (strut type 1) under Load Case 1 (strut spring constant reduced from $1.69E+05$ lb/in to $0.905E+05$ lb/in). The GENOPT/BIGBOSOR4 model is conservative because the largest influence of tank flexibility on any strut attached at a given axial location (attached to a given propellant tank support ring) is used for all of the struts at that axial location. For example, in Load Case 1 (axial acceleration) the reduced strut spring constant, $0.905E+05$ lb/in, is used for all of the struts attached to the aft propellant tank support ring. The same conservative approach is used for the struts attached to the forward propellant tank support ring. This is probably the primary reason that the predictions from GENOPT/BIGBOSOR4 for modal vibration frequencies are conservative (lower) when compared with predictions from STAGS for modes (A) – (D) in Fig. 16a. Modes (A) – (D) all involve significant extension/compression of the springs (struts), while the propellant tank shell translates and rotates approximately as a rigid body in the GENOPT/BIGBOSOR4 model.

The three vibration modes in Fig. 16b are each called “shell deformation vibration mode” because the struts participate very little in these modes. Instead, mostly the cylindrical portion of the propellant tank vibrates with “ n ” circumferential waves. The struts have diminishing influence on the modal vibration frequency as the number of circumferential waves in the shell deformation modes increases. Usually the modal vibration frequencies for these “shell deformation vibration modes” agree better with the STAGS [16 – 19] predictions than the types of vibration modes shown in Fig. 16a. The four vibration modes shown in Fig. 16a involve significant extension/compression of the struts, the reduced effective axial stiffness of which is computed with use of the approximate and conservative GENOPT/BIGBOSOR4 model just described.

How is the reduced effective axial spring stiffness computed? For each of the two load cases and for each of the two “rings” of struts, aft and forward, the reduced effective axial strut stiffness is computed in the following way:

Item 1. Forces in the struts and lengths of the struts are computed from a linear static equilibrium analysis of the propellant tank with springs (struts) with an arbitrarily assigned spring constant.

Item 2. The 6 x 6 integrated wall stiffness matrix $C(i,j)$ for a laminated composite strut tube is computed, and from this $C(i,j)$ are computed the axial “EA” stiffness and spring constant of the compound strut that consists of the laminated composite strut tube plus metallic end fittings with given “EA” axial stiffness and given length. For example, in the case of the optimized long propellant tank with aft and forward “rings” of struts (the specific case called “test”) the spring constant of each compound strut in the aft ring of struts is $1.69E+05$ lb/in as listed near the beginning of this section.

Item 3. A linear equilibrium model of the propellant tank is set up in which the struts are replaced by the forces computed in **Item 1**. From this **Item 3** model the component of tank displacement is computed at the attachment point of each strut to the centroid of the external tank support ring and resolved in the direction of the strut axis. The maximum resolved component of tank wall displacement from all the struts in a given ring of struts (aft or forward) is stored in an array called $DISMAX(i)$, $i = 1$ for aft ring of struts, $i = 2$ for forward ring of struts.

Item 4. New, reduced spring constants, $k(\text{reduced})(i)$, $i = 1$ for aft struts and $i = 2$ for forward struts, are computed from the equations:

$$F(i) = k(\text{original})(i)x \quad (1)$$

$$F(i) = k(\text{reduced})(i)(x + DISMAX(i)) \quad (2)$$

which, through the elimination of the unknown, x , lead to the following equation:

$$k(\text{reduced})(i) = F(i) / [F(i) / k(\text{original})(i) + DISMAX(i)] \quad (3)$$

in which $i = 1$ for the aft “ring” of struts, and $i = 2$ for the forward “ring” of struts, and $F(i)$ is the force in the strut (derived in **Item 1**) that corresponds to the maximum resolved displacement component, $DISMAX(i)$. The quantity, $k(\text{reduced})(i)$, is called $FKTOTL(JRING)$ in the output file, test.OPM. The quantity, $k(\text{original})(i)$, is called “SPRCON” (“SPRing CONstant”). For example, with the optimized long propellant tank, “test”, in Load Case 1 the reduced effective spring constant of each compound strut in the aft ring of struts is $FKTOTL(1) = 0.90485E+05$ lb/in and the “original” spring constant, $k(\text{original})(1) = SPRCON(1) = 1.6918E+05$ lb/in, as listed near the beginning of this section. Similarly, under Load Case 1 the reduced effective spring constant of each compound strut in the forward ring of struts is $FKTOTL(2) = 1.2149E+05$ lb/in and the “original” spring constant, $k(\text{original})(2) = SPRCON(2) = 1.8157E+05$ lb/in as listed near the beginning of this section.

Analogously, in Load Case 2 the reduced effective spring constant of each compound strut in the aft ring of struts is $1.0843E+05$ lb/in, and the reduced effective spring constant of each compound strut in the forward ring of struts is $1.0227E+05$ lb/in. For the appropriate load case these reduced spring constants are to be used in

Item 5.

Item 5. New forces in the struts are computed from the same type of linear static equilibrium analysis of the propellant tank with springs (struts) as that used in **Item 1**, now with use of the reduced (“effective”) spring constants computed in **Item 4** instead of the arbitrarily assigned spring constants used in **Item 1**. These new strut forces are to be used in the computations of column and shell buckling of the struts, maximum stress components in the laminated composite struts, maximum effective stress in the propellant tank wall, and buckling load factors of the propellant tank. **The reduced strut spring constants are to be used only in the modal vibration model of the propellant tank with attached springs and in the computation of the maximum strut forces developed under the loading associated with the launch-hold condition (1 g axial acceleration, 25 psi internal ullage pressure and 200-degree propellant tank cool-down).**

Section 13. DESIGN SENSITIVITY OF THE OPTIMIZED LONG PROPELLANT TANK WITH TWO SETS OF STRUTS WITH FOUR PAIRS OF STRUTS IN EACH SET (the specific case called "test")

Figures 17 – 19 show sample "design sensitivity" plots corresponding to the optimized design of the long propellant tank with aft and forward sets of struts. Many additional “design sensitivity” plots are given in [20]. The “design sensitivity” plots are generated by the GENOPT/BIGBOSOR4 model from analyses in which a user-selected decision variable varies over a user-selected range while all other decision variables are held constant. A typical characteristic of these plots, which pertain to a previously optimized design, is that several design margins become critical or nearly critical at the value of the user-selected decision variable that corresponds to its optimized value. NOTE: Figures 17 – 19 were created before the August 2012 and February 2013 updates were incorporated into the “tank” software, struct.tank and behavior.tank.

Section 14. OTHER PREDICTIONS PERTAINING TO THE GENOPT/BIGBOSOR4 MODEL OF THE OPTIMIZED LONG PROPELLANT TANK WITH TWO SETS OF STRUTS WITH FOUR PAIRS OF STRUTS IN EACH SET (the specific case called "test")

Other plots

Plots of the optimized configuration are given in Figs. 4 – 6. Several of the behaviors corresponding to the optimized design are plotted: vibration modes in Figs. 16a and 16b, shell buckling modes of the struts in Fig. 20, propellant tank prebuckling deformations in Figs. 21a-d, and propellant tank buckling modes in Figs. 22 and 23. These plots are generated by the “stand-alone” version of BIGBOSOR4 as described in Table 1 of [20]. The struts are not shown in Figs. 21 – 23 because, in the model of propellant tank prebuckling and buckling, the struts are replaced by the concentrated loads that these struts apply to the propellant tank. The struts are not shown in Figs. 16a and 16b because the plotting software associated with BIGBOSOR4 does not have the capability of plotting springs. All GENOPT/BIGBOSOR4 predictions are from linear theory.

Linear GENOPT/BIGBOSOR4 stress analysis of the optimized design with tapered doublers

The GENOPT/BIGBOSOR4 predictions for the optimized long propellant tank with aft and forward sets of struts, 4 pairs at each axial location, are given for Load Case 1 by the following:

```
***** (ALLOWABLE STRESS)/(ACTUAL STRESS) *****
 1  9.9997E-01 fiber tension : matl=1 , A , seg=11, node=4 , layer=1 ,z=-0.46
 2  1.4762E+00 fiber compres.: matl=1 , A , seg=1 , node=1 , layer=1 ,z=-0.46
 3  1.4424E+00 transv tension: matl=1 , A , seg=14, node=5 , layer=1 ,z=-0.45
```

```

4  1.4762E+00 transv compres: matl=1 , A , seg=1 , node=1 , layer=1 , z=-0.46
5  1.1141E+00 effect. stress: matl=2 , A , seg=1 , node=3 , layer=2 , z= 0.04
6  1.5371E+00 effect. stress: matl=3 , A , seg=16, node=2 , layer=3 , z= 0.05
7  1.1232E+00 effect. stress: matl=4 , A , seg=15, node=52, layer=2 , z= 0.03
8  1.3502E+00 effect. stress: matl=5 , A , seg=28, node=10, layer=2 , z= 0.03
*****

```

Maximum stress components for Load Case 1 STRESS2(i),i=1,6=

fiber tension	fiber compres.	transv tension	transv compres	in-plane shear	effect. stress
5.0002E+04	3.3871E+04	3.4666E+04	3.3871E+04	0.0000E+00	4.4879E+04

The GENOPT/BIGBOSOR4 predictions just listed are from linear theory.

In the GENOPT/TANK/BIGBOSOR4 model of the tank/strut system, the internal orthogrid “layer” (layer=1 in the list above) of the aluminum propellant tank is designated as being fabricated with material type 1 (matl=1 in the list above). The quantity “z” is the coordinate normal to the reference surface of the shell. Negative z is inside the propellant tank shell wall reference surface, and positive z is outside the reference surface. z = -0.45 inch and z = -0.46 inch correspond to the tips of the internal orthogrid stringers; z = +0.04, +0.05 and +0.03 inch correspond to the outer surface of the skin of the propellant tank shell wall. The allowable stress in material type 1 is $TNKSTRA(i,j) = 50000$ psi, as listed in Table 2. The factor of safety for stress in the propellant tank is taken as $TNKSTRF(i,j) = 1.0$, as listed in Table 2. A typical stress margin is given by:

$$(\text{stress margin}) = (\text{allowable stress}) / [(\text{actual stress}) \times (\text{factor of safety})] - 1.0.$$

The locations of the most critical stresses in the propellant tank generated under Load Case 1 (10 g axial acceleration plus 25 psi internal pressure + 200-degree tank cool-down) are identified in the entries 1, 5 and 7 in the list above under the heading “(ALLOWABLE STRESS)/(ACTUAL STRESS)”. Entries 1, 5 and 7 have values that are closest to unity. Therefore, they represent critical (Entry 1) and nearly critical (Entries 5 and 7) stresses (corresponding design margins are near zero). Layer 1 is the layer consisting of the smeared internal orthogrid stiffeners (Fig. 1c); Layer 2 is the skin; Layer 3 is the external tapered doubler. The locations of the critical and nearly critical effective stresses corresponding to Load Case 1 are indicated in Fig. 21a(A).

Comparison of BIGBOSOR4 predictions of orthogrid stringer tip tensile stress in the knuckle regions of the ellipsoidal domes from three BIGBOSOR4 models

About 98 per cent of the Load Case 1 stress from entries 1, 2, 4 and 5 (aft dome) and 8 (forward dome) in the list above entitled, $(\text{ALLOWABLE STRESS}) / (\text{ACTUAL STRESS})$, is generated by only two of the components of loading: the uniform internal pressure, 25 psi, plus 10g axial acceleration. The maximum tensile stress at the tips of the stringers in the internal orthogrid (called “fiber tension” above) is 50000 psi from all four components of the loading: axial acceleration, internal pressure, tank cool-down, and concentrated loads from the struts. This 50000 psi maximum is obtained from linear theory. It occurs in the knuckle region of the aft ellipsoidal dome, and it is indicated as Critical Point No. 2 in Fig. 21a(A).

Three BIGBOSOR4 models were set up corresponding to the optimized design of the propellant tank loaded by the uniform internal pressure = 25 psi (no thermal loading, no loading by struts) in order to find the maximum tensile stress at the tips of the stringers in the internal orthogrid “layer” of the propellant tank shell wall in the knuckle regions of the ellipsoidal domes:

1. **Model 1:** a model with the use of **linear** theory for the prediction of maximum stringer tip tensile stress in the knuckle regions of the ellipsoidal domes loaded by uniform internal pressure = 25 psi plus 10g axial acceleration (BIGBOSOR4 analysis type, INDIC = 3), and

2. **Model 2:** a model with the use of **linear** theory for the prediction of maximum stringer tip tensile stress in the knuckle regions of the ellipsoidal domes loaded by uniform internal pressure = 25 psi only (BIGBOSOR4 analysis type, INDIC = 3), and

3. **Model 3:** a model with the use of **nonlinear** theory for the prediction of maximum stringer tip tensile stress in the knuckle regions of the ellipsoidal domes loaded by uniform internal pressure = 25 psi only (BIGBOSOR4 analysis type, INDIC = 0).

The following maximum tensile stresses at the tips of the stringers in the internal orthogrid in the knuckle regions of the aft and forward ellipsoidal domes were found:

From Model 1: maximum tensile stress = 48917 psi (aft dome); 39053 psi (forward dome)

From Model 2: maximum tensile stress = 34535 psi (aft dome); 39270 psi (forward dome)

From Model 3: maximum tensile stress = 30210 psi (aft dome); 34013 psi (forward dome)

The BIGBOSOR4 predictions of stress at the tips of the stringers of the internal orthogrid “layer” in the knuckle region of the aft ellipsoidal dome are plotted in Fig. 21b. The effect of the 10 g axial acceleration is greater than the effect of the application of linear versus nonlinear theory. Nonlinear theory yields smaller maximum tensile stresses at the tips of the orthogrid stringers because the net (membrane) meridional tension field in the knuckle region of each dome, generated by the uniform internal pressure component of the loading, diminishes the amount of meridional bending in the knuckle region from that predicted with the use of linear theory.

Linear theory is used throughout in the GENOPT/BIGBOSOR4 model that is employed during optimization. Only linear theory can be used in the BIGBOSOR4 model of the propellant tank with concentrated strut loads because the branch of BIGBOSOR4 that computes the static response of a shell of revolution to non-axisymmetric loading is based on Fourier superposition of the static responses from each number of circumferential waves in the Fourier series expansion of the applied loading. The loading is non-axisymmetric because of the concentrated loads applied by the struts to the centroids of the propellant tank external support rings.

Use of the BIGBOSOR4 model to simulate the STAGS model with doublers of constant average thickness

It is of interest to simulate the STAGS model to be discussed in the next major section with the use of a modified BIGBOSOR4 model. In the STAGS model to be described in the next major section the doubly tapered external aft and forward propellant tank doublers used in the BIGBOSOR4 model (Figs. 1b and 1c) are replaced by external doublers of constant thickness equal to the average thickness of the doubly tapered doublers. The uniform doubler thickness used in the STAGS model equals 0.443 inch; the maximum thickness of the optimized doubly tapered doubler used in the GENOPT/BIGBOSOR4 model, (decision variable candidate called “DUBTHK(1)” as indicated in Fig. 1c) equals 0.886 inch. With the tapered doublers replaced by constant thickness doublers in the BIGBOSOR4 model of the otherwise optimized tank/strut system, the following stress predictions for Load Case 1 are obtained from BIGBOSOR4:

Load Case 1: Constant doubler thickness = 0.443 inch.

```
ALLOWABLE STRESS)/(ACTUAL STRESS) *****
 1  6.3778E-01 fiber tension : matl=1 , A , seg=17, node=1 , layer=1 , z=-0.4539
 2  4.1974E-01 fiber compres.: matl=1 , A , seg=16, node=13, layer=1 , z=-0.454
 3  1.4616E+00 transv tension: matl=1 , A , seg=14, node=6 , layer=1 , z=-0.454
 4  1.4762E+00 transv compres: matl=1 , A , seg=1 , node=1 , layer=1 , z=-0.4608
 5  1.1141E+00 effect. stress: matl=2 , A , seg=1 , node=3 , layer=2 , z=0.0357
 6  8.8860E-01 effect. stress: matl=3 , A , seg=16, node=13, layer=3 , z=0.472
 7  1.2751E+00 effect. stress: matl=4 , A , seg=15, node=50, layer=2 , z=0.029
 8  1.3502E+00 effect. stress: matl=5 , A , seg=28, node=10, layer=2 , z=0.0289
*****
```

The maximum tensile and compressive stresses at the tips of the internal orthogrid stringers (entries 1 and 2 in bold face) are much higher in the BIGBOSOR4 model in which the external doublers with constant average thickness are used. Compare especially the first two entries in the above list, that is:

```
ALLOWABLE STRESS)/(ACTUAL STRESS) *****
 1  6.3778E-01 fiber tension : matl=1 , A , seg=17, node=1 , layer=1 , z=-0.4539
 2  4.1974E-01 fiber compres.: matl=1 , A , seg=16, node=13, layer=1 , z=-0.454
```

with the first two entries in the previous analogous list, which pertains to the BIGBOSOR4 model with the tapered doublers, that is:

```
***** (ALLOWABLE STRESS)/(ACTUAL STRESS) *****
 1  9.9997E-01 fiber tension : matl=1 , A , seg=11, node=4 , layer=1 , z=-0.46
 2  1.4762E+00 fiber compres.: matl=1 , A , seg=1 , node=1 , layer=1 , z=-0.46
```

The locations of the maximum tensile and compressive stresses at the internal orthogrid stringer tips have changed as well as their values. The change in the BIGBOSOR4 predictions resulting from the use of constant thickness doublers with thickness equal to 0.443 inch is dramatic. This dramatic increase in the maximum stress predicted by the modified BIGBOSOR4 model strongly indicates the need for the introduction of tapered doublers into the STAGS model to be described in the next major section.

Figure 21c shows, for Load Case 1, a comparison of the deformations of the forward part of the propellant tank meridian at circumferential coordinate, $\theta = 6.0$ degrees, predicted from the BIGBOSOR4 model with the doubly tapered doubler [Fig. 21c(A), maximum doubler thickness = 0.886 inch] and the BIGBOSOR4 model with the constant thickness doubler [Fig. 21c(B), uniform doubler thickness = 0.443 inch].

Figure 21d gives a comparison, from two BIGBOSOR4 models, of stresses at the forward cylinder/dome junction at the tips of the internal orthogrid stringers in the circumferential region between $\theta = 0$ degrees and $\theta = 21$ degrees. Because BIGBOSOR4 does not plot stresses in layered shell walls, each data point in this figure had to be generated from a separate execution of BIGBOSOR4 with the circumferential angle, θ , specified in the BIGBOSOR4 input file. Compare the BIGBOSOR4 results plotted in Fig. 21d with the STAGS results from the refined 45-degree STAGS model with constant thickness doublers plotted in Fig. 26f.

Convergence study with respect to the maximum number, N, of circumferential waves, n, in the Fourier series expansion used in the BIGBOSOR4 linear stress analysis of the propellant tank

In the BIGBOSOR4 model the concentrated loads applied by the struts to the centroids of the aft and forward external propellant tank support rings (Figs. 1b and 1c) are modeled as line loads with relatively narrow triangular “pulses” centered on the circumferential angles, θ , where the struts are pinned to these rings. In the specific case called “test” there are four pairs of struts pinned to the centroid of each external propellant tank support ring (optimized configuration displayed in Figs. 5 and 6). For example, in Load Case 1 (axial acceleration plus uniform internal ullage pressure plus uniform tank cool-down) for the optimized configuration shown in Figs. 5 and 6 the line load corresponding to the axial component of concentrated strut loading applied by one ring of struts has the following normalized distribution over 180 degrees of circumference (circumferential coordinate = θ in degrees):

$\theta=$	0.	1.	6.	11.	79.	84.	89.	91.	96.	101.	169.	174.	179.	180.
load=	0.	0.	1.	0.	0.	1.	0.	0.	1.	0.	0.	1.	0.	0.

with the load distribution, “load”, being even (symmetric) about the circumferential coordinates, $\theta = 0$ degrees and $\theta = 180$ degrees. As can be seen from the above list, each triangular “pulse” in the line load representation of the four concentrated strut loads applied at $\theta = 6, 84, 96$ and 174 degrees subtends 10 degrees. It is this circumferential distribution of line load with its four triangular “pulses” that must be expanded in a Fourier series. In the BIGBOSOR4 linear stress analysis of the propellant tank subjected to concentrated strut loads, 10g lateral acceleration (Load Case 2), 25 psi internal ullage pressure, and -200 degrees tank cool-down, the static response of the propellant tank is determined by Fourier superposition of the static responses from each number of circumferential waves, n , over a range from $n = 0$ circumferential waves to $n = -N$ circumferential waves. (As described in the BIGBOSOR4 user’s manual, minus wave numbers correspond to series expansions in which the normal displacement, w , of the shell wall reference surface is expanded in a cosine series [cosine($n \times \theta$)], the meridional displacement, u , is expanded in a cosine series, and the circumferential displacement, v , is expanded in a sine series. In other words, the displacement field is symmetric about the circumferential coordinates, $\theta = 0$ degrees and $\theta = 180$ degrees.) In the work on which this paper is based the maximum number of circumferential waves in the Fourier series expansion of the displacement field is automatically set to $N = -60$. It is of interest to perform a convergence study in which the minimum stress ratios, (ALLOWABLE STRESS)/(ACTUAL STRESS), are computed for various values of N . Results of such a study are as follows:

Load Case 2: "test" maximum stresses at $\theta = 83.999$ deg, max. $N = -60$ circ. waves

```
***** (ALLOWABLE STRESS)/(ACTUAL STRESS) *****
 1  1.0178E+00 fiber tension : matl=1 , A , seg=18, node=8 , layer=1 , z=-0.4539
 2  1.4028E+00 fiber compres.: matl=1 , A , seg=16, node=1 , layer=1 , z=-0.454
 3  1.8272E+00 transv tension: matl=1 , A , seg=15, node=50, layer=1 , z=-0.029
 4  1.6713E+00 transv compres: matl=1 , A , seg=28, node=13, layer=1 , z=-0.4539
 5  1.4297E+00 effect. stress: matl=2 , A , seg=1 , node=3 , layer=2 , z=0.0357
 6  1.3454E+00 effect. stress: matl=3 , A , seg=16, node=2 , layer=3 , z=0.0534
 7  1.0012E+00 effect. stress: matl=4 , A , seg=15, node=52, layer=2 , z=0.029
 8  1.2199E+00 effect. stress: matl=5 , A , seg=28, node=10, layer=2 , z=0.0289
*****
```

Load Case 2: "test" maximum stresses at $\theta = 83.999$ deg, max. $N = -30$ circ. waves

```
***** (ALLOWABLE STRESS)/(ACTUAL STRESS) *****
 1  1.0087E+00 fiber tension : matl=1 , A , seg=18, node=8 , layer=1 , z=-0.4539
 2  1.3993E+00 fiber compres.: matl=1 , A , seg=16, node=1 , layer=1 , z=-0.454
 3  1.8271E+00 transv tension: matl=1 , A , seg=15, node=50, layer=1 , z=-0.029
```

```

4 1.6713E+00 transv compres: matl=1 , A , seg=28, node=13, layer=1 ,z=-0.4539
5 1.4297E+00 effect. stress: matl=2 , A , seg=1 , node=3 , layer=2 ,z=0.0357
6 1.3450E+00 effect. stress: matl=3 , A , seg=16, node=2 , layer=3 ,z=0.0534
7 1.0010E+00 effect. stress: matl=4 , A , seg=15, node=52, layer=2 ,z=0.029
8 1.2199E+00 effect. stress: matl=5 , A , seg=28, node=10, layer=2 ,z=0.0289
*****

```

Load Case 2: "test" maximum stresses at theta = 83.999 deg, max. N = -15 circ. waves

```

***** (ALLOWABLE STRESS)/(ACTUAL STRESS) *****
1 9.9110E-01 fiber tension : matl=1 , A , seg=18, node=8 , layer=1 ,z=-0.4539
2 1.5343E+00 fiber compres.: matl=1 , A , seg=16, node=1 , layer=1 ,z=-0.454
3 1.8378E+00 transv tension: matl=1 , A , seg=15, node=50, layer=1 ,z=-0.029
4 1.6713E+00 transv compres: matl=1 , A , seg=28, node=13, layer=1 ,z=-0.4539
5 1.4297E+00 effect. stress: matl=2 , A , seg=1 , node=3 , layer=2 ,z=0.0357
6 1.3754E+00 effect. stress: matl=3 , A , seg=16, node=2 , layer=3 ,z=0.0534
7 1.0203E+00 effect. stress: matl=4 , A , seg=15, node=52, layer=2 ,z=0.029
8 1.2199E+00 effect. stress: matl=5 , A , seg=28, node=10, layer=2 ,z=0.0289
*****

```

It is seen that for N = -60 circumferential waves the stress ratios listed above have converged with respect to N. It is clear that the tapered doublers and external propellant tank support rings (Figs. 1b and 1c) are sturdy enough in the optimized design to filter out static responses with high numbers of circumferential waves, n.

Convergence study with respect to the meridional nodal point density used in the BIGBOSOR4 linear stress analysis of the propellant tank

In the three sets of results listed above the number of nodal points in Shell Segments 15, 16, 17 and 18 (Fig. 1b) are 51, 11, 11 and 11, respectively. A BIGBOSOR4 linear stress analysis of the same design and loading was conducted with the number of nodal points in Shell Segments 15, 16, 17 and 18 increased to 97, 31, 31 and 31, respectively. The BIGBOSOR4 results are listed below.

Load Case 2: "test" maximum stresses at theta = 83.999 deg, max. N = -60 circ. waves

```

***** (ALLOWABLE STRESS)/(ACTUAL STRESS) *****
1 1.0160E+00 fiber tension : matl=1 , A , seg=18, node=21, layer=1 ,z=-0.4539
2 1.3945E+00 fiber compres.: matl=1 , A , seg=16, node=1 , layer=1 ,z=-0.454
3 1.8191E+00 transv tension: matl=1 , A , seg=15, node=94, layer=1 ,z=-0.029
4 1.6713E+00 transv compres: matl=1 , A , seg=28, node=13, layer=1 ,z=-0.4539
5 1.4297E+00 effect. stress: matl=2 , A , seg=1 , node=3 , layer=2 ,z=0.0357
6 1.1244E+00 effect. stress: matl=3 , A , seg=16, node=2 , layer=3 ,z=0.0371
7 1.0045E+00 effect. stress: matl=4 , A , seg=15, node=98, layer=2 ,z=0.029
8 1.2199E+00 effect. stress: matl=5 , A , seg=28, node=10, layer=2 ,z=0.0289
*****

```

Compare the results just listed with the first of the three sets of results listed in the previous sub-section. Notice that all the results just listed are close to those previous results except for Entry No. 6:

6 1.1244E+00 effect. stress: matl=3 , A , seg=16, node=2 , layer=3 ,z=0.0371

which previously had been as follows:

6 1.3454E+00 effect. stress: matl=3 , A , seg=16, node=2 , layer=3 ,z=0.0534

The significant difference in the two No. 6 entries for "effect. Stress" (effective stress) is caused, not by failure of convergence with respect to nodal point density, but because Segment 16 includes the lower part of the

forward tapered doubler (Figs. 1b and 1c), and the location, “seg=16, node=2” is different in the two different discretized models. In the model with more nodal points in Segment 16, for which the outermost fiber of the shell wall is at $z = 0.0371$ inch, “seg=16, node=2” is much closer to the junction of Segment 15 and Segment 16 than is so with the original model, for which the outermost fiber of the shell wall is at $z = 0.0534$ inch. (z is the coordinate normal to the shell wall reference surface, positive in the outward direction.) The more nodal points in Segment 16, the closer the effective stress in Entry No. 6 will be to that in Entry No. 7 because the corresponding two axial coordinates of Entries 6 and 7 approach each other as the number of nodal points in Segment 16 is increased.

Determination of the circumferential location at which to compute the most critical stresses

In the GENOPT/BIGBOSOR4 model the stress ratios such as those just listed are computed at the circumferential coordinate, **theta**, that corresponds to the maximum strut load in a given “ring” of struts, aft or forward. It is assumed that this circumferential coordinate, **theta**, corresponds to the most harmful stress. It is the stress at that circumferential location that is used to generate the stress margins during optimization cycles. As seen from the results listed in this sub-section, there may exist a different circumferential location with one or more stress components that are more critical than those corresponding to the circumferential coordinate at which the largest strut load is applied. For example, in the previous sub-section the most critical circumferential coordinate, **theta**, is assumed to be that corresponding to the strut pinned to the centroid of the external propellant tank support ring at $\theta = 84$ degrees. The converged maximum tensile stress (minimum stress ratio, allowable/actual, at the tips of the stringers in the internal orthogrid “layer” of the shell wall is given above for circumferential coordinate, **theta** = 84 degrees as:

Load Case 2: "test" maximum stresses at theta = 83.999 deg, max. N = -60 circ. waves

```
***** (ALLOWABLE STRESS)/(ACTUAL STRESS) *****
  1  1.0178E+00 fiber tension : matl=1 , A , seg=18, node=8 , layer=1 , z=-0.4539
```

However, at circumferential coordinate, **theta** = 76 degrees, we have the following minimum stress ratios:

Load Case 2: "test" maximum stresses at theta = 76.000 deg, max. N = -60 circ. waves

```
***** (ALLOWABLE STRESS)/(ACTUAL STRESS) *****
  1  8.6849E-01 fiber tension : matl=1 , A , seg=18, node=9 , layer=1 , z=-0.4539
  2  1.6715E+00 fiber compres.: matl=1 , A , seg=28, node=13, layer=1 , z=-0.4539
  3  1.9234E+00 transv tension: matl=1 , A , seg=15, node=50, layer=1 , z=-0.029
  4  1.6715E+00 transv compres: matl=1 , A , seg=28, node=13, layer=1 , z=-0.4539
  5  1.4301E+00 effect. stress: matl=2 , A , seg=1 , node=3 , layer=2 , z=0.0357
  6  1.5424E+00 effect. stress: matl=3 , A , seg=16, node=2 , layer=3 , z=0.0534
  7  1.1236E+00 effect. stress: matl=4 , A , seg=15, node=52, layer=2 , z=0.029
  8  1.2204E+00 effect. stress: matl=5 , A , seg=28, node=10, layer=2 , z=0.0289
*****
```

Note that Entry 1, “fiber tension” (at the tips of the stringers in the internal orthogrid “layer” of the shell wall), is more critical at the circumferential coordinate, **theta** = 76 degrees than at **theta** = 84 degrees. However, it is expected that such differences in one or more of the most critical stress components will not be overly dramatic, and that therefore the existing strategy used during optimization cycles will be adequate for the determination of preliminary optimized designs. Alternatively, and almost certainly a better practice, one could compensate for such an eventuality by setting the factor of safety for stress greater than unity. After all, that is what factors of

safety are for: to compensate for characteristics of a problem that are not covered by the formulation of the problem or that cannot easily be known in advance.

Section 15. COMPARISON OF PREDICTIONS FROM GENOPT/BIGBOSOR4 WITH THOSE FROM STAGS FOR THE OPTIMIZED LONG PROPELLANT TANK WITH TWO SETS OF STRUTS, AFT AND FORWARD, 4 PAIRS OF STRUTS AT EACH AXIAL LOCATION (the specific case called “test”)

Summary

A summary of the comparison of predictions from STAGS [16 – 19] and GENOPT/BIGBOSOR4 for the optimized design of the tank/strut system called “test” is listed in Table 7.

About STAGS and its application to the optimized tank/strut system called “test”

Version 6.1 of the STAGS computer program [16-19] was used to validate the design of the optimized long propellant tank with two “rings” of struts, aft and forward, 4 pairs of struts in each “ring” of struts (STAGS models are shown in Figs. 24 and 26d; BIGBOSOR4 models are shown in Figs. 1a, 1b, 1c and 4 – 6).

The capabilities and properties of the STAGS computer program [16 – 19] are summarized in Appendix 2. The “official” version of STAGS, developed by Almroth, Brogan, Rankin and others during the past 40 years, has recently been considerably improved by Michael Jacoby, who created STAGS pre- and post-processing code called “**StagsViewer**”. The StagsViewer application is written entirely in the C computer language, is intended for LINUX and UNIX based systems with graphics hardware acceleration, and employs the OpenMotif and OpenGL standards. The construction of finite element models is accomplished via a simple general purpose easy-to-use scripting language built into the StagsViewer code that contains many advanced features (such as surface patch intersections) and that simplifies the specification of many commonly used modeling techniques. Through interaction with the GUI, a user of StagsViewer can build up complex models in an intuitive way. The STAGS models displayed in Figs. 24 and 26d were created by the pre-processor of StagsViewer.

The StagsViewer **pre-processor** produces a STAGS model in what in STAGS jargon is called “Element Unit” input data format. The “official” version of STAGS can also generate finite element models in what in STAGS jargon is called “Shell Unit” input data format. In many cases of interest in the advanced nonlinear analysis of shells, use of the STAGS Shell Unit input data format simplifies the construction of segmented models.

However, generating more geometrically-general models can be challenging with use of the STAGS Shell Unit format. In the current work many STAGS Shell Units would have been required to develop the model, and certain features such as the struts would have required additional STAGS Element Units or STAGS User-written subroutines. The StagsViewer meshing capability was developed for just such general configurations. To give some idea of the compactness and ease of creation of finite element models, we note that the meshing script for the STAGS model shown in Fig. 24 is 322 lines long, including blank lines and comments. Execution time is less than 2 seconds. The model contains 26422 nodes, 256 linear beam (STAGS E210) elements, 360 linear triangular shell (STAGS E320) elements, and 25920 quadrilateral shell (STAGS E410) elements. There are 158964 degrees of freedom in the STAGS model displayed in Fig. 24. This model includes 34 separate material properties, 6 beam sections and 27 separate shell wall specifications. Partial compatibility of translational freedoms is used to connect the struts to the centroids of the aft and forward external propellant tank support rings, thereby providing a pin joint that is eccentrically located with respect to the reference

surface of the tank wall. The translational freedoms at the warm ("ground") ends of each strut are fixed and rotational freedoms are free, thereby forming pin joints to rigid "ground" at those locations.

In addition to finite element pre-processing, the StagsViewer can also **post-process** STAGS results in a manner similar to that of many of the large commercially available tools, such as Patran, I-deas, and others. All of the figures in this paper pertaining to STAGS finite element results were produced with use of the post-processor of StagsViewer. The StagsViewer post-processing files are generated by the STAGS processor call "STAPL". The post-processor of StagsViewer allows for easy interactive visualization of deflected shapes, continuous and discrete color contouring of stress, strain and other result quantities, buckling and vibration mode shape animation, load step animation, and the interrogation of results. The results can be exported as encapsulated postscript or jpeg "screen shots". One-button creation of GIF-based animations is also readily accomplished.

The STAGS finite element analyses described in this paper were performed on an Apple Macbook Pro running the Mac OSX 10.5.8 operating system, with a 2.5 Ghz Intel Core 2 Duo processor with 4 Gb of RAM memory and an NVIDIA GeForce 8600M GT graphics card. For the model shown in Figure 24, a typical STAGS linear stress analysis takes approximately 45 seconds of CPU time.

For the most part, the details of the STAGS finite element model faithfully represent the modeling idealizations employed in the GENOPT/BIGBOSOR4 model. For example, the struts are pinned to the centroids of the aft and forward external propellant tank support rings and to rigid "ground", and these ring centroids are located eccentrically with respect to the reference surface of the propellant tank, as is indicated in Fig. 1c. However, there are three areas where the STAGS model differs from the GENOPT/BIGBOSOR4 model:

- (1) In the STAGS models uniform temperature (-200 degrees) is applied throughout.
- (2) In the STAGS models only uniform thickness sections are employed (no tapering of the external doublers).
- (3) In the STAGS models the widths of the 12 segments in each ellipsoidal dome are somewhat different from those in the GENOPT/BIGBOSOR4 models, and each of the 12 segments is ellipsoidal in the STAGS models, whereas in the GENOPT/BIGBOSOR4 models each of the 12 segments is torispherical with average meridional radius of curvature in each dome segment equal to the average local meridional radius of curvature of the ellipsoid in that segment.

With the introduction of these departures of the STAGS model from the GENOPT/BIGBOSOR4 model, only the standard features in STAGS need be used; **the development of STAGS user-written subroutines is not required.** In the case of Item (1), the linear temperature gradient in the GENOPT/BIGBOSOR4 model exists only in the struts; the supported tank is of uniform temperature (-200 degrees), while rigid "ground" is assumed to be at room temperature (0 degrees). Rather than apply a temperature gradient along the struts in the STAGS model, the coefficient of thermal expansion of the strut material is adjusted in the STAGS model so that, when multiplied by a uniform -200 degree temperature, the free contraction of the strut is the same as that of the strut with the actual coefficient of thermal expansion subjected to a linear temperature gradient between 0 and -200 degrees from "ground" to tank. In the case of Item (2), the average thickness of the doubler is used in the STAGS model and this doubler is not tapered.

Through comparisons of STAGS predictions with those from GENOPT/BIGBOSOR4 (Table 7) the three differences, (1) - (3), are found to have little impact on the predictions of vibration frequencies (Table 7a), loads in the struts (Table 7b), stresses in the struts (Table 7c), and buckling load factors for the struts buckling as columns (Table 7d) and for the struts buckling as thin shells (Table 7e). This makes sense. In the case of

vibration frequencies, the STAGS and GENOPT/BIGBOSOR4 predictions depend on properties averaged over the entire structure (shell deformation vibration modes, Fig. 25b and 25f) or depend on the strain energy stored in the struts (vibration modes in which strut extension and compression is combined with one or more shell deformation modes, Figs. 25a, 25c, 25d, 25e, 25g, and 25h). In the case of loads in the struts, stresses in the struts, and buckling of the struts, the predictions depend on overall equilibrium of the tank/strut system, not on details of the propellant tank wall construction in the neighborhood of the strut/tank junction.

Item (3), widths of the shell segments in the domes, influences buckling of the domes of the tank wall for configurations in which the “rings” of struts are attached at the same axial stations as the dome/cylinder junctions, as shown in Fig. 1a (the specific case called “test”). In those particular configurations part of the external doubler spans the entire width of the dome shell segment closest to the cylindrical part of the tank. Since this width differs in the STAGS and BIGBOSOR4 models there can occur a corresponding difference in the prediction of buckling load factors associated with buckling in the knuckle regions of the domes under internal pressure. See Fig. 31, for example.

With respect to the predictions of localized tank stresses in the neighborhoods of the strut/tank junctions, the uniform thickness approximation of the tapered doublers used in the STAGS models is inadequate (too conservative, that is, the maximum stresses in the STAGS model are too high, Figs. 21d, 26e and 26f). It is emphasized that the analyst should consider very carefully what kinds of idealizations are appropriate for what kinds of high-quality predictions to be required from the STAGS model.

The significant differences in the predictions from STAGS and GENOPT/TANK listed in Table 7f (launch hold force in the struts) are probably caused by the inability of the GENOPT/TANK model to account for thermal shrinkage of the struts; the model of springs in the BIGBOSOR4 computer program [14] does not account for thermal extension or shrinkage of the springs. In the STAGS model there exists thermal shrinkage of the struts.

The STAGS modal vibration analysis (Figs. 25a – 25h) includes the prestress generated by the uniform 25 psi internal pressure and the 200-degree tank cool-down. The mass of the propellant is lumped into the tank shell wall. The effect of the prestress generated from the uniform 25 psi internal pressure is more significant than that generated from the 200-degree tank cool-down because the former creates uniform hoop tension over the entire length of the cylindrical part of the tank that is not created by the latter. Without this hoop tensile prestress in the cylindrical part of the tank, the vibration frequencies associated with maximum non-axisymmetric modal shell deformation in the cylindrical part of the tank (as shown, for example, in Figs. 25b and 25f in which the prestress is present) occur at a significantly lower frequency for $n = 2$ circumferential waves and dramatically lower frequencies for $n > 2$ circumferential waves. The GENOPT/BIGBOSOR4 model includes the effect of shell wall prestress generated by the uniform 25 psi internal pressure but does not include the effect of prestress generated by the 200-degree tank cool-down. Here is the effect of the prestress generated by the uniform 25 psi internal pressure on the **modal vibration frequencies** as computed from the GENOPT/BIGBOSOR4 model with use of the “variable density” option (the option in which the relevant tank/BIGBOSOR4 software is `bosdec.density.var` and `addbosor4.density.var`):

	Prestress from the 25 psi internal pressure included	Prestress from the 25 psi internal pressure neglected
$n = 0$ circumferential waves	12.069 Hz	12.070 Hz
$n = 1$ circumferential wave	12.161 Hz	12.154 Hz

n = 2 circumferential waves	13.237 Hz	11.331 Hz
n = 3 circumferential waves	13.327 Hz	6.704 Hz
n = 4 circumferential waves	16.676 Hz	4.705 Hz

As expected, there is virtually no influence of prestress on the frequencies for the modes with $n = 0$ and $n = 1$ circumferential waves (modes of the type shown in Fig. 16a), significant influence on the frequency for the mode with $n = 2$ circumferential waves, and dramatic influence on the frequencies for the modes with $n > 2$ circumferential waves (modes of the type shown in Fig. 16b).

Buckling analyses of several sorts were performed with STAGS. The models shown in Figs. 24 and 26d are used. In these models the struts are idealized as beams. The propellant mass in these buckling analyses is no longer lumped into the tank wall. Instead, there is imposed a spatially linearly varying normal pressure head acting on the tank wall generated by the accelerated propellant.

The following strategy was first attempted. In STAGS there are two load sets, Load Set A and Load Set B. The total buckling load is the sum of the buckling eigenvalue multiplied by Load Set A plus the constant Load Set B. Load Set A includes only the inertial loads, and Load Set B includes the uniform 25 psi internal pressure plus the 200-degree tank cool-down. Unfortunately, when a linear bifurcation buckling analysis is performed with STAGS, this “Load Set A plus Load Set B” formulation leads to many very low spurious (non-physical) buckling eigenvalues and mode shapes that involve buckling deformations of the tank wall. The reasons for this are unclear. (Perhaps the “spurious” buckling modes are actual buckling modes that would occur if there existed 25 psi external pressure plus 200-degree tank warm up instead of internal pressure and tank cool-down.) There are so many closely spaced spurious eigenvalues that it is not possible to determine the lowest non-spurious buckling load factors for Load Case 1 and for Load Case 2. Therefore, the problem formulation was changed. The buckling predictions presented here in Table 7d and 7e and Figs. 30 and 31 are from models in which all of the loads are included in Load Set A. With this new formulation, the STAGS bifurcation buckling analysis does not produce a myriad of spurious shell modes as was previously encountered. Comparisons of buckling predictions between STAGS using the models shown in Figs. 24 and 26d and GENOPT/BIGBOSOR4 are discussed in a following section. The buckling modes predicted by STAGS are displayed in Figs. 30 and 31.

Buckling of the struts as thin shells rather than as columns is also investigated with use of a different STAGS model: a STAGS finite element model of a strut by itself to which a uniform axial stress resultant is applied. This axial resultant is obtained from the forces developed in the struts as calculated with use of the complete STAGS model shown in Figure 24. STAGS predictions of strut buckling as thin shells are displayed in Figs. 28 and 29.

For the STAGS stress analyses, all of the loads are placed in Load Set A, and a straightforward linear static analysis is performed. Results from these analyses are discussed in a following section. It is emphasized that the finite element discretization employed in the full model shown in Figure 24 is too coarse accurately to capture some of the stress gradients of interest. Accordingly, for Load Case 1 a 1/8 model (45 degrees of circumference) of the tank was constructed (Fig. 26d), taking advantage of the eight-fold symmetry of the structure and the eight-fold symmetry of its response under **Load Case 1**. This model is composed of 28889 nodes, 32 linear beam elements (STAGS E210), 180 three-node triangular shell elements (STAGS E320) and 28440 quadrilateral shell elements (STAGS E410), with a total of 173660 degrees-of-freedom. The strut end conditions are as before. The refined 45-degree STAGS model also has symmetry enforced along the model boundaries at the circumferential coordinates, $\theta = 0$ degrees and $\theta = 45$ degrees. In addition to the linear

stress analysis (Figs. 26e and 26f), this refined 45-degree STAGS model is also used to capture shell buckling of the aft ellipsoidal dome under Load Case 1 (Fig. 31). Hoop compression develops in the knuckle region of the dome as a result of the 25 psi uniform internal ullage pressure plus the axially linearly varying normal pressure head from the axially accelerated propellant. Results from this model are discussed in a following section.

Modal vibration

Figures 25a – 25h show the vibration modes and eigenvalues (frequencies) predicted by STAGS for the optimized design. The STAGS modes are either fairly pure shell deformation modes, such as those shown in Figs. 25b and 25f or, unlike the vibration modes from BIGBOSOR4 displayed in Fig. 16a(A) – 16a(D), mixtures of:

1. axial vibration motion of the propellant tank combined with an axisymmetric shell deformation mode (Fig. 25c),
2. 1st lateral-pitching mode of the propellant tank combined with a non-axisymmetric shell deformation mode (Figs. 25a and 25d),
3. 2nd lateral-pitching mode of the propellant tank combined with a non-axisymmetric shell deformation mode (Fig. 25g), and
4. torsional (rolling) mode of the propellant tank combined with a non-axisymmetric shell deformation mode (Figs. 25e and 25h).

Figures 16 and 25 demonstrate that the predictions from the GENOPT/BIGBOSOR4 model are reasonably close to those from STAGS and that the fundamental vibration mode from STAGS is slightly higher than the allowable minimum frequency, $FREQA = 10$ Hz, multiplied by the factor of safety for modal vibration frequency, $FREQF = 1.2$ (Table 2).

Linear stress analysis of the tank/strut system under Load Case 1 from a 360-degree STAGS model

Figure 26a shows the prediction from STAGS of the effective stress in the outer surface of the skin of the propellant tank caused by Load Case 1. What is physically the outer surface of the propellant tank skin is called “inner surface” by STAGS because of the way this particular STAGS model was set up. The prediction of stress by STAGS is from the linear analysis branch of STAGS.

Corresponding to the 360-degree STAGS model displayed in Fig. 24, Fig. 26b shows the prediction of the stress at the tips of the internal orthogrid stringers in the forward part of the propellant tank caused by Load Case 1. Figure 26c shows the same for the aft part of the propellant tank. Unfortunately, the STAGS 360-degree finite element model shown in Fig. 24 is too crude to obtain a converged prediction of maximum tensile and compressive stresses at the tips of the orthogrid stringers.

Linear stress analysis of the tank/strut system under Load Case 1 from a refined STAGS 45-degree model

Figure 26d shows a much more refined STAGS model that subtends only 45 degrees of the circumference of the propellant tank. This 45-degree STAGS model is suitable only for the prediction of stresses under Load Case 1. Fig. 26e (left-hand side) shows a detail of the stresses at the tips of the orthogrid stringers from the refined STAGS 45-degree model. Compare the predictions of maximum stress from the 45-degree refined STAGS model with those from the cruder 360-degree STAGS model shown in Fig. 26b. Figure 26f shows the stringer

tip stresses as a function of the circumferential coordinate at the forward cylinder/dome junction as predicted by the refined STAGS 45-degree model. Compare Fig. 26f with the plots displayed in Fig. 21d for the BIGBOSOR4 model.

Comparison of STAGS and BIGBOSOR4 predictions from linear theory for stress under Load Case 2

Figure 27a shows the prediction from STAGS of the effective stress in outer surface of the skin of the propellant tank caused by Load Case 2. Figure 27b shows the stress at the tips of the internal orthogrid stringers caused by Load Case 2. The GENOPT/BIGBOSOR4 predictions for Load Case 2 are given by the following:

```
***** (ALLOWABLE STRESS)/(ACTUAL STRESS) *****
 1  1.0177E+00 fiber tension : matl=1 , A , seg=18, node=8 , layer=1 , z=-0.45
 2  1.4027E+00 fiber compres.: matl=1 , A , seg=16, node=1 , layer=1 , z=-0.45
 3  1.8272E+00 transv tension: matl=1 , A , seg=15, node=50, layer=1 , z=-0.03
 4  1.6713E+00 transv compres: matl=1 , A , seg=28, node=13, layer=1 , z=-0.45
 5  1.4297E+00 effect. stress: matl=2 , A , seg=1 , node=3 , layer=2 , z= 0.04
 6  1.3454E+00 effect. stress: matl=3 , A , seg=16, node=2 , layer=3 , z= 0.05
 7  1.0012E+00 effect. stress: matl=4 , A , seg=15, node=52, layer=2 , z= 0.03
 8  1.2199E+00 effect. stress: matl=5 , A , seg=28, node=10, layer=2 , z= 0.03
*****
```

Maximum stress components for Load Case 2 STRESS2(i),i=1,6=

fiber tension	fiber compres.	transv tension	transv compres	in-plane shear	effect. stress
4.9129E+04	3.5645E+04	2.7364E+04	2.9917E+04	0.0000E+00	4.9938E+04

In the list above “matl 1” represents the internal orthogrid “layer” of the propellant tank shell wall. z = -0.45 inch corresponds to the tips of the internal orthogrid stringers. z = +0.03, +0.04 and +0.05 inch correspond to the outer surface of the skin of the propellant tank shell wall. The locations of the most critical stresses in the propellant tank generated under Load Case 2 (10 g lateral acceleration plus 25 psi internal pressure + 200-degree tank cool-down) as predicted by BIGBOSOR4 are identified as the entries 1 and 7 in the list above with the heading “(ALLOWABLE STRESS)/(ACTUAL STRESS)”. Entries 1 and 7 have values that are closest to unity. Therefore, they represent nearly critical effective stresses (corresponding design margins near zero). The locations of nearly critical stresses corresponding to Load Case 2 as predicted by BIGBOSOR4 for the optimized tank/strut system are indicated in Fig. 21a(B).

STAGS analysis of buckling of a strut as a thin shell

Figure 28 shows STAGS predictions of the buckling mode shape and buckling load factor of an aft strut buckling as a long thin cylindrical shell under Load Case 1. This is a STAGS model of the entire strut, including the end fittings. Figure 29 shows the predictions from STAGS of a short segment of the same strut under Load Case 1 [Fig. 29(A)] and Load Case 2 [Fig. 29(B)].

STAGS prediction of buckling of the tank/strut system

Figures 30 and 31 show buckling modes of the tank/strut system predicted by STAGS. In these STAGS models all the load components (10g acceleration plus 25 psi uniform internal ullage pressure plus 200-degree tank cool-down) are included in Load Set A (“eiganvalue” loads). There is no Load Set B (loads not to be multiplied

by the eigenvalue, that is, by the buckling load factor). For problems of the type described in this paper STAGS has difficulty finding non-spurious buckling modes when there exist non-trivial loads in both Load Set A and Load Set B. The buckling load factors obtained by STAGS agree reasonably well with those obtained by GENOPT/TANK/BIGBOSOR4, especially for buckling of the struts under Load Case 1 [Fig. 30(A)] and Load Case 2 [Fig. 30(B,C)], as is seen in Part (d) of Table 7. The STAGS prediction of buckling of the aft dome under Load Case 1 (STAGS buckling load factor = 5.0047) is about 18 per cent higher than that predicted by BIGBOSOR4 (BIGBOSOR4 buckling load factor = 4.107) although the buckling mode shapes are similar. This difference is caused almost entirely by the arc-width of the lower part of the aft doubler in the BIGBOSOR4 model (tapered doubler in Segment 12 shown on the right-hand side of Fig. 1b) being significantly smaller (7.147 inches) than that at the equivalent location in the STAGS model (10.09 inches). Modifying the BIGBOSOR4 model by changing the tapered doubler with maximum thickness equal to 0.886 inch to a doubler of constant thickness equal to 0.443 inch raises the buckling load factor predicted by BIGBOSOR4 from 4.107 to 4.238. Increasing the width of the lower part of the constant thickness doubler from 7.14687 inches to 10.09 inches raises the buckling load factor predicted by BIGBOSOR4 from 4.238 to 5.036, which agrees very well with the prediction from STAGS: 5.005.

Discussion of the results listed in Table 7

Table 7 lists comparisons between predictions by STAGS and GENOPT/TANK/BIGBOSOR4 for various behaviors of the long propellant tank with aft and forward sets of struts, 4 strut pairs at each axial location (the specific case called “test”). The following comments apply:

(a) The lowest modal vibration frequency from STAGS is slightly higher than the minimum allowable frequency, 10 Hz, multiplied by the factor of safety for vibration frequency, 1.2, and slightly higher than the lowest modal frequency predicted by the GENOPT/TANK model. The three vibration modes most likely to be excited during launch, tank axial motion, tank lateral/pitching mode 1 and tank lateral/pitching mode 2, are conservatively estimated by the GENOPT/TANK model, but not overly conservatively estimated. The lowest shell deformation modes predicted by STAGS corresponding to $n = 2, 3$ and 4 circumferential waves are somewhat lower than those predicted by GENOPT/TANK because these modes in the STAGS model are (except in the $n = 2$ case) combined with overall average motions of the propellant tank, a combined mode that is not possible with the approximate decoupled GENOPT/TANK model. However, these somewhat lower shell deformation modal frequencies are above the minimum required frequency, FREQA, times its factor of safety, FREQF (Table 2).

(b) The prediction of maximum compressive force and maximum tensile force in the aft (Lower) and forward (Upper) “rings” of struts for Load Case 1 and Load Case 2 differ by as much as about 9 per cent, with GENOPT/TANK/BIGBOSOR4 (except in one less significant case) yielding conservative values for compressive (destabilizing) forces and somewhat unconservative values for tensile forces.

(c) For the most significant stress components in the laminated composite struts the GENOPT/TANK/BIGBOSOR4 predictions are generally conservative. In the one fairly significant case in which STAGS yields a higher value [Load Case 1 Fiber Compression in the lower (aft) struts] the two predictions are fairly close: STAGS yielding 23318 psi and GENOPT/TANK/BIGBOSOR4 yielding 22060 psi, a difference of about 5 per cent.

(d) Contributing to the reasonably small discrepancy between the STAGS and GENOPT/BIGBOSOR4 predictions of strut column buckling are the differing predictions of compressive strut forces from STAGS and GENOPT/BIGBOSOR4 as listed in Part (b) of Table 7. To get from the column buckling load factor of the aft (Lower) strut under Load Set 1 predicted by GENOPT (4.163) to that predicted by STAGS (3.99) we have $4.163 \times (\text{strut load from GENOPT})/(\text{strut load from STAGS}) = 4.163 \times (22693/24841) = 3.80$, not too far below the actual STAGS value of 3.99. To get from the column buckling load factor of the aft strut under Load Set 2 predicted by GENOPT (2.398) to that predicted by STAGS (2.74) we have $2.398 \times (\text{strut load from GENOPT})/(\text{strut load from STAGS}) = 2.398 \times (39393/36298) = 2.60$, not too far below the actual STAGS value of 2.74. To get from the column buckling load factor of the forward strut under Load Set 2 predicted by GENOPT (2.645) to that predicted by STAGS (3.00) we have $2.645 \times (\text{strut load from GENOPT})/(\text{strut load from STAGS}) = 2.645 \times (40611/38568) = 2.785$, about 7 per cent below the actual STAGS value of 3.00. It is emphasized that the results listed in Part d of Table 7 were obtained from models in which all the components of loading (10 g acceleration, 25 psi internal pressure, and 200-degree propellant tank cool-down) are in Load Set A (“eigenvalue” loads). There is no Load Set B.

(e) GENOPT/BIGBOSOR4 predictions of buckling of the struts as thin shells are conservative. This conservativeness is mostly due to the conservativeness of the prediction by GENOPT/TANK/BIGBOSOR4 of the maximum compressive force in the struts. [See Item (b) in Table 7.] To get from the shell buckling load factor of the aft (Lower) strut under Load Set 1 predicted by GENOPT (5.314) to that predicted by STAGS (4.73) we have $5.314 \times (\text{strut load from GENOPT})/(\text{strut load from STAGS}) = 5.314 \times (22693/24841) = 4.85$, not far above the actual STAGS value of 4.73. To get from the shell buckling load factor of the aft strut under Load Set 2 predicted by GENOPT (3.095) to that predicted by STAGS (3.24) we have $3.095 \times (\text{strut load from GENOPT})/(\text{strut load from STAGS}) = 3.095 \times (39393/36298) = 3.36$, not far above the actual STAGS value of 3.24. To get from the shell buckling load factor of the forward strut under Load Set 2 predicted by GENOPT (3.210) to that predicted by STAGS (3.65) we have $3.210 \times (\text{strut load from GENOPT})/(\text{strut load from STAGS}) = 3.210 \times (40611/38568) = 3.380$, about 7.5 per cent below the actual STAGS value of 3.65.

(f) GENOPT/BIGBOSOR4 yields unconservative predictions of forces in the struts from the launch-hold condition. The launch-hold forces in the aft and forward set of struts from each of the three elements of loading (25 psi ullage pressure, 1g axial acceleration, and 200 degrees tank cool-down) applied separately are as follows:

strut	25psi internal pressure		1g axial acceleration		200 deg tank cool-down	
	GENOPT	STAGS	GENOPT	STAGS	GENOPT	STAGS
aft	-7532	-9284	-3948	-3956	+20652	+23710
forward	-7099	-7672	+3774	+3984	+19466	+22347

The biggest difference between GENOPT and STAGS predictions is the strut force caused by tank cool-down: about 3000 lbs higher from STAGS than from GENOPT.

Notice that superposition of the strut forces from each of the three elements of loading applied separately is not valid in the GENOPT/TANK/BIGBOSOR4 model, even though that model is mathematically linear. For example, if we sum the three strut forces in the aft strut, $-7532 - 3948 + 20652$ we obtain $+9172$ lbs, significantly

different from the 7317 lbs listed in Part (f) of Table 7. The reason that superposition of strut forces from various loadings applied separately does not hold in the GENOPT/TANK/BIGBOSOR4 model is that the strut forces computed by GENOPT/TANK/BIGBOSOR4 account for the flexibility of the propellant tank in an approximate way: by computation of the **total** tank wall displacement at the attachment point of a strut in the direction of the axis of that strut caused by all the loads applied together. Subsequently that component of **total** tank wall displacement resolved along the axis of that strut is treated as a spring in series with the spring represented by the strut itself. The final forces in the struts at a given axial location are computed from a GENOPT/TANK linear stress model in which all the struts attached to the tank at a given axial location have the same reduced axial stiffness: a stiffness that is equal to the minimum stiffness determined from each of the struts at that axial location.

The significant discrepancy between the predictions of GENOPT/TANK/BIGBOSOR4 and STAGS, and the unconservative nature of this discrepancy, revealed in Part (f) of Table 7, indicate the need in the GENOPT/TANK/BIGBOSOR4 model for the introduction of factors of safety, FORCEF(i,j), for maximum strut force (Table 2) that are greater than 1.0.

Section 16. OPTIMIZED SHORT PROPELLANT TANK WITH ONE "RING" OF STRUTS WITH FOUR PAIRS OF STRUTS ATTACHED TO THE ONE TANK SUPPORT RING

Figures 7 – 10 pertain to this section. Tables 12 – 14 of [20] list input data for the GENOPT processors, BEGIN, DECIDE, and MAINSETUP, respectively. Table 15 of [20] lists the output for the optimized design from the GENOPT processor, OPTIMIZE, executed in a "fixed design" mode. Table 16 of [20] lists input data for the GENOPT processor, CHANGE, by means of which the optimized design is archived. Figures 7 – 10 in this paper show the configuration of the short tank with its single "ring" of struts for the starting design (Figs. 7 and 8) and for the optimized design (Figs. 9 and 10). **No STAGS models of this case were created.** The results listed here were obtained after the August 2012 and February 2013 updates to the "tank" software, struct.tank and behavior.tank, were compiled.

The optimized values of the decision variables and linked variables for the short propellant tank with one ring of supporting struts are as follows:

Optimized Design Found With The Temporary Version Of Bigbosor4/Bosdec And With Curing Temperature, TEMTUR=170 Degrees For The Short Propellant Tank With One Ring Of Struts With 4 Pairs Of Struts In That Ring Of Struts And With The Tank End Of The Struts Attached At The Midlength Of The Tank (Dimensions in inches)

VALUES OF DESIGN VARIABLES CORRESPONDING TO BEST FEASIBLE DESIGN

VAR. NO.	CURRENT VALUE	DEFINITION
1	2.220E-02	thickness of the tank aft dome skin: THKAFT
2	7.152E-02	thickness of the tank cylinder skin: THKMID
3	3.031E-02	thickness of the forward tank dome skin: THKFWD
4	3.000E+00	spacing of the tank orthogrid stringers: STRSPC
5	3.003E+00	spacing of the tank orthogrid rings: RNGSPC
6	1.557E-01	thickness of the tank orthogrid stringers: STRTHK
7	1.000E+00	height of the tank orthogrid stringers: STRHI

```

8      1.579E-01  thickness of the tank orthogrid rings: RNGTHK
9      1.000E+00  height of the tank orthogrid rings: RNGHI
10     1.750E+02  global axial coordinate of tank support ring: ZTANK(1 )
11     1.067E+02  global axial coordinate of "ground": ZGRND(1 )
12     6.000E+00  circ.angle (deg.) to pinned tank end of strut: ATANK(1 )
13     4.500E+01  circ.angle to pinned "ground" end of strut: AGRND(1 )
14     5.177E+00  inner diam. of support tube active at launch: IDTUBE(1 )
15     1.000E-06  height of mid-tank T-ring web: WEBHI
16     1.000E-06  thickness of mid-tank T-ring web: WEBTHK
17     1.000E-06  width (height) of mid-tank T-ring flange: FLGHI
18     1.000E-06  thickness of mid-tank T-ring flange: FLGTHK
19     3.000E+01  axial length of the propellant tank doubler: DUBAXL(1 )
20     1.852E-01  max.thickness of the propellant tank doubler: DUBTHK(1 )
21     1.000E-01  thickness of the tank reinforcement ring: TRNGTH(1 )
22     5.000E-01  height of the tank reinforcement ring: TRNGHI(1 )
23     5.587E-03  thickness of a lamina: THICK(1 )
24     5.587E-03  thickness of a lamina: THICK(2 )
25     5.587E-03  thickness of a lamina: THICK(3 )
26     5.587E-03  thickness of a lamina: THICK(4 )
27     5.587E-03  thickness of a lamina: THICK(5 )
28     5.587E-03  thickness of a lamina: THICK(6 )
29     1.264E+01  layup angle: ANGLE(1 )
30     -1.264E+01  layup angle: ANGLE(2 )
31     1.000E+01  layup angle: ANGLE(3 )
32     -1.000E+01  layup angle: ANGLE(4 )
33     6.532E+01  layup angle: ANGLE(5 )
34     -6.532E+01  layup angle: ANGLE(6 )

```

During optimization, design margins are computed for each of the two load cases for each optimization cycle. In the work reported here design margins are computed for each of the two load cases identified above in the section entitled "Section 8. TWO LOAD CASES".

For example, the "behaviors", corresponding design margins and objective computed for the optimized tank/strut system for the short tank with one "ring" of struts, 4 pairs of struts attached to the tank at the midlength of the short cylindrical part of the tank, are as follows:

Corresponding Values Of "Behaviors", Design Margins And Objective (Critical and almost critical design margins are listed in bold face.)

```

***** RESULTS FOR LOAD CASE NO. 1 (axial acceleration = 10g) *****
PARAMETERS WHICH DESCRIBE BEHAVIOR (e.g. modal vibration, stress, buckling load, strut force)

```

BEH. NO.	CURRENT VALUE	DEFINITION
1	1.582E+01	modal vibration frequency (cps): FREQ(1 ,1)
2	1.375E+01	modal vibration frequency (cps): FREQ(1 ,2)

3	4.216E+01	modal vibration frequency (cps): FREQ(1 ,3)
4	4.092E+01	modal vibration frequency (cps): FREQ(1 ,4)
5	5.179E+03	maximum stress in material 1: STRES1(1 ,1)
6	3.518E+04	maximum stress in material 1: STRES1(1 ,2)
7	4.247E+03	maximum stress in material 1: STRES1(1 ,3)
8	1.042E+03	maximum stress in material 1: STRES1(1 ,5)
9	1.438E+00	buckling of a strut as a column: COLBUK(1 ,1)
10	2.869E+00	buckling of strut as a shell: SHLBUK(1 ,1)
11	2.408E+03	launch-hold force in a strut: FORCE(1 ,1)
12	5.036E+04	maximum stress in the propellant tank: TNKSTR(1 ,1)
13	1.504E+01	propellant tank buckling load factor: TNKBUK(1 ,1)

***** RESULTS FOR **LOAD CASE NO. 1** (axial acceleration = 10g) *****
MARGINS CORRESPONDING TO CURRENT DESIGN (F.S.= FACTOR OF SAFETY)
MARGIN CURRENT

NO.	VALUE	DEFINITION
1	3.183E-01	(FREQ(1,1)/FREQA(1,1))/ FREQF(1 ,1)-1; F.S.=1.20
2	1.462E-01	(FREQ(1,2)/FREQA(1,2))/ FREQF(1 ,2)-1; F.S.=1.20
3	2.513E+00	(FREQ(1,4)/FREQA(1,4))/ FREQF(1 ,4)-1; F.S.=1.20
5	1.710E+01	(STRES1A(1,1)/STRES1(1,1))/ STRES1F(1,1)-1; F.S.=1.50
6	9.843E-01	(STRES1A(1,2)/STRES1(1,2))/ STRES1F(1,2)-1; F.S.=1.50
7	6.572E-01	(STRES1A(1,3)/STRES1(1,3))/ STRES1F(1,3)-1; F.S.=1.50
8	3.023E+00	(STRES1A(1,5)/STRES1(1,5))/ STRES1F(1,5)-1; F.S.=1.50
9	4.377E-01	(COLBUK(1,1)/COLBUKA(1,1))/COLBUKF(1,1)-1; F.S.=1.00
10	4.347E-01	(SHLBUK(1,1)/SHLBUKA(1,1))/SHLBUKF(1,1)-1; F.S.=2.00
11	5.229E+00	(FORCEA(1,1)/FORCE(1,1)) / FORCEF(1,1)-1; F.S.=1.00
12	-7.085E-03	(TNKSTRA(1,1)/TNKSTR(1,1))/ TNKSTRF(1,1)-1; F.S.=1.00
13	1.404E+01	(TNKBUK(1,1)/TNKBUKA(1,1))/TNKBUKF(1,1)-1; F.S.=1.00

***** RESULTS FOR **LOAD CASE NO. 2** (lateral acceleration = 10g) *****
PARAMETERS WHICH DESCRIBE **BEHAVIOR** (e.g. modal vibration, stress, buckling load, strut force)

BEH.	CURRENT	
NO.	VALUE	DEFINITION
1	1.378E+01	modal vibration frequency (cps): FREQ(2 ,1)
2	1.201E+01	modal vibration frequency (cps): FREQ(2 ,2)
3	4.172E+01	modal vibration frequency (cps): FREQ(2 ,3)
4	4.065E+01	modal vibration frequency (cps): FREQ(2 ,4)
5	5.412E+04	maximum stress in material 1: STRES1(2 ,1)
6	4.872E+04	maximum stress in material 1: STRES1(2 ,2)
7	7.043E+03	maximum stress in material 1: STRES1(2 ,3)
8	1.868E+03	maximum stress in material 1: STRES1(2 ,5)
9	9.991E-01	buckling of a strut as a column: COLBUK(2 ,1)
10	1.994E+00	buckling of strut as a shell: SHLBUK(2 ,1)
11	2.408E+03	launch-hold force in a strut: FORCE(2 ,1)
12	5.034E+04	maximum stress in the propellant tank: TNKSTR(2 ,1)
13	3.533E+01	propellant tank buckling load factor: TNKBUK(2 ,1)

***** RESULTS FOR **LOAD CASE NO. 2** (lateral acceleration = 10g) *****
MARGINS CORRESPONDING TO CURRENT DESIGN (F.S.= FACTOR OF SAFETY)

MARGIN CURRENT

NO.	VALUE	DEFINITION	
1	1.484E-01	(FREQ(2,1)/FREQA(2,1))/ FREQF(2,1)-1;	F.S.=1.20
2	5.784E-04	(FREQ(2,2)/FREQA(2,2))/ FREQF(2,2)-1;	F.S.=1.20
3	2.477E+00	(FREQ(2,3)/FREQA(2,3))/ FREQF(2,3)-1;	F.S.=1.20
4	2.387E+00	(FREQ(2,4)/FREQA(2,4))/ FREQF(2,4)-1;	F.S.=1.20
5	7.315E-01	(STRES1A(2,1)/STRES1(2,1))/ STRES1F(2,1)-1;	F.S.=1.50
6	4.327E-01	(STRES1A(2,2)/STRES1(2,2))/ STRES1F(2,2)-1;	F.S.=1.50
7	-7.768E-04	(STRES1A(2,3)/STRES1(2,3))/ STRES1F(2,3)-1;	F.S.=1.50
8	1.245E+00	(STRES1A(2,5)/STRES1(2,5))/ STRES1F(2,5)-1;	F.S.=1.50
9	-8.537E-04	(COLBUK(2,1)/COLBUKA(2,1))/COLBUKF(2,1)-1;	F.S.=1.00
10	-2.893E-03	(SHLBUK(2,1)/SHLBUKA(2,1))/SHLBUKF(2,1)-1;	F.S.=2.00
11	5.229E+00	(FORCEA(2,1)/FORCE(2,1))/ FORCEF(2,1)-1;	F.S.=1.00
12	-6.714E-03	(TNKSTRA(2,1)/TNKSTR(2,1))/ TNKSTRF(2,1)-1;	F.S.=1.00
13	3.433E+01	(TNKBUK(2,1)/TNKBUKA(2,1))/TNKBUKF(2,1)-1;	F.S.=1.00

***** **DESIGN OBJECTIVE** *****

CURRENT VALUE OF THE OBJECTIVE FUNCTION:

VAR.	CURRENT	DEFINITION
NO.	VALUE	
1	1.214E+00	WGTxTOTMAS/TNKNRM +(1-WGT)xCONDCT/CONNRM: CONDCT

in which:

WGT, TOTMAS, TNKNRM, CONDCT, CONNRM=
5.0000E-01 4.6899E+00 3.0000E+00 5.7932E-04 6.0000E-04

No STAGS models of the short propellant tank with one ring of struts were created.

Section 17. DEPENDENCE OF OPIMIZED EMPTY TANK MASS AND TOTAL CONDUCTANCE INTO THE TANK AS FUNCTIONS OF THE NUMBER OF STRUT PAIRS IN EACH "RING" OF STRUTS

The relationships of optimized empty tank mass and total conductance into the tank to the number of strut pairs are displayed in Figs. 32 and 33. Figure 32 pertains to the long propellant tank with two rings of struts, aft and forward, and Fig. 33 pertains to the short propellant tank with one ring of struts attached at the midlength of the propellant tank.

Table 3 lists the optimized designs of the long propellant tank with 3, 4 and 5 pairs of struts at each (aft and forward) axial location. Table 4 lists the behaviors of the optimized designs of the long propellant tank for Load Case 1 and Load Case 2. Table 5 lists the optimized designs of the short propellant tank with 3, 4 and 5 pairs of struts attached at the midlength of the short tank. Table 6 lists the behaviors of the optimized designs of the

short propellant tank for Load Case 1 and Load Case 2. The results listed in Tables 3 – 6 were obtained after the August 2012 and February 2013 updates to the “tank” software, struct.tank and behavior.tank, were compiled.

Section 18. CONCLUSIONS

1. Predictions from STAGS and from GENOPT/BIGBOSOR4 for the optimized long propellant tank with aft and forward sets of struts agree well enough to justify the use of GENOPT/BIGBOSOR4 for the purpose of preliminary design.
2. In the GENOPT/TANK/BIGBOSOR4 models it is important in modal vibration computations to include the flexibility of the propellant tank in calculations of the effective axial stiffness of a supporting strut. The reduced effective axial strut stiffness depends on the direction of g-loading to which the propellant tank is subjected. Therefore, the modal vibration frequencies depend (to a lesser degree) on that direction of g-loading.
3. The GENOPT/TANK/BIGBOSOR4 model, by predicting lower vibration frequencies than does STAGS, is conservative (but not overly conservative) in its prediction of modal vibration frequencies corresponding to modes that are the most likely to be excited during launch. This conservativeness is a consequence of the way in which the flexibility of the propellant tank is accounted for in the GENOPT/TANK/BIGBOSOR4 modal vibration model.
4. Important results for the optimized propellant tank/strut systems are plotted in Figs. 32 and 33 as functions of the number of strut pairs. The "best" optimum for the long propellant tank supported by two rings of struts is probably that with four pairs of struts at each of the two axial locations because the optimum obtained with 3 pairs of struts at each axial location, although associated with a smaller objective, has clearance problems, as is demonstrated in Fig. 12. The “best” optimum for the short propellant tank supported at its midlength by one ring of struts is probably that with three pairs of struts.
5. Optimizations were obtained in the presence of two load cases: a first that includes 25 psi uniform ullage pressure plus 200-degree tank cool-down plus a 10g **axial** acceleration and a second that includes the 25 psi ullage pressure plus 200-degree tank cool-down plus a 10g **lateral** acceleration. The second load case generates a greater number of critical and almost critical design margins than the first. However, 10g lateral acceleration is probably much too severe. In future optimizations the lateral acceleration should probably be substantially reduced and perhaps the axial acceleration should also be reduced somewhat.
6. Optimizations via SUPEROPT of the long propellant tank with two "rings" of struts, aft and forward, require somewhat more than 24 hours on the first author's very fast computer.
7. All the results in this report were obtained for arbitrarily assigned material properties, overall propellant tank dimensions and launch vehicle diameter, accelerations, and factors of safety. All the results presented here were obtained from only one value of each of these quantities. (See the values listed in Table 2.) Further work should be done with the use of other values for these quantities.
8. The effect of cool-down of the supporting struts was not included in this study because the bigbosor4/bosdec software is not capable of including thermal lengthening or shortening of springs.

9. The launch vehicle from which the propellant tank/strut system is supported is assumed to be rigid. BIGBOSOR4 cannot in its present form handle the presence of springs that connect different flexible shell segments to one another. Instead, each spring must be connected to rigid "ground".
10. There are no clearance constraints introduced into the present tank/strut model. It is up to the End user to specify upper and lower bounds of decision variables that do not allow struts to pass through each other or through the propellant tank.
11. For the particular ply properties used for the laminated composite strut tubes in this study the curing temperature, TEMTUR, has a significant effect on the values of the maximum stress components in the laminated composite strut tube walls. However, the value of TEMTUR only has a minor effect on the configuration of the optimized tank/strut system.
12. Short propellant tanks, such as that corresponding to Figs. 7 – 10, must be optimized with use of the "temporary" versions of bigbosor4 (addbosor4.density.var) and bosdec (bosdec.density.var) in addition (perhaps) to the "permanent" or "regular" versions of bigbosor4 (addbosor4.regular) and bosdec (bosdec.tank). The "regular" version of bigbosor4 does not handle shell segments the material density of which varies along the meridian of a given segment of the shell of revolution (the propellant tank). As listed in APPENDIX 2 of [20], a temporary "fix" is created that is valid only for the specific case of a propellant tank modeled as a three-layered shell of revolution. The three-layered model of the propellant tank shell wall is described above.
13. Long propellant tanks, such as that corresponding to the specific case called "test", should probably be optimized with use of the "temporary" versions of bigbosor4 and bosdec. As listed in [20], the "temporary" versions of bigbosor4/bosdec yield significantly better (smaller) objectives than do the "permanent" versions of bigbosor4/bosdec. However, the difference is not nearly as dramatic for the long tank as it is for the short tank. For directions on how to obtain optimum designs of the tank/strut system with use of the temporary versions of BIGBOSOR4 and BOSDEC see the section entitled, "TWO BIGBOSOR4/BOSDEC MODELS OF LUMPING..." in [20].
14. It is often difficult to find a "global" optimum design because the GENOPT processor, SUPEROPT, converges to multiple local minima of the objective, $WGT \times (TOTMAS/TNKNRM) + (1 - WGT) \times (CONDCT/CONNRM)$.
15. In optimizations the End user should always assign a significant non-zero value to the composite strut tube curing temperature, TEMTUR. TEMTUR = 170 degrees is used in the study reported here.
16. In every case reported here the laminated composite strut tube walls have a total of 12 layers with a symmetric layup: [1,2,3,4,5,6,6,5,4,3,2,1]. This seems to be suitable for a heavy, long propellant tank subjected to high axial and especially high lateral accelerations. However, for short tanks and perhaps for both long and short tanks subjected to a milder environment, it might be best to optimize with strut tubes that have a total of only eight layers with a symmetric layup: [1,2,3,4,4,3,2,1].
17. No attempt in this work was made to ensure that the optimized designs of the struts have an integral number of plies of a given specified thickness in the laminated composite wall of the strut tube.

18. Relatively crude STAGS models such as that shown in Fig. 24 are adequate for the prediction of modal vibration frequencies and buckling load factors. However, a more refined STAGS model, such as that shown in Fig. 26d, may be required for reasonably accurate predictions of maximum stress.

19. Replacement of the tapered external doublers in the GENOPT/BIGBOSOR4 model by doublers of constant average thickness in the STAGS model has little influence on the prediction of modal vibration frequencies and buckling load factors. However, as demonstrated in Fig. 21d, that replacement has a dramatic effect on the prediction of maximum stress at the tips of the stringers in the internal orthogrid “layer” of the propellant tank.

20. For the problems described in this paper it is difficult to find with STAGS non-spurious buckling modes when only the loads associated with the 10g acceleration are included in Load Set A (“eigenvalue” loads) and the 25 psi internal ullage pressure plus the 200-degree tank cool-down are included in Load Set B (load components not to be multiplied by the eigenvalue, that is, by the buckling load factor).

Section 19. SUGGESTIONS FOR FURTHER WORK

1. STAGS models of the optimized design should be constructed in which the external propellant tank doublers are tapered. Tapering of the doublers dramatically reduces the amplitudes of the stress concentrations caused by the concentrated loads applied by the struts to the wall of the propellant tank.

2. A STAGS model should be constructed with a denser finite element mesh in the meridional direction in the knuckle region of the aft dome, where the GENOPT/BIGBOSOR4 model predicts a significantly higher tensile stress at the tips of the internal orthogrid stringers (50000 psi) than do either of the two STAGS models (the 360-degree model and the 45-degree model) used in this work (about 44000 psi from the 45-degree STAGS model).

3. A version of BIGBOSOR4 should be created in which springs are permitted to connect two different shell segments. Presently, one end of each spring can be connected to a shell segment but the other end of that spring must be connected to rigid ground. Then this proposed new version of BIGBOSOR4 should be used to optimize payload/strut systems in which both ends of each strut are connected to flexible shells of revolution.

4. Little has been done here to handle struts with a thermal disconnect feature (called "PODS" in [6]) or to optimize for both launch (Phase 1) and orbital (Phase 2) conditions. Perhaps new decision variables should be introduced with respect to the "thermal disconnect part" of a strut. These would typically be the ply thicknesses and layup angles of an inner laminated strut tube that has a much lower conductivity than the much bigger launch tube part of the strut. Then the tank/strut system would have to be optimized for conditions in orbit as well as for launch conditions and for launch-hold conditions.

5. In the cases reported here and in other cases reported in [20] GENOPT has difficulty finding a “global” optimum design. The optimizer, ADS [4,5], used in connection with GENOPT is a gradient-based optimizer that easily finds local optima. Perhaps it would be a good idea to use the response surface method [21 – 26] in the search for a “global” optimum design.

APPENDIX 1

Certain updates were made to the “tank” FORTRAN source libraries, “struct” and “behavior”, in August 2012 and February 2013. The August 2012 updates give rise to significantly less conservative estimates of the maximum compressive loads in the struts in Load Case 2 (lateral acceleration). The February 2013 updates pertain to buckling of the struts as columns: previously the reduced “effective” axial stiffness, FKTOTL was used for column buckling, whereas presently the original axial stiffness, SPRCON (“SPRing CONstant”) is used for column buckling. The optimized design, behaviors, margins and objective listed above in the sections entitled, “Section 10. DECISION VARIABLE CANDIDATES FOR THE OPTIMIZED SPECIFIC CASE CALLED “test”: THE LONG PROPELLANT TANK WITH TWO SETS OF STRUTS, AFT AND FORWARD, 4 PAIRS OF STRUTS IN EACH SET” and “Section 11. VALUES OF ‘BEHAVIORS’, CORRESPONDING DESIGN MARGINS AND OBJECTIVE FOR THE OPTIMIZED SPECIFIC CASE CALLED ‘test’” were obtained **before** the August 2012 and February 2013 updates were made. However, the behaviors, margins and objective listed there were generated for that same optimized design **after** these August 2012 and February 2013 updates were made. **The design listed there is the one for which STAGS models are constructed and processed.** The tank/strut system was not re-optimized at that time. Listed below are the **re-optimized design**, design margins and objective obtained **after** the August 2012 and February 2013 updates were incorporated into the “tank” FORTRAN source libraries called “struct” (struct.tank) and “behavior” (behavior.tank):

Re-Optimized Design Found With The Temporary Version Of Bigbosor4/Bosdec And With Curing Temperature, TEMTUR=170 Degrees For The Long Propellant Tank With Two Rings Of Struts With 4 Pairs Of Struts In Each Ring Of Struts. (Dimensions in inches and degrees) (The design, the design margins and objective listed next were obtained **after re-optimization** via one execution of SUPEROPT **after** the August 2012 and February 2013 updates had been incorporated into the “tank” FORTRAN source libraries, “struct” and “behavior”. NOTE: **STAGS models of the re-optimized design listed below were never processed.**)

VALUES OF DESIGN VARIABLES CORRESPONDING TO BEST FEASIBLE DESIGN		
VAR. NO.	CURRENT VALUE	DEFINITION
1	6.133E-02	thickness of the tank aft dome skin: THKAFT
2	5.453E-02	thickness of the tank cylinder skin: THKMID
3	5.825E-02	thickness of the forward tank dome skin: THKFWD
4	7.891E+00	spacing of the tank orthogrid stringers: STRSPC
5	7.907E+00	spacing of the tank orthogrid rings: RNGSPC
6	2.601E-01	thickness of the tank orthogrid stringers: STRTHK
7	6.714E-01	height of the tank orthogrid stringers: STRHI
8	4.095E-01	thickness of the tank orthogrid rings: RNGTHK
9	6.714E-01	height of the tank orthogrid rings: RNGHI
10	1.500E+02	global axial coordinate of tank support ring: ZTANK(1)
11	4.500E+02	global axial coordinate of tank support ring: ZTANK(2)
12	8.672E+01	global axial coordinate of "ground": ZGRND(1)
13	5.142E+02	global axial coordinate of "ground": ZGRND(2)
14	6.000E+00	circ.angle (deg.) to pinned tank end of strut: ATANK(1)
15	6.001E+00	circ.angle (deg.) to pinned tank end of strut: ATANK(2)
16	4.500E+01	circ.angle to pinned "ground" end of strut: AGRND(1)

```

17 4.499E+01 circ.angle to pinned "ground" end of strut: AGRND(2 )
18 5.617E+00 inner diam. of support tube active at launch: IDTUBE(1 )
19 5.981E+00 inner diam. of support tube active at launch: IDTUBE(2 )
20 1.000E-06 height of mid-tank T-ring web: WEBHI
21 1.000E-06 thickness of mid-tank T-ring web: WEBTHK
22 1.000E-06 width (height) of mid-tank T-ring flange: FLGHI
23 1.000E-06 thickness of mid-tank T-ring flange: FLGTHK
24 3.000E+01 axial length of the propellant tank doubler: DUBAXL(1 )
25 7.272E-01 max.thickness of the propellant tank doubler: DUBTHK(1 )
26 3.218E-01 thickness of the tank reinforcement ring: TRNGTH(1 )
27 1.609E+00 height of the tank reinforcement ring: TRNGHI(1 )
28 7.049E-03 thickness of a lamina: THICK(1 )
29 7.049E-03 thickness of a lamina: THICK(2 )
30 7.049E-03 thickness of a lamina: THICK(3 )
31 7.049E-03 thickness of a lamina: THICK(4 )
32 7.049E-03 thickness of a lamina: THICK(5 )
33 7.049E-03 thickness of a lamina: THICK(6 )
34 6.695E-03 thickness of a lamina: THICK(7 )
35 6.695E-03 thickness of a lamina: THICK(8 )
36 6.695E-03 thickness of a lamina: THICK(9 )
37 6.695E-03 thickness of a lamina: THICK(10)
38 6.695E-03 thickness of a lamina: THICK(11)
39 6.695E-03 thickness of a lamina: THICK(12)
40 1.002E+01 layup angle: ANGLE(1 )
41 -1.002E+01 layup angle: ANGLE(2 )
42 1.002E+01 layup angle: ANGLE(3 )
43 -1.002E+01 layup angle: ANGLE(4 )
44 4.854E+01 layup angle: ANGLE(5 )
45 -4.854E+01 layup angle: ANGLE(6 )
46 1.000E+01 layup angle: ANGLE(7 )
47 -1.000E+01 layup angle: ANGLE(8 )
48 1.000E+01 layup angle: ANGLE(9 )
49 -1.000E+01 layup angle: ANGLE(10)
50 4.980E+01 layup angle: ANGLE(11)
51 -4.980E+01 layup angle: ANGLE(12)

```

***** MARGINS FOR LOAD CASE NO. 1 (axial acceleration, etc.) *****

(Critical and nearly critical margins are listed in bold face.)

MARGINS CORRESPONDING TO CURRENT DESIGN (F.S.= FACTOR OF SAFETY)

MARGIN NO.	CURRENT VALUE	DEFINITION
1	1.055E-02	(FREQ(1 ,1)/FREQA(1 ,1)) / FREQF(1 ,1)-1; F.S.= 1.20
2	3.920E-03	(FREQ(1 ,2)/FREQA(1 ,2)) / FREQF(1 ,2)-1; F.S.= 1.20
3	9.678E-02	(FREQ(1 ,3)/FREQA(1 ,3)) / FREQF(1 ,3)-1; F.S.= 1.20
4	1.138E-01	(FREQ(1 ,4)/FREQA(1 ,4)) / FREQF(1 ,4)-1; F.S.= 1.20
5	1.501E+01	(STRES1A(1 ,1)/STRES1(1 ,1)) / STRES1F(1 ,1)-1; F.S.= 1.50
6	1.800E+00	(STRES1A(1 ,2)/STRES1(1 ,2)) / STRES1F(1 ,2)-1; F.S.= 1.50
7	6.527E-01	(STRES1A(1 ,3)/STRES1(1 ,3)) / STRES1F(1 ,3)-1; F.S.= 1.50

8	3.193E+00	(STRES1A(1,5)/STRES1(1,5)) / STRES1F(1,5)-1; F.S.= 1.50
9	5.270E-01	(STRES2A(1,1)/STRES2(1,1)) / STRES2F(1,1)-1; F.S.= 1.50
10	5.637E+00	(STRES2A(1,2)/STRES2(1,2)) / STRES2F(1,2)-1; F.S.= 1.50
11	7.711E-02	(STRES2A(1,3)/STRES2(1,3)) / STRES2F(1,3)-1; F.S.= 1.50
12	2.196E-01	(STRES2A(1,5)/STRES2(1,5)) / STRES2F(1,5)-1; F.S.= 1.50
13	1.368E+00	(COLBUK(1,1)/COLBUKA(1,1)) / COLBUKF(1,1)-1; F.S.= 1.00
14	1.256E+04	(COLBUK(1,2)/COLBUKA(1,2)) / COLBUKF(1,2)-1; F.S.= 1.00
15	1.196E+00	(SHLBUK(1,1)/SHLBUKA(1,1)) / SHLBUKF(1,1)-1; F.S.= 2.00
16	6.724E+01	(SHLBUK(1,2)/SHLBUKA(1,2)) / SHLBUKF(1,2)-1; F.S.= 2.00
17	1.014E+00	(FORCEA(1,1)/FORCE(1,1)) / FORCEF(1,1)-1; F.S.= 1.00
18	7.095E-03	(FORCEA(1,2)/FORCE(1,2)) / FORCEF(1,2)-1; F.S.= 1.00
19	3.362E-03	(TNKSTRA(1,1)/TNKSTR(1,1)) / TNKSTRF(1,1)-1; F.S.= 1.00
20	3.355E-03	(TNKSTRA(1,2)/TNKSTR(1,2)) / TNKSTRF(1,2)-1; F.S.= 1.00
21	1.774E+01	(TNKBUK(1,1)/TNKBUKA(1,1)) / TNKBUKF(1,1)-1; F.S.= 1.00
22	1.774E+01	(TNKBUK(1,2)/TNKBUKA(1,2)) / TNKBUKF(1,2)-1; F.S.= 1.00

***** MARGINS FOR LOAD CASE NO. 2 (lateral acceleration, etc.) *****

(Critical and nearly critical margins are listed in bold face.)

MARGINS CORRESPONDING TO CURRENT DESIGN (F.S.= FACTOR OF SAFETY)

MARGIN NO.	CURRENT VALUE	DEFINITION
1	3.824E-03	(FREQ(2,1)/FREQA(2,1)) / FREQF(2,1)-1; F.S.= 1.20
2	7.493E-03	(FREQ(2,2)/FREQA(2,2)) / FREQF(2,2)-1; F.S.= 1.20
3	9.623E-02	(FREQ(2,3)/FREQA(2,3)) / FREQF(2,3)-1; F.S.= 1.20
4	1.136E-01	(FREQ(2,4)/FREQA(2,4)) / FREQF(2,4)-1; F.S.= 1.20
5	2.965E-01	(STRES1A(2,1)/STRES1(2,1)) / STRES1F(2,1)-1; F.S.= 1.50
6	8.261E-01	(STRES1A(2,2)/STRES1(2,2)) / STRES1F(2,2)-1; F.S.= 1.50
7	1.236E-02	(STRES1A(2,3)/STRES1(2,3)) / STRES1F(2,3)-1; F.S.= 1.50
8	2.066E-02	(STRES1A(2,5)/STRES1(2,5)) / STRES1F(2,5)-1; F.S.= 1.50
9	3.208E-01	(STRES2A(2,1)/STRES2(2,1)) / STRES2F(2,1)-1; F.S.= 1.50
10	8.509E-01	(STRES2A(2,2)/STRES2(2,2)) / STRES2F(2,2)-1; F.S.= 1.50
11	9.511E-03	(STRES2A(2,3)/STRES2(2,3)) / STRES2F(2,3)-1; F.S.= 1.50
12	7.115E-02	(STRES2A(2,5)/STRES2(2,5)) / STRES2F(2,5)-1; F.S.= 1.50
13	4.278E-01	(COLBUK(2,1)/COLBUKA(2,1)) / COLBUKF(2,1)-1; F.S.= 1.00
14	6.240E-01	(COLBUK(2,2)/COLBUKA(2,2)) / COLBUKF(2,2)-1; F.S.= 1.00
15	3.238E-01	(SHLBUK(2,1)/SHLBUKA(2,1)) / SHLBUKF(2,1)-1; F.S.= 2.00
16	2.096E-01	(SHLBUK(2,2)/SHLBUKA(2,2)) / SHLBUKF(2,2)-1; F.S.= 2.00
17	1.173E+00	(FORCEA(2,1)/FORCE(2,1)) / FORCEF(2,1)-1; F.S.= 1.00
18	4.478E-02	(FORCEA(2,2)/FORCE(2,2)) / FORCEF(2,2)-1; F.S.= 1.00
19	-9.033E-03	(TNKSTRA(2,1)/TNKSTR(2,1)) / TNKSTRF(2,1)-1; F.S.= 1.00
20	-9.048E-03	(TNKSTRA(2,2)/TNKSTR(2,2)) / TNKSTRF(2,2)-1; F.S.= 1.00
21	1.346E+01	(TNKBUK(2,1)/TNKBUKA(2,1)) / TNKBUKF(2,1)-1; F.S.= 1.00
22	1.346E+01	(TNKBUK(2,2)/TNKBUKA(2,2)) / TNKBUKF(2,2)-1; F.S.= 1.00

***** DESIGN OBJECTIVE *****

CURRENT VALUE OF THE OBJECTIVE FUNCTION:

VAR. NO.	CURRENT VALUE	DEFINITION
1	9.099E-01	WGTxTOTMAS/TNKNRM + (1-WGT)xCONDCT/CONNRM

APPENDIX 2

ABOUT STAGS (Structural Analysis of General Shells)

In this paper optimum designs obtained by GENOPT/TANK are evaluated later via STAGS models. **NOTE: STAGS is not used inside the optimization loop.**

STAGS [16 – 19] is a finite element code for the **general-purpose nonlinear analysis of stiffened shell structures of arbitrary shape and complexity**. Its capabilities include stress, stability, vibration, and transient analyses with both material and geometric nonlinearities permitted in all analysis types. STAGS includes enhancements, such as a higher order thick shell element, more advanced nonlinear solution strategies, and more comprehensive post-processing features such as a link with the STAGS postprocessor, STAPL.

Research and development of STAGS by Brogan, Almroth, Rankin, Stanley, Cabiness, Stehlin and others, formerly of the Computational Mechanics Department of the Lockheed Palo Alto Research Laboratory, was under continuous sponsorship from U.S. government agencies and internal Lockheed funding for more than 40 years. During this time particular emphasis was placed on improvement of the capability to solve difficult nonlinear problems such as the prediction of the behavior of axially compressed stiffened panels loaded far into their locally postbuckled states. STAGS has been extensively used worldwide for the evaluation of stiffened panels and shells loaded well into their locally postbuckled states.

A large rotation algorithm that is independent of the finite element library was incorporated into STAGS. With this algorithm there is no artificial stiffening due to large rotations. The finite elements in the STAGS library do not store energy under arbitrary rigid-body motion and the first and second variations of the strain energy are consistent. These properties lead to quadratic convergence during Newton iterations.

Solution control in nonlinear problems includes specification of load levels or use of the **advanced Riks-Crisfield path parameter** that enables traversal of limit points into the post-buckling regime. Two load systems with different histories (Load Sets A and B) can be defined and controlled separately during the solution process. Flexible restart procedures permit switching from one strategy to another during an analysis. This includes shifts from bifurcation buckling to nonlinear collapse analyses and back and shifts from static to transient and transient to static analyses with modified boundary conditions and loading. STAGS provides solutions to the generalized eigenvalue problem for **buckling and vibration from a linear or nonlinear stress state**.

Quadric surfaces can be modeled with minimal user input as individual substructures called "**shell units**" in which the analytic geometry is represented exactly. "Shell units" can be connected along edges or internal grid lines with partial or complete compatibility. In this way complex structures can be assembled from relatively simple units. Alternatively, a structure of arbitrary shape can be modeled with use of "element units".

Geometric imperfections can be generated automatically in a variety of ways, thereby permitting imperfection-sensitivity studies to be performed. For example, **imperfections can be generated by superposition of several buckling modes determined from previous STAGS analyses of a given case.**

A variety of material models is available, including both plasticity and creep. STAGS handles isotropic and anisotropic materials, including composites consisting of up to 60 layers of arbitrary orientation. Four plasticity models are available, including isotropic strain hardening, the White Besseling (mechanical sublayer model), kinematic strain hardening, and deformation theory.

Two independent load sets, each composed from simple parts that may be specified with minimal input, define a spatial variation of loading. Any number of point loads, prescribed displacements, line loads, surface tractions, thermal loads, and "live" pressure (hydrostatic pressure which remains normal to the shell surface throughout large deformations) can be combined to make a load set. For transient analysis the user may select from a menu of loading histories, or a general temporal variation may be specified in a user-written subroutine.

Boundary conditions (B.C.) may be imposed either by reference to certain standard conditions or by the use of single- and multi-point constraints. Simple support, symmetry, antisymmetry, clamped, or user-defined B.C. can be defined on a "shell unit" edge. Single-point constraints which allow individual freedoms to be free, fixed, or a prescribed non-zero value may be applied to grid lines and surfaces in "shell units" or "element units". A useful feature for buckling analysis allows these constraints to differ for the prestress and eigenvalue analyses. Lagrangian constraint equations containing up to 100 terms may be defined to impose multi-point constraints.

STAGS has a variety of finite elements suitable for the analysis of stiffened plates and shells. Simple four node quadrilateral plate elements with a cubic lateral displacement field (called "410" and "411" elements) are effective and efficient for the prediction of postbuckling thin shell response. A linear (410) or quadratic (411) membrane interpolation can be selected. For thicker shells in which transverse shear deformation is important, STAGS provides the Assumed Natural Strain (ANS) nine node element (called "480" element). A two node beam element compatible with the four node quadrilateral plate element is provided to simulate stiffeners and beam assemblies. Other finite elements included in STAGS are described in the STAGS literature [16 – 19].

APPENDIX 3

A small part of the file called "bigbosor4.springs", which is included as part of the compressed "tar" file: ...genopt/case/tank/tanktank2.tar.gz [20]

ADDITION OF SPRINGS IN BIGBOSOR4 CONNECTING A "FAKE" RING TO GROUND

David Bushnell

March 25, 2008

ABSTRACT

Connection of an otherwise unconstrained shell structure to ground by means of linear elastic springs pinned at their ends simulates a strut-supported structure with pin-ended struts. The springs are entered into the BIGBOSOR4 input file as discrete elastic structures attached at one end to user-defined discrete points around the circumference of a "fake" ring joined to the shell and attached at the other end to user-defined discrete

points at ground. Even so, since BIGBOSOR4 can handle only axisymmetric structures, the effect of the springs is "smeared out" by BIGBOSOR4 over the circumference where the springs are attached to the "fake" ring. Essentially, the springs act as a thick conical shell extending from the "fake" ring where the springs are attached to the shell structure to ground where the springs are attached to ground. The overall extensional and shear stiffnesses of this imaginary conical shell match those of the assemblage of springs. In a linear non-axisymmetric stress and buckling analysis the springs contribute strain energy to the structure only in the $n = 0$ and $n = 1$ circumferential wave harmonics. The springs thus prevent rigid body displacements of the structure. The internal concentrated loads applied by the springs to the "fake" ring (and therefore to the shell) are computed by BIGBOSOR4 and listed in the BIGBOSOR4 output file. These concentrated loads can be applied to the same shell structure without springs in a separate and subsequent execution of BIGBOSOR4 in order to determine local deformations and stresses caused by them and in order to determine lowered "effective" spring constants because the springs react against a deformable structure, not against a rigid structure. An example is given of a sequence of two BIGBOSOR4 runs, the first run involving a spring-supported cylindrical shell subjected to an overall static bending moment at its top end and the second run involving the same shell with the springs replaced by line loads applied to the "fake" ring that simulate the concentrated spring reaction loads applied by the springs to the bottom of the cylindrical shell in the first execution of BIGBOSOR4.

The entire "bigbosor4.springs" file is very long [20]. Therefore, only this abstract is included here.

APPENDIX 4

PART 1:

Part of the BIGBOSOR4 prompting files, PROMPT3.DAT and PROMPT.DAT, that relate to inertial loading and loading by normal pressure caused by axial acceleration, GAXIAL, and lateral acceleration, GLATRL, of a fluid-filled tank. (NOTE: The first line in the following list is from the BIGBOSOR4 prompting file, PROMPT3.DAT. All the other lines are from the BIGBOSOR4 prompting file, PROMPT.DAT.)

```
-----
702.1 Do you want response to harmonic forcing (INDIC = 3 or 4)?
57.1 OMEGDR = driving frequency for harmonic forcing (rad/sec)
58.1 GLATRL = no. of g's lateral forcing (base excitation only)
59.1 GAXIAL = no. of g's axial forcing (base excitation only)
134.1 Is there a tank filled with fluid?
134.2
```

This section is entered only if there exists at least one non-zero component of acceleration of gravity (axial, lateral, or both), such as would be experienced by a payload in a launch vehicle.

If you answer "Y" (you are allowed only one fluid-filled tank per case!), you will next be asked to supply the following information:

1. The WEIGHT density (e.g. lb/in**3) of the fluid, GAMMA
2. The axial length of the tank, AXLONG
3. The radius of the largest parallel circle in the tank, RBIG
4. The axial coordinate of the bottom of the tank, ZBEGIN

5. The segment numbers that comprise the tank, ISTANK(j), j=1,2,..
6. Whether the inside of the tank is on the left or right side of the wall as you travel along the meridian.

NOTE: The tank is assumed to be completely full of the fluid. BOSOR4 uses the above information plus the meridional geometry of the tank and the axial and lateral g's, GAXIAL and GLATRL, to which the tank is subjected to compute the pressure of the fluid acting on the tank wall:

$$p(\text{fluid}) = k * \text{GAMMA} \{ \text{abs}(\text{GLATRL}) * [\text{RBIG} - (\text{GLATRL} / \text{abs}(\text{GLATRL})) * r * \cos(\text{theta})] + \text{GAXIAL} * [0.5 * \text{AXLONG} * (1 + \text{GAXIAL} / \text{abs}(\text{GAXIAL})) - (z - \text{ZBEGIN})] \}$$

in which r is the radius of the parallel circle at z, z is the axial coordinate of an arbitrary point on the tank meridian, and theta is the circumferential coordinate. The factor k is +1.0 if the inside of the tank is on the left side of the wall as you travel along the meridian in the direction of increasing arc length, s; k= -1.0 otherwise. (See p 66, bottom, of "BOSOR4: Program for stress, buckling, and vibration of complex shells of revolution", in STRUCTURAL MECHANICS SOFTWARE SERIES, Vol. 1, N. Perrone and W. Pilkey, editors, Univ. Press of Virginia, pp 11-141 (1974)).

- 136.1 WEIGHT density (e.g. lb/in**3) of the fluid, GAMMA
- 138.1 Axial length of the tank, AXLONG
- 140.1 Radius of largest parallel circle in the tank, RBIG
- 142.1 Axial coordinate of the bottom of the tank, ZBEGIN
- 144.0

Next, please provide the numbers of the segments of the tank wall that "see" the normal pressure applied by the fluid.

NOTE: INCLUDE ONLY THOSE SEGMENTS THAT EXPERIENCE A DELTA-p from the fluid across the wall!

- 146.1 How many BOSOR4 segments in the tank "see" delta-p(fluid)?
- 146.2

NOTE: Include only those segments upon which a net fluid pressure acts on the wall of the tank!

- 148.1 Segment number, ISTANK
- 149.1 Is the inside of the tank to the left of increasing arc, s?

PART 2:

Part of the BIGBOSOR4 input file, test.ALL, relating to inertial loading and loading by normal pressure caused by axial acceleration, GAXIAL, and lateral acceleration, GLATRL, of a fluid-filled tank.

Y	\$ Do you want response to harmonic forcing (INDIC = 3 or 4)?
0.1000000E-05	\$ OMEGDR = driving frequency for harmonic forcing (rad/sec)
Y	\$ Is the harmonic forcing thru base excitation?
386.4000	\$ Value of acceleration of gravity in this case's units
0.000000	\$ GLATRL = no. of g's lateral forcing (base excitation only)
10.00000	\$ GAXIAL = no. of g's axial forcing (base excitation only)
Y	\$ Is there a tank filled with fluid?
0.2560000E-02	\$ WEIGHT density (e.g. lb/in**3) of the fluid, GAMMA
400.0000	\$ Axial length of the tank, AXLONG
100.0000	\$ Radius of largest parallel circle in the tank, RBIG
100.0000	\$ Axial coordinate of the bottom of the tank, ZBEGIN
28	\$ How many BOSOR4 segments in the tank "see" delta-p(fluid)?
1	\$ Segment number, ISTANK(1)
Y	\$ Is the inside of the tank to the left of increasing arc, s?
2	\$ Segment number, ISTANK(2)
Y	\$ Is the inside of the tank to the left of increasing arc, s?
3	\$ Segment number, ISTANK(3)
Y	\$ Is the inside of the tank to the left of increasing arc, s?
4	\$ Segment number, ISTANK(4)
Y	\$ Is the inside of the tank to the left of increasing arc, s?
5	\$ Segment number, ISTANK(5)
Y	\$ Is the inside of the tank to the left of increasing arc, s?
6	\$ Segment number, ISTANK(6)
Y	\$ Is the inside of the tank to the left of increasing arc, s?
7	\$ Segment number, ISTANK(7)
Y	\$ Is the inside of the tank to the left of increasing arc, s?
8	\$ Segment number, ISTANK(8)
Y	\$ Is the inside of the tank to the left of increasing arc, s?
9	\$ Segment number, ISTANK(9)
Y	\$ Is the inside of the tank to the left of increasing arc, s?
10	\$ Segment number, ISTANK(10)
Y	\$ Is the inside of the tank to the left of increasing arc, s?
11	\$ Segment number, ISTANK(11)
Y	\$ Is the inside of the tank to the left of increasing arc, s?
12	\$ Segment number, ISTANK(12)
Y	\$ Is the inside of the tank to the left of increasing arc, s?
13	\$ Segment number, ISTANK(13)
Y	\$ Is the inside of the tank to the left of increasing arc, s?
14	\$ Segment number, ISTANK(14)
Y	\$ Is the inside of the tank to the left of increasing arc, s?
15	\$ Segment number, ISTANK(15)
Y	\$ Is the inside of the tank to the left of increasing arc, s?
16	\$ Segment number, ISTANK(16)
Y	\$ Is the inside of the tank to the left of increasing arc, s?
17	\$ Segment number, ISTANK(17)
Y	\$ Is the inside of the tank to the left of increasing arc, s?
18	\$ Segment number, ISTANK(18)
Y	\$ Is the inside of the tank to the left of increasing arc, s?

```

19      $ Segment number, ISTANK( 19)
Y      $ Is the inside of the tank to the left of increasing arc, s?
20      $ Segment number, ISTANK( 20)
Y      $ Is the inside of the tank to the left of increasing arc, s?
21      $ Segment number, ISTANK( 21)
Y      $ Is the inside of the tank to the left of increasing arc, s?
22      $ Segment number, ISTANK( 22)
Y      $ Is the inside of the tank to the left of increasing arc, s?
23      $ Segment number, ISTANK( 23)
Y      $ Is the inside of the tank to the left of increasing arc, s?
24      $ Segment number, ISTANK( 24)
Y      $ Is the inside of the tank to the left of increasing arc, s?
25      $ Segment number, ISTANK( 25)
Y      $ Is the inside of the tank to the left of increasing arc, s?
26      $ Segment number, ISTANK( 26)
Y      $ Is the inside of the tank to the left of increasing arc, s?
27      $ Segment number, ISTANK( 27)
Y      $ Is the inside of the tank to the left of increasing arc, s?
28      $ Segment number, ISTANK( 28)
Y      $ Is the inside of the tank to the left of increasing arc, s?

```

NOTE: The effects of quasi-static accelerations, GAXIAL and GLATRL, are generated through harmonic loading with a very, very low driving frequency, OMEGDR:

0.1000000E-05 \$ OMEGDR = driving frequency for harmonic forcing (rad/sec)

Hence, the effect of the propellant is included in the BIGBOSOR4 models for buckling and stress by normal pressure applied by the accelerating propellant to the wall of the accelerating propellant tank, not by instead lumping the propellant mass into the middle layer of the propellant tank shell wall, as is done for the modal vibration model.

REFERENCES

- [1] Bushnell, D., "GENOPT--A program that writes user-friendly optimization code", International Journal of Solids and Structures, Vol. 26, No. 9/10, pp. 2031-380, 1990. The same paper is contained in a bound volume of papers from the International Journal of Solids and Structures published in memory of the late Professor Charles D. Babcock, Jr, formerly with the California Institute of Technology.
- [2] Bushnell, D., "Automated optimum design of shells of revolution with application to ring-stiffened cylindrical shells with wavy walls", AIAA paper 2000-1663, 41st AIAA Structures Meeting, Atlanta, GA, April 2000. Also see Lockheed Martin report, same title, LMMS P534574, November 1999
- [3] Bushnell, D., "BOSOR4: Program for stress, stability, and vibration of complex, branched shells of revolution", in STRUCTURAL ANALYSIS SYSTEMS, Vol. 2, edited by A. Niku-Lari, pp. 25-54, (1986)
- [4] Vanderplaats, G. N., "ADS--a FORTRAN program for automated design synthesis, Version 2.01", Engineering Design Optimization, Inc, Santa Barbara, CA, January, 1987
- [5] Vanderplaats, G. N. and Sugimoto, H., "A general-purpose optimization program for engineering design", Computers and Structures, Vol. 24, pp 13-21, 1986

- [6] Bushnell, D., "Improved optimum design of dewar supports", COMPUTERS and STRUCTURES, Vol. 29, No. 1, pp. 1-56 (1988)
- [7] Bushnell, D., "Use of GENOPT and BIGBOSOR4 to obtain an optimum design of a deep submergence tank", unpublished report to the DOER company, Alameda, CA, June 30, 2009
- [8] Bushnell, D., "Use of GENOPT and BIGBOSOR4 to obtain optimum designs of a double-walled inflatable spherical vacuum chamber", unpublished report for Michael Mayo, December, 2010 (accepted for 53rd AIAA Structures Meeting, Honolulu, Hawaii, April 2012)
- [9] Bushnell, D., "SPHERE - Program for minimum weight design of isogrid-stiffened spherical shells under uniform external pressure", Lockheed Report F372046, January, 1990
- [10] Bushnell, D., "Optimum design of imperfect isogrid-stiffened ellipsoidal shells...", written and placed in the file ..genopt/case/torisp/sdm50.report.pdf. Also see "A shortened version of the report on minimum weight design of imperfect isogrid-stiffened ellipsoidal shells under uniform external pressure", AIAA Paper 2009-2702, 50th AIAA Structures, Structural Dynamics and Materials Conference, 2009
- [11] Bushnell, D., "Use of GENOPT and BIGBOSOR4 to obtain optimum designs of a double-walled inflatable cylindrical vacuum chamber", unpublished report, November, 2010
- [12] Bushnell, D. and Thornburgh, R. P., "Use of GENOPT and BIGBOSOR4 to optimize weld lands in axially compressed stiffened cylindrical shells and evaluation of the optimized designs by STAGS", AIAA Paper 2010-2927, AIAA 51st Structures Meeting, Orlando, Florida, April 2010
- [13] Bushnell, D. and Rankin, C., "Use of GENOPT and BIGBOSOR4 to obtain optimum designs of an axially compressed cylindrical shell with a composite truss-core sandwich wall", AIAA Paper 2011-1811, 52nd AIAA Structures Meeting, Denver, CO, April, 2011
- [14] Bushnell, D., "Addition of springs in BIGBOSOR4 connecting a "fake" ring to ground", Item No. 29 in the file, /home/progs/bigbisor4/doc/bigbisor4.news, dated March 25, 2008. See the file included in the "genopt" section of [20] called "bigbisor4.springs". This file, bigbisor4.springs, is located in the directory, ...genopt/case/tank, as part of the compressed "tar" file called "tanktank2.tar.gz". The file, .../genopt/case/tank/tanktank2.tar.gz, is part of the very big compressed "tar" file that can be downloaded from the "Downloads" page of the "shellbuckling.com" website [20]. See Appendix 3 for an abstract.
- [15] Bushnell, D., "Theoretical basis of the PANDA computer program for preliminary design of stiffened panels under combined in-plane loads", Computers & Structures, Vol. 27, No. 4, pp. 541-563, 1987
- [16] B. O. Almroth, F. A. Brogan, "The STAGS Computer Code", NASA CR-2950, NASA Langley Research Center, Hampton, Va.(1978)
- [17] C. C. Rankin, P. Stehlin and F. A. Brogan, "Enhancements to the STAGS computer code", NASA CR 4000, NASA Langley Research Center, Hampton, Va, November 1986

[18] Riks, E., Rankin C. C., Brogan F. A., "On the solution of mode jumping phenomena in thin walled shell structures", First ASCE/ASM/SES Mechanics Conference, Charlottesville, VA, June 6-9, 1993, in: Computer Methods in Applied Mechanics and Engineering, Vol.136, 1996.

[19] G. A. Thurston, F. A. Brogan and P. Stehlin, "Postbuckling analysis using a general purpose code", AIAA Journal, 24, (6) (1986) pp. 1013-1020.

[20] Bushnell, D. and Bushnell, W.D., Shell buckling website, <http://shellbuckling.com/>, in particular the "GENOPT" page of that website and the two unpublished full reports and their associated figures and tables, "Optimization of Propellant Tanks Supported by Optimized Laminated Composite Tubular Struts", by David Bushnell, January – March 2012, and "Optimization of Propellant Tanks Supported by One or Two Optimized Laminated Composite Skirts", by David Bushnell, February – June 2012. These two detailed reports and associated figures and tables, written before Michael Jacoby and Charles Rankin generated the STAGS models and predictions, can be downloaded by website visitors. NOTE: These detailed reports give configurations that are now out of date because certain errors were found and other software modifications were made after the detailed reports were written. In spite of this, the detailed reports are instructive because of other information given in them. In order to download the two unpublished full reports and their associated figures and tables, go to the "Downloads" page of the website, <http://shellbuckling.com/>, and download a very large compressed "tar" file (about 700 Mbytes) containing the latest versions of the following computer programs/documentation/cases created over many years by David Bushnell: BOSOR4, BIGBOSOR4, BOSOR5, PANDA2 and GENOPT, and a small file, "How to Run on LINUX". Generate the proper directory structure for the five programs; go to the directory, .../genopt/case/tank; copy the file, tanktank2.tar.gz to a working directory; go to that working directory; decompress (gunzip) the file, tanktank2.tar.gz; disassemble the resulting file, tanktank2.tar (tar xvf tanktank2.tar); and uncompress and disassemble three of the resulting files, general.info.tar.gz, tank.tar.gz (strut-supported tank), and tank2.tar.gz (skirt-supported tank). All of the files referred to in this paper can be obtained by this procedure. The two "unpublished full reports" mentioned at the beginning of this reference are located in the "folder" called "tanktank2", which appears in a list of the entities that exist following your command, "tar xvf tanktank2.tar". The "folder" called "tanktank2" contains the two "folders", tank.paper (strut-supported propellant tank) and tank2paper (skirt-supported propellant tank). The tank.paper "folder" contains several "folders", in particular the two "folders" called "tankfigsdoc" (the "tank" figures) and "tanktablesdoc" (the "tank" tables) and the file called "tankpapertext.pdf" (the text of the unpublished full report on the strut-supported tank). The tank2paper "folder" contains several "folders", in particular the two "folders" called "tank2figsdoc" (the "tank2" figures) and "tank2tablesdoc" (the "tank2" tables) and the file called "tank2papertext.pdf" (the text of the unpublished full report on the skirt-supported tank). The word, "folder", which is jargon used on the iMAC computers, can be replaced by the word, "directory", appropriate for workstations.

[21] Haftka, R.T., and Watson, L.T., "Multidisciplinary Design Optimization with Quasiseparable Subsystems," Optimization and Engineering, 6, 9–20, March 2005. | View Publication

[22] Liu, B., Haftka, R.T., and Watson L.T., "Global-Local Structural Optimization Using Response Surfaces of Local Optimization Margins," Structural and Multidisciplinary Optimization, 27(5), 352-359, 2004.

[23] Papila, M., and Haftka, R.T., "Response Surface Approximations: Noise, Error Repair, and Modeling Errors," AIAA Journal 38(12), pp. 2336-2343, 2000.

[24] Hosder, S., Watson, L.T., Grossman, B., Mason, W.H., and Kim, H., "Polynomial Response Surface Approximations for Multidisciplinary Design Optimization of a High Speed Civil Transport," *Optimization and Engineering*, 2, 431-452, 2001.

[25] Venter, G., Haftka, R.T., and Starnes, J.H., Jr. "Construction of Response Surface Approximation for Design Optimization," *AIAA Journal*, 36(12), pp. 2242-2249, 1998.

[26] Roux, W.J., Stander, N., and Haftka, R.T., "Response Surface Approximations for Structural Optimization," *International Journal for Numerical Methods in Engineering*, 42, pp. 517-534, 1998.

DEDICATION

This paper is dedicated to Dr. Charles C. Rankin (August 19, 1942 – August 11, 2012) See next pages.



Dr. Charles C. Rankin (August 19, 1942 – August 11, 2012)

IN MEMORIAM

Personal

Our co-author and colleague, Charles Rankin, was a great man, loved by many for his great sense of humor, respected by many for his towering intellect and superb accomplishments in the field of structural mechanics. He will remain forever in the minds and hearts of his many friends and colleagues.

Biography

Charles Rankin received his PhD in Molecular Physics from the University of Chicago in 1968 and his BS in Chemistry from the University of North Carolina in 1964. It is unusual that his degrees are in a different field than that of his major technical contributions, demonstrating his exceptional ability not only to learn and master new disciplines but also to rise to the top of his new field of endeavor.

Charles worked at Lockheed (now Lockheed Martin) practically his entire career. He retired from the Lockheed Martin Advanced Technology Center, Palo Alto, in 2003 and worked at Rhombus Consultants Group in Palo Alto from 2003 until July 2012. From 1983 on he devoted most of his time to the continuing development of the STAGS computer program, primarily under contract with the NASA Langley Research Center in Hampton, Virginia. During this time he received several Lockheed Martin recognition awards and NASA Group Achievement Awards relating to work on Aging Aircraft Structural Integrity and work on the Space Shuttle External Tank. He was at the height of his powers until he was hospitalized with advanced cancer in July 2012 from which he died on August 11, 2012.

During the last ten years of his life Charles served on the AIAA Structures Technical Committee. For almost ten years (2003 – 2012) he was a member of the ABAQUS Fracture Customer Review Team. For eight years (2004 – 2012) he served on the NASA Engineering and Safety Center (NESC) Structures Technical Discipline Team. He served as a member of the NESC Space Shuttle External Tank Intertank Stringer Cracking Investigation Team in 2011 and participated in the International Workshop on Structural Integrity of Aging Airplanes in 1992. He served three times on a board for evaluation of a student's defense of a PhD dissertation or MS thesis.

Charles was always an avid hiker and served the Sierra Club as a leader of long hikes in the San Francisco Bay area and in the Sierra Nevada of California.

Technical Contributions

Charles Rankin is known for his salient fundamental contributions over more than 30 years to the field of solid and structural mechanics. All of these contributions have been formulated by Charles and implemented into his general-purpose nonlinear static and dynamic finite element code called STAGS (**S**tructural **A**nalysis of **G**eneral **S**hells), widely used especially at NASA Langley Research Center. Charles was no mere programmer implementing into a code the mechanics theories of others; he developed these theories mainly by himself. Many of Charles' fundamental contributions are now finding their way into the most widely used commercial structural computer programs such as MSC_NASTRAN, ANSYS and ABAQUS. In this way Charles' important original contributions will for the foreseeable future have a major impact on research and engineering in academia, government and industry.

Specifically Charles Rankin's technical contributions are as follows:

- 1.** Formulation of a finite-element-independent co-rotational theory and its implementation into the STAGS computer program in the 1980s [18, 29, 31, 33] that was original with Charles and that has just recently been and is now being introduced into widely used commercial computer codes. This method permits the simulation of highly nonlinear phenomena in thin-walled structures such as the reliable determination via Newton's method of far post-buckling static and dynamic equilibrium states of stiffened, composite shell structures universally used by the aerospace industry. Charles' unique co-rotational formulation avoids finite-element "lockup". It has been especially well received by the developers of commercial structural computer codes because it operates outside the finite element kernels that differ not only from code to code but also from finite element to finite element within each commercial software package. Unique to STAGS is an extension to large strain for various selected strain measures [5, 7], again in a process that is virtually independent of the details of the finite element kernel. A Google search with use of the string, "corotational finite element", produces about 74000 results, indicating that this original contribution of Charles has now become an important standard in computational mechanics the world over.
- 2.** Formulation (with Eduard Riks) and implementation into STAGS of an arc-length method that permits the traversal of limit points from pre-buckling to post-buckling of imperfect shells under destabilizing loads [16, 21, 24, 25]. Charles optimized the solution stepping algorithm for the reliable determination of the nonlinear equilibrium state at each successive loading step. This strategy includes the unique ability to switch solutions paths and continue "in the path direction" of a particular buckling eigenvector in order to enable a more reliable and accurate investigation of post-buckling behavior. Charles' unique strategy permits the accurate prediction of "mode-jumping" [19, 23], a dynamic phenomenon in which a given post-buckled state evolves dynamically, at a given load level, into an entirely different, non-neighboring, post-buckled state. STAGS is the first general-purpose computer program to include these sophisticated formulations and strategies that are now finding their way into the major commercial codes.
- 3.** Formulation and implementation into STAGS of an algorithm to determine multiple bifurcation eigenvalues and eigenvectors from nonlinearly determined rather than from linearly determined pre-buckled equilibrium states. This original contribution by Charles is essential for the successful simulation of "mode jumping" [8, 19, 23], a phenomenon that is especially prominent in compressed stiffened thin shells of the type universally used by the aerospace industry. It is also essential for the determination of the behavior of an axially compressed imperfect stiffened cylindrical shell loaded well beyond its initial buckling load to ultimate failure in its far post-buckled state.
- 4.** Formulation and implementation of a solution strategy that permits the successive introduction into a given nonlinear finite element model of a shell structure a sequence of buckling modal imperfections [8]. This strategy, original with Charles, is required in order to determine static and dynamic nonlinear post-buckled equilibrium states of thin shells with closely spaced bifurcation points in the nonlinear regime, for the determination of secondary and tertiary (and so on) equilibrium bifurcations, and for successful nonlinear continuation beyond these secondary and tertiary bifurcations [8, 13]. This very complex nonlinear behavior is typical of extremely light-weight stiffened thin shell structures such as the huge external tank of the Space Shuttle and optimally designed aircraft fuselages. Charles' unique strategy is crucial if the ultimate failure of such thin shell structures is to be determined reliably. Numerous comparisons in the literature between test and the theory implemented in STAGS demonstrate the accuracy of predictions by STAGS.

5. Formulation and implementation of a strategy that permits successive smooth transitions from static to transient and from transient to static analyses of a given structure during execution of a sequence of nonlinear computer runs sometimes required for the complete determination of the ultimate failure of a thin shell structure [8]. A crucial aspect of this strategy is the use of advanced static arc-length methods to enable the reliable return to a converged nonlinear static equilibrium state from a nonlinear transient state by means of appropriate load relaxation.

6. Formulation and implementation of a strategy that permits the simulation of unzipping of a through crack in a shell possibly with multiple crack tips and turning of a crack during loading [9, 26, 28, 30]. This unique and sophisticated strategy requires the use of a combination of advanced arc-length procedures and load-relaxation return to nonlinear static equilibrium, all done seamlessly in STAGS without user intervention. STAGS is the only code to report the actual energy release rate during the entire crack growth process. This crack tip behavior simulation capability, originally unique to STAGS, is crucial for solution of the problem of fatigue failure and catastrophic delamination in composite and metallic aircraft fuselages [2, 4, 9, 15]. Charles' formulations are now finding their way into ABAQUS, primarily via Charles' service on the ABAQUS Fracture Customer Review Team.

7. Formulation and implementation of a "sandwich" finite element that efficiently accounts for soft, shear-deformable cores and stiff face sheets [11, 36]. The STAGS sandwich element makes clever use of existing shell elements for the face sheets, and adds a separation between the face sheets. The space is filled with an 8-node solid element whose displacement field is taken from the face sheets; this process allows for a very high order resolution of the dominant shear field between the face sheets. An additional important aspect of the sandwich element is that one is able to raise the through-the-thickness order by stacking phantom face sheets within the core to provide a more flexible displacement field. Phantom face sheets are shell elements with no stiffness, with a displacement field driven by the core shear field.

8. The development of unique nonlinear material models in separate "material modules" which are independent of the rest of the software. This formulation makes it straightforward to introduce into large commercial finite element codes various composite-response progressive failure models that include many different failure threshold and growth criteria [14, 22, 28]. Notable among these models created by Charles is the simulation of composite fatigue delamination in a mixed-mode setting [2] and advanced decohesion finite elements for the simulation of composite delamination [4]: an initial version implemented into STAGS in 1999 and revised and improved since then. These sophisticated models have been implemented in ABAQUS.

Publications by Dr Charles C. Rankin

1. "Use of GENOPT and BIGBOSOR4 to obtain optimum designs of multi-walled inflatable spherical and cylindrical vacuum chambers", (with David Bushnell), AIAA 53rd Structures, Structural Dynamics and Materials Conference, Honolulu, Hawaii, April 2012
2. "Simulation of Composite Fatigue Delamination in a Mixed-Mode Setting," with Bryan Hurlbut, presented at the 2011 Simulia (ABAQUS) Customer Conference (2011).
3. "Use of GENOPT and BIGBOSOR4 to Obtain Optimum Designs of an Axially Compressed Cylindrical Shell with a Composite Truss-Core Sandwich Wall," with David Bushnell, presented at the 52nd AIAA SDM

Conference, Paper #2011-1811 (2011).

4. “Advanced Decohesion Elements for the Simulation of Composite Delamination,” with Marc Regelbrugge & Bryan Hurlbut, presented at the 2010 Simulia (ABAQUS) Customer Conference (2010).

5. “The Use of Shell Elements for the Analysis of Large Strain Response,” presented at the 48th AIAA SDM Conference, Paper #2007-2384 (2007).

6. “Design Equations & System Implications of Thin Film Membrane Mirrors & Windows,” with Jason Lindler & Eric Flint, presented at the 48th AIAA SDM Conference, Paper #2007-1815 (2007).

7. “Application of Linear Finite Elements to Finite Strain Using Corotation,” presented at the 47th AIAA SDM Conference, Paper #2006-1751 (2006).

8. “Difficulties in Optimization of Imperfect Stiffened Cylindrical Shells,” with David Bushnell, presented at the 47th AIAA SDM Conference, Paper #2006-1943 (2006).

9. “Residual Strength Calculations of Stiffened Metal Panels Containing Cracks,” with Eduard Riks, presented at the 46th AIAA SDM Conference, Paper #2005-2007 (2005).

10. “Optimum design of Stiffened Panels with Sub-stiffeners,” with David Bushnell, presented at the 46th AIAA SDM Conference, Paper #2005-1932 (2005).

11. “Finite Element Modeling of the Buckling Response of Sandwich Panels,” with Cheryl Rose, David Moore and Norman Knight, presented at the 43rd AIAA SDM Conference, Paper #2002-1517 (2002).

12. “Optimization of Perfect and Imperfect Ring and Stringer-Stiffened Cylindrical Shells with PANDA2 and Evaluation of the Optimum Design with STAGS,” with David Bushnell, presented at the 43rd AIAA SDM Conference, Paper #2002-1408 (2002).

13. “Tools for the Evaluation of the Residual Strength of Cracked Pressurized Fuselage Shells,” with Eduard Riks, presented at the 42nd AIAA SDM Conference, Paper #2001-1325 (2001).

14. “Controlling Nonlinear Procedures During Progressive Failure Analysis,” with N. Knight & F. Brogan, presented at the 41st AIAA SDM Conference, Paper #2000-1460 (2000).

15. “On the Simulation of Crack Propagation in Pressurized Fuselages,” with E. Riks, presented at the 41st AIAA SDM Conference, Paper #2000-1594 (2000)

16. “Modeling and Nonlinear Structural Analysis of a Large-Scale Launch Vehicle,” with Richard Young, J. of Spacecraft & Rockets, Vol. 36, No. 6, pp. 804-811 (1999).

17. “Line-to-Line Contact Behavior of Shell Structures,” with W. Loden, L. Swenson, and L. Chien, presented at the 40th AIAA SDM Conference, Paper #99-1237 (1999).

18. “On the Choice of Best Possible Corotational Element Frame,” presented at the 3rd International

Conference on Computational Mechanics at Atlanta, GA. (1998)

19. "Optimization of Stiffened Panels in which Mode Jumping Is Accounted For," with D. Bushnell, presented at the 38th AIAA SDM Conference, AIAA Paper 97-1141, (1997)

20. "Modeling and Nonlinear Analysis of a Large Scale Launch Vehicle under Combined Thermal & Mechanical Loads," with R. D. Young, presented at the 37th AIAA SDM Conference, AIAA Paper No. 1996-1551, (1996).

21. "Computer Simulation of the Buckling Behavior of Thin Shells Under Quasi Static Loads," with E. Riks, Archives of Computational Methods in Engineering, Vol. 4, No. 4, pp 325-351 (1997).

22. "Nonlinear Response and Residual Strength of Damaged Stiffened Shells Subjected to Combined Loads," with James Starnes, Vicki Britt, and Cheryl Rose. Presented at the 37th AIAA SDM Conference, Paper #1996-1555 (1996).

23. "On the Solution of Mode Jumping Phenomena in Thin-Walled Shell Structures," with E. Riks and Francis A. Brogan, Comp. Meth. Appl. Mech. Eng., Vol 136, pp 59-92 (1996).

24. "Simulation of Propagating Instabilities in Structures using the STAGS Finite Element Code," with W. Loden, presented at the AMD-MD Summer Conference, UCLA, (1995)

25. "Computer Simulation of Dynamic Buckling Phenomena under Quasi Static Loads," with E. Riks, J. Starnes, and A. Waters, (published where and when?).

26. "The Buckling Behavior of a Central Crack in a Plate under Tension," with E. Riks, Eng. Fracture Mechanics, pp 529-548, 1992.

27. "Applications of the USA-STAGS-CFA Code to Nonlinear Fluid-Structure Interaction Problems in Underwater Shock of Submerged Structures," Proceedings of the 60th Shock and Vibration Symposium, Vol. 1, Virginia Beach, VA, Nov. 1989, pp 121-138.

28. "Damage Propagation in Stiffened Fuselage Shells Containing Cracks," presented at International Workshop on Structural Integrity of Aging Airplanes, April, 1992.

29. "Finite Rotation Analysis and Consistent Linearization Using Projectors," with B. Nour-Omid, Comp. Meth. Appl. Mech. Eng., Vol. 93, pp 353-384, January, 1991.

30. "Bulging Cracks in Pressurized Fuselages: A Procedure for Computation," with E. Riks and F. A. Brogan, in Analytical and Computational Models of Shells, A. K. Noor, T. Belytschko and J. Simo eds., American Society of Mechanical Engineers, New York, 1989.

31. "The Use of Projectors to Improve Finite Element Performance," with Bahram Nour-Omid, Computers & Structures, Vol. 30, pp 257-267, October, 1988.

32. "Analysis of Structural Collapse by the Reduced Basis Technique Using a Mixed Local-Global

Formulation,” with P. Stehlin, LMSC-F035663, Lockheed Palo Alto Research Laboratory, Palo Alto, CA, May, 1986, presented at the 27th AIAA/ASME/ASCE Structures, Structural Dynamics, and Materials Conference, San Antonio, May, 1986.

33. “An Element-Independent Corotational Procedure for the Treatment of Large Rotations,” with F. A. Brogan, ASME J. Pressure Vessel Technology, pp 165-174, May, 1986

34. B. O. Almroth & Charles C. Rankin, “Imperfection Sensitivity of Cylindrical Shells,” in Recent Advances in Engineering Mechanics and their Impact on Civil Engineering Practice, Vol. II, pp 1701-1704, Proceedings of the Fourth Engineering Mechanics Division Specialty Conference, Eds. W.F. Chen and A.D.M Lewis, Published by the American Society of Civil Engineers (New York, 1983)

35. “A Semi-Implicit Dynamic Relaxation Algorithm for Static Nonlinear Structural Analysis,” with K. C. Park, in “Research in Structural and Solid Mechanics – 1982,” compiled by J. M. Housner and A. K. Noor, NASA CP-2245, pp. 1-24.

36. “Transient Response of Soft Bonded Multilayered Shells,” with C. J. Bonner, D. W. Lindow, and P. G. Underwood, AIAA Journal, Vol. 13, No. 3, pp 350-356, 1975.

37. “Classical S-Matrix for Linear Reactive Collisions of H + Cl,” with W. H. Miller, J. Chem. Phys., pp 3150, 1971.

38. “Quantum Solution of Collinear Reactive systems: H + Cl,” with J. C. Light, J. Chem. Phys., pp 1701, 1969.

39. “Relaxation of a Gas of Harmonic Oscillators,” with J. C. Light, Journal of Chemical Physics, pp 1305, 1967.

40. “Statistical Theory of Chemical Kinetics: Application to Neutral Atom Molecule Reactions,” with J. C. Light and P. Pechukas, J. Chem. Phys., pp 794, 1966.

41. “Transient Response of Soft Bonded Multilayered Shells,” with C. J. Bonner, D. W. Lindow, and P. G. Underwood, presented at the 15th SDM conference, AIAA Paper No. 1974-342, 1974..

42. “STAGS Example Problems Manual,” with N. F. Knight, NASA CR-2006-214281, March 2006.

43. “The Computational Structural Mechanics testbed Structural Element Processor ES5: STAGS Shell Element,” with F. A. Brogan, NASA CR-4358, May 1991.

44. “Controlling Progressive Failure Analyses using Artificial Viscous Damping,” with N. F. Knight and F. A. Brogan, AIAA Paper 2001-1180.

45. “Enhancements to the STAGS Computer Code,” with P. Stehlin and F. A. Brogan, NASA CR-4000, November 1986.

46. "STAGS Computational Procedure for Progressive Failure Analysis of Laminated Composite Structures," with N. F. Knight and F. A. Brogan, *International Journal of Non-Linear Mechanics*, Vol. 37, No. 4-5, pp. 833-849 (2002).
47. "Sandwich Modeling with an Application to the Residual Strength Analysis of a Damaged Compression Panel," with E. Riks, *International Journal of Non-Linear Mechanics*, Vol. 37, No. 4-5, pp. 897-908 (2002).
48. "Sandwich Modeling with an Application to the Residual Strength Analysis of a Damaged Compression Panel," with E. Riks, AIAA Paper No. 2001-1323, April 2001.
49. "Numerical Aspects of Shell Stability Analysis", with E. riks and F. A. Brogan, in *Computational Mechanics of Nonlinear Response of Shells*, W. B. Kratzir and E. Onate (eds), Springer-Verlag, Berlin, pp. 125-151, 1990.
50. "110 Mount Element," , with W. C. Perry, Lockheed report LMSC-D062175, 1985.
51. "Enhanced Analysis Capability in USA/STAGS," with T. L. Geers, J. A. Derutz, G. M. Stanley, and W. C. Perry, Lockheed Report No. LMSC-D877665, 1983.
52. "Computational Tools for Stability Analysis," with E. Riks, AIAA Paper No. 1997-1138, presented at the 41st SDM, 1997.
53. "Application of the Thurston Bifurcation Solution strategy to Problems with Modal Interaction," with F. A. Brogan, AIAA Paper No. 1988-2286.
54. "Consistent Linearization of the Element-Independent Corotational Formulation for the Structural Analysis of General Shells," Lockheed Report No. LMSC-F202439, March 1987.
55. "Some Computational Tools for the Analysis of through Cracks in stiffened Fuselage Shells," with F. A. Brogan and E. Riks, *Computational mechanics*, Vol. 13, pp. 143-156, 1993.
56. "An Element-Independent Corotational Procedure for the Treatment of Large Rotations," with F. A. Brogan, in *Collapse Analysis of Structures*, L. Sobel and K. Thomas (eds), pp. 85-100, ASME PVP Vol. 84, (1984).
57. "STAGS User Manual – Version 5.0," with F. A. Brogan, W. A. Logan, H. D. Cabiness, Rhombus Consultants Group, Inc. January 2005. Previously released as LMSC-P032594.
58. "Formulation of Improved Plasticity Calculations in the STAGSC-1 and NICE-SPAR Computer Codes," with G. Stanley and J. Deruntz, Lockheed Report No. LMSC-F183026, 1987.
59. "Improved Plasticity and Imperfections in the STAGSC-1 Computer Code –Phase 2: Implementation," with F. A. Brogan, Lockheed Report No. LMSC-F386402, 1990.

Table 1 Glossary of variables used in the generic case, "tank"
(This is part of the tank.DEF file, created automatically by
the GENOPT processor, GENTEXT, with use of information, variable
names and one-line definitions provided by the GENOPT user.)

C	ARRAY	NUMBER OF	PROMPT	ROLE	NUMBER	NAME	DEFINITION OF VARIABLE
C	?	(ROWS, COLS)	(tank.PRO)				
C	n	(0, 0)	2	10	GRAV	= acceleration of gravity	
C	n	(0, 0)	2	20	DIAVEH	= diameter of launch vehicle	
C	n	(0, 0)	2	30	AFTDIA	= diameter of the aft dome of the tank	
C	n	(0, 0)	2	35	AFTHI	= height of the aft dome of the tank	
C	n	(0, 0)	2	40	FWDDIA	= diameter of the forward dome of the tank	
C	n	(0, 0)	2	45	FWDHI	= height of the forward dome of the tank	
C	n	(0, 0)	2	50	FLTANK	= axial dist. from aft dome apex to fwd dome apex	
C	n	(0, 0)	2	55	ZAPEX	= global axial coordinate of the aft dome apex	
C	n	(0, 0)	2	60	DENPRP	= weight density of the propellant	
C	n	(0, 0)	2	65	ZCG	= global axial coordinate of the tank cg	
C	n	(0, 0)	1	70	THKAFT	= thickness of the tank aft dome skin	
C	n	(0, 0)	1	75	THKMID	= thickness of the tank cylinder skin	
C	n	(0, 0)	1	80	THKFWD	= thickness of the forward tank dome skin	
C	n	(0, 0)	1	90	STRSPC	= spacing of the tank orthogrid stringers	
C	n	(0, 0)	1	95	RNGSPC	= spacing of the tank orthogrid rings	
C	n	(0, 0)	1	100	STRTHK	= thickness of the tank orthogrid stringers	
C	n	(0, 0)	1	105	STRHI	= height of the tank orthogrid stringers	
C	n	(0, 0)	1	110	RNGTHK	= thickness of the tank orthogrid rings	
C	n	(0, 0)	1	115	RNGHI	= height of the tank orthogrid rings	
C	n	(0, 0)	2	125	ETANK	= Young's modulus of the cold tank material	
C	n	(0, 0)	2	130	NUTANK	= Poisson's ratio of the tank material	
C	n	(0, 0)	2	135	DENTNK	= mass density of the tank material	
C	n	(0, 0)	2	140	ALTNK	= coef.thermal expansion of tank material	
C	n	(0, 0)	2	150	IAXIS	= tank is vertical (1) or horizontal (2)	
C	n	(0, 0)	2	160	IZTANK	= strut support ring number in ZTANK(IZTANK)	
C	y	(10, 0)	1	165	ZTANK	= global axial coordinate of tank support ring	
C	y	(10, 0)	1	170	ZGRND	= global axial coordinate of "ground"	
C	y	(10, 0)	2	180	STRTYP	= type of strut arrangement	
C	n	(0, 0)	2	190	INPAIRS	= strut type number in NPAIRS(INPAIRS)	
C	y	(3, 0)	2	195	NPAIRS	= number of strut pairs	
C	y	(3, 0)	2	205	FITTNK	= length of end fitting attached to tank ring	
C	y	(3, 0)	2	210	FEATNK	= axial "EA" stiffness of tank-end strut fitting	
C	y	(3, 0)	2	215	ALFITT	= Coef.of thermal expansion of tank end fitting	
C	y	(3, 0)	2	220	FITVEH	= length of strut end fitting attached to "ground"	
C	y	(3, 0)	2	225	FEAVEH	= axial "EA" stiffness of "ground" end strut fitting	
C	y	(3, 0)	2	230	ALFITV	= coef.of thermal expan. of "ground" end fitting	
C	y	(3, 0)	1	240	ATANK	= circ.angle (deg.) to pinned tank end of strut	
C	y	(3, 0)	1	245	AGRND	= circ.angle to pinned "ground" end of strut	
C	y	(3, 0)	1	255	IDTUBE	= inner diam. of support tube active at launch	
C	y	(3, 0)	2	265	FACLEN	= length factor for strut buckling as a shell	
C	y	(3, 0)	2	270	DTSUP	= Average strut temperature minus ambient	
C	y	(3, 0)	2	275	ODINNR	= outer diam.of the orbital tube assembly	
C	y	(3, 0)	2	280	FLINNR	= Length of the orbital tube assembly	
C	n	(0, 0)	2	285	NTUBES	= Choose 1 or 2 tubes in the orbital tube assembly	
C	n	(0, 0)	2	295	ISTRUT	= index for simple strut (1), "PODS" strut (2)	
C	y	(3, 0)	2	305	WALTYP	= type of wall constructions in strut type STRTYP	
C	n	(0, 0)	1	315	WEBHI	= height of mid-tank T-ring web	
C	n	(0, 0)	1	320	WEBTHK	= thickness of mid-tank T-ring web	
C	n	(0, 0)	1	325	FLGHI	= width (height) of mid-tank T-ring flange	

C	n	(0,	0)	1	330	FLGTHK	= thickness of mid-tank T-ring flange
C	y	(3,	0)	2	340	RNGTYP	= propellant tank reinforcement type
C	n	(0,	0)	2	350	IDUBAXL	= propellant tank reinforcement type number in
DUBAXL(IDUBAXL)								
C	y	(3,	0)	1	355	DUBAXL	= axial length of the propellant tank doubler
C	y	(3,	0)	1	360	DUBTHK	= max.thickness of the propellant tank doubler
C	y	(3,	0)	1	370	TRNGTH	= thickness of the tank reinforcement ring
C	y	(3,	0)	1	375	TRNGHI	= height of the tank reinforcement ring
C	y	(3,	0)	2	380	TRNGE	= hoop modulus of the tank ring
C	y	(3,	0)	2	385	ALRNGT	= coef.of thermal expansion of the tank ring
C	n	(0,	0)	2	395	ITHICK	= thickness index in THICK(ITHICK)
C	y	(15,	0)	1	400	THICK	= thickness of a lamina
C	y	(15,	0)	1	405	ANGLE	= layup angle
C	y	(15,	0)	2	410	MATTYP	= Material type
C	n	(0,	0)	2	420	JLAYTYP	= wall type number in LAYTYP(ILAYTYP,JLAYTYP)
C	n	(0,	0)	2	425	ILAYTYP	= layer number in LAYTYP(ILAYTYP,JLAYTYP)
C	y	(90,	3)	2	430	LAYTYP	= layer type index
C	n	(0,	0)	2	440	IE1	= material type in E1(IE1)
C	y	(3,	0)	2	445	E1	= modulus in the fiber direction
C	y	(3,	0)	2	450	E2	= modulus transverse to fibers
C	y	(3,	0)	2	455	G12	= in-plane shear modulus
C	y	(3,	0)	2	460	NU	= small Poisson's ratio
C	y	(3,	0)	2	465	G13	= x-z out-of-plane shear modulus
C	y	(3,	0)	2	470	G23	= y-z out-of-plane shear modulus
C	y	(3,	0)	2	475	ALPHA1	= coef.of thermal expansion along fibers
C	y	(3,	0)	2	480	ALPHA2	= coef.of thermal expan.transverse to fibers
C	y	(3,	0)	2	485	TEMTUR	= curing delta temperature (positive)
C	y	(3,	0)	2	490	COND1	= conductivity along the fibers
C	y	(3,	0)	2	495	COND2	= conductivity transverse to fibers
C	y	(3,	0)	2	500	DENSTY	= weight density of the material
C	n	(0,	0)	2	510	WGT	= objective=WGT*(empty tank mass) +(1-
WGT)*(conductance)								
C	n	(0,	0)	2	515	TNKNRM	= normalizing empty tank mass
C	n	(0,	0)	2	520	CONNRM	= normalizing total strut conductance
C	n	(0,	0)	2	530	IPHASE	= IPHASE=1=launch phase; IPHASE=2=orbital phase
C	n	(0,	0)	2	540	NCASES	= Number of load cases (number of environments) in
PRESS(NCASES)								
C	y	(20,	0)	3	545	PRESS	= propellant tank ullage pressure
C	y	(20,	0)	3	550	GAXIAL	= quasi-static axial g-loading
C	y	(20,	0)	3	555	GLATRL	= quasi-static lateral g-loading
C	y	(20,	0)	3	560	TNKCOOL	= propellant tank cool-down from cryogen
C	n	(0,	0)	2	570	JFREQ	= vibration mode type in FREQ(NCASES,JFREQ)
C	y	(20,	4)	4	575	FREQ	= modal vibration frequency (cps)
C	y	(20,	4)	5	580	FREQA	= minimum allowable frequency (cps)
C	y	(20,	4)	6	585	FREQF	= factor of safety for frequency
C	n	(0,	0)	2	595	JSTRES1	= stress component number in STRES1(NCASES,JSTRES1)
C	y	(20,	6)	4	600	STRES1	= maximum stress in material 1
C	y	(20,	6)	5	605	STRES1A	= maximum allowable stress in material 1
C	y	(20,	6)	6	610	STRES1F	= factor of safety for stress, matl 1
C	y	(20,	6)	4	615	STRES2	= maximum stress in material 2
C	y	(20,	6)	5	620	STRES2A	= maximum allowable stress in material 2
C	y	(20,	6)	6	625	STRES2F	= factor of safety for stress, matl 2
C	y	(20,	6)	4	630	STRES3	= maximum stress in material 3
C	y	(20,	6)	5	635	STRES3A	= maximum allowable stress in material 3
C	y	(20,	6)	6	640	STRES3F	= factor of safety for stress, matl 3
C	n	(0,	0)	2	645	JCOLBUK	= strut set number (1 for aft-most set) in
COLBUK(NCASES,JCOLBUK)								
C	y	(20,	3)	4	650	COLBUK	= buckling of a strut as a column
C	y	(20,	3)	5	655	COLBUKA	= allowable for column buckling of strut
C	y	(20,	3)	6	660	COLBUKF	= factor of safety for Euler strut buckling
C	y	(20,	3)	4	665	SHLBUK	= buckling of strut as a shell
C	y	(20,	3)	5	670	SHLBUKA	= allowable for shell buckling of strut
C	y	(20,	3)	6	675	SHLBUKF	= factor of safety for shell buckling of strut
C	y	(20,	3)	4	680	FORCE	= launch-hold force in a strut
C	y	(20,	3)	5	685	FORCEA	= maximum allowable launch-hold force in strut

```

C   y   ( 20, 3)   6   690   FORCEF   = factor of safety for launch-hold force
C   y   ( 20, 3)   4   695   TNKSTR  = maximum stress in the propellant tank
C   y   ( 20, 3)   5   700   TNKSTRA = allowable for propellant tank stress
C   y   ( 20, 3)   6   705   TNKSTRF = factor of safety for tank stress
C   y   ( 20, 3)   4   710   TNKBUK  = propellant tank buckling load factor
C   y   ( 20, 3)   5   715   TNKBUKA = allowable for propellant tank buckling
C   y   ( 20, 3)   6   720   TNKBUKF = factor of safety for tank buckling
C   n   (  0, 0)   7   730   CONDCT  = WGTxTOTMAS/TNKNRM +(1-WGT)xCONDCT/CONNRM
C=====

```

**Table 2 Input data for the GENOPT processor, BEGIN (test.BEG file)
(These input data are provided by the End user for the specific
case called “test”; See Figs. 1 – 3.)**

```

=====
      N          $ Do you want a tutorial session and tutorial output?
386.4000      $ acceleration of gravity: GRAV
      300      $ diameter of launch vehicle: DIAVEH
      200      $ diameter of the aft dome of the tank: AFTDIA
      50       $ height of the aft dome of the tank: AFTHI
      200      $ diameter of the forward dome of the tank: FWDDIA
      50       $ height of the forward dome of the tank: FWDHI
      400      $ axial dist. from aft dome apex to fwd dome apex: FLTANK
      100      $ global axial coordinate of the aft dome apex: ZAPEX
0.2560000E-02 $ weight density of the propellant: DENPRP
      300      $ global axial coordinate of the tank cg: ZCG
0.1000000    $ thickness of the tank aft dome skin: THKAFT
0.1000000    $ thickness of the tank cylinder skin: THKMID
0.1000000    $ thickness of the forward tank dome skin: THKFWD
      10       $ spacing of the tank orthogrid stringers: STRSPC
      10       $ spacing of the tank orthogrid rings: RNGSPC
0.5000000    $ thickness of the tank orthogrid stringers: STRTHK
      1        $ height of the tank orthogrid stringers: STRHI
0.5000000    $ thickness of the tank orthogrid rings: RNGTHK
      1        $ height of the tank orthogrid rings: RNGHI
0.1000000E+08 $ Young's modulus of the cold tank material: ETANK
0.3000000    $ Poisson's ratio of the tank material: NUTANK
0.2500000E-03 $ mass density of the tank material: DENTNK
0.1000000E-04 $ coef.thermal expansion of tank material: ALTNK
      1        $ tank is vertical (1) or horizontal (2): IAXIS
      2        $ Number IZTANK of rows in the array ZTANK: IZTANK
      150     $ global axial coordinate of tank support ring: ZTANK( 1)
      450     $ global axial coordinate of tank support ring: ZTANK( 2)
      50      $ global axial coordinate of "ground": ZGRND( 1)
      550     $ global axial coordinate of "ground": ZGRND( 2)
      1        $ type of strut arrangement: STRTYP( 1)
      2        $ type of strut arrangement: STRTYP( 2)
      2        $ Number INPAIRS of rows in the array NPAIRS: INPAIRS
      4        $ number of strut pairs: NPAIRS( 1)
      4        $ number of strut pairs: NPAIRS( 2)
      5        $ length of end fitting attached to tank ring: FITTNK( 1)

```

```

5          $ length of end fitting attached to tank ring: FITTNK( 2)
0.1000000E+08 $ axial "EA" stiffness of tank-end strut fitting: FEATNK( 1)
0.1000000E+08 $ axial "EA" stiffness of tank-end strut fitting: FEATNK( 2)
0.1000000E-04 $ Coef.of thermal expansion of tank end fitting: ALFITT( 1)
0.1000000E-04 $ Coef.of thermal expansion of tank end fitting: ALFITT( 2)
5          $ length of strut end fitting attached to "ground": FITVEH( 1)
5          $ length of strut end fitting attached to "ground": FITVEH( 2)
0.1000000E+08 $ axial "EA" stiffness of "ground" end strut fitting: FEAVEH( 1)
0.1000000E+08 $ axial "EA" stiffness of "ground" end strut fitting: FEAVEH( 2)
0.1000000E-04 $ coef.of thermal expan. of "ground" end fitting: ALFITV( 1)
0.1000000E-04 $ coef.of thermal expan. of "ground" end fitting: ALFITV( 2)
10         $ circ.angle (deg.) to pinned tank end of strut: ATANK( 1)
10         $ circ.angle (deg.) to pinned tank end of strut: ATANK( 2)
25         $ circ.angle to pinned "ground" end of strut: AGRND( 1)
25         $ circ.angle to pinned "ground" end of strut: AGRND( 2)
5          $ inner diam. of support tube active at launch: IDTUBE( 1)
5          $ inner diam. of support tube active at launch: IDTUBE( 2)
0.1000000    $ length factor for strut buckling as a shell: FACLEN( 1)
0.1000000    $ length factor for strut buckling as a shell: FACLEN( 2)
-100        $ Average strut temperature minus ambient: DTSUP( 1)
-100        $ Average strut temperature minus ambient: DTSUP( 2)
2           $ outer diam.of the orbital tube assembly: ODINNR( 1)
2           $ outer diam.of the orbital tube assembly: ODINNR( 2)
4           $ Length of the orbital tube assembly: FLINNR( 1)
4           $ Length of the orbital tube assembly: FLINNR( 2)
1           $ Choose 1 or 2 tubes in the orbital tube assembly: NTUBES
1           $ index for simple strut (1), "PODS" strut (2): ISTRUT
1           $ type of wall constructions in strut type STRTYP: WALTYP( 1)
2           $ type of wall constructions in strut type STRTYP: WALTYP( 2)
0.000001    $ height of mid-tank T-ring web: WEBHI
0.000001    $ thickness of mid-tank T-ring web: WEBTHK
0.000001    $ width (height) of mid-tank T-ring flange: FLGHI
0.000001    $ thickness of mid-tank T-ring flange: FLGTHK
1           $ propellant tank reinforcement type: RNGTHYP( 1)
1           $ propellant tank reinforcement type: RNGTHYP( 2)
1           $ Number IDUBAXL of rows in the array DUBAXL: IDUBAXL
30          $ axial length of the propellant tank doubler: DUBAXL( 1)
0.1000000    $ max.thickness of the propellant tank doubler: DUBTHK( 1)
0.2000000    $ thickness of the tank reinforcement ring: TRNGTH( 1)
1.000000    $ height of the tank reinforcement ring: TRNGHI( 1)
0.1000000E+08 $ hoop modulus of the tank ring: TRNGE( 1)
0.1000000E-04 $ coef.of thermal expansion of the tank ring: ALRNGT( 1)
12          $ Number ITHICK of rows in the array THICK: ITHICK
0.1000000    $ thickness of a lamina: THICK( 1)
0.1000000    $ thickness of a lamina: THICK( 2)
0.1000000    $ thickness of a lamina: THICK( 3)
0.1000000    $ thickness of a lamina: THICK( 4)
0.1000000    $ thickness of a lamina: THICK( 5)
0.1000000    $ thickness of a lamina: THICK( 6)
0.1000000    $ thickness of a lamina: THICK( 7)
0.1000000    $ thickness of a lamina: THICK( 8)
0.1000000    $ thickness of a lamina: THICK( 9)
0.1000000    $ thickness of a lamina: THICK( 10)

```

```

0.1000000    $ thickness of a lamina: THICK( 11)
0.1000000    $ thickness of a lamina: THICK( 12)
  45         $ layup angle: ANGLE(  1)
 -45         $ layup angle: ANGLE(  2)
  45         $ layup angle: ANGLE(  3)
 -45         $ layup angle: ANGLE(  4)
  45         $ layup angle: ANGLE(  5)
 -45         $ layup angle: ANGLE(  6)
  45         $ layup angle: ANGLE(  7)
 -45         $ layup angle: ANGLE(  8)
  45         $ layup angle: ANGLE(  9)
 -45         $ layup angle: ANGLE( 10)
  45         $ layup angle: ANGLE( 11)
 -45         $ layup angle: ANGLE( 12)
   1         $ Material type: MATTYP(  1)
   1         $ Material type: MATTYP(  2)
   1         $ Material type: MATTYP(  3)
   1         $ Material type: MATTYP(  4)
   1         $ Material type: MATTYP(  5)
   1         $ Material type: MATTYP(  6)
   1         $ Material type: MATTYP(  7)
   1         $ Material type: MATTYP(  8)
   1         $ Material type: MATTYP(  9)
   1         $ Material type: MATTYP( 10)
   1         $ Material type: MATTYP( 11)
   1         $ Material type: MATTYP( 12)
   2         $ Number JLAYTYP of columns in the array, LAYTYP: JLAYTYP
  12         $ Number ILAYTYP of rows in this column of LAYTYP: ILAYTYP
   1         $ layer type index: LAYTYP(  1,  1)
   2         $ layer type index: LAYTYP(  2,  1)
   3         $ layer type index: LAYTYP(  3,  1)
   4         $ layer type index: LAYTYP(  4,  1)
   5         $ layer type index: LAYTYP(  5,  1)
   6         $ layer type index: LAYTYP(  6,  1)
   6         $ layer type index: LAYTYP(  7,  1)
   5         $ layer type index: LAYTYP(  8,  1)
   4         $ layer type index: LAYTYP(  9,  1)
   3         $ layer type index: LAYTYP( 10,  1)
   2         $ layer type index: LAYTYP( 11,  1)
   1         $ layer type index: LAYTYP( 12,  1)
  12         $ Number ILAYTYP of rows in this column of LAYTYP: ILAYTYP
   7         $ layer type index: LAYTYP(  1,  2)
   8         $ layer type index: LAYTYP(  2,  2)
   9         $ layer type index: LAYTYP(  3,  2)
  10         $ layer type index: LAYTYP(  4,  2)
  11         $ layer type index: LAYTYP(  5,  2)
  12         $ layer type index: LAYTYP(  6,  2)
  12         $ layer type index: LAYTYP(  7,  2)
  11         $ layer type index: LAYTYP(  8,  2)
  10         $ layer type index: LAYTYP(  9,  2)
   9         $ layer type index: LAYTYP( 10,  2)
   8         $ layer type index: LAYTYP( 11,  2)
   7         $ layer type index: LAYTYP( 12,  2)

```

```

1          $ Number IE1      of rows in the array  E1: IE1
0.2100000E+08 $ modulus in the fiber direction: E1( 1)
1600000.    $ modulus transverse to fibers: E2( 1)
679000.0    $ in-plane shear modulus: G12( 1)
0.2300000E-01 $ small Poisson's ratio: NU( 1)
627000.0    $ x-z out-of-plane shear modulus: G13( 1)
334000.0    $ y-z out-of-plane shear modulus: G23( 1)
0.1000000E-05 $ coef.of thermal expansion along fibers: ALPHA1( 1)
0.1000000E-04 $ coef.of thermal expan.transverse to fibers: ALPHA2( 1)
170         $ curing delta temperature (positive): TEMTUR( 1)
0.7270000E-02 $ conductivity along the fibers: COND1( 1)
0.4370000E-02 $ conductivity transverse to fibers: COND2( 1)
0.5700000E-01 $ weight density of the material: DENSTY( 1)
0.5000000    $ objective=WGT*(empty tank mass) +(1-WGT)*(conductance): WGT
10.00000    $ normalizing empty tank mass: TNKNRM
0.2000000E-02 $ normalizing total strut conductance: CONNRM
1           $ IPHASE=1=launch phase; IPHASE=2=orbital phase: IPHASE
2           $ Number NCASES  of load cases (environments): NCASES
25.00000    $ propellant tank ullage pressure: PRESS( 1)
25.00000    $ propellant tank ullage pressure: PRESS( 2)
10          $ quasi-static axial g-loading: GAXIAL( 1)
0           $ quasi-static axial g-loading: GAXIAL( 2)
0           $ quasi-static lateral g-loading: GLATRL( 1)
10          $ quasi-static lateral g-loading: GLATRL( 2)
-200.0000   $ propellant tank cool-down from cryogen: TNKCOOL( 1)
-200.0000   $ propellant tank cool-down from cryogen: TNKCOOL( 2)
4           $ Number JFREQ    of columns in the array, FREQ: JFREQ
10          $ minimum allowable frequency (cps): FREQA( 1, 1)
10          $ minimum allowable frequency (cps): FREQA( 2, 1)
10          $ minimum allowable frequency (cps): FREQA( 1, 2)
10          $ minimum allowable frequency (cps): FREQA( 2, 2)
10          $ minimum allowable frequency (cps): FREQA( 1, 3)
10          $ minimum allowable frequency (cps): FREQA( 2, 3)
10          $ minimum allowable frequency (cps): FREQA( 1, 4)
10          $ minimum allowable frequency (cps): FREQA( 2, 4)
1.200000    $ factor of safety for frequency: FREQF( 1, 1)
1.200000    $ factor of safety for frequency: FREQF( 2, 1)
1.200000    $ factor of safety for frequency: FREQF( 1, 2)
1.200000    $ factor of safety for frequency: FREQF( 2, 2)
1.200000    $ factor of safety for frequency: FREQF( 1, 3)
1.200000    $ factor of safety for frequency: FREQF( 2, 3)
1.200000    $ factor of safety for frequency: FREQF( 1, 4)
1.200000    $ factor of safety for frequency: FREQF( 2, 4)
5           $ Number JSTRES1 of columns in the array, STRES1: JSTRES1
140571      $ maximum allowable stress in material 1: STRES1A( 1, 1)
140571      $ maximum allowable stress in material 1: STRES1A( 2, 1)
104714      $ maximum allowable stress in material 1: STRES1A( 1, 2)
104714      $ maximum allowable stress in material 1: STRES1A( 2, 2)
10557       $ maximum allowable stress in material 1: STRES1A( 1, 3)
10557       $ maximum allowable stress in material 1: STRES1A( 2, 3)
14529       $ maximum allowable stress in material 1: STRES1A( 1, 4)
14529       $ maximum allowable stress in material 1: STRES1A( 2, 4)
6290        $ maximum allowable stress in material 1: STRES1A( 1, 5)

```

```

6290      $ maximum allowable stress in material 1: STRES1A( 2, 5)
1.500000 $ factor of safety for stress, matl 1: STRES1F( 1, 1)
1.500000 $ factor of safety for stress, matl 1: STRES1F( 2, 1)
1.500000 $ factor of safety for stress, matl 1: STRES1F( 1, 2)
1.500000 $ factor of safety for stress, matl 1: STRES1F( 2, 2)
1.500000 $ factor of safety for stress, matl 1: STRES1F( 1, 3)
1.500000 $ factor of safety for stress, matl 1: STRES1F( 2, 3)
1.500000 $ factor of safety for stress, matl 1: STRES1F( 1, 4)
1.500000 $ factor of safety for stress, matl 1: STRES1F( 2, 4)
1.500000 $ factor of safety for stress, matl 1: STRES1F( 1, 5)
1.500000 $ factor of safety for stress, matl 1: STRES1F( 2, 5)
140571    $ maximum allowable stress in material 2: STRES2A( 1, 1)
140571    $ maximum allowable stress in material 2: STRES2A( 2, 1)
104714    $ maximum allowable stress in material 2: STRES2A( 1, 2)
104714    $ maximum allowable stress in material 2: STRES2A( 2, 2)
10557     $ maximum allowable stress in material 2: STRES2A( 1, 3)
10557     $ maximum allowable stress in material 2: STRES2A( 2, 3)
14529     $ maximum allowable stress in material 2: STRES2A( 1, 4)
14529     $ maximum allowable stress in material 2: STRES2A( 2, 4)
6290      $ maximum allowable stress in material 2: STRES2A( 1, 5)
6290      $ maximum allowable stress in material 2: STRES2A( 2, 5)
1.500000 $ factor of safety for stress, matl 2: STRES2F( 1, 1)
1.500000 $ factor of safety for stress, matl 2: STRES2F( 2, 1)
1.500000 $ factor of safety for stress, matl 2: STRES2F( 1, 2)
1.500000 $ factor of safety for stress, matl 2: STRES2F( 2, 2)
1.500000 $ factor of safety for stress, matl 2: STRES2F( 1, 3)
1.500000 $ factor of safety for stress, matl 2: STRES2F( 2, 3)
1.500000 $ factor of safety for stress, matl 2: STRES2F( 1, 4)
1.500000 $ factor of safety for stress, matl 2: STRES2F( 2, 4)
1.500000 $ factor of safety for stress, matl 2: STRES2F( 1, 5)
1.500000 $ factor of safety for stress, matl 2: STRES2F( 2, 5)
140571    $ maximum allowable stress in material 3: STRES3A( 1, 1)
140571    $ maximum allowable stress in material 3: STRES3A( 2, 1)
104714    $ maximum allowable stress in material 3: STRES3A( 1, 2)
104714    $ maximum allowable stress in material 3: STRES3A( 2, 2)
10557     $ maximum allowable stress in material 3: STRES3A( 1, 3)
10557     $ maximum allowable stress in material 3: STRES3A( 2, 3)
14529     $ maximum allowable stress in material 3: STRES3A( 1, 4)
14529     $ maximum allowable stress in material 3: STRES3A( 2, 4)
6290      $ maximum allowable stress in material 3: STRES3A( 1, 5)
6290      $ maximum allowable stress in material 3: STRES3A( 2, 5)
1.500000 $ factor of safety for stress, matl 3: STRES3F( 1, 1)
1.500000 $ factor of safety for stress, matl 3: STRES3F( 2, 1)
1.500000 $ factor of safety for stress, matl 3: STRES3F( 1, 2)
1.500000 $ factor of safety for stress, matl 3: STRES3F( 2, 2)
1.500000 $ factor of safety for stress, matl 3: STRES3F( 1, 3)
1.500000 $ factor of safety for stress, matl 3: STRES3F( 2, 3)
1.500000 $ factor of safety for stress, matl 3: STRES3F( 1, 4)
1.500000 $ factor of safety for stress, matl 3: STRES3F( 2, 4)
1.500000 $ factor of safety for stress, matl 3: STRES3F( 1, 5)
1.500000 $ factor of safety for stress, matl 3: STRES3F( 2, 5)
2         $ Number JCOLBUK of columns in the array, COLBUK: JCOLBUK
1         $ allowable for column buckling of strut: COLBUKA( 1, 1)

```

```

1      $ allowable for column buckling of strut: COLBUKA( 2, 1)
1      $ allowable for column buckling of strut: COLBUKA( 1, 2)
1      $ allowable for column buckling of strut: COLBUKA( 2, 2)
1      $ factor of safety for Euler strut buckling: COLBUKF( 1, 1)
1      $ factor of safety for Euler strut buckling: COLBUKF( 2, 1)
1      $ factor of safety for Euler strut buckling: COLBUKF( 1, 2)
1      $ factor of safety for Euler strut buckling: COLBUKF( 2, 2)
1      $ allowable for shell buckling of strut: SHLBUKA( 1, 1)
1      $ allowable for shell buckling of strut: SHLBUKA( 2, 1)
1      $ allowable for shell buckling of strut: SHLBUKA( 1, 2)
1      $ allowable for shell buckling of strut: SHLBUKA( 2, 2)
2      $ factor of safety for shell buckling of strut: SHLBUKF( 1, 1)
2      $ factor of safety for shell buckling of strut: SHLBUKF( 2, 1)
2      $ factor of safety for shell buckling of strut: SHLBUKF( 1, 2)
2      $ factor of safety for shell buckling of strut: SHLBUKF( 2, 2)
15000 $ maximum allowable launch-hold force in strut: FORCEA( 1, 1)
15000 $ maximum allowable launch-hold force in strut: FORCEA( 2, 1)
15000 $ maximum allowable launch-hold force in strut: FORCEA( 1, 2)
15000 $ maximum allowable launch-hold force in strut: FORCEA( 2, 2)
1      $ factor of safety for launch-hold force: FORCEF( 1, 1)
1      $ factor of safety for launch-hold force: FORCEF( 2, 1)
1      $ factor of safety for launch-hold force: FORCEF( 1, 2)
1      $ factor of safety for launch-hold force: FORCEF( 2, 2)
50000.00 $ allowable for propellant tank stress: TNKSTRA( 1, 1)
50000.00 $ allowable for propellant tank stress: TNKSTRA( 2, 1)
50000.00 $ allowable for propellant tank stress: TNKSTRA( 1, 2)
50000.00 $ allowable for propellant tank stress: TNKSTRA( 2, 2)
1      $ factor of safety for tank stress: TNKSTRF( 1, 1)
1      $ factor of safety for tank stress: TNKSTRF( 2, 1)
1      $ factor of safety for tank stress: TNKSTRF( 1, 2)
1      $ factor of safety for tank stress: TNKSTRF( 2, 2)
1      $ allowable for propellant tank buckling: TNKBUKA( 1, 1)
1      $ allowable for propellant tank buckling: TNKBUKA( 2, 1)
1      $ allowable for propellant tank buckling: TNKBUKA( 1, 2)
1      $ allowable for propellant tank buckling: TNKBUKA( 2, 2)
1      $ factor of safety for tank buckling: TNKBUKF( 1, 1)
1      $ factor of safety for tank buckling: TNKBUKF( 2, 1)
1      $ factor of safety for tank buckling: TNKBUKF( 1, 2)
1      $ factor of safety for tank buckling: TNKBUKF( 2, 2)
=====

```

Table 3 Feasible Optimum Designs for the Long Propellant Tank with 3, 4 and 5 Pairs of Struts at Each of 2 Axial Locations (Dimensions in inches and degrees. These optimum designs were obtained after the August 2012 and February 2013 updates to the "tank" software, struct.tank and behavior.tank.)

Decision Variable	3 strut pairs	4 strut pairs	5 strut pairs
THKAFT	1.030E-01	6.133E-02	5.509E-02
THKMID	5.488E-02	5.453E-02	5.308E-02
THKFWD	4.807E-02	5.825E-02	4.904E-02
STRSPC	9.202E+00	7.891E+00	6.772E+00
RNGSPC	9.515E+00	7.907E+00	6.467E+00
STRTHK	2.341E-01	2.601E-01	2.569E-01
STRHI	5.355E-01	6.714E-01	6.119E-01
RNGTHK	2.329E-01	4.095E-01	4.510E-01
RNGHI	5.355E-01	6.714E-01	6.119E-01
ZTANK(1)	1.500E+02	1.500E+02	1.500E+02
ZTANK(2)	4.500E+02	4.500E+02	4.500E+02
ZGRND(1)	7.753E+01	8.672E+01	9.860E+01
ZGRND(2)	5.350E+02	5.142E+02	5.025E+02
ATANK(1)	6.186E+00	6.000E+00	6.000E+00
ATANK(2)	6.173E+00	6.001E+00	6.000E+00
AGRND(1)	5.719E+01	4.500E+01	3.599E+01
AGRND(2)	6.000E+01	4.499E+01	3.600E+01
IDTUBE(1)	6.481E+00	5.617E+00	5.128E+00
IDTUBE(2)	7.080E+00	5.981E+00	5.409E+00
DUBAXL(1)	3.000E+01	3.000E+01	3.000E+01
DUBTHK(1)	5.308E-01	7.272E-01	7.817E-01
TRNGTH(1)	9.484E-02	3.218E-01	4.793E-01
TRNGHI(1)	4.742E-01	1.609E+00	2.396E+00
THICK(1)	8.017E-03	7.049E-03	6.406E-03
THICK(7)	7.899E-03	6.695E-03	6.045E-03
ANGLE(1)	1.003E+01	1.002E+01	1.000E+01
ANGLE(3)	1.003E+01	1.002E+01	1.119E+01
ANGLE(5)	1.003E+01	4.854E+01	4.883E+01
ANGLE(7)	1.000E+01	1.000E+01	1.108E+01
ANGLE(9)	1.000E+01	1.000E+01	1.111E+01
ANGLE(11)	1.000E+01	4.980E+01	4.903E+01
Objective = WGTxTOTMAS/TNKNRM + (1-WGT)xCONDCT/CONNRM			
with WGT = 0.5, TNKNRM = 10.0 lb-sec ² /inch, CONNRM = 0.002 BTU/hr-deg.R			
Objective	7.305E-01	9.099E-01	1.049E+00
TOTMAS	7.9226E+00	1.0473E+01	1.1246E+01
CONDCT	1.3377E-03	1.5450E-03	1.9469E-03

Table 4 Behaviors of Feasible Optimum Designs for the Long Propellant Tank with 3, 4 and 5 Pairs of Struts at Each of 2 Axial Locations. These behaviors correspond to the optimum designs that were obtained after the August 2012 and February 2013 updates to the "tank" software, struct.tank and behavior.tank. See the previous table.)

Behavior	3 strut pairs	4 strut pairs	5 strut pairs
Load Case 1:			
FREQ(1,1)	1.297E+01	1.213E+01	1.234E+01
FREQ(1,2)	1.285E+01	1.205E+01	1.277E+01
FREQ(1,3)	1.287E+01	1.316E+01	1.331E+01
FREQ(1,4)	1.323E+01	1.337E+01	1.345E+01
STRES1(1,1)	8.599E+03	5.854E+03	5.632E+03
STRES1(1,2)	2.516E+04	2.493E+04	2.496E+04
STRES1(1,3)	4.301E+03	4.258E+03	4.257E+03
STRES1(1,4)	8.493E+01	1.000E-10	1.000E-10
STRES1(1,5)	6.380E+02	1.000E+03	1.001E+03
STRES2(1,1)	4.178E+04	6.137E+04	6.210E+04
STRES2(1,2)	9.007E+03	1.052E+04	1.051E+04
STRES2(1,3)	5.059E+03	6.534E+03	6.539E+03
STRES2(1,4)	9.131E+02	1.000E-10	1.000E-10
STRES2(1,5)	1.235E+03	3.438E+03	3.626E+03
COLBUK(1,1)	2.556E+00	2.368E+00	2.899E+00
COLBUK(1,2)	5.369E+03	1.256E+04	1.221E+04
SHLBUK(1,1)	3.420E+00	4.392E+00	4.340E+00
SHLBUK(1,2)	8.180E+01	1.365E+02	1.389E+02
FORCE(1,1)	6.808E+03	7.446E+03	8.520E+03
FORCE(1,2)	1.574E+04	1.489E+04	1.458E+04
TNKSTR(1,1)	5.215E+04	4.983E+04	4.999E+04
TNKSTR(1,2)	5.216E+04	4.983E+04	4.999E+04
TNKBUK(1,1)	6.194E+00	1.874E+01	1.955E+01
TNKBUK(1,2)	6.192E+00	1.874E+01	1.955E+01
Load Case 2:			
FREQ(2,1)	1.194E+01	1.205E+01	1.227E+01
FREQ(2,2)	1.197E+01	1.209E+01	1.266E+01
FREQ(2,3)	1.280E+01	1.315E+01	1.330E+01
FREQ(2,4)	1.322E+01	1.336E+01	1.344E+01
STRES1(2,1)	4.786E+04	7.228E+04	7.407E+04
STRES1(2,2)	2.980E+04	3.823E+04	2.716E+04
STRES1(2,3)	5.201E+03	6.952E+03	7.053E+03

STRES1(2,4)	1.079E+03	1.000E-10	1.000E-10
STRES1(2,5)	1.351E+03	4.108E+03	4.213E+03
STRES2(2,1)	4.523E+04	7.095E+04	7.368E+04
STRES2(2,2)	2.628E+04	3.772E+04	2.781E+04
STRES2(2,3)	5.138E+03	6.972E+03	7.060E+03
STRES2(2,4)	9.999E+02	1.000E-10	1.000E-10
STRES2(2,5)	1.297E+03	3.915E+03	4.226E+03
COLBUK(2,1)	1.988E+00	1.428E+00	2.597E+00
COLBUK(2,2)	2.440E+00	1.624E+00	2.729E+00
SHLBUK(2,1)	2.659E+00	2.648E+00	3.888E+00
SHLBUK(2,2)	2.953E+00	2.419E+00	3.646E+00
FORCE(2,1)	4.690E+03	6.904E+03	8.202E+03
FORCE(2,2)	1.379E+04	1.436E+04	1.426E+04
TNKSTR(2,1)	5.173E+04	5.046E+04	4.955E+04
TNKSTR(2,2)	5.172E+04	5.046E+04	4.955E+04
TNKBUK(2,1)	1.698E+01	1.446E+01	1.222E+01
TNKBUK(2,2)	1.707E+01	1.446E+01	1.222E+01

=====

Table 5 Feasible Optimum Designs for the Short Propellant Tank with 3, 4 and 5 Pairs of Struts Attached at the Midlength of the Tank
(Dimensions in inches and degrees. These optimum designs were obtained after the August 2012 and February 2013 updates to the "tank" software, struct.tank and behavior.tank.)

Decision Variable	3 strut pairs	4 strut pairs	5 strut pairs
THKAFT	2.619E-02	2.220E-02	5.315E-02
THKMID	6.518E-02	7.152E-02	1.089E-01
THKFWD	2.827E-02	3.031E-02	3.638E-02
STRSPC	3.000E+00	3.000E+00	3.000E+00
RNGSPC	4.370E+00	3.003E+00	3.519E+00
STRTHK	1.444E-01	1.557E-01	1.464E-01
STRHI	9.977E-01	1.000E+00	5.449E-01
RNGTHK	2.635E-01	1.579E-01	1.763E-01
RNGHI	9.977E-01	1.000E+00	5.449E-01
ZTANK(1)	1.750E+02	1.750E+02	1.750E+02
ZGRND(1)	9.595E+01	1.067E+02	1.059E+02
ATANK(1)	6.000E+00	6.000E+00	6.000E+00
AGRND(1)	5.357E+01	4.500E+01	3.600E+01
IDTUBE(1)	5.853E+00	5.177E+00	4.630E+00
DUBAXL(1)	3.000E+01	3.000E+01	3.000E+01
DUBTHK(1)	1.517E-01	1.852E-01	5.590E-01
TRNGTH(1)	1.000E-01	1.000E-01	4.041E-01
TRNGHI(1)	5.000E-01	5.000E-01	2.021E+00
THICK(1)	5.730E-03	5.587E-03	5.782E-03
ANGLE(1)	1.358E+01	1.264E+01	1.139E+01
ANGLE(3)	1.000E+01	1.000E+01	1.162E+01
ANGLE(5)	6.121E+01	6.532E+01	8.000E+01
Objective = WGTxTOTMAS/TNKNRM +(1-WGT)xCONDCT/CONNRM with WGT = 0.5, TNKNRM = 3.0 lb-sec ² /inch, CONNRM = 0.0006 BTU/hr-deg.R			
Objective	1.139E+00	1.214E+00	1.367E+00
TOTMAS	4.6626E+00	4.6609E+00	4.8641E+00
CONDCT	3.9246E-04	5.2505E-04	6.6764E-04

Table 6 Behaviors of Feasible Optimum Designs for the Short Propellant Tank with 3, 4 and 5 Pairs of Struts Attached at the Tank Midlength. (These behaviors correspond to the optimum designs that were obtained after the August 2012 and February 2013 updates to the "tank" software, struct.tank and behavior.tank. See the previous table.)

Behavior	3 strut pairs	4 strut pairs	5 strut pairs
Load Case 1:			
FREQ(1,1)	1.349E+01	1.582E+01	1.834E+01
FREQ(1,2)	1.263E+01	1.375E+01	1.280E+01
FREQ(1,3)	4.270E+01	4.216E+01	4.919E+01
FREQ(1,4)	4.050E+01	4.092E+01	4.726E+01
STRES1(1,1)	4.637E+03	5.179E+03	6.524E+03
STRES1(1,2)	3.933E+04	3.518E+04	3.026E+04
STRES1(1,3)	4.246E+03	4.247E+03	4.243E+03
STRES1(1,4)	1.000E-10	1.000E-10	1.000E-10
STRES1(1,5)	1.290E+03	1.042E+03	4.516E+02
COLBUK(1,1)	1.165E+00	1.438E+00	1.847E+00
SHLBUK(1,1)	2.324E+00	2.869E+00	3.831E+00
FORCE(1,1)	3.208E+03	2.408E+03	1.727E+03
TNKSTR(1,1)	5.020E+04	5.036E+04	4.997E+04
TNKBUK(1,1)	2.410E+01	1.504E+01	1.179E+01
Load Case 2:			
FREQ(2,1)	1.284E+01	1.378E+01	1.713E+01
FREQ(2,2)	1.203E+01	1.201E+01	1.195E+01
FREQ(2,3)	4.257E+01	4.172E+01	4.886E+01
FREQ(2,4)	4.045E+01	4.065E+01	4.701E+01
STRES1(2,1)	5.713E+04	5.412E+04	4.722E+04
STRES1(2,2)	4.514E+04	4.872E+04	4.952E+04
STRES1(2,3)	7.039E+03	7.043E+03	7.054E+03
STRES1(2,4)	1.000E-10	1.000E-10	1.000E-10
STRES1(2,5)	2.357E+03	1.868E+03	7.472E+02
COLBUK(2,1)	1.008E+00	9.991E-01	1.022E+00
SHLBUK(2,1)	2.010E+00	1.994E+00	2.121E+00
FORCE(2,1)	3.208E+03	2.408E+03	1.727E+03
TNKSTR(2,1)	5.021E+04	5.034E+04	5.044E+04
TNKBUK(2,1)	3.782E+01	3.533E+01	8.574E+00

Table 7 Comparisons between predictions from STAGS and from GENOPT/TANK for the earlier optimized long propellant tank with aft (Lower) and forward (Upper) sets of struts, 4 pairs of struts in each set. (The earlier optimum design is that obtained before the August 2012 and February 2013 updates to the GENOPT/TANK software, behavior.tank and struct.tank. This earlier optimum design is listed in the section entitled: “Section 10. DECISION VARIABLE CANDIDATES FOR THE OPTIMIZED SPECIFIC CASE CALLED “test”: THE LONG PROPELLANT TANK WITH TWO SETS OF STRUTS, AFT AND FORWARD, 4 PAIRS OF STRUTS IN EACH SET”)

=====

(a) Comparison of major-mass modes (modes in which there is significant strut extension/compression) followed by shell deformation modes (modes in which there is much less strut energy):

Mode Description	Vibration Frequency (Hz)	
	STAGS	GENOPT/TANK
Tank axial motion	13.46	12.06
Tank lateral-pitching mode 1	12.19 and 13.90	12.16
Tank lateral-pitching mode 2	16.25	15.28
Tank rolling motion	15.92 and 19.82	17.79
n=2 circ. waves tank shell deformation	13.02	13.24
n=3 circ. waves tank shell deformation	12.19 and 13.90	13.33
n=4 circ. waves tank shell deformation	15.92 and 16.19	16.68

(b) Comparison of Strut Forces from Load Case 1 and Load Case 2:

1. Load Case 1: 10G axial acceleration + 25psi internal pressure + tank cool-down

Strut	Value	Strut Forces (lbs.)	
		STAGS	GENOPT/TANK
Lower (aft)	Max.	-24611	-22693
	Min.	-24841	
Upper (forward)	Max.	53035	53554
	Min.	52767	

2. Load Case 2: 10G lateral acceleration + 25psi internal pressure + tank cool-down

Strut	Value	Strut Forces (lbs.)	
		STAGS	GENOPT/TANK
Lower (aft)	Max.	64401	60463
	Min.	-36298	-39393
Upper (forward)	Max.	65057	60471
	Min.	-38568	-40611

(c) Comparison of maximum strut stresses from Load Case 1 and Load Case 2:

1. Load Case 1: 10G axial acceleration + 25psi internal pressure + tank cool-down

Strut	Direction	Sense	Stress (psi)	
			STAGS	GENOPT/TANK
Lower (aft)	Fiber	Tension	973	4724
		Compression	23318	22060
	Transverse	Tension	510	4240
		Compression	816	0
	Shear	n/a	1216	914
	Upper (forward)	Fiber	Tension	43607
Compression			4088	14160
Transverse		Tension	2288	6671
		Compression	327	0
Shear		n/a	1881	2328

2. Load Case 2: 10G lateral acceleration + 25psi internal pressure + tank cool-down

Strut	Direction	Sense	Stress (psi)	
			STAGS	GENOPT/TANK
Lower (aft)	Fiber	Tension	61017	63980
		Compression	34391	37110
	Transverse	Tension	2135	7016
		Compression	1334	0
	Shear	n/a	3182	3659
	Upper (forward)	Fiber	Tension	53763
Compression			31873	34380
Transverse		Tension	2807	7035
		Compression	1664	0
Shear		n/a	2307	2584

(d) Comparison of struts buckling as columns:

Strut	Load Case	Compressive Load (lbs.)	Buckling Load Factor	
			STAGS (does not include tank flexibility)	GENOPT/TANK (does not include tank flexibility)
Lower (aft)	10G Axial	24841	3.99	4.163
	10G Lateral	36298	2.74	2.398
Upper (forward)	10G Axial	Tension	n/a	n/a
	10G Lateral	38568	3.00	2.645

(e) Comparison of struts buckling as thin shells:

Strut	Load Case	Compressive Load (lbs.)	Buckling Load Factor	
			STAGS	GENOPT/TANK
Lower (aft)	10G Axial	24841	4.73	5.314
	10G Lateral	36298	3.24	3.095
Upper (forward)	10G Axial	Tension	n/a	n/a
	10G Lateral	38568	3.65	3.210

(f) Comparison of strut forces in the Launch Hold condition:

Strut	Strut Force (lbs.)	
	STAGS	GENOPT/TANK
Lower (aft)	11157	7317
Upper (forward)	18143	14390

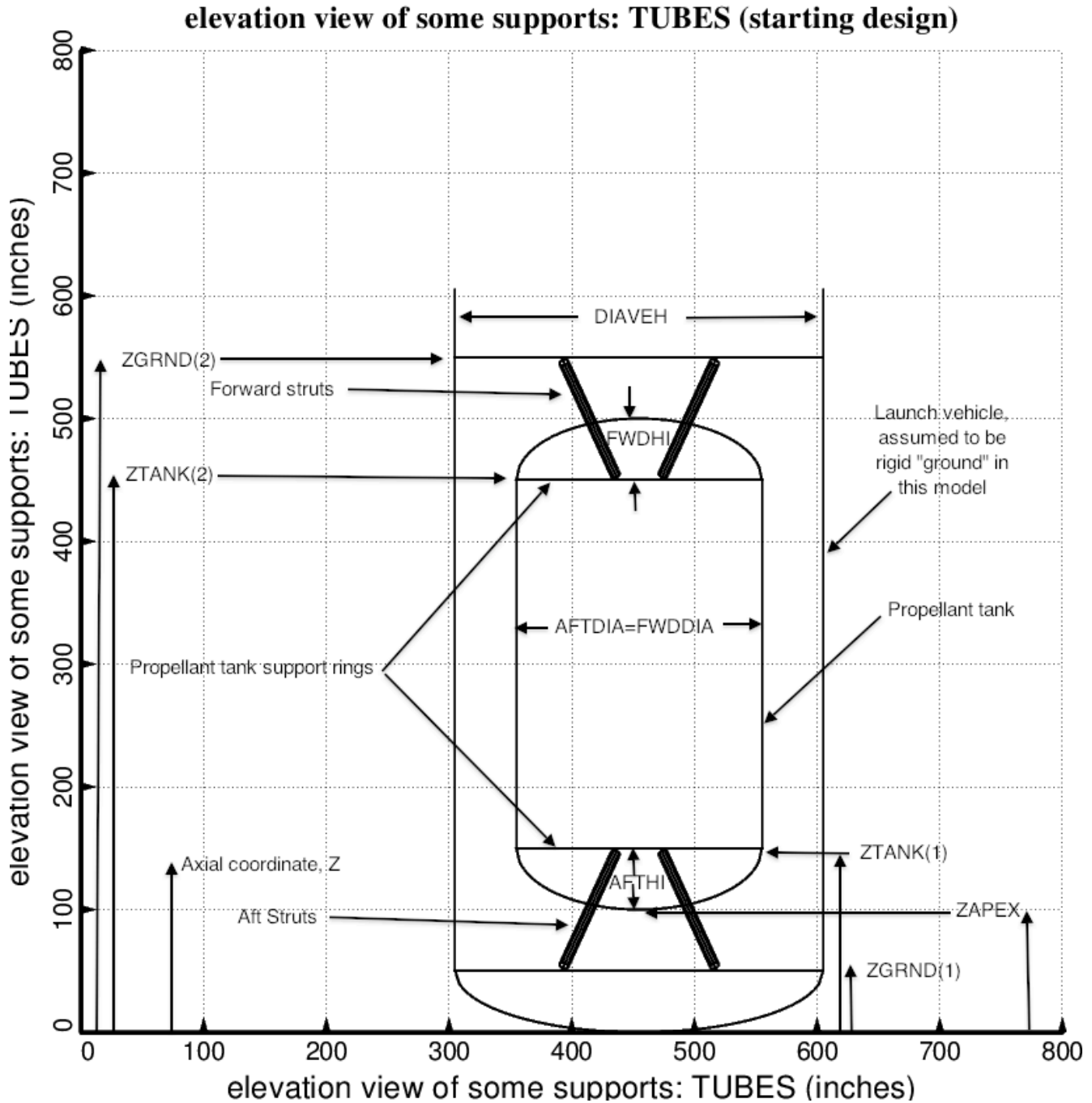


Fig. 1a **Starting design of the long propellant tank with two sets of struts, aft and forward**, with 4 pairs of struts in each of these two sets. Compare with the optimized configuration shown in Fig. 4. (NOTE: In this elevation view of the starting design only one of the four pairs of struts is displayed at each of the aft and forward axial locations. See Fig. 2 for the plan view of all four pairs of struts at the aft axial location and Fig. 3 for those at the forward axial location.) The GENOPT-user-created names of several of the decision variable candidates are given. These decision variable candidates are defined in Tables 1 and 2. The end domes of the propellant tank are 2:1 ellipsoidal shells in the particular cases described here, but may have any ratios of major to minor axes.

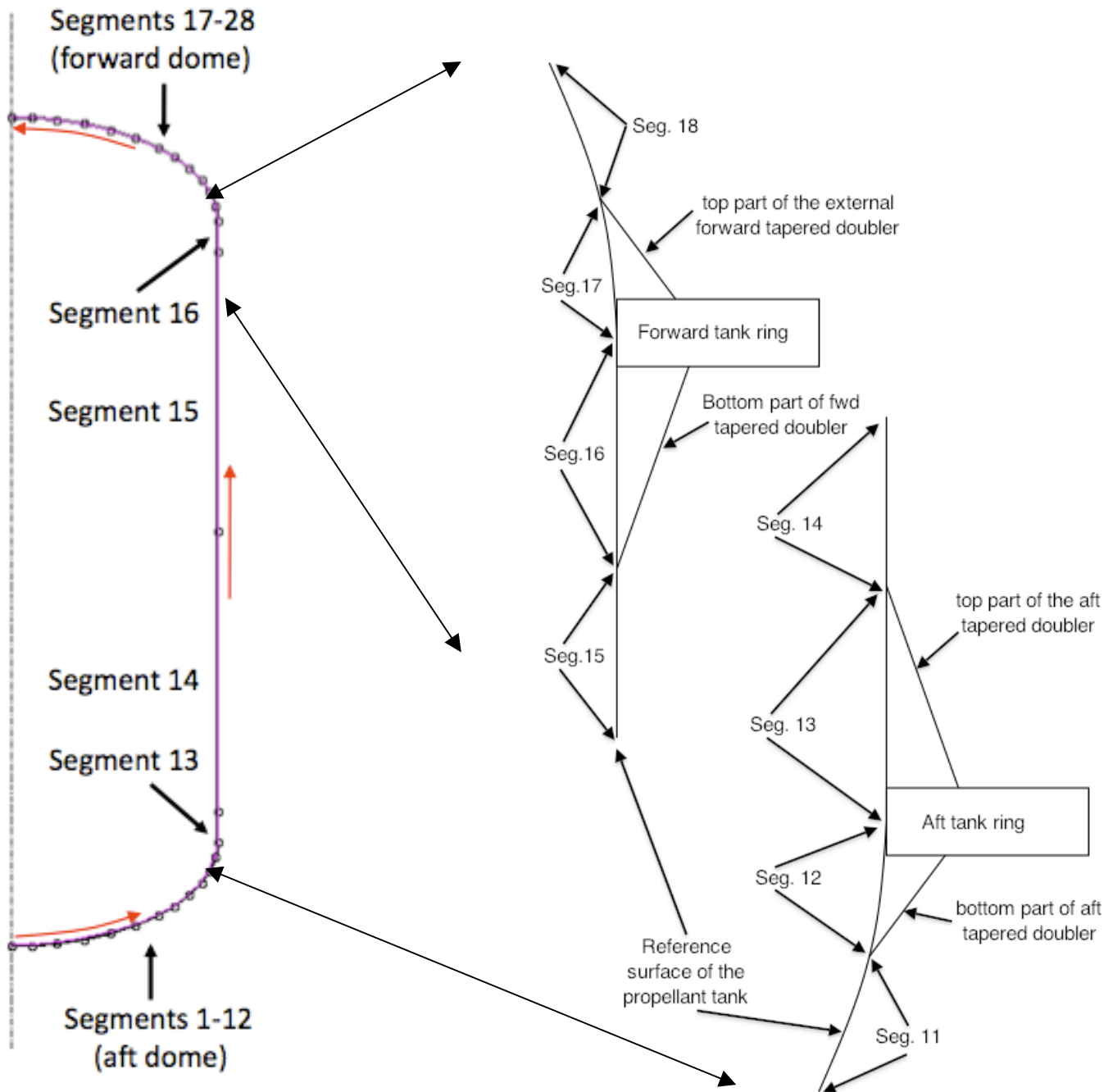


Fig. 1b **BIGBOSOR4 model of the propellant tank.** This tank model contains 28 shell segments. The points shown in the leftmost image lie on the shell reference surface. These points indicate **only the end points of each shell segment** in the model. Each shell segment contains many nodal points, as follows: 13 nodal points in each of Segments 1 – 13 and 16 – 28, and 53 nodal points in each of Segments 14 and 15 (the two long cylindrical segments of the propellant tank). Red arrows indicate the direction of increasing arc length along the meridian of the tank. Images on the right-hand side: details of the forward and aft reinforcements where the struts are attached to the centroids of the forward and aft external propellant tank support rings.

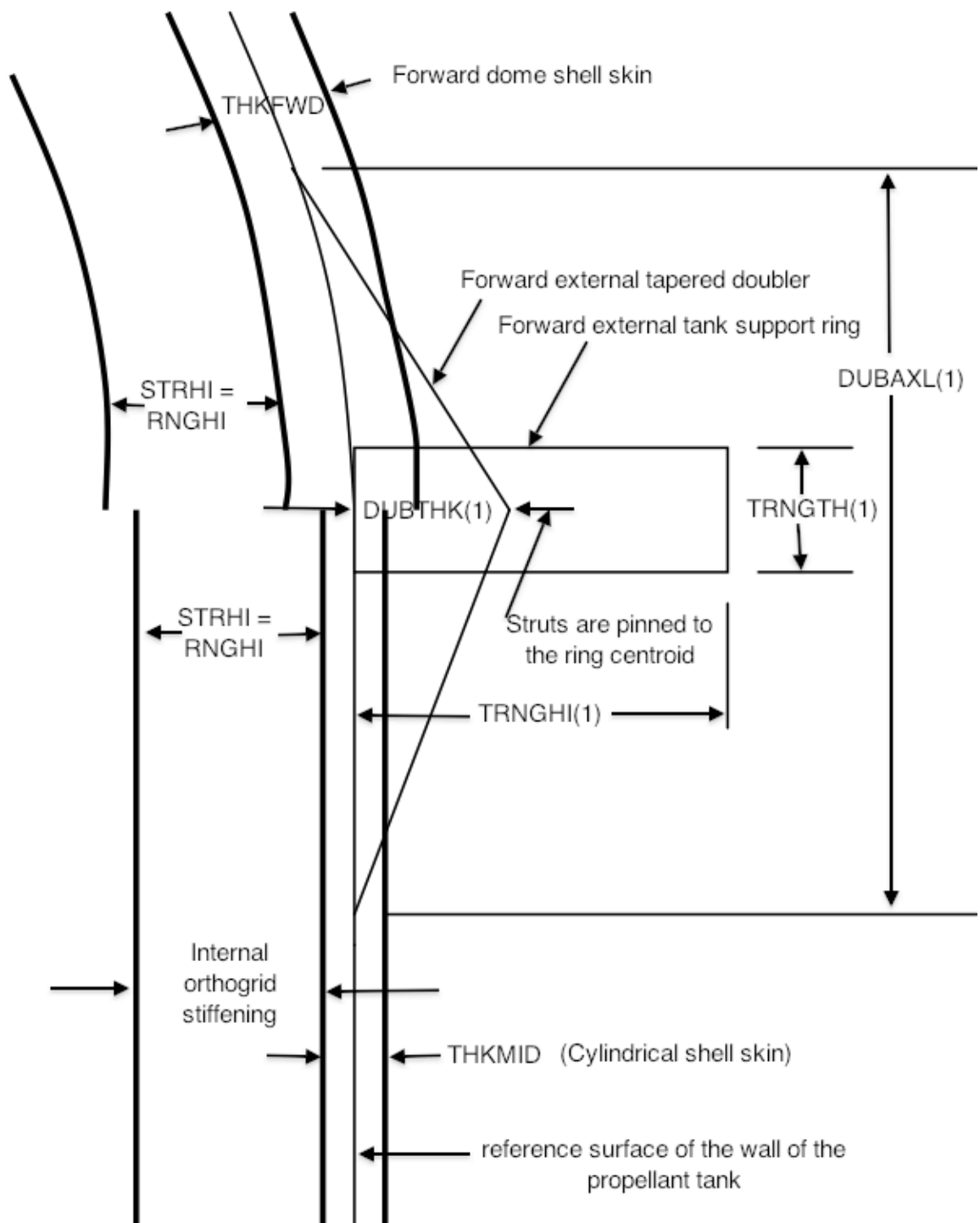


Fig. 1c Configuration of the forward part of the propellant tank in the neighborhood of the forward cylinder/dome junction. The names of several of the decision variable candidates are given. (See Tables 1, 2.)

Plan view of AFT set of supports: TUBES (starting design)

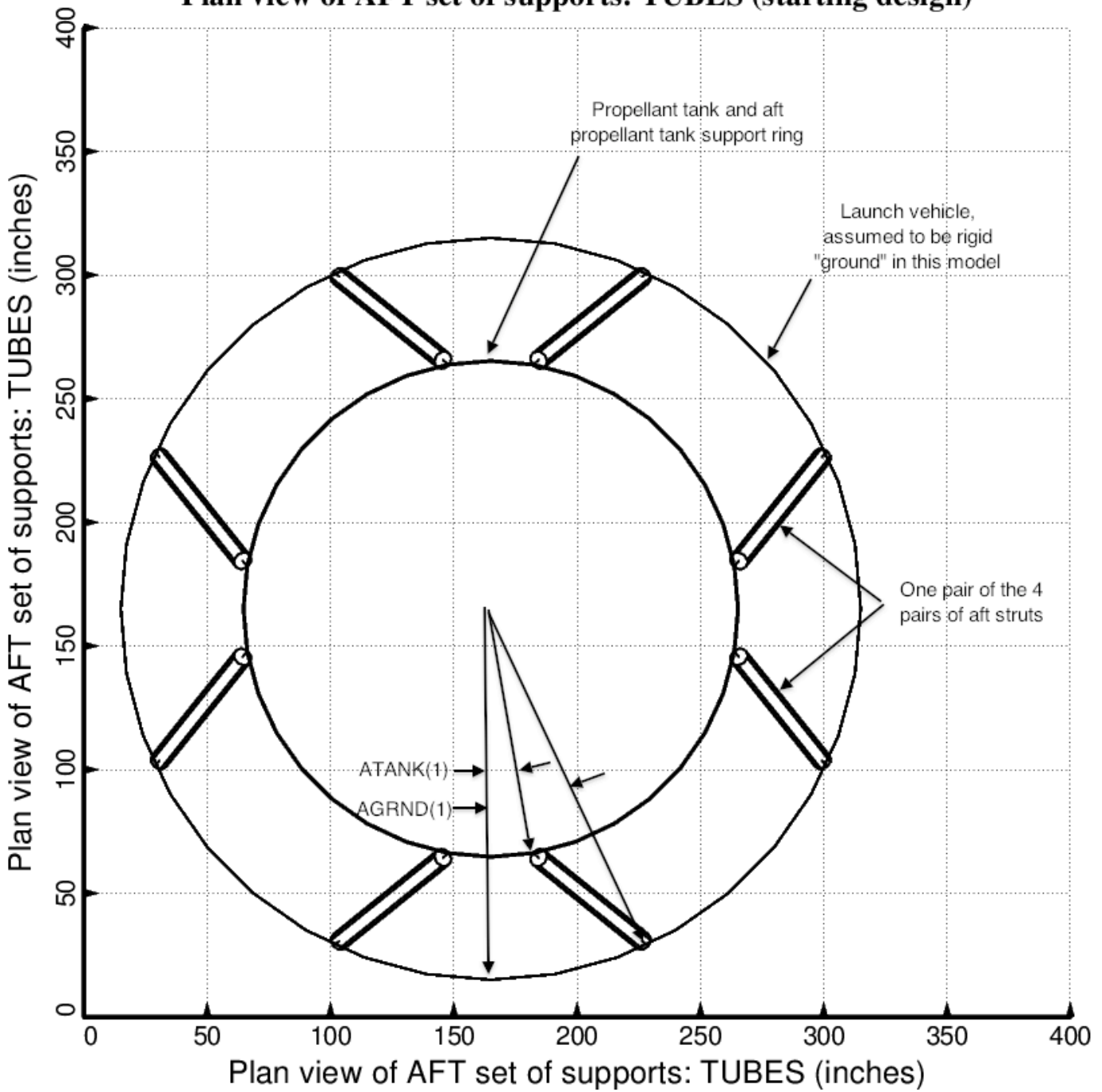


Fig. 2 Starting design of the long propellant tank with two sets of struts, aft and forward, with 4 pairs of struts in each of these two sets. Shown here is a plan view of the starting design of the **aft** set of struts. Compare with the optimized configuration shown in Fig. 5. See Tables 1 and 2 for the definitions of ATANK and AGRND.

Plan view of FWD set of supports: TUBES (starting design)

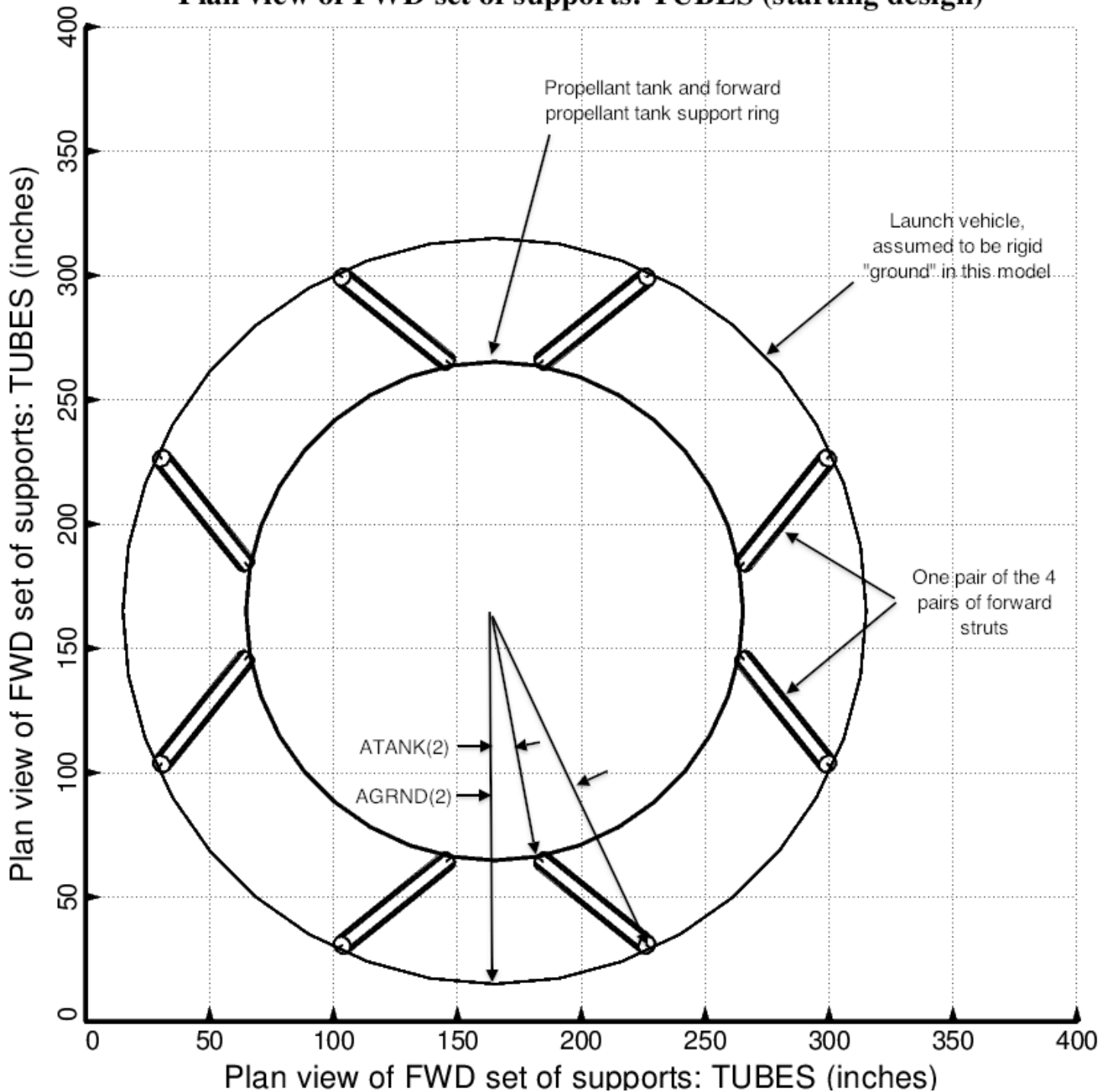


Fig. 3 **Starting design of the long propellant tank with two sets of struts, aft and forward**, with 4 pairs of struts in each of these two sets. Shown here is the plan view of the starting design of the **forward** set of struts. Compare with the optimized configuration shown in Fig. 6. See Tables 1 and 2 for the definitions of ATANK and AGRND.

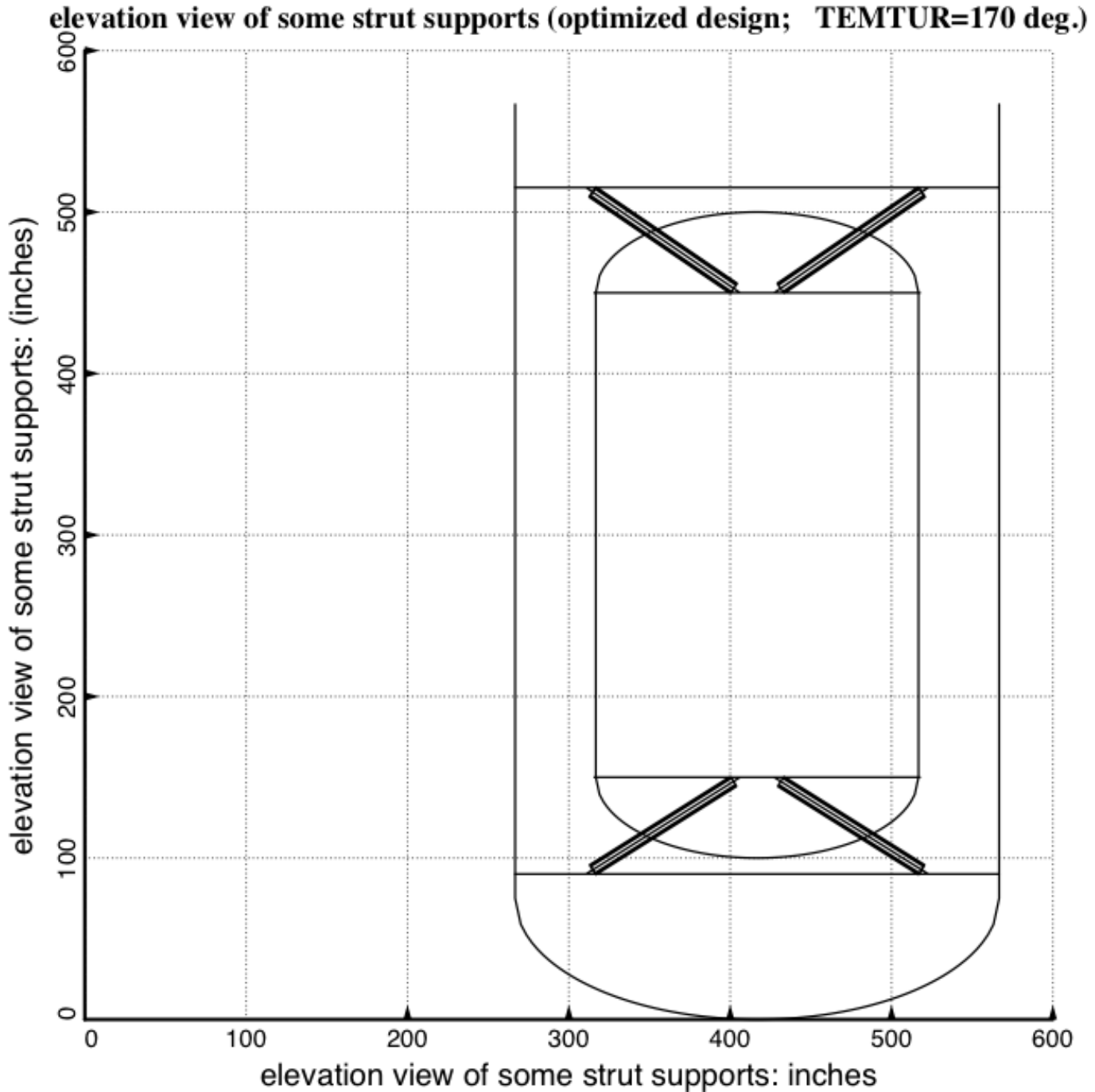


Fig. 4 **Optimized design of the long propellant tank with two sets of struts, aft and forward**, with 4 pairs of struts in each of these two sets. Compare with the starting configuration shown in Fig. 1a. (NOTE: In this elevation view only one of the four pairs of struts is displayed at each axial location, aft and forward). This optimum design was found with use of the “temporary” (varying density) versions of bosdec (bosdec.density.var) and addbosor4 (addbosor4.density.var). “Temporary” means that the density including the mass of the propellant “lumped” into the propellant tank shell wall varies along a shell segment meridian.

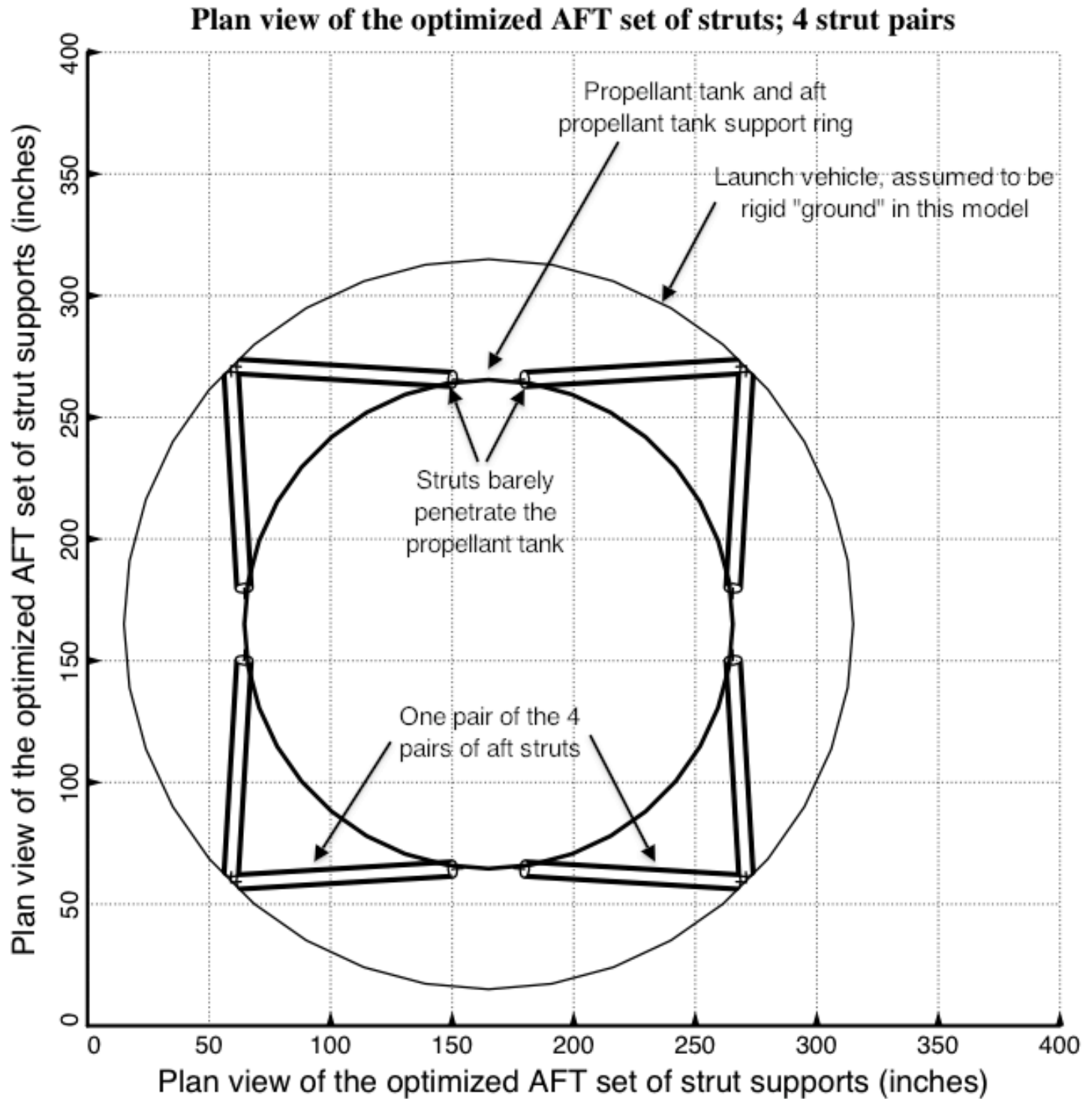


Fig. 5 **Optimized design of the long propellant tank with two sets of struts, aft and forward**, with 4 pairs of struts in each of these two sets. Shown here is a plan view of the optimized **aft** set of 4 pairs of struts. Compare with the starting configuration shown in Fig. 2. This optimum design was found with use of the “temporary” (varying density) versions of bosdec (bosdec.density.var) and addbosor4 (addbosor4.density.var).

Plan view of FWD set of supports (optimized configuration; TEMTUR=170 deg.)

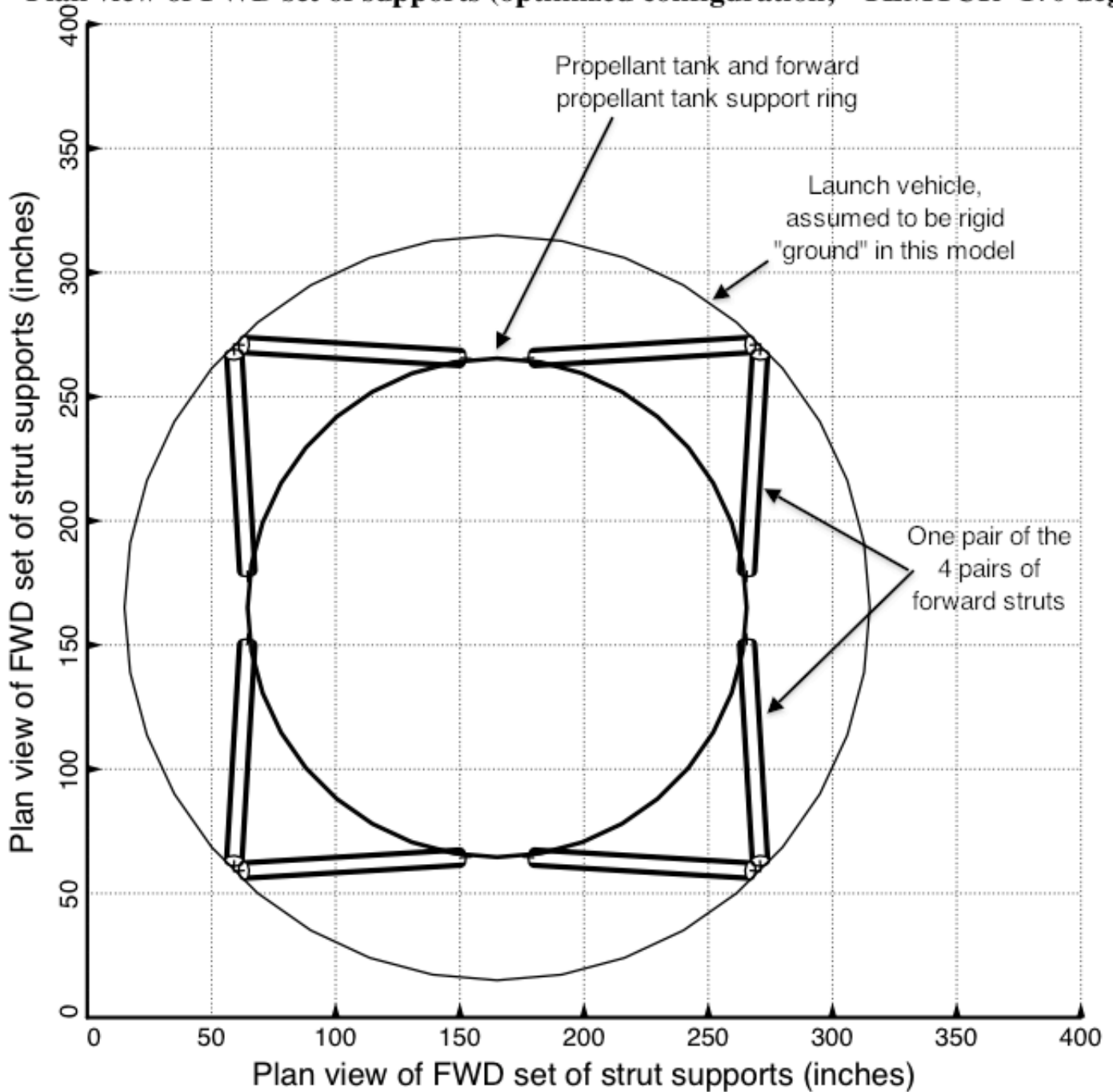


Fig. 6 **Optimized design of the long propellant tank with two sets of struts, aft and forward**, with 4 pairs of struts in each of these two sets. Shown here is the plan view of the optimized **forward** set of struts. Compare with the starting configuration shown in Fig. 3. This optimum design was found with use of the “temporary” (varying density) versions of bosdec (bosdec.density.var) and addbosor4 (addbosor4.density.var).

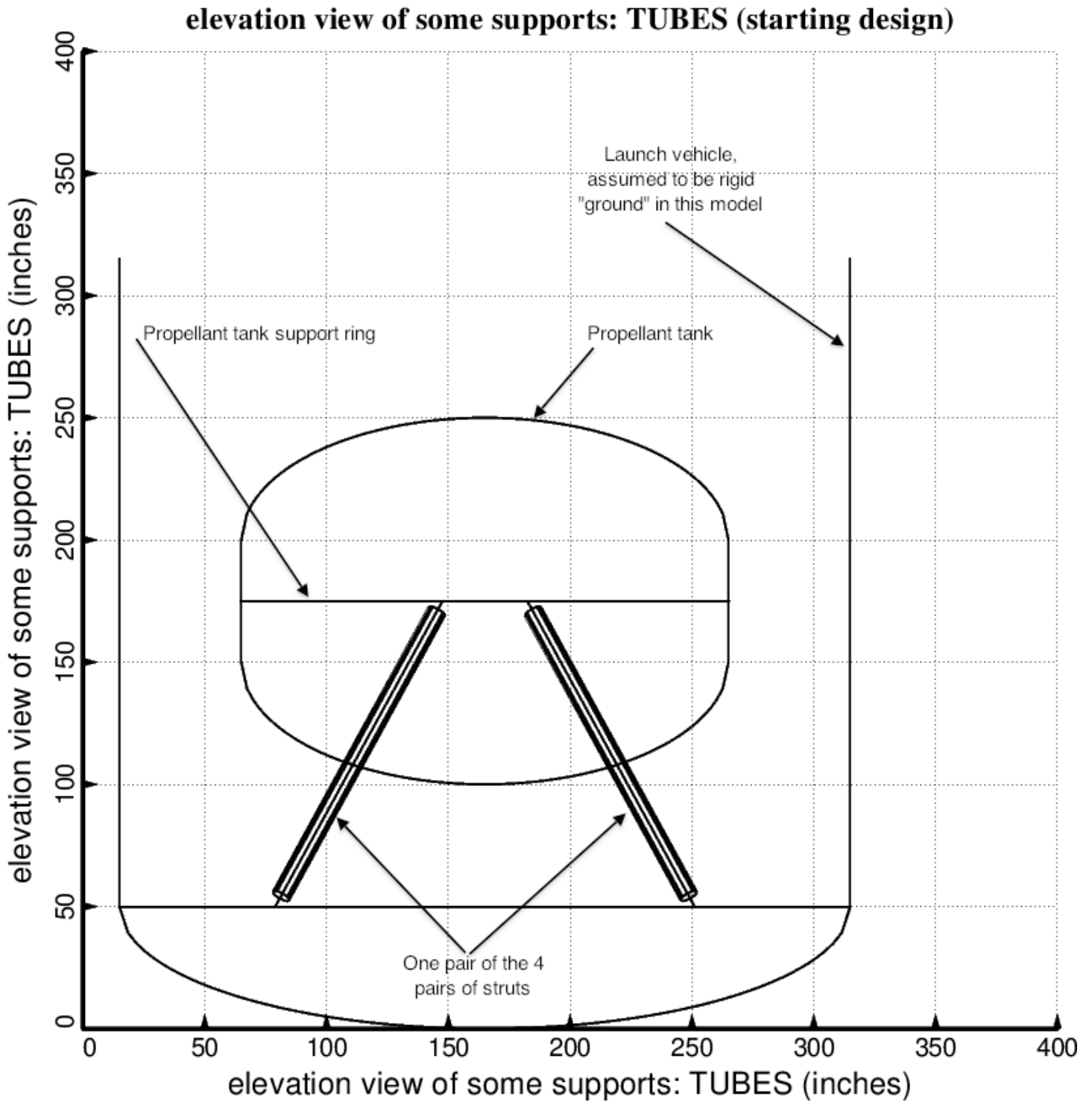


Fig. 7 **Starting design of the short propellant tank with one set of struts**, called “aft”, with 4 pairs of struts in this one set. Compare with the optimized configuration shown in Fig. 9. (NOTE: In this elevation view only one of the four pairs of struts is displayed)

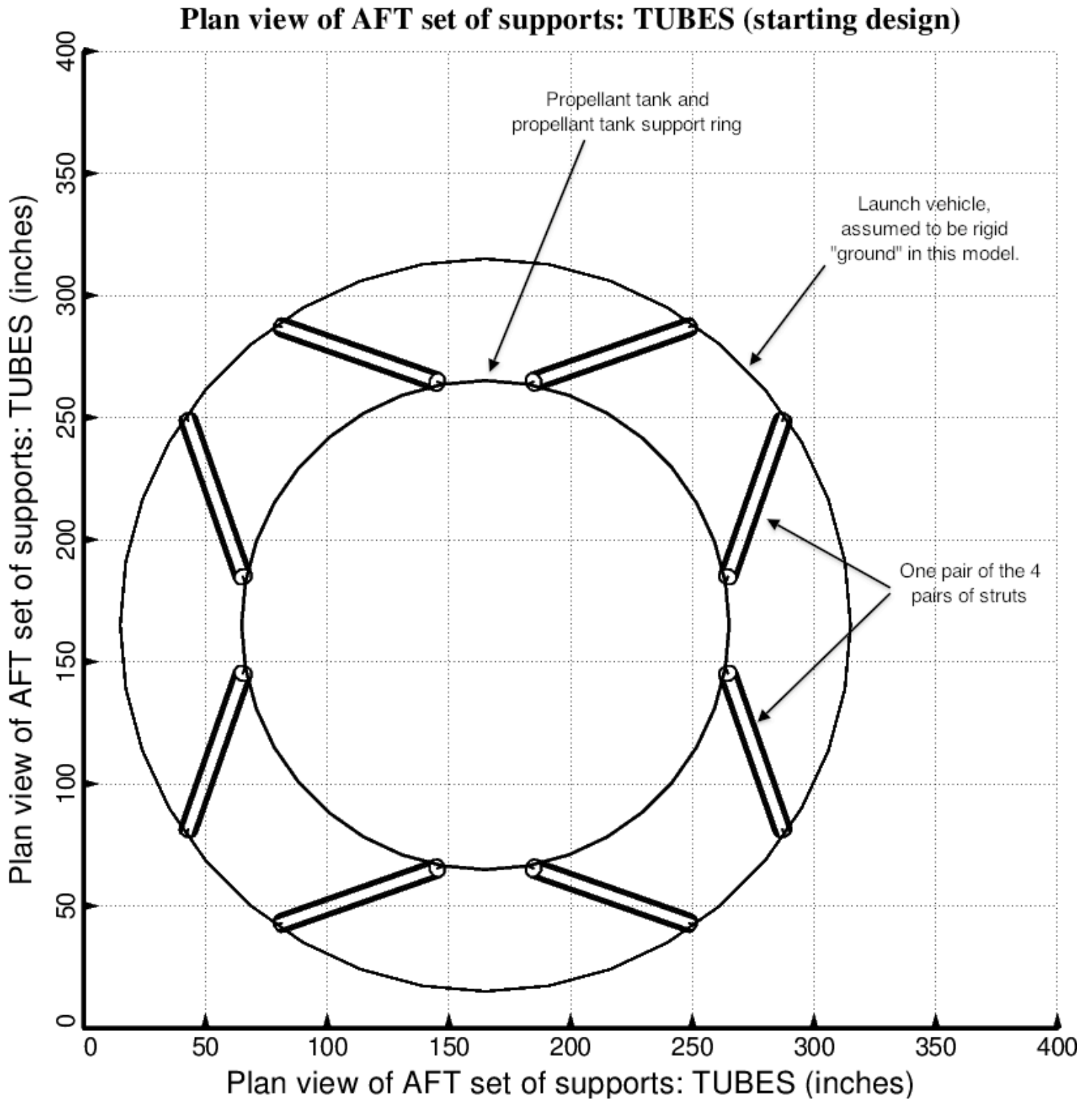


Fig. 8 Starting design of the short propellant tank with one set of struts, called “aft”, with 4 pairs of struts in this one set. Compare with the optimized configuration shown in Fig. 10.

elevation view of some supports (optimized configuration; TEMTUR=170 deg.)

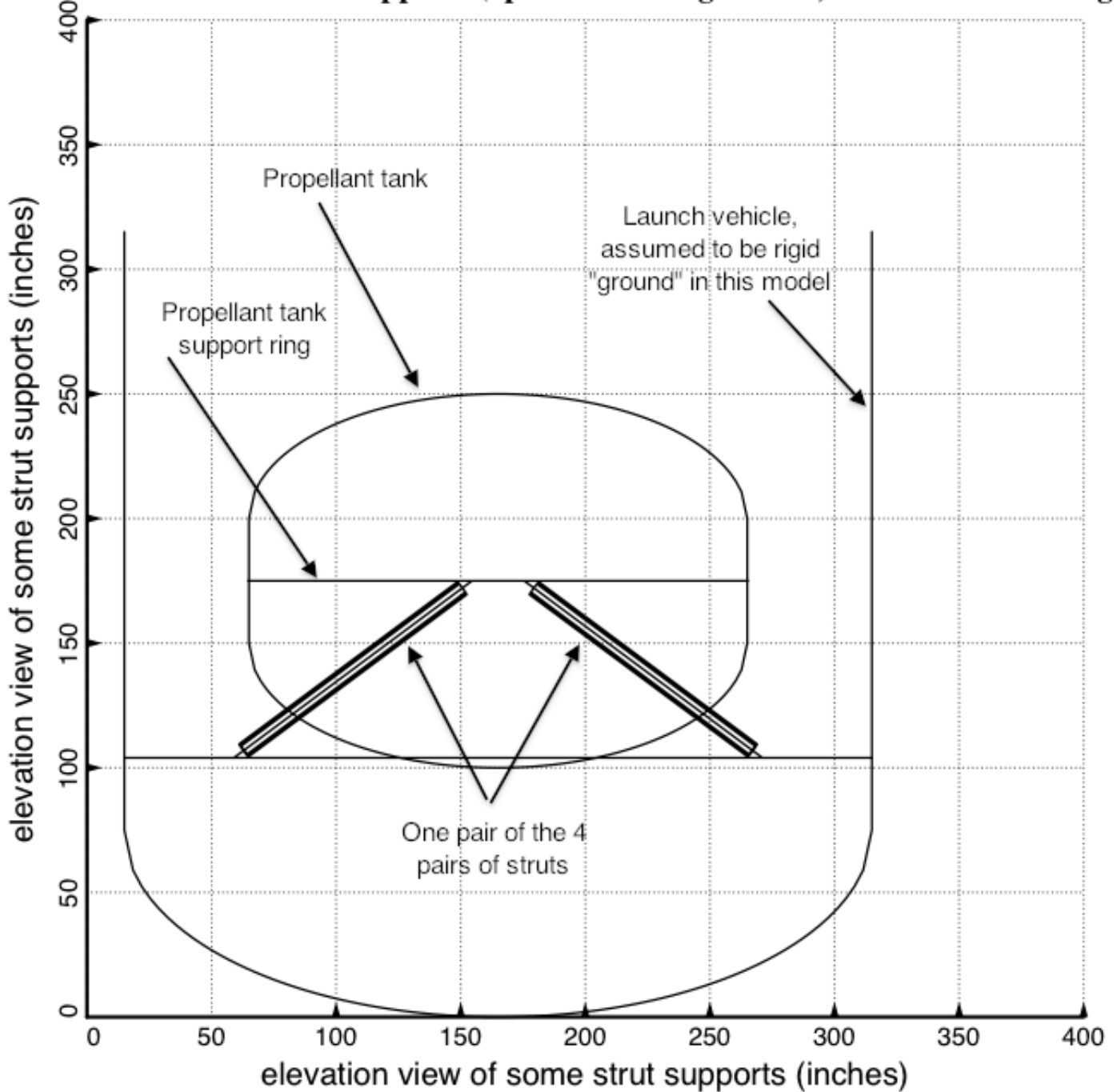


Fig. 9 **Optimized design of the short propellant tank with one set of struts**, called “aft”, with 4 pairs of struts in this one set. Compare with the starting configuration shown in Fig. 7. (NOTE: In this elevation view only one of the four pairs of struts is displayed). This optimum design was found with use of the “temporary” (varying density) versions of bosdec (bosdec.density.var) and addbosor4 (addbosor4.density.var).

Plan view of AFT set of supports (optimized configuration; TEMTUR=170 deg.)

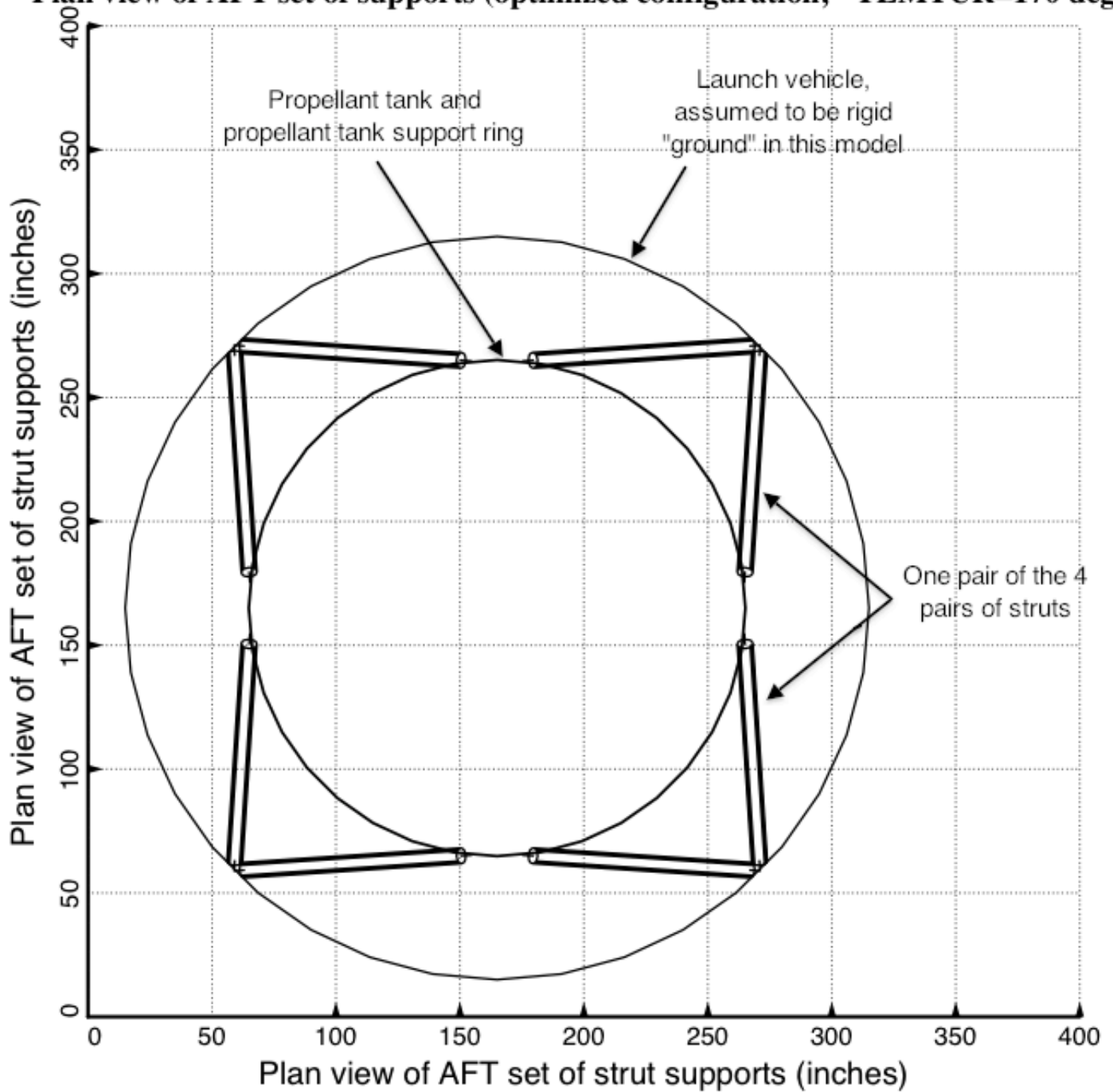


Fig. 10 **Optimized design of the short propellant tank with one set of struts**, called “aft”, with 4 pairs of struts in this one set. Compare with the starting configuration shown in Fig. 8. This optimum design was found with use of the “temporary” (varying density) versions of bosdec (bosdec.density.var) and addbosor4 (addbosor4.density.var).

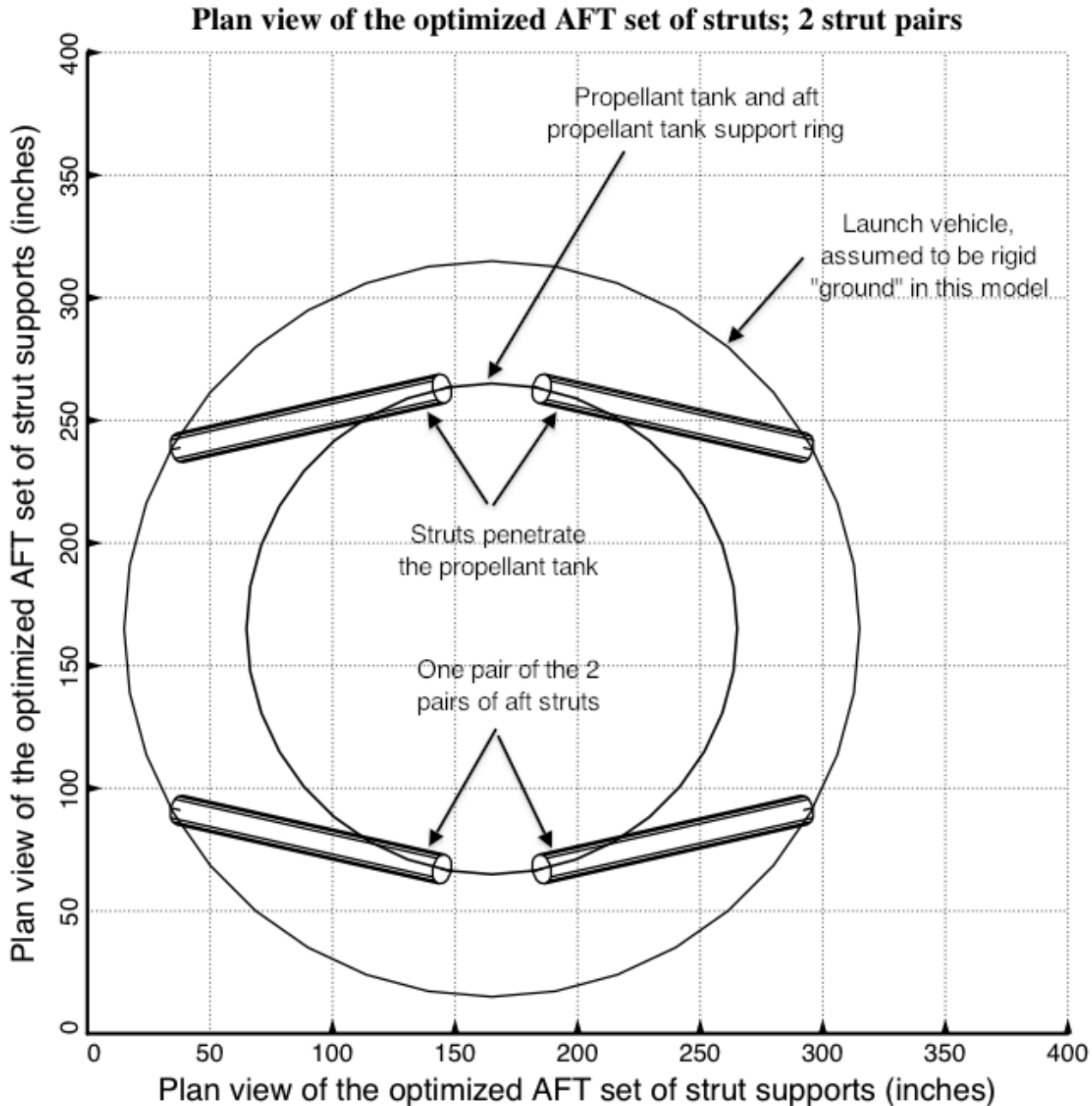


Fig. 11 Optimized design of the long propellant tank with two sets of struts, aft and forward, with 2 pairs of struts in each of these two sets. This is the aft set of 2 strut pairs. Notice that the struts penetrate the propellant tank. In the work reported here no constraint was introduced to avoid clearance problems of this type. Also, notice that the configuration appears to be “softer” with regard to lateral or pitching motions in the vertical direction in the plane of the paper than with regard to motions in the horizontal direction in the plane of the paper. **The GENOPT/TANK software optimizes with respect to lateral/pitching motions only in the horizontal direction in this figure. Therefore, it is not valid to optimize a tank/strut system with less than three pairs of struts at each axial location in the propellant tank.**

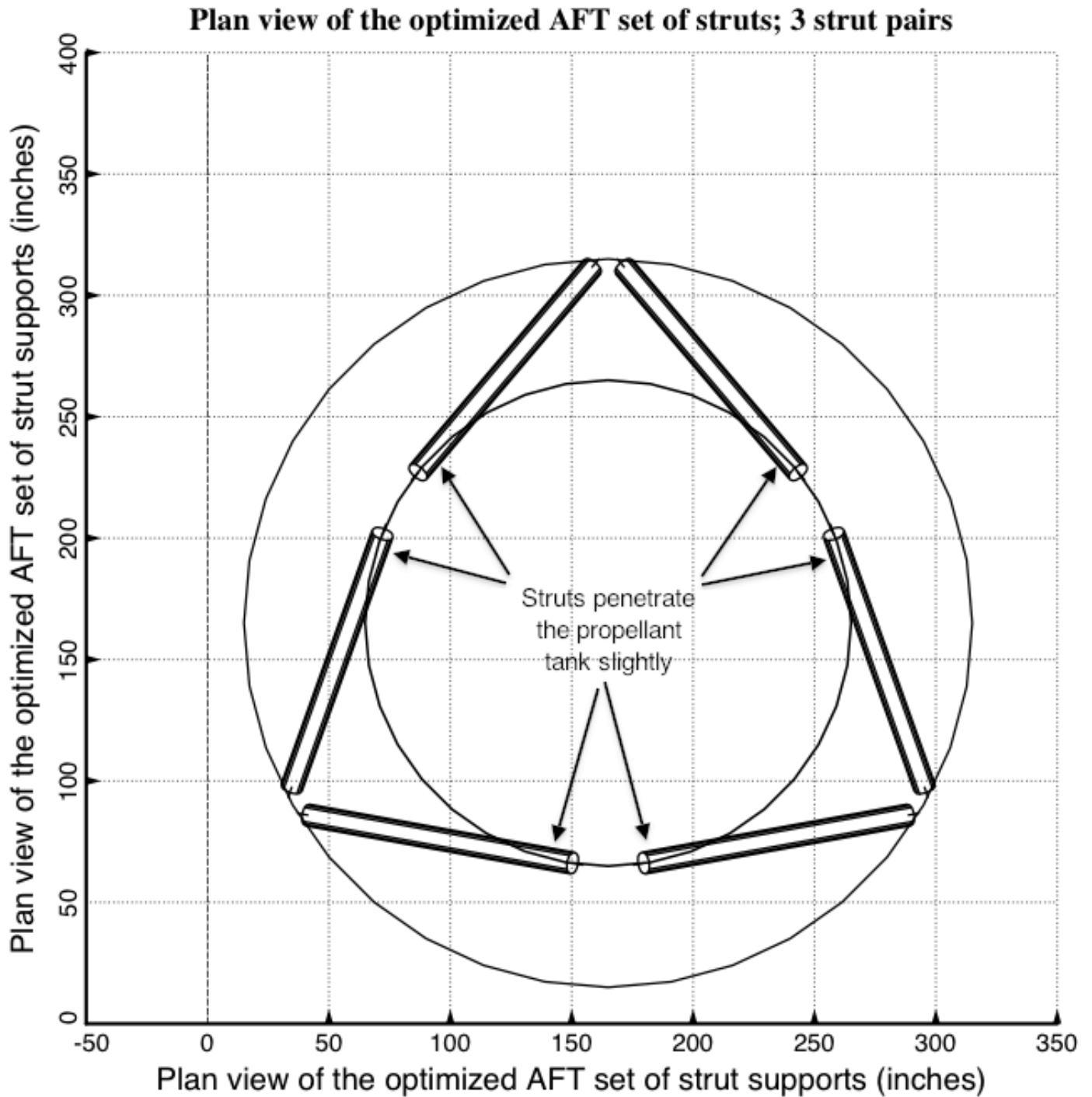


Fig. 12 **Optimized design of the long propellant tank with two sets of struts, aft and forward, with 3 pairs of struts in each of these two sets.** Notice that there is a small clearance problem at the end of the struts attached to the propellant tank. In the work reported here no constraint was introduced to avoid clearance problems of this type.

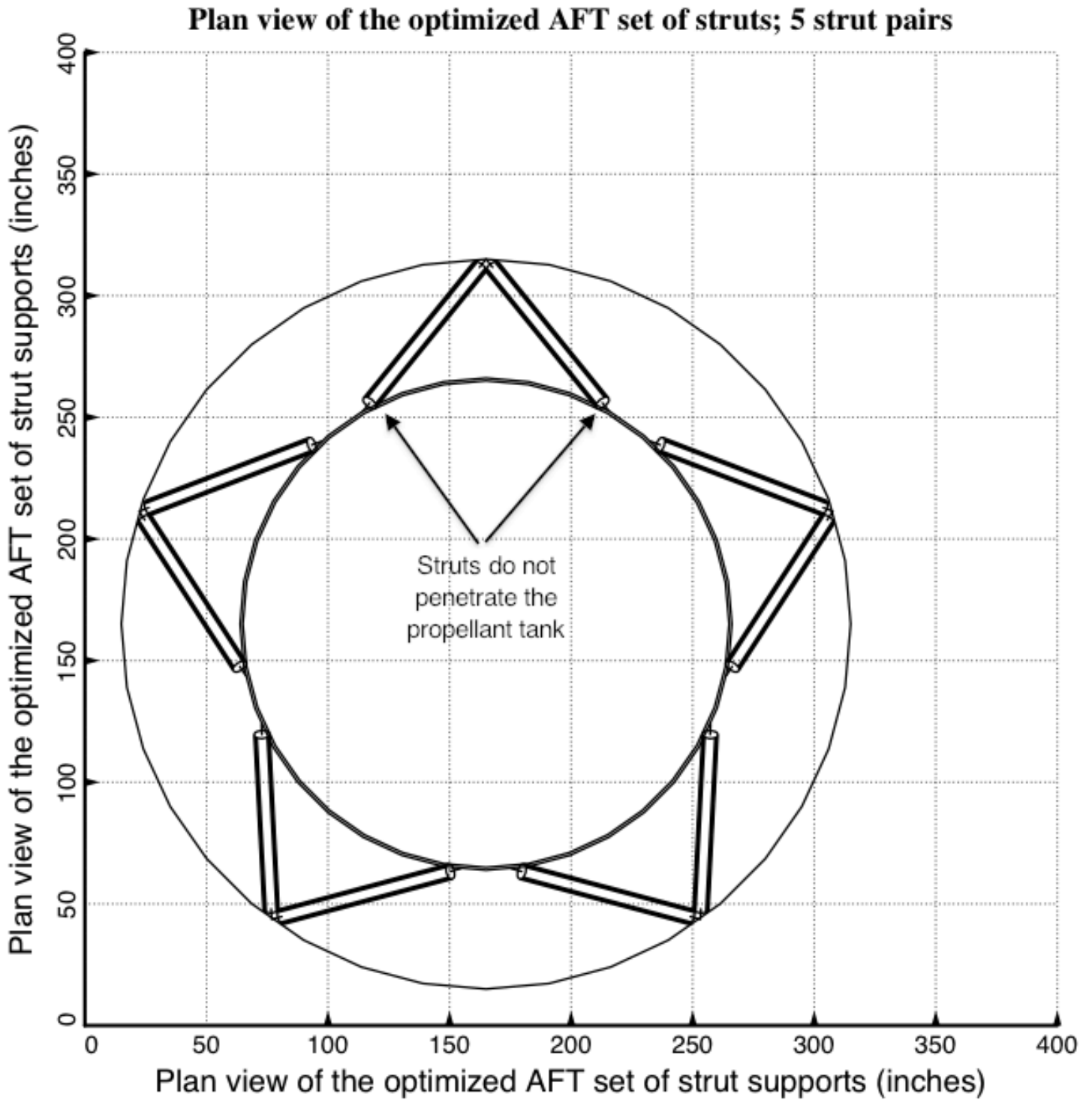


Fig. 13 **Optimized design of the long propellant tank with two sets of struts, aft and forward, with 5 pairs of struts in each of these two sets.** Notice that there is almost no clearance problem at the end of the struts attached to the propellant tank.

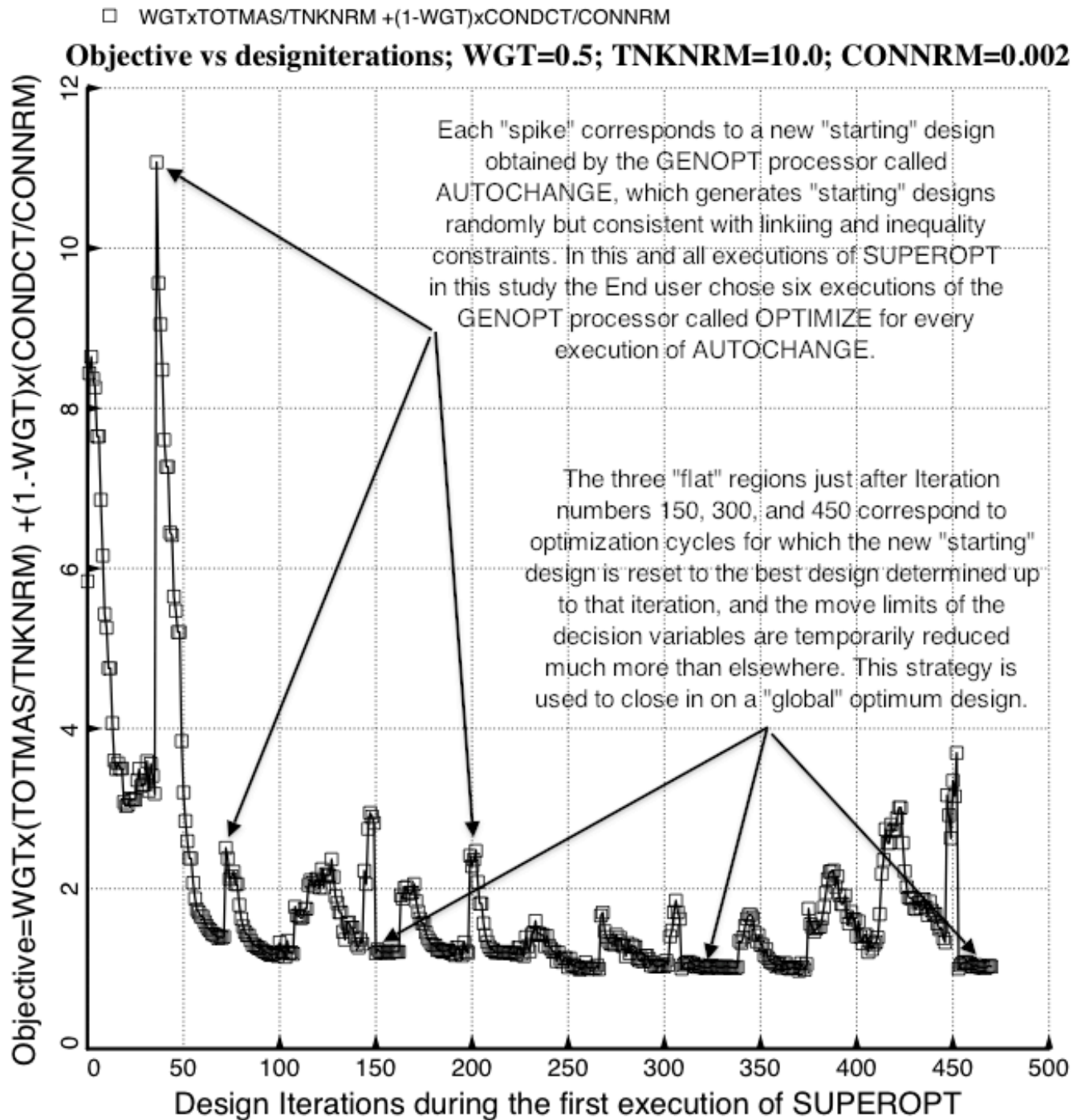


Fig. 14 **Results from the specific case called "test"**: Optimization of the long propellant tank with two sets of struts (aft and forward), 4 pairs of struts in each set. This plot is created with use of the files generated after completion of the first execution of the GENOPT processor called "SUPEROPT" during the very long execution of the GENOPT processor called "SUPERDUPEROPT" (96 hours for 4 automatic successive executions of SUPEROPT). WGT, TNKNRM and CONNRM are specified by the End user in "BEGIN".

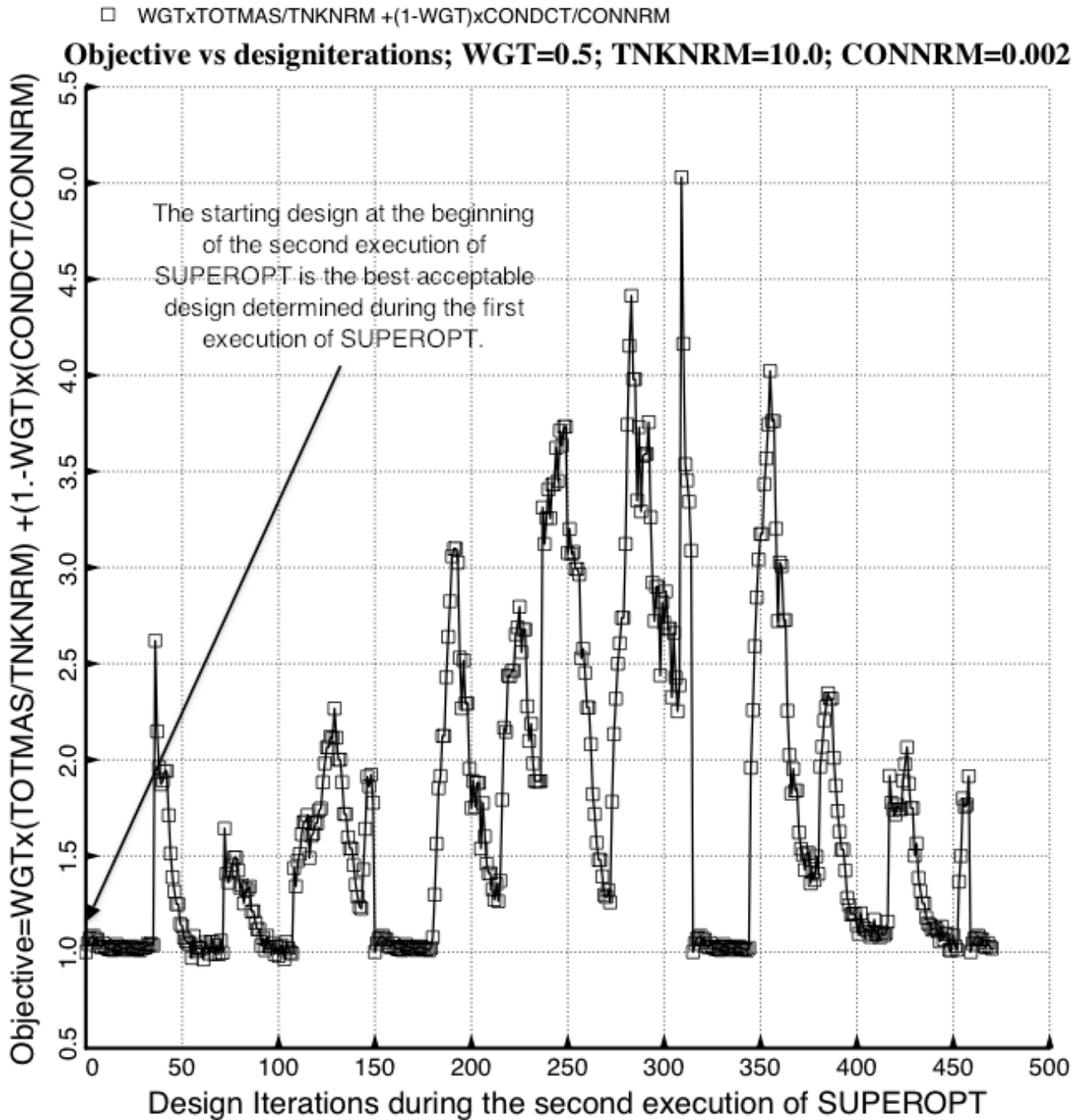


Fig. 15 **Results from the specific case called “test”**: Optimization of the long propellant tank with two sets of struts (aft and forward), 4 pairs of struts in each set. This plot is created with use of the files generated after completion of the second execution of the GENOPT processor called “SUPEROPT” during the very long execution of the GENOPT processor called “SUPERDUPEROPT” (96 hours for 4 automatic successive executions of SUPEROPT). Results from the third and fourth executions of SUPEROPT exist in [20] but are not shown in this paper.

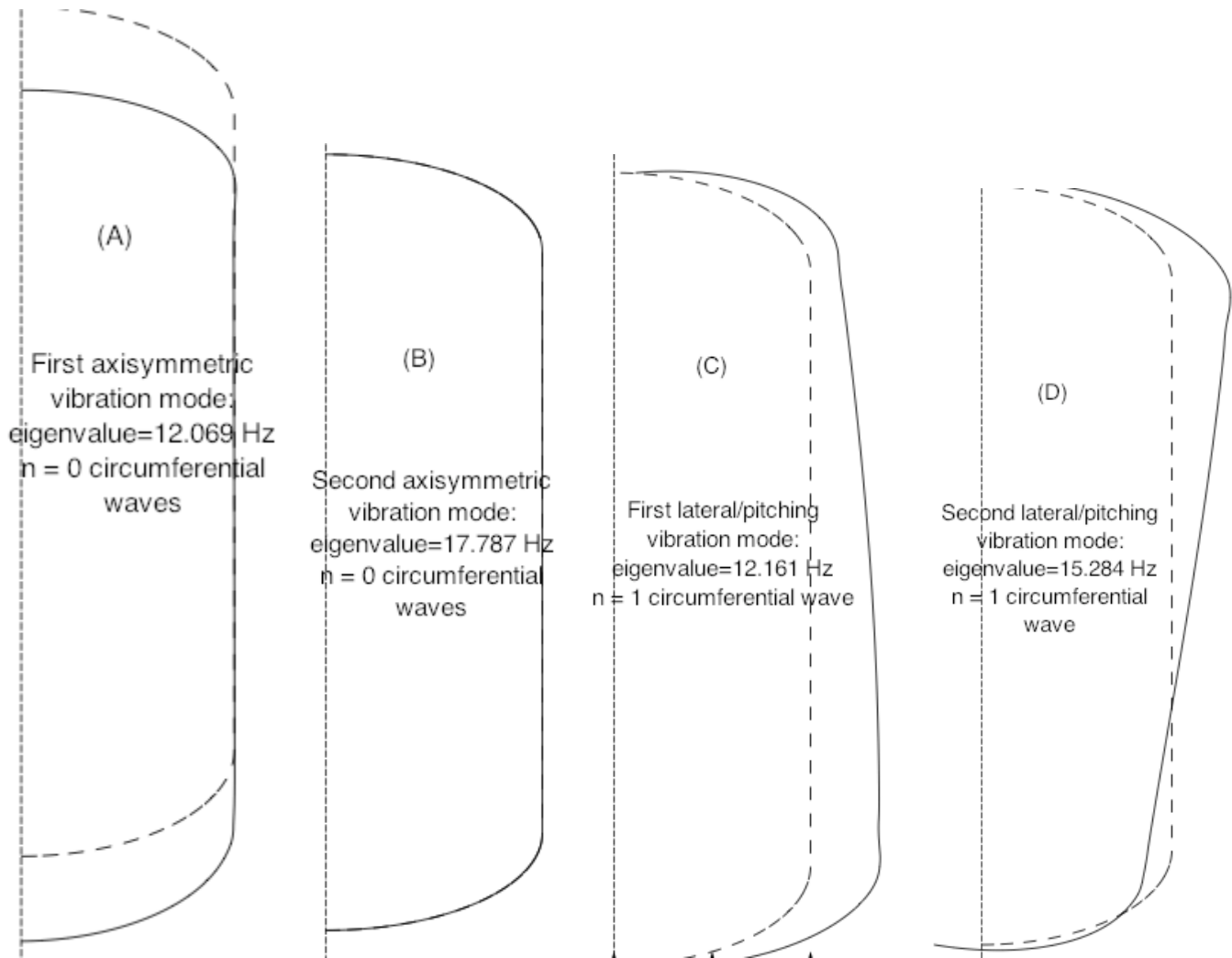


Fig. 16a **Four Vibration modes from GENOPT/TANK/BIGBOSOR4 for the optimized propellant tank with aft and forward sets of struts, 4 pairs of struts at each axial location. These are vibration modes in which the propellant tank moves approximately as a rigid body and there exists significant extension and compression of the supporting struts.** The struts are not shown because BIGBOSOR4 cannot plot springs. Compare (A) with the prediction from STAGS shown in Fig. 25c, (B) with the predictions from STAGS shown in Figs. 25e and 25h, (C) with the predictions from STAGS shown in Figs. 25a and 25d, and (D) with predictions from STAGS shown in Fig. 25g.

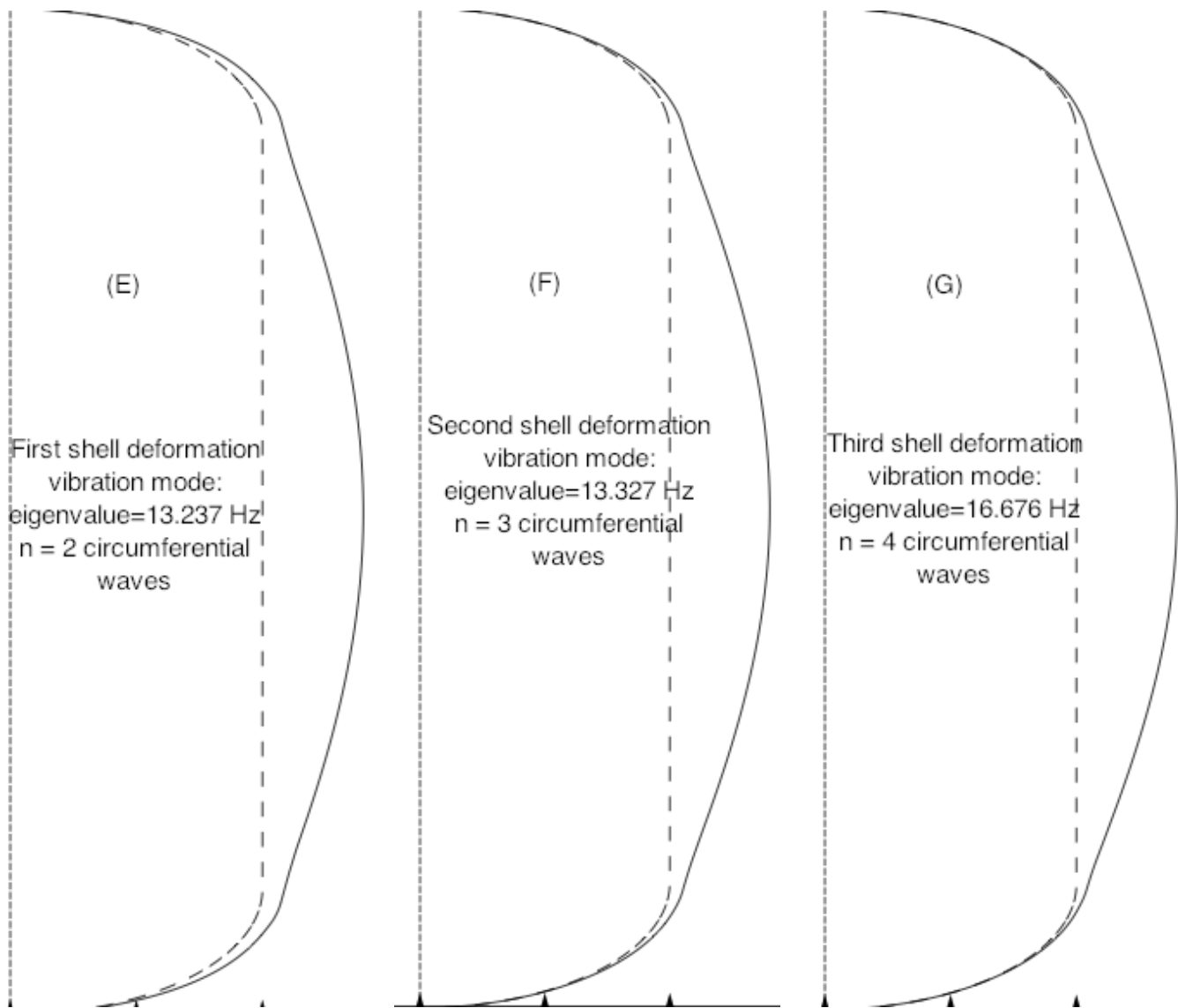


Fig. 16b **Three Vibration modes from GENOPT/TANK/BIGBOSOR4 for the optimized propellant tank with aft and forward sets of struts, 4 pairs of struts at each axial location. These are vibration modes in which the cylindrical part of the propellant tank deforms primarily as a thin shell, and there exists little extension and compression of the supporting struts.** The struts are not shown because BIGBOSOR4 cannot plot springs. Compare (E) with the prediction from STAGS shown in Fig. 25b, (F) with the predictions from STAGS shown in Figs. 25a and 25d, and (G) with the predictions from STAGS shown in Fig. 25f.

- (FREQ(1,1)/FREQA(1,1)) / FREQF(1,1)-1; F.S.= 1.20
- (FREQ(1,2)/FREQA(1,2)) / FREQF(1,2)-1; F.S.= 1.20
- △ (STRES2A(1,3)/STRES2(1,3)) / STRES2F(1,3)-1; F.S.= 1.50
- + (FORCEA(1,2)/FORCE(1,2)) / FORCEF(1,2)-1; F.S.= 1.00
- × (TNKSTRA(1,1)/TNKSTR(1,1)) / TNKSTRF(1,1)-1; F.S.= 1.00
- ◇ (TNKSTRA(1,2)/TNKSTR(1,2)) / TNKSTRF(1,2)-1; F.S.= 1.00
- ▽ (FREQ(2,1)/FREQA(2,1)) / FREQF(2,1)-1; F.S.= 1.20
- ⊠ (FREQ(2,2)/FREQA(2,2)) / FREQF(2,2)-1; F.S.= 1.20
- ⊞ (FREQ(2,3)/FREQA(2,3)) / FREQF(2,3)-1; F.S.= 1.20
- ⊚ (FREQ(2,4)/FREQA(2,4)) / FREQF(2,4)-1; F.S.= 1.20
- ⊗ (STRES1A(2,3)/STRES1(2,3)) / STRES1F(2,3)-1; F.S.= 1.50
- ⊙ (STRES2A(2,3)/STRES2(2,3)) / STRES2F(2,3)-1; F.S.= 1.50
- ⊕ (COLBUK(2,1)/COLBUKA(2,1)) / COLBUKF(2,1)-1; F.S.= 1.00
- ⊖ (COLBUK(2,2)/COLBUKA(2,2)) / COLBUKF(2,2)-1; F.S.= 1.00
- ⊗ (SHLBUK(2,1)/SHLBUKA(2,1)) / SHLBUKF(2,1)-1; F.S.= 2.00
- (SHLBUK(2,2)/SHLBUKA(2,2)) / SHLBUKF(2,2)-1; F.S.= 2.00
- (FORCEA(2,2)/FORCE(2,2)) / FORCEF(2,2)-1; F.S.= 1.00
- (TNKSTRA(2,1)/TNKSTR(2,1)) / TNKSTRF(2,1)-1; F.S.= 1.00
- (TNKSTRA(2,2)/TNKSTR(2,2)) / TNKSTRF(2,2)-1; F.S.= 1.00

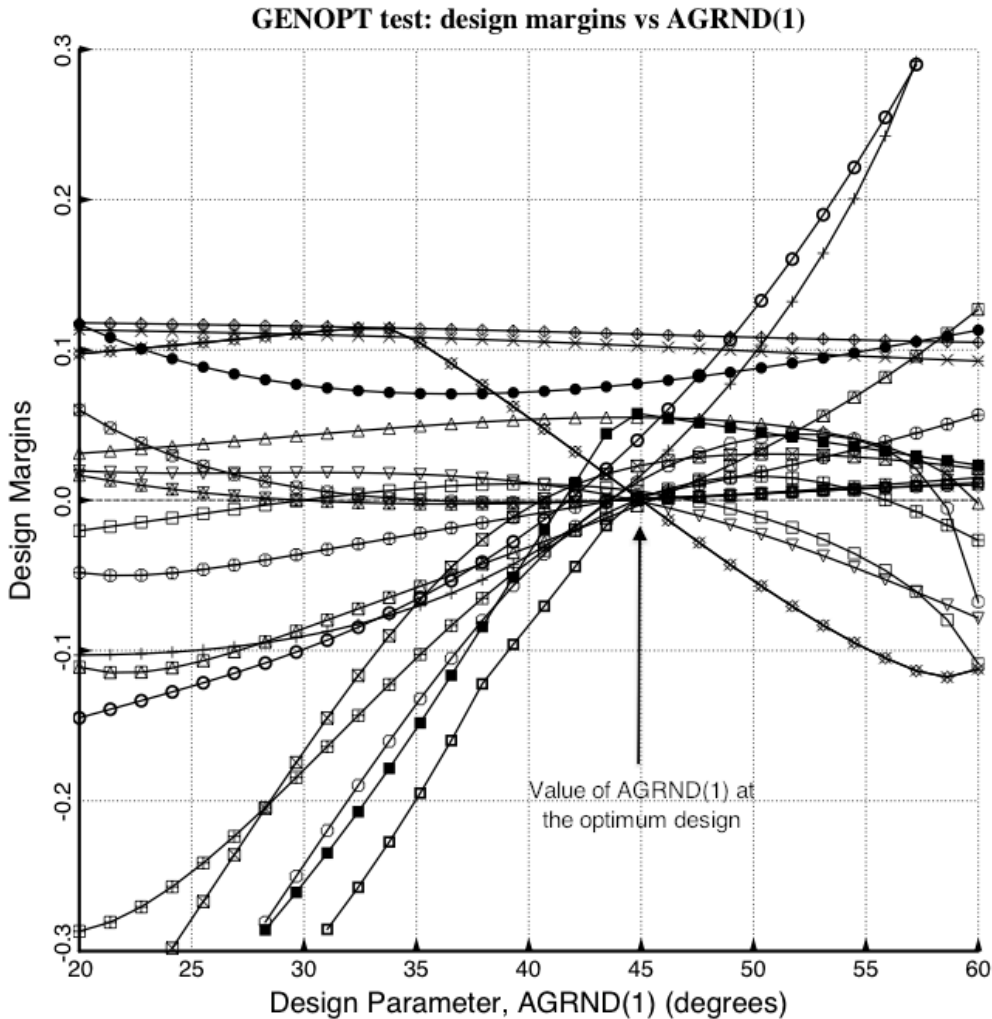


Fig. 17 Results from the specific case called “test”: Optimized long propellant tank with two sets of struts (aft and forward), 4 pairs of struts in each set. Shown here are “**design sensitivity**” plots from an analysis in which all decision variables are held constant except for AGRND(1) = circumferential angle to the pinned “ground” end of the forward slanting strut in the first strut pair in the aft set of struts (Fig. 2). Typical behavior at the optimum design is exhibited: several margins are critical or near-critical at the optimum value of AGRND(1).

- (FREQ(1,1)/FREQA(1,1))/FREQ(1,1)-1; F.S.= 1.20
- (FREQ(1,2)/FREQA(1,2))/FREQ(1,2)-1; F.S.= 1.20
- △ (STRES2A(1,3)/STRES2(1,3))/STRES2F(1,3)-1; F.S.= 1.50
- + (FORCEA(1,2)/FORCE(1,2))/FORCEF(1,2)-1; F.S.= 1.00
- × (TNKSTRA(1,1)/TNKSTR(1,1))/TNKSTRF(1,1)-1; F.S.= 1.00
- ◇ (TNKSTRA(1,2)/TNKSTR(1,2))/TNKSTRF(1,2)-1; F.S.= 1.00
- ▽ (FREQ(2,1)/FREQA(2,1))/FREQ(2,1)-1; F.S.= 1.20
- ⊠ (FREQ(2,2)/FREQA(2,2))/FREQ(2,2)-1; F.S.= 1.20
- × (FREQ(2,3)/FREQA(2,3))/FREQ(2,3)-1; F.S.= 1.20
- ◆ (FREQ(2,4)/FREQA(2,4))/FREQ(2,4)-1; F.S.= 1.20
- ⊕ (STRES1A(2,3)/STRES1(2,3))/STRES1F(2,3)-1; F.S.= 1.50
- ⊗ (STRES2A(2,3)/STRES2(2,3))/STRES2F(2,3)-1; F.S.= 1.50
- ⊞ (COLBUK(2,1)/COLBUKA(2,1))/COLBUKF(2,1)-1; F.S.= 1.00
- ⊠ (COLBUK(2,2)/COLBUKA(2,2))/COLBUKF(2,2)-1; F.S.= 1.00
- ⊞ (SHLBUK(2,1)/SHLBUKA(2,1))/SHLBUKF(2,1)-1; F.S.= 2.00
- (SHLBUK(2,2)/SHLBUKA(2,2))/SHLBUKF(2,2)-1; F.S.= 2.00
- (FORCEA(2,2)/FORCE(2,2))/FORCEF(2,2)-1; F.S.= 1.00
- (TNKSTRA(2,1)/TNKSTR(2,1))/TNKSTRF(2,1)-1; F.S.= 1.00
- (TNKSTRA(2,2)/TNKSTR(2,2))/TNKSTRF(2,2)-1; F.S.= 1.00

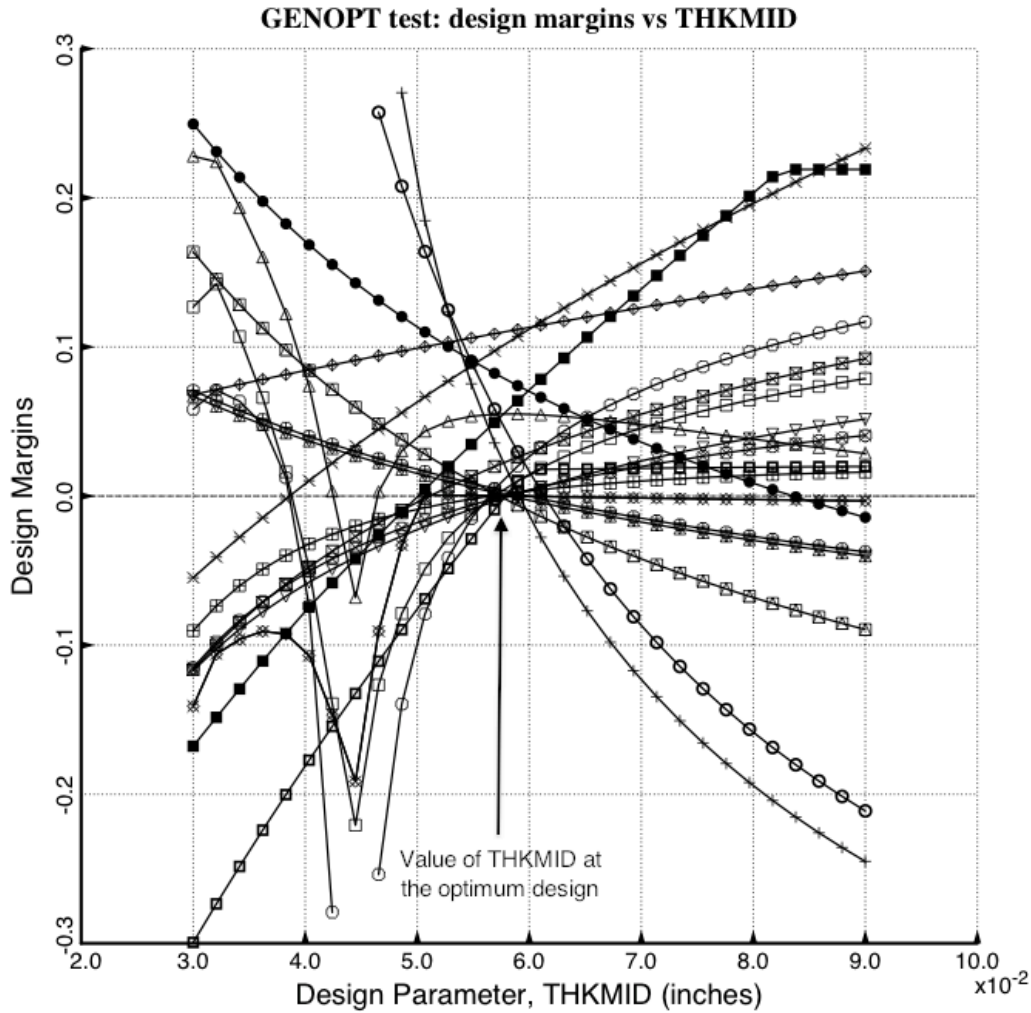


Fig. 18 Results from the specific case called “test”: Optimized long propellant tank with two sets of struts (aft and forward), 4 pairs of struts in each set. Shown here are “**design sensitivity**” plots from an analysis in which all decision variables are held constant except for THKMID = thickness of the skin of the cylindrical part of the propellant tank (Fig. 1c). Typical behavior at the optimum design is exhibited: several margins are critical or near-critical at the optimum value of THKMID.

- (FREQ(1,1)/FREQA(1,1)) / FREQF(1,1)-1; F.S.= 1.20
- (FREQ(1,2)/FREQA(1,2)) / FREQF(1,2)-1; F.S.= 1.20
- △ (STRES2A(1,3)/STRES2(1,3)) / STRES2F(1,3)-1; F.S.= 1.50
- + (FORCEA(1,2)/FORCE(1,2)) / FORCEF(1,2)-1; F.S.= 1.00
- × (TNKSTRA(1,1)/TNKSTR(1,1)) / TNKSTRF(1,1)-1; F.S.= 1.00
- ◇ (TNKSTRA(1,2)/TNKSTR(1,2)) / TNKSTRF(1,2)-1; F.S.= 1.00
- ▽ (FREQ(2,1)/FREQA(2,1)) / FREQF(2,1)-1; F.S.= 1.20
- ⊠ (FREQ(2,2)/FREQA(2,2)) / FREQF(2,2)-1; F.S.= 1.20
- ⊞ (FREQ(2,3)/FREQA(2,3)) / FREQF(2,3)-1; F.S.= 1.20
- ⊚ (FREQ(2,4)/FREQA(2,4)) / FREQF(2,4)-1; F.S.= 1.20
- ⊗ (STRES1A(2,3)/STRES1(2,3)) / STRES1F(2,3)-1; F.S.= 1.50
- ⊙ (STRES2A(2,3)/STRES2(2,3)) / STRES2F(2,3)-1; F.S.= 1.50
- ⊕ (COLBUK(2,1)/COLBUKA(2,1)) / COLBUKF(2,1)-1; F.S.= 1.00
- ⊖ (COLBUK(2,2)/COLBUKA(2,2)) / COLBUKF(2,2)-1; F.S.= 1.00
- ⊗ (SHLBUK(2,1)/SHLBUKA(2,1)) / SHLBUKF(2,1)-1; F.S.= 2.00
- ⊙ (SHLBUK(2,2)/SHLBUKA(2,2)) / SHLBUKF(2,2)-1; F.S.= 2.00
- ⊕ (FORCEA(2,2)/FORCE(2,2)) / FORCEF(2,2)-1; F.S.= 1.00
- ⊖ (TNKSTRA(2,1)/TNKSTR(2,1)) / TNKSTRF(2,1)-1; F.S.= 1.00
- (TNKSTRA(2,2)/TNKSTR(2,2)) / TNKSTRF(2,2)-1; F.S.= 1.00

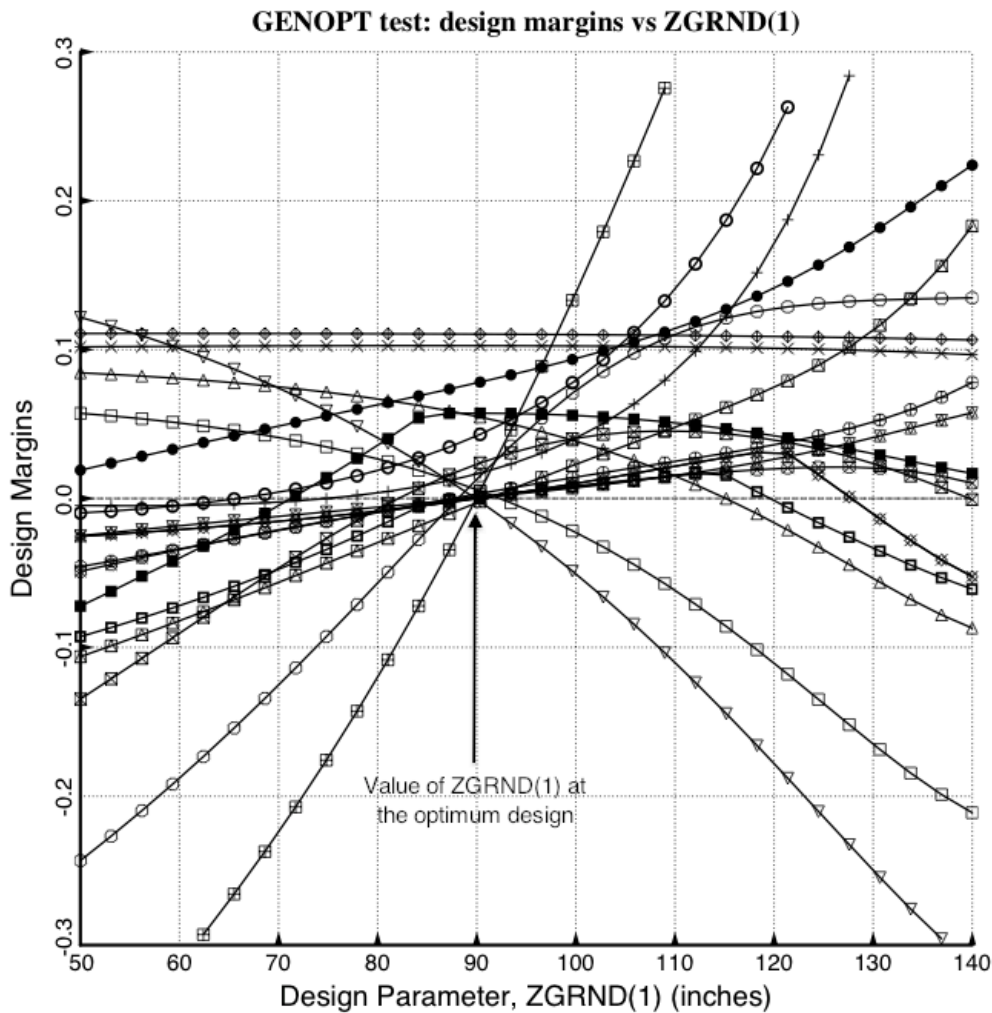


Fig. 19 Results from the specific case called “test”: Optimized long propellant tank with two sets of struts (aft and forward), 4 pairs of struts in each set. Shown here are “**design sensitivity**” plots from an analysis in which all decision variables are held constant except for ZGRND(1) = the global axial coordinate of the “ground” ends of the aft set of struts (Fig.1a). Typical behavior at the optimum design is exhibited: several margins are critical or near-critical at the optimum value of ZGRND(1).

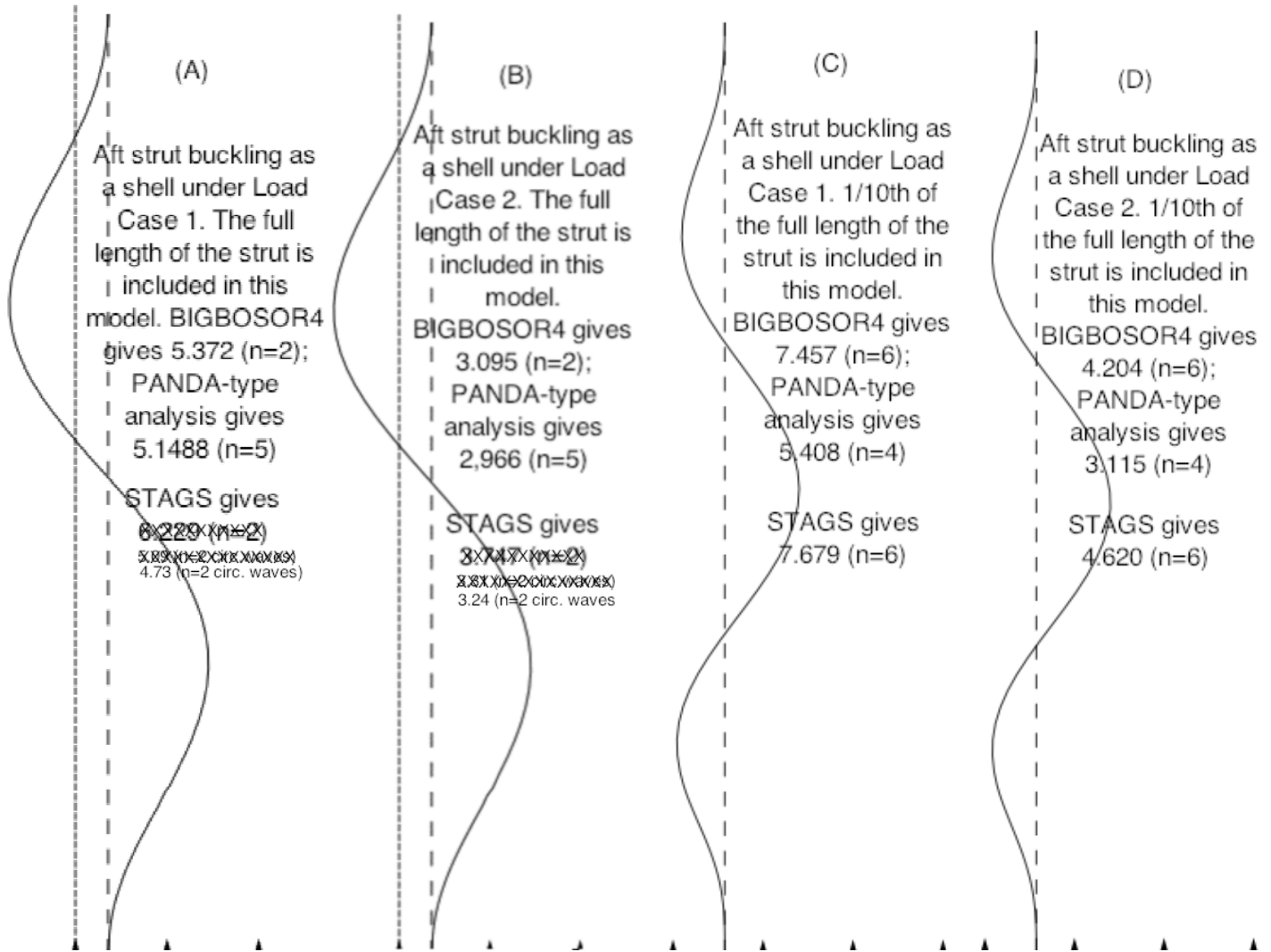


Fig 20 Aft strut buckling mode shapes for the strut buckling as a thin shell rather than as a column. For computation of the design margin corresponding to buckling of the strut as a thin shell, GENOPT selects the lower of the load factors from the BIGBOSOR4 model and the PANDA-type model [15]. The strut shell buckling mode shapes displayed here are predicted by BIGBOSOR4 for the optimized long propellant tank with two sets of struts, aft and forward, 4 pairs of struts in each set. Buckling load factors from BIGBOSOR4 [2,3], from a PANDA-type of analysis [15] and from STAGS [16 – 19] are listed. The differences in the BIGBOSOR4 and STAGS predictions for the buckling load factors in (A) and (B) are primarily due to the different predictions from GENOPT/TANK and STAGS of maximum compressive load in an aft strut in Load Case 1 (axial acceleration): -22693 lbs according to GENOPT/TANK and -24841 lbs according to STAGS, and in Load Case 2 (lateral acceleration): -39393 lbs according to GENOPT/TANK and -36298 lbs according to STAGS. [See Table 7(b).]. The shell buckling modes shown in Parts (A) and (B) are from strut models that contain the entire length of the strut minus the lengths of the end fittings. The shell buckling modes shown in Parts (C) and (D) are from strut models that contain only 1/10th of that length. Notice that the buckling load factors predicted from the PANDA-type model are much less sensitive to the length of strut included in the strut shell buckling model than are the load factors predicted by BIGBOSOR4 and STAGS.

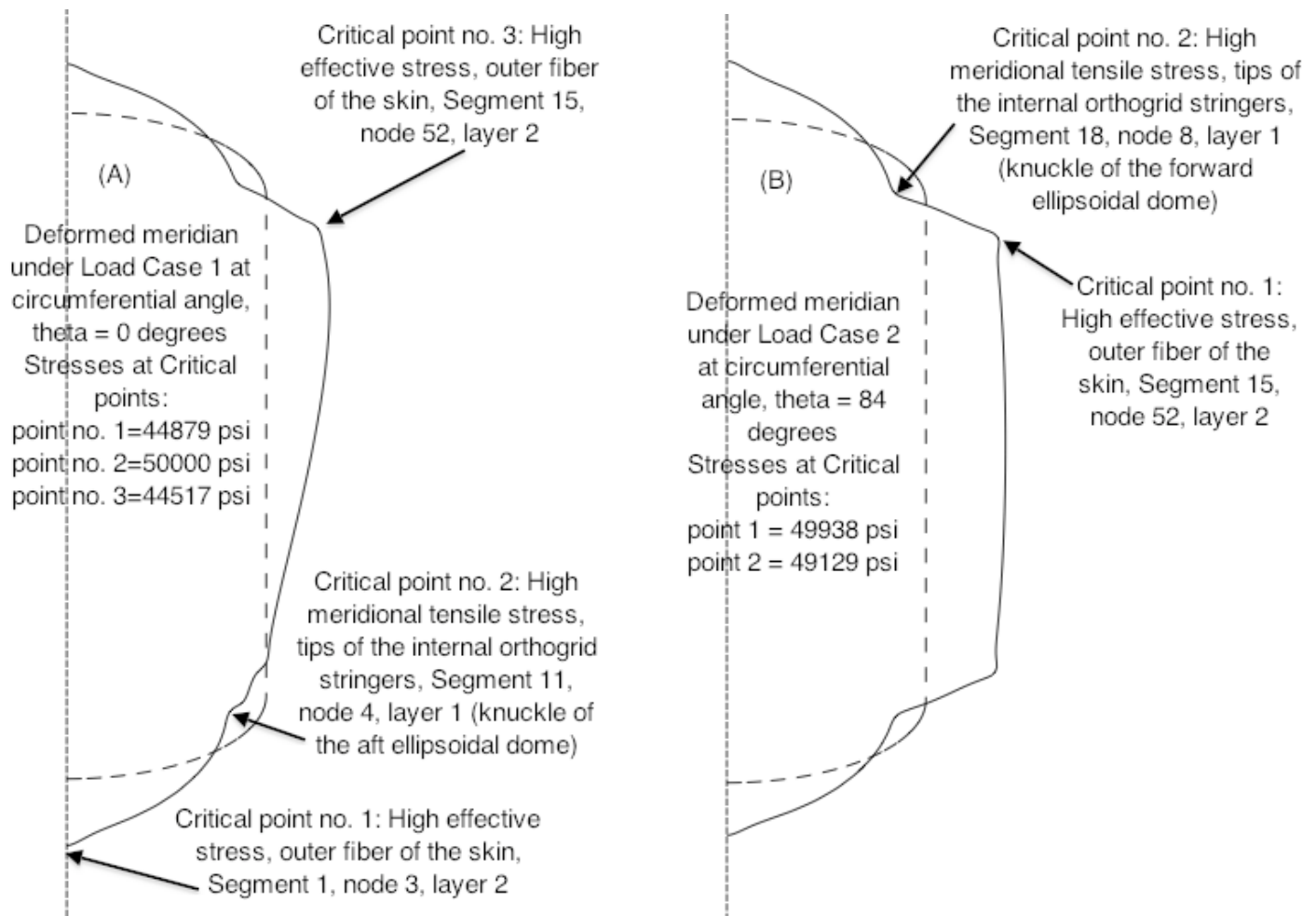


Fig. 21a Deformed meridians, critical and near-critical stresses and their locations under (A) Load Case 1 (10g axial acceleration plus 25 psi internal pressure + 200-degree tank cool-down) and (B) Load Case 2 (10g lateral acceleration plus 25 psi internal pressure + 200-degree tank cool-down) as predicted from the GENOPT/TANK model of the specific case called “test”. (See Figs. 4 – 6.) The struts are not shown because in the linear non-axisymmetric stress analysis the struts are replaced in the GENOPT/BIGBOSOR4 model by the concentrated loads that they apply to the propellant tank. Compare the maximum stresses shown here with the STAGS predictions of the maximum stresses plotted in Figs. 26a-26f for Load Case 1 and in Figs. 27a and 27b for Load Case 2. The deformations of the lower and upper domes are entirely caused by the 25 psi uniform internal ullage pressure plus the linearly varying normal propellant pressure heads generated from the 10g axial and lateral acceleration components. The somewhat odd appearances of these axisymmetric deformations in the immediate neighborhoods of the apexes of the domes (very local outward bulges) are caused by the following:

1. The innermost layer of the dome, which represents the internal orthogrid with smeared stiffeners, is orthotropic rather than isotropic because the thickness and spacing of the optimized orthogrid stringers (STRTHK=0.1370 and STRSPC=3.426 inches, respectively) are different from those of the orthogrid rings (RNGTHK=0.3431 and RNGSPC=4.042 inches, respectively).
2. The pole conditions imposed by BIGBOSOR4 at the apexes of domes are strictly valid only for isotropic material. The STAGS model displayed in Figs. 26a and 26c show a similar local outward bulge.

- The optimized specific case, "test", Linear BIGBOSOR4 theory (INDIC=3); GAXIAL=10
- The optimized specific case, "test", Linear BIGBOSOR4 theory (INDIC=3); GAXIAL=0
- △ The optimized specific case, "test", Nonlinear BIGBOSOR4 theory (INDIC=0); GAXIAL=0

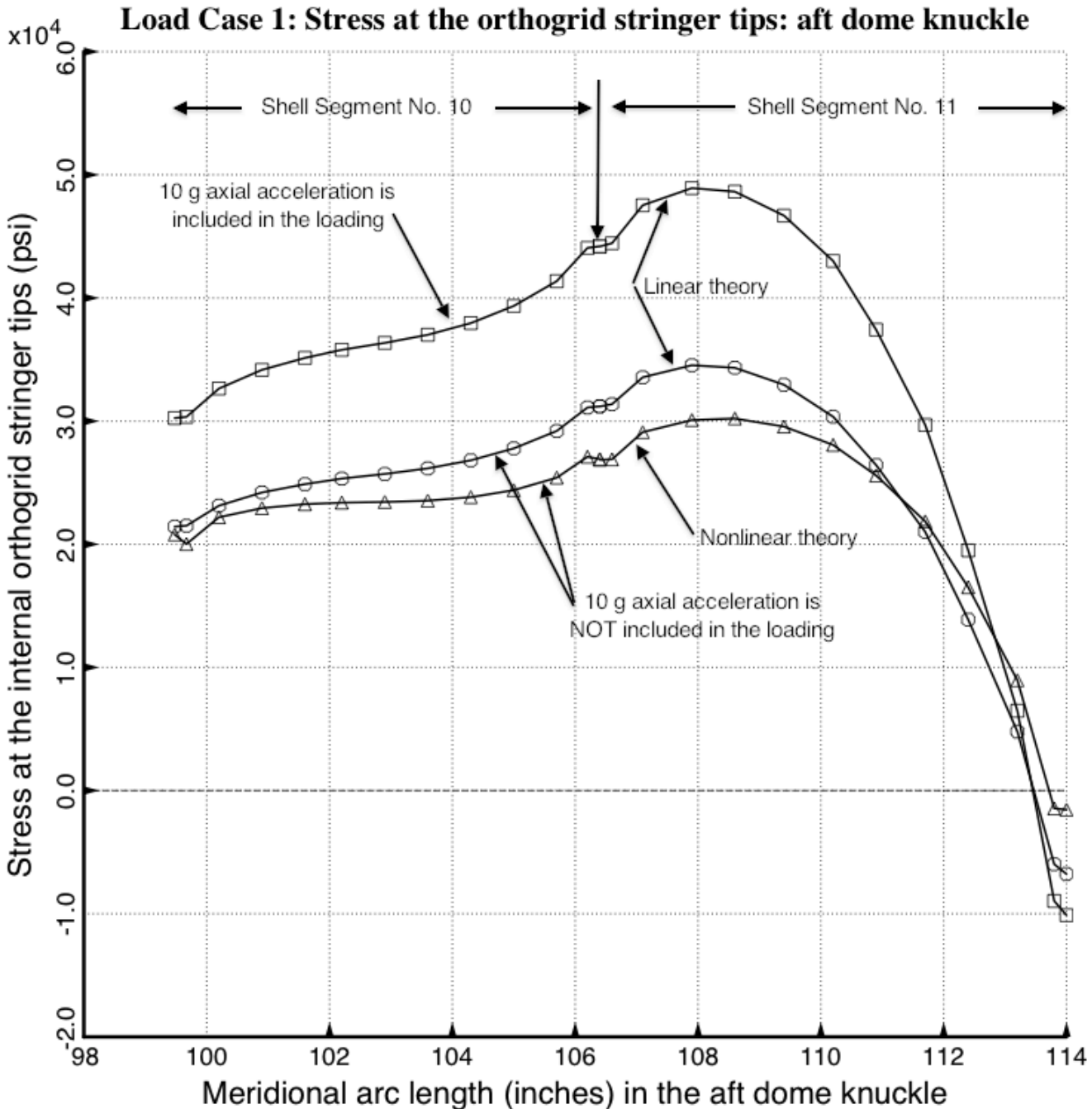


Fig. 21b Stress from Load Case 1 at the tips of the internal orthogrid stringers in the knuckle region of the aft ellipsoidal dome of the optimized propellant tank from three different BIGBOSOR4 models. The thermal loading (tank cool-down) and the concentrated loads applied by the struts to the propellant tank were not included in the BIGBOSOR4 models that generated the curves shown here. The locations of shell segments 10 and 11 are indicated in Fig. 1b.

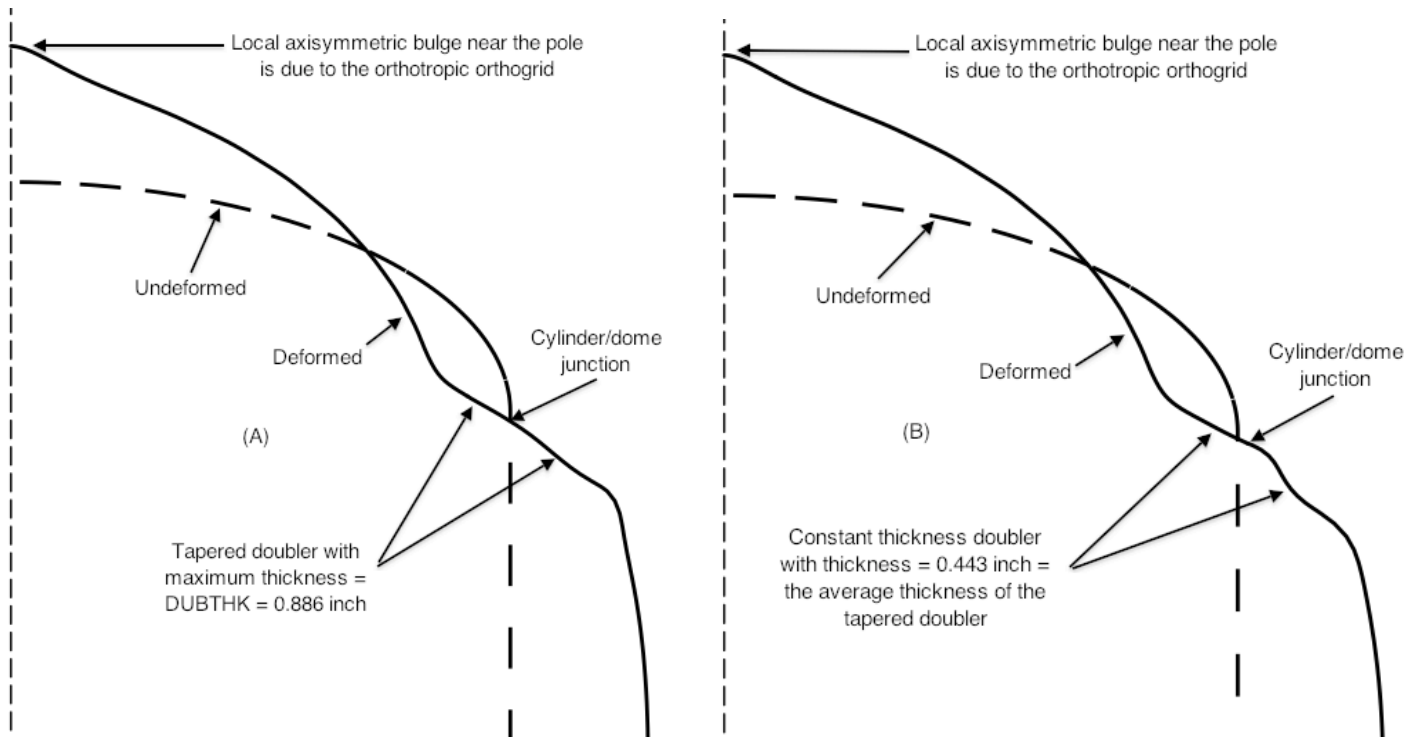


Fig. 21c Enlarged views of the prebuckled states of the forward part of the optimized “test” propellant tank as deformed under Load Case 1 (10g axial acceleration + 25 psi internal pressure + 200-degree tank cool-down) along the meridian at the circumferential coordinate, $\theta = 6.0$ degrees, as predicted by two GENOPT/BIGBOSOR4 models. (A) The external doubler, approximately centered at the junction of the forward dome with the cylindrical part of the tank (Figs. 1b and 1c), is double-linearly tapered as shown in Fig. 1c, with its maximum thickness, DUBTHK = 0.886 inch, at the dome/cylinder junction, which is also where the forward ring of struts is attached to the centroid of the forward external propellant tank support ring. (B) The same overall geometry except that the external doubler has constant thickness over its entire 30-inch axial width equal to 0.443 inch, which is equal to the average thickness of the double-linearly tapered doubler. The deformation shown in (A) is the same as that shown in part (A) of Fig. 21a. The compressive stress at the forward dome/cylinder junction at the tips of the internal orthogrid stringers corresponding to (A) is about –23000 psi. **The maximum compressive stress at the same location corresponding to (B) is about –119000 psi, as shown in Fig. 21d.** This huge difference in the maximum compressive stress at the tips of the internal orthogrid stringers at the forward dome/cylinder junction is caused by the huge difference in the amount of local meridional bending of the wall of the propellant tank there (approximately midway between the two arrows), evident when the local deformation shown in (A) is compared with that in (B). **The STAGS models correspond to (B).** The maximum compressive stress at the tips of the orthogrid stringers predicted by the STAGS 360-degree model is close to –41240 psi, as shown in Fig. 26b and that predicted by the STAGS refined 45-degree model is close to –114000 psi, as shown in Fig. 26f. The STAGS 360-degree model shown in Fig. 24 is adequate for the prediction of vibration modal frequencies and buckling load factors, but not for the prediction of very localized stress concentrations that occur in the propellant tank where the struts apply concentrated loads. **The difference in predictions from the BIGBOSOR4 model with tapered doublers (A) and that with constant thickness doublers (B) highlights the need for a STAGS model with tapered doublers.**

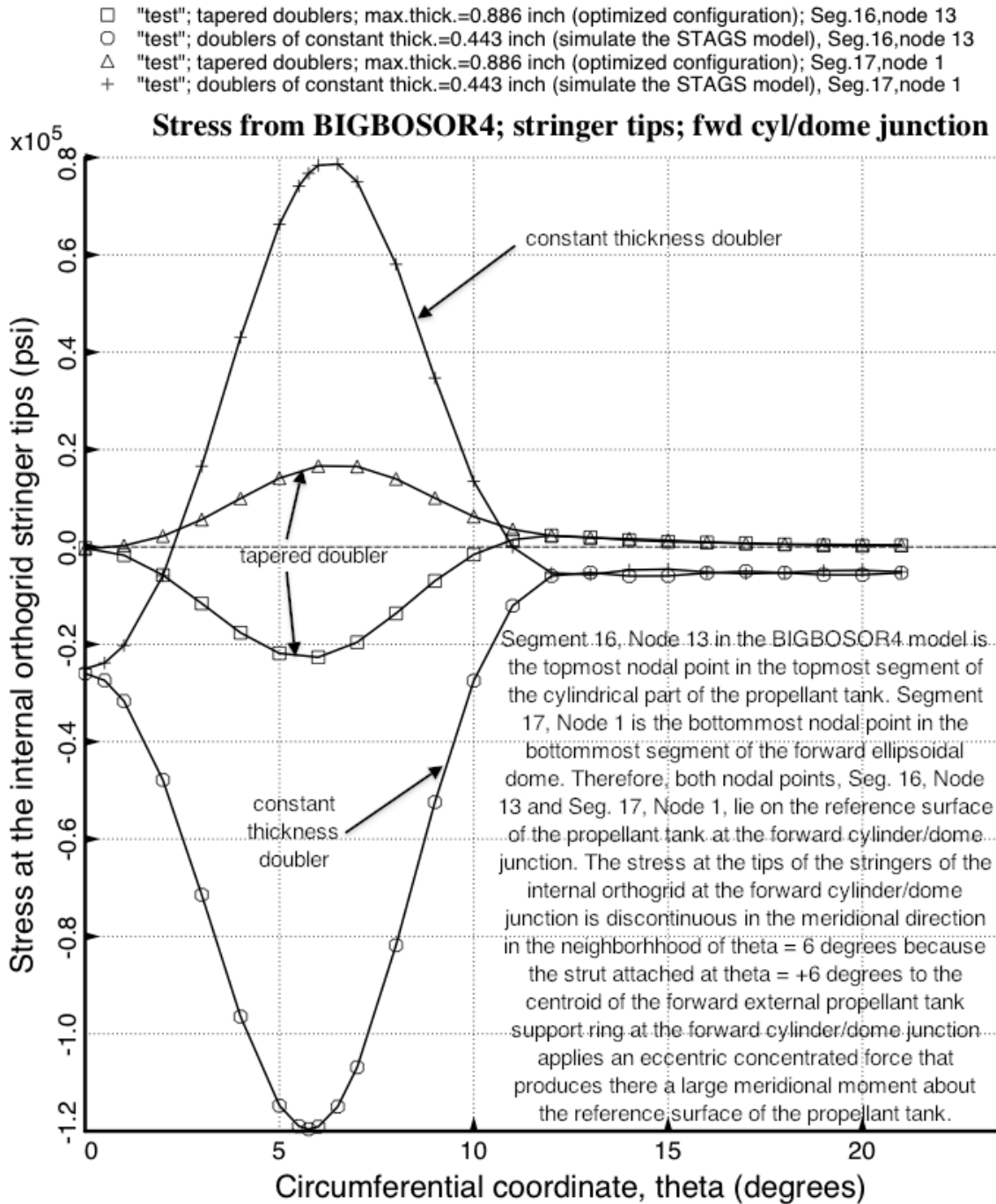


Fig. 21d The specific case, "test", propellant tank under **Load Case 1** (10 g axial acceleration, 25 psi internal pressure and 200 degree tank cool-down). **Plots of the stress at the tips of the internal orthogrid stringers from two BIGBOSOR4 models: Model 1 has tapered doublers with maximum thickness = 0.886 inch (the optimized configuration) and Model 2 has constant thickness doublers with thickness = 0.443 inch (BIGBOSOR4 simulation of the STAGS model).** The dramatic difference in the prediction of maximum stress from the two BIGBOSOR4 models, Model 1 and Model 2, arises mainly from the dramatic difference in the maximum meridional curvature changes at the forward cylinder/dome junction near the pinned struts (Fig.21c).

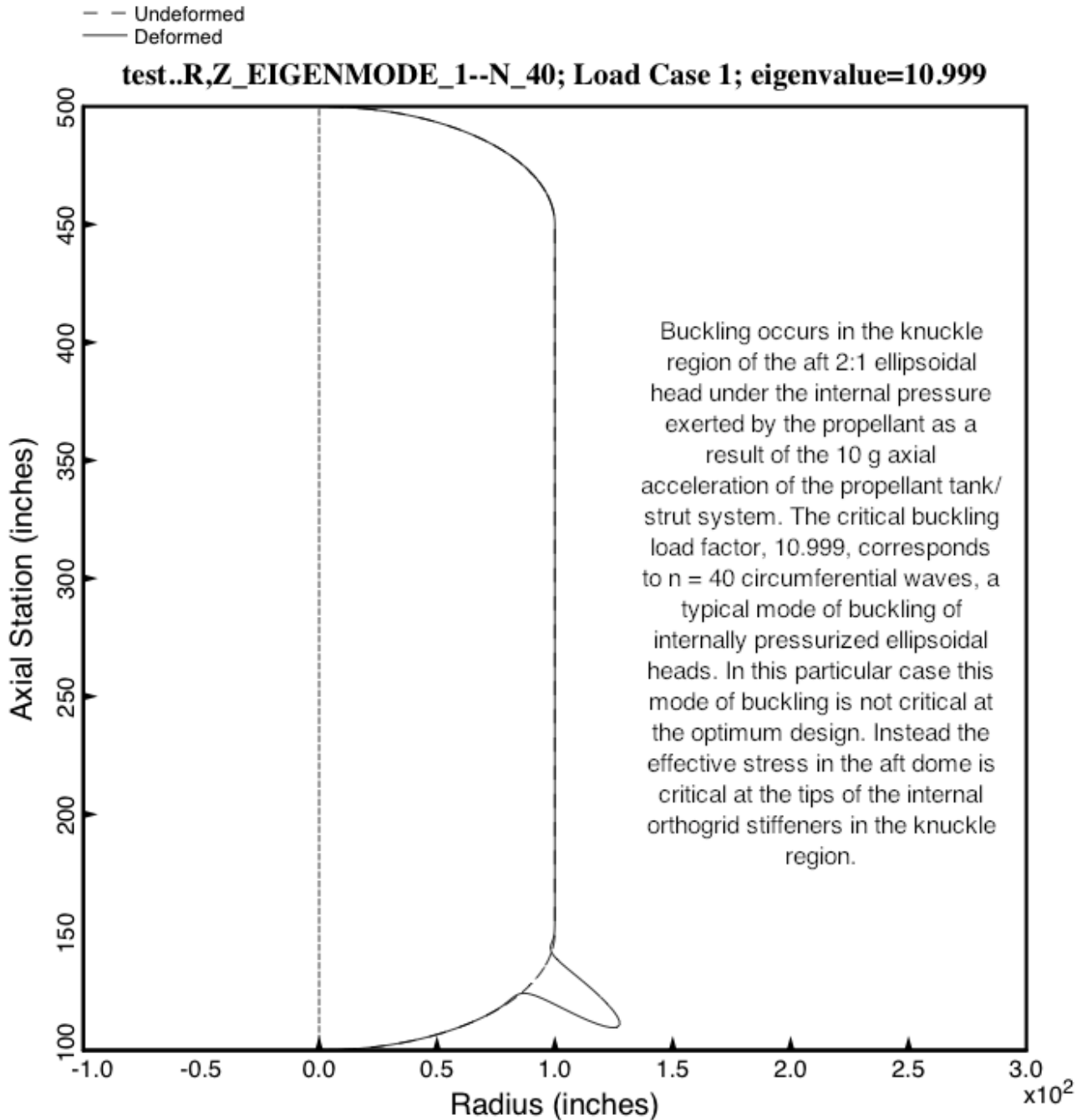


Fig. 22 Results from the specific case called “test”: Optimized long propellant tank with two sets of struts (aft and forward), 4 pairs of struts in each set. **Shown here is the buckling mode of the propellant tank under Load Case 1**, 10g axial acceleration (upward acceleration). The aft dome buckles before the forward dome because the internal pressure exerted by the axially accelerating propellant is greatest at the bottom of the tank. NOTE: The buckling load factor would have been much less than 10.999 if the 25-psi internal ullage pressure had been included in Load Set A rather than in Load Set B (4.107 as listed in Fig. 31 versus 10.999 listed here).

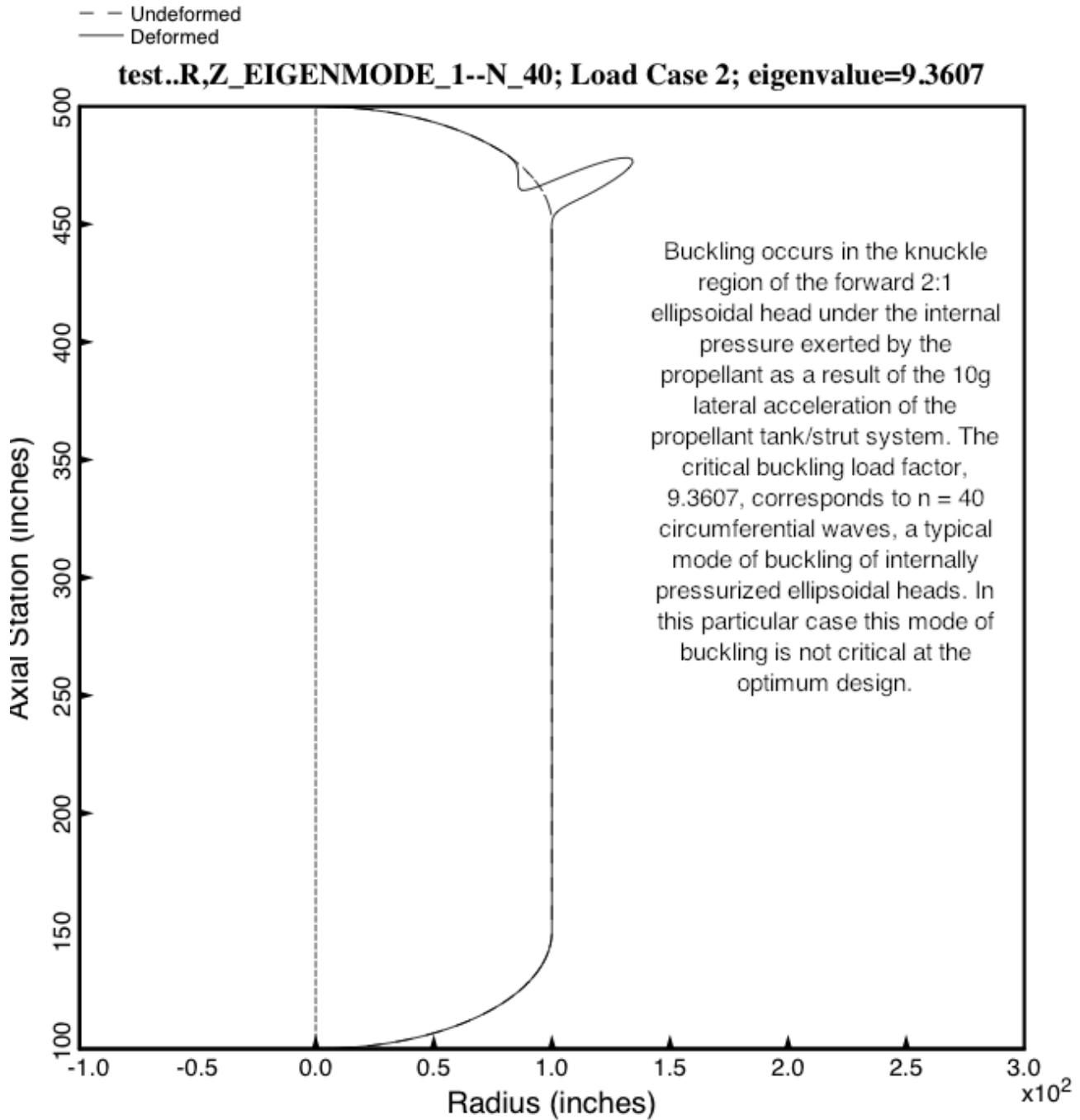
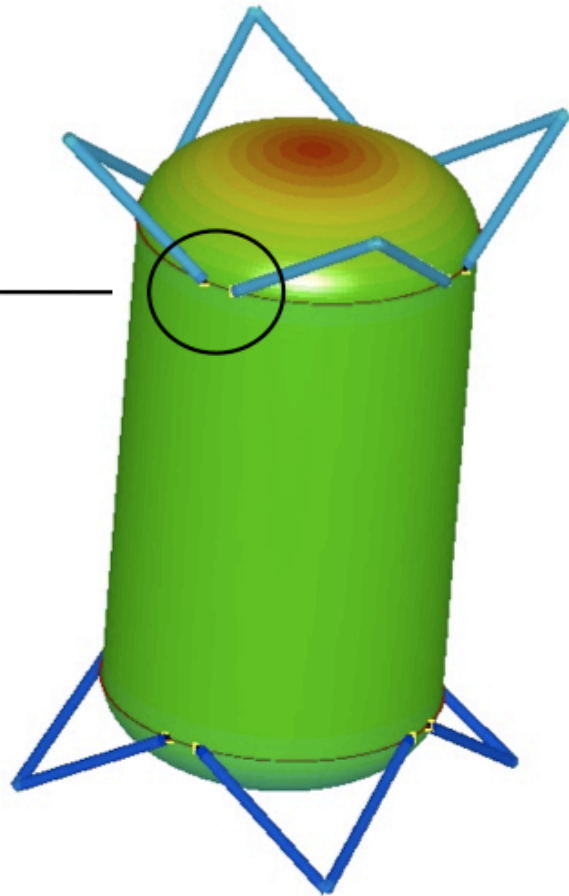
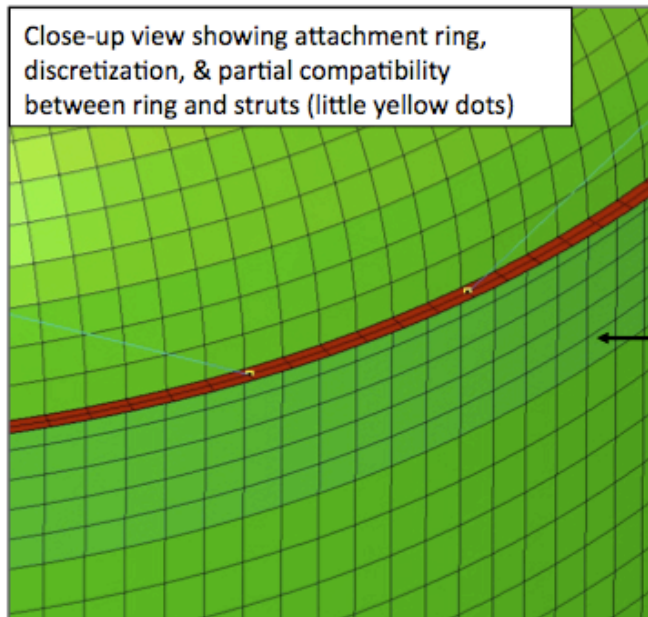


Fig. 23 Results from the specific case called “test”: Optimized long propellant tank with two sets of struts (aft and forward), 4 pairs of struts in each set. **Shown here is the buckling mode of the propellant tank under Load Case 2, 10g lateral acceleration (leftward acceleration).** The forward dome buckles at a lower load factor than the aft dome because the skin thickness of the forward dome, $THKFWD = 0.05775$ inch, is significantly less than the skin thickness of the aft dome, $THKAFT = 0.07150$ inch.



Also revised "full" model to make sure it was 100% consistent with "slice" model

- Found small error in shell offsets which was corrected
- Changed strut attachment ring idealization to shells
- Analyzed to same loads

Fig. 24 STAGS finite element model of the optimized long propellant tank with two sets of struts, aft (Lower) and forward (Upper), with 4 pairs of struts at each axial location. The struts are pinned to the centroids of the aft and forward propellant tank external support rings and to rigid "ground". The STAGS "410" finite element is used in the model of the propellant tank shell wall.

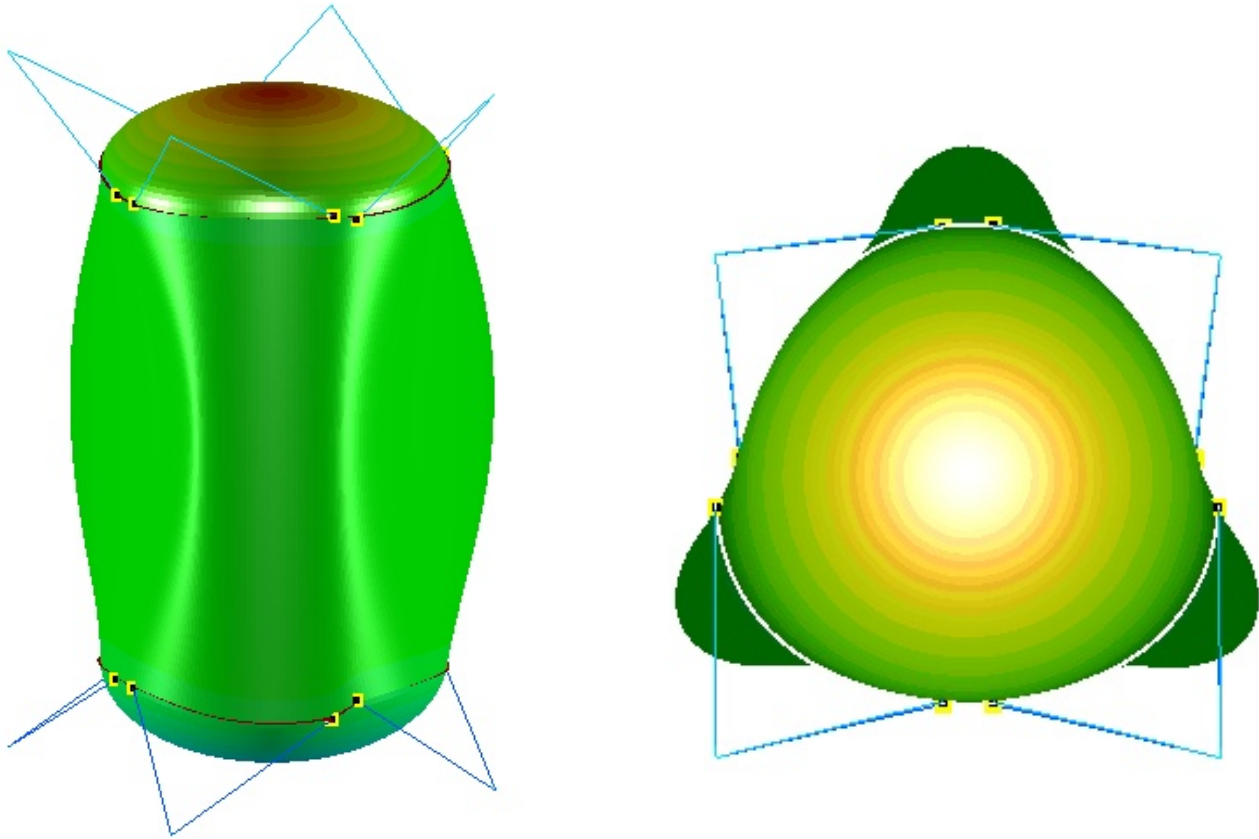


Fig. 25a **The lowest vibration mode from the STAGS model. The modal vibration frequency predicted by STAGS is 12.19 Hz.** This mode is a combination of shell deformation with $n = 3$ circumferential waves and uniform lateral motion of the propellant tank approximately as a rigid body with significant tension and compression in the supporting struts. The lateral tank motion with associated tension and compression in the struts can most easily be appreciated from the image on the right-hand side of this figure. In that image the uniform lateral component of the total motion of the tank is upward in the plane of the paper. The two components of vibration motion, lateral tank motion and $n = 3$ shell deformation motion, which are combined in a single mode in this STAGS model, are decoupled in the GENOPT/BIGBOSOR4 model displayed in Figs. 16a and 16b: the lateral/pitching motion depicted in Fig. 16a(C) with a frequency of 12.161 Hz and the $n = 3$ shell deformation motion depicted in Fig. 16b(F) with a frequency of 13.327 Hz.

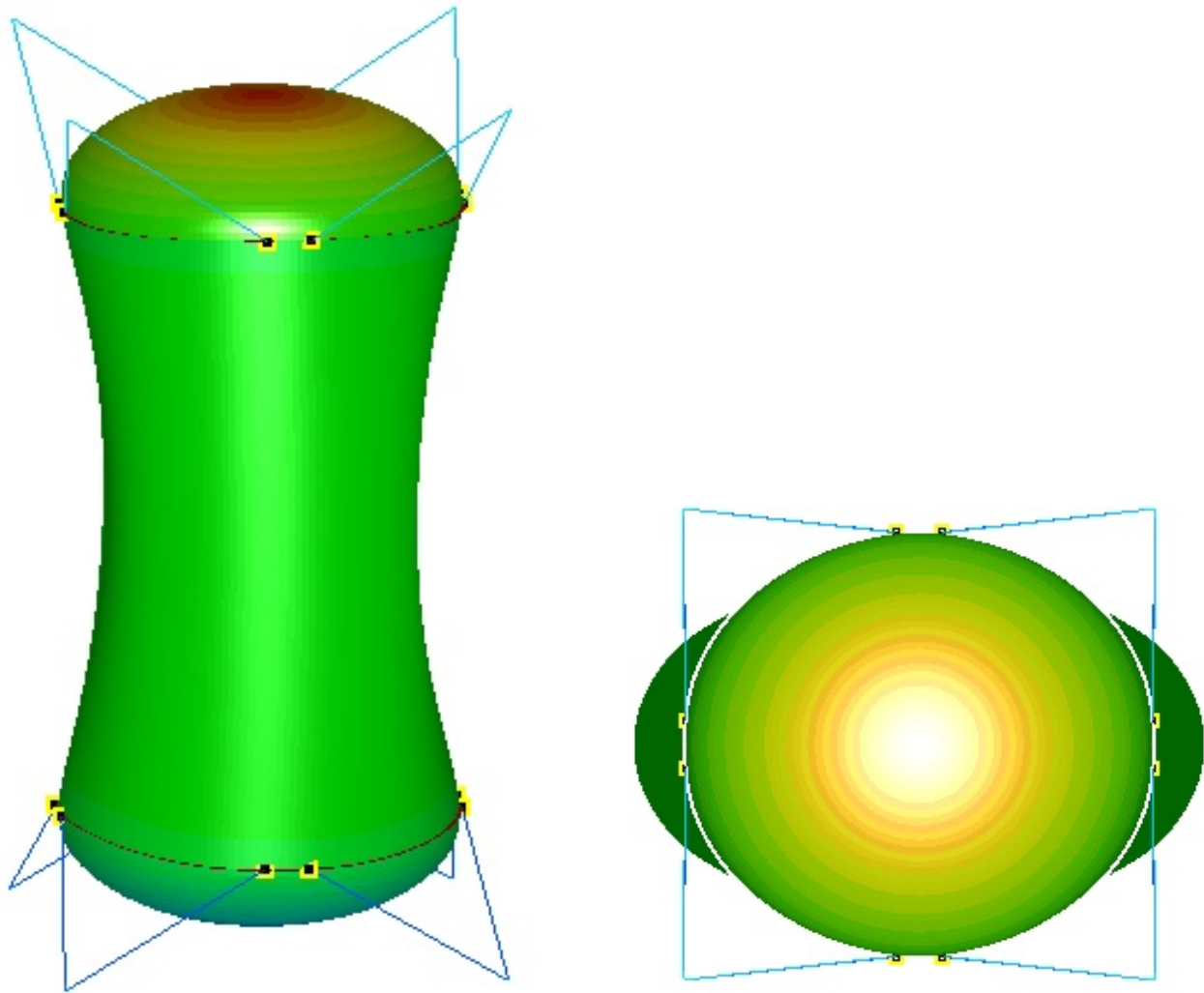


Fig. 25b **The second vibration mode from the STAGS model. The modal vibration frequency predicted by STAGS is 13.02 Hz.** This mode is essentially pure shell deformation with $n = 2$ circumferential waves. The analogous $n = 2$ shell deformation mode predicted by GENOPT/BIGBOSOR4 is displayed in Fig. 16b(E) with its associated modal vibration frequency equal to 13.237 Hz.

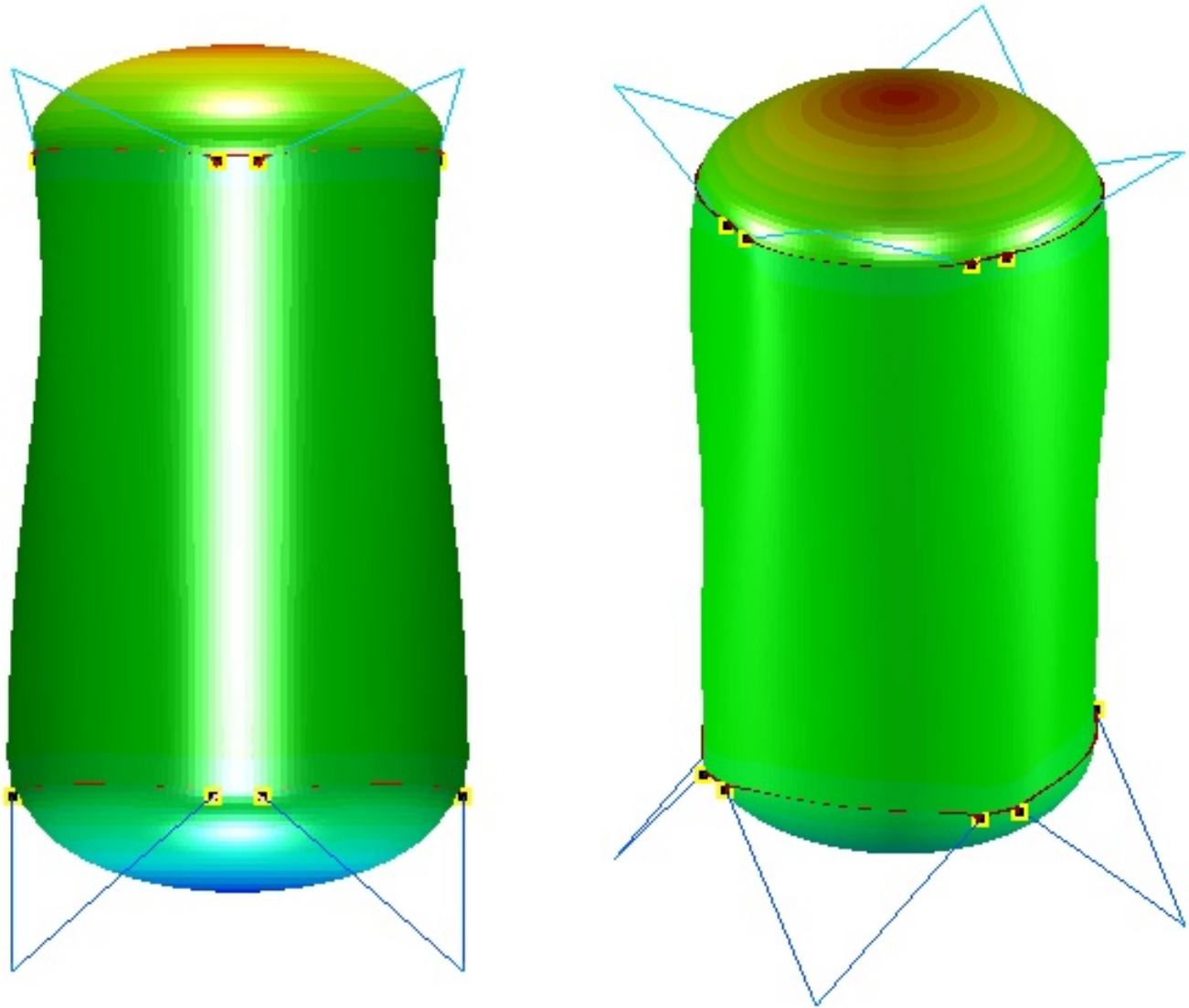


Fig. 25c Two views of the third vibration mode from the STAGS model. The modal vibration frequency predicted by STAGS is 13.46 Hz. This mode is a combination of shell “breathing” ($n = 0$ circumferential waves) and axial motion of the propellant tank approximately as a rigid body with significant tension and compression in the supporting struts. The axial tank motion with associated tension in the lower set of struts and compression in the upper set of struts can most easily be appreciated from the image on the left-hand side of the figure. In that image the axial component of the total motion of the tank is upward in the plane of the paper, as can be seen by the deformation of the aft struts (elongation) versus that of the forward struts (shortening). The axial motion of the propellant tank in the GENOPT/BIGBOSOR4 model is shown in Fig. 16a(A). It is associated with the modal vibration frequency 12.069 Hz, which is the lowest frequency determined by the GENOPT/BIGBOSOR4 model.

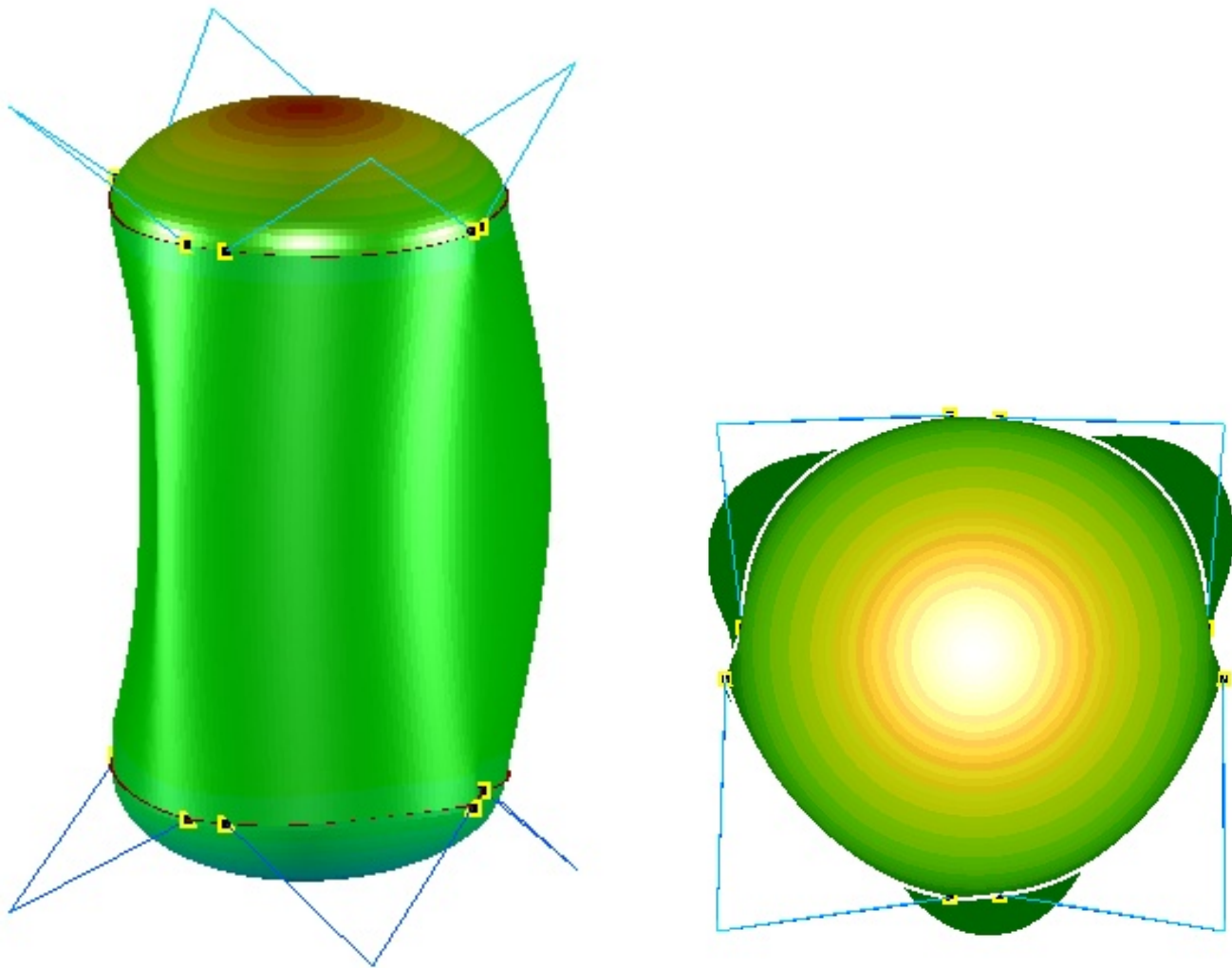


Fig. 25d **The fourth vibration mode from the STAGS model. The modal vibration frequency predicted by STAGS is 13.90 Hz.** This mode is analogous to that displayed by the STAGS model in Fig. 25a: a combination of shell deformation with $n = 3$ circumferential waves and uniform lateral motion of the propellant tank approximately as a rigid body with significant tension and compression in the supporting struts. While the two superficially similar STAGS vibration modes that are orthogonal to each other shown here and in Fig. 25a can exist, there is no analogous situation in which there exist multiple modes with primarily lateral tank motion in the decoupled GENOPT/BIGBOSOR4 model. As with Fig. 25a, the two components of total motion from STAGS shown here should be compared with the predictions from GENOPT/BIGBOSOR4 shown in Figs. 16a(C) and 16b(F).

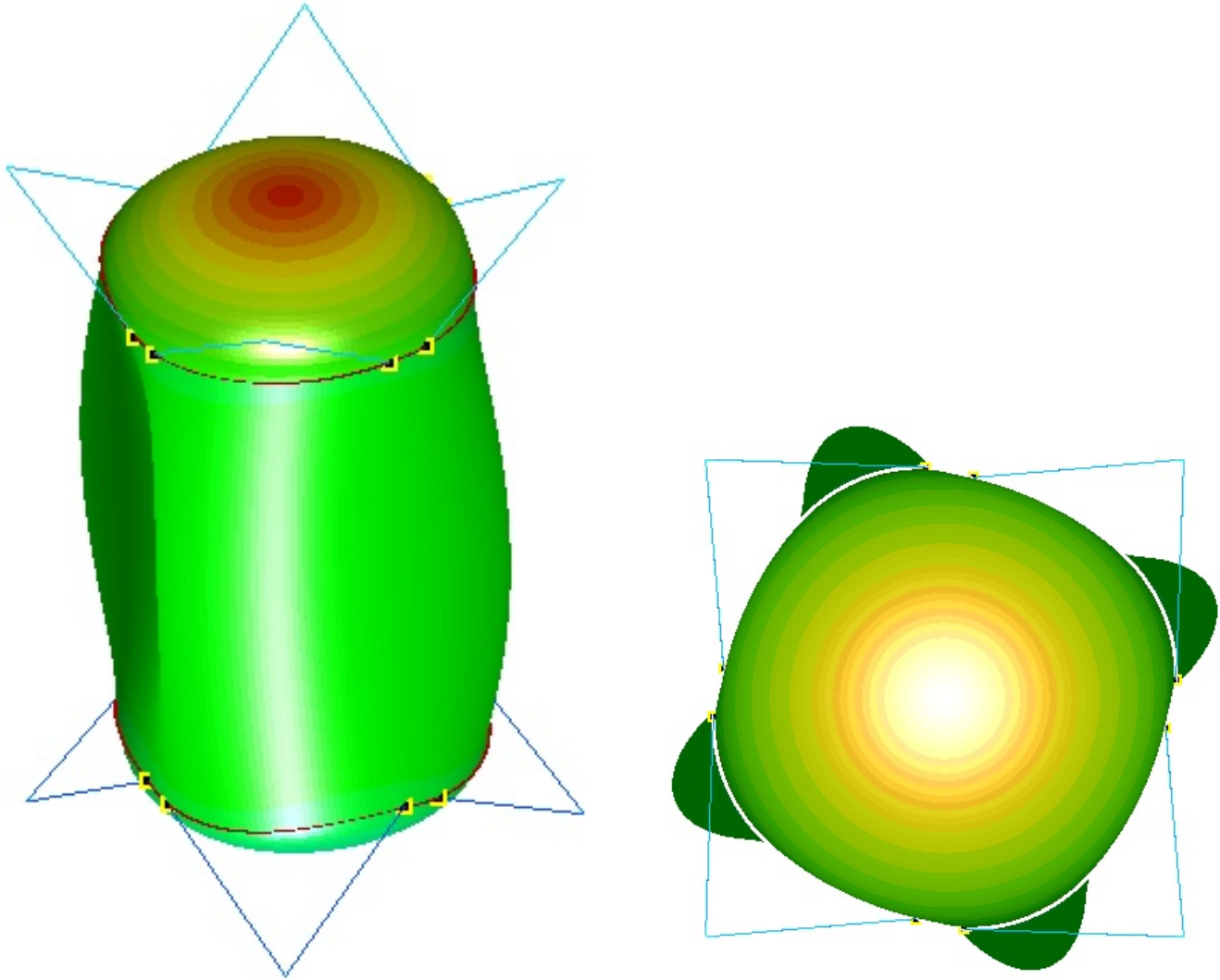


Fig. 25e **The fifth vibration mode from the STAGS model. The modal vibration frequency predicted by STAGS is 15.92 Hz.** This mode is a combination of shell deformation with $n = 4$ circumferential waves and uniform rolling of the propellant tank approximately as a rigid body with significant tension and compression in the supporting struts. The rolling motion with associated tension and compression in the struts can most easily be appreciated from the image on the right-hand side of the figure. In that image the approximately “uniform” rolling component of the total motion of the tank is counterclockwise. The two components of vibration motion, rolling tank motion and $n = 4$ shell deformation motion, which are combined in a single mode in this STAGS model, are decoupled in the GENOPT/BIGBOSOR4 model displayed in Figs. 16a and 16b: the tank rolling motion depicted in Fig. 16a(B) with a frequency of 17.787 Hz and the $n = 4$ shell deformation motion depicted in Fig. 16b(G) with a frequency of 16.676 Hz.

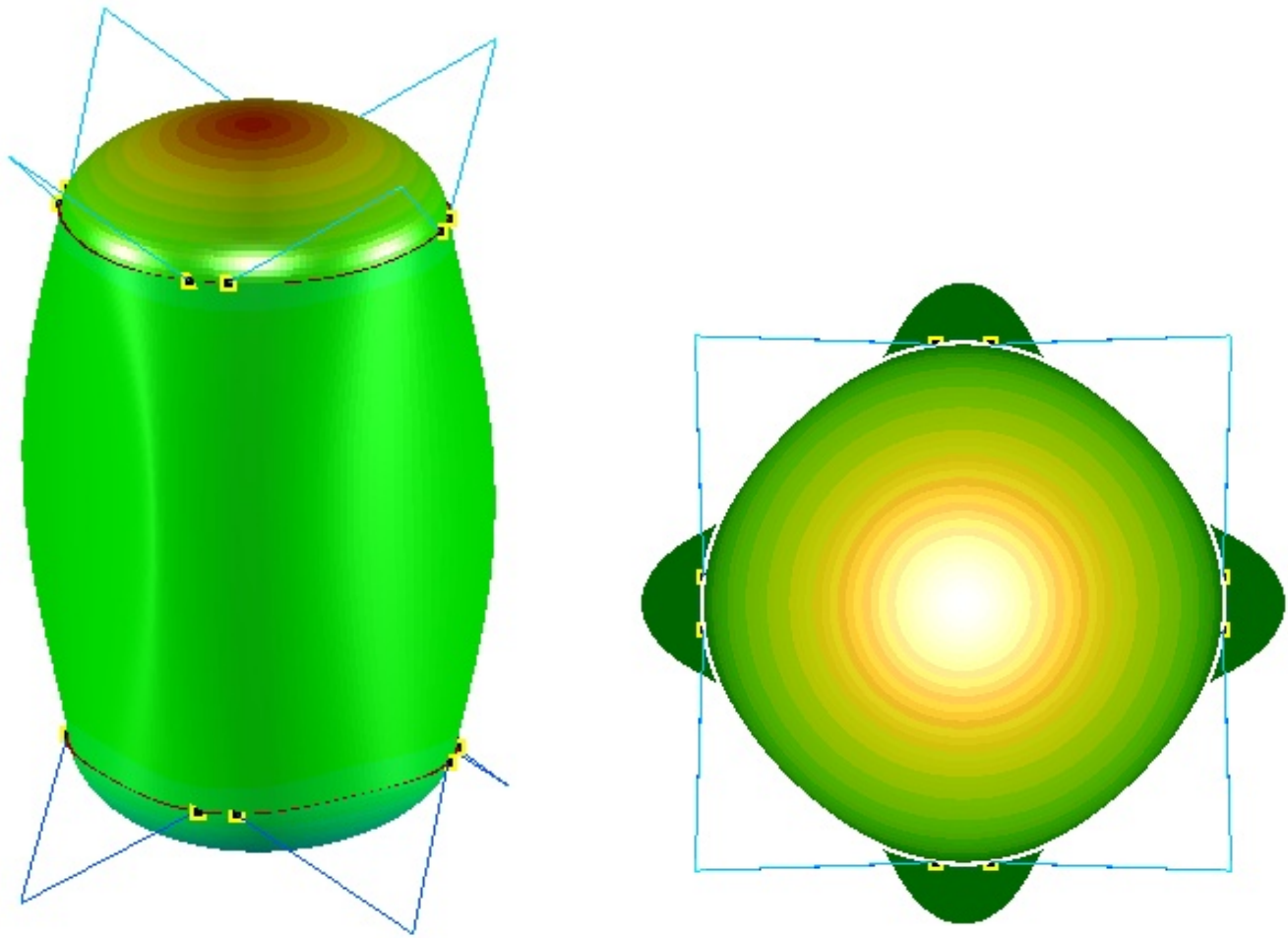


Fig. 25f **The sixth vibration mode from the STAGS model. The modal vibration frequency predicted by STAGS is 16.19 Hz.** This mode is essentially pure shell deformation with $n = 4$ circumferential waves. The analogous $n = 4$ shell deformation mode predicted by GENOPT/BIGBOSOR4 is displayed in Fig. 16b(G) with its associated modal vibration frequency equal to 16.676 Hz.

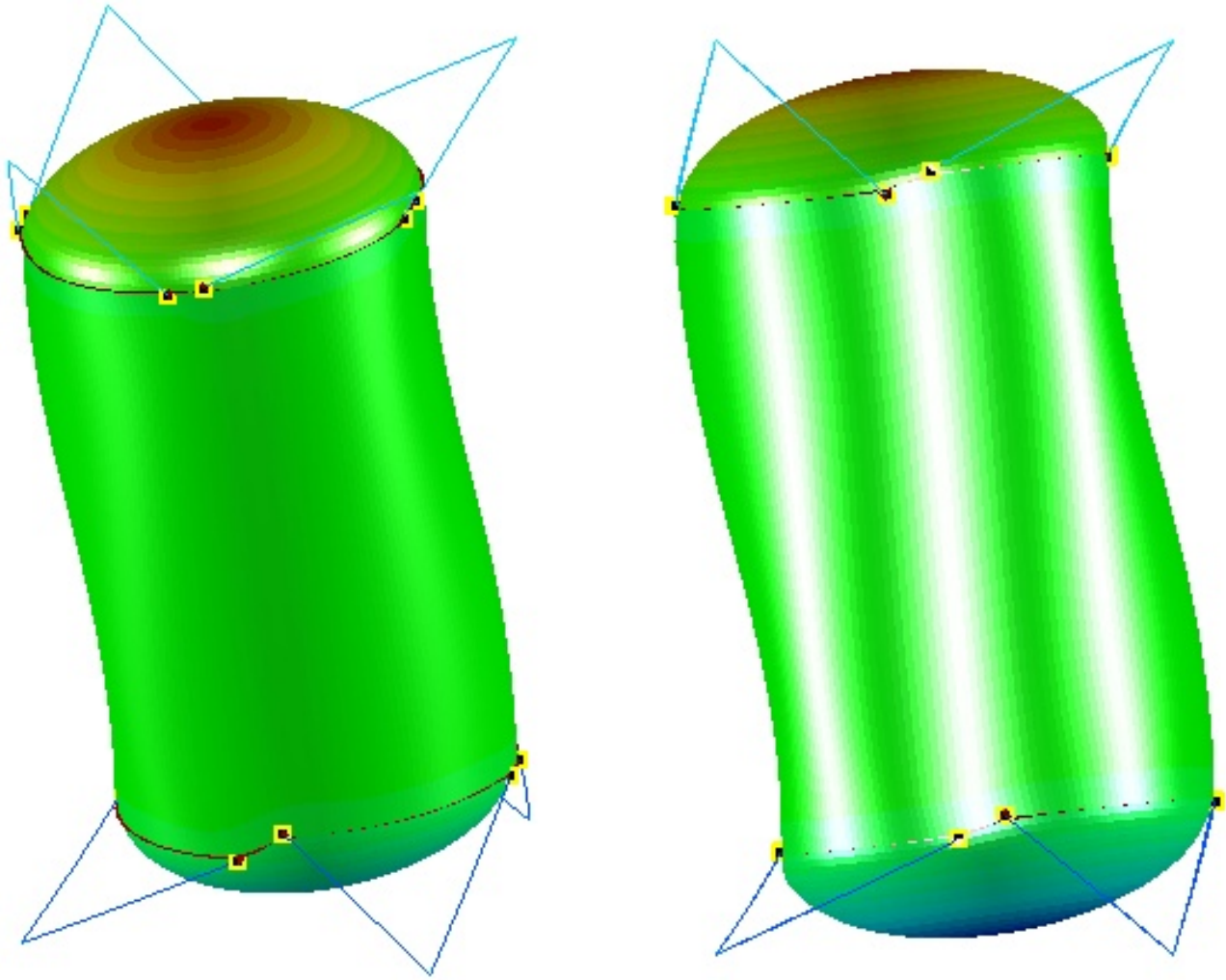


Fig. 25g **Two views of the seventh vibration mode from the STAGS model. The modal vibration frequency predicted by STAGS is 16.25 Hz.** This mode is a combination of shell deformation with $m = 2$ axial half-waves and mostly pitching motion of the propellant tank approximately as a rigid body with significant tension and compression in the supporting struts. The GENOPT/BIGBOSOR4 model predicts mostly pitching tank motion with a modal vibration frequency equal to 15.284 Hz, as displayed in Fig. 16a(D). Shell deformation modes with m greater than one-half axial wave were not computed for the GENOPT/BIGBOSOR4 model.

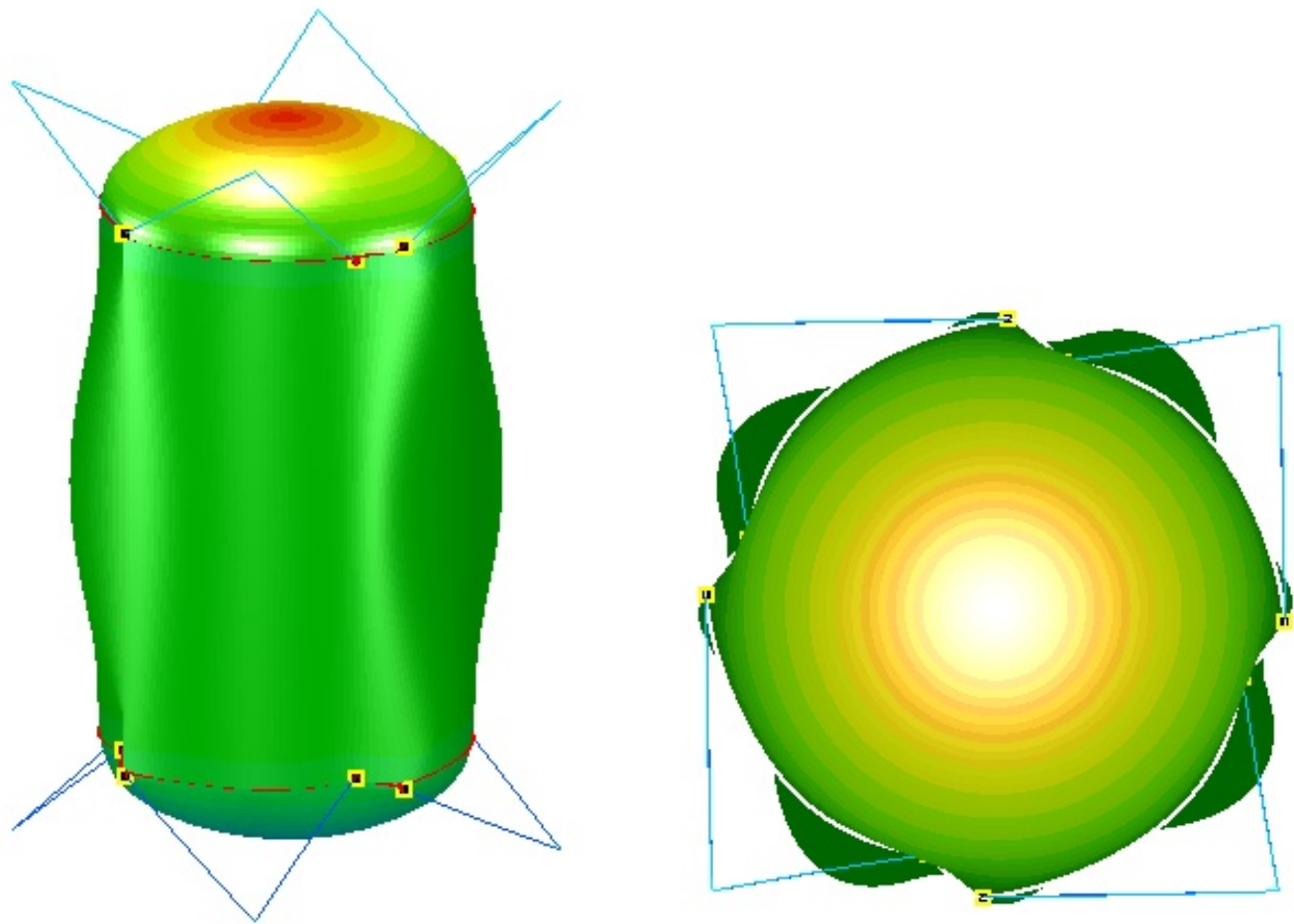


Fig. 25h **The eighth vibration mode from the STAGS model. The modal vibration frequency predicted by STAGS is 19.82 Hz.** The situation here is analogous to that depicted by the STAGS model in Fig. 25d ($n = 3$ circumferential waves + some tank lateral motion) and compared with Fig. 25a ($n = 3$ circumferential waves + some tank lateral motion). This mode is analogous to that displayed in Fig. 25e: a combination of shell deformation with $n = 4$ circumferential waves and rolling motion of the propellant tank approximately as a rigid body with significant tension and compression in the supporting struts. While the two superficially similar STAGS vibration modes that are orthogonal to each other shown here and in Fig. 25e can exist, there is no analogous situation in which there exist multiple modes with primarily tank rolling motion in the decoupled GENOPT/BIGBOSOR4 model. As with Fig. 25e the two components of total motion from STAGS shown here should be compared with the predictions from GENOPT/BIGBOSOR4 shown in Figs. 16a(B) and 16b(G).

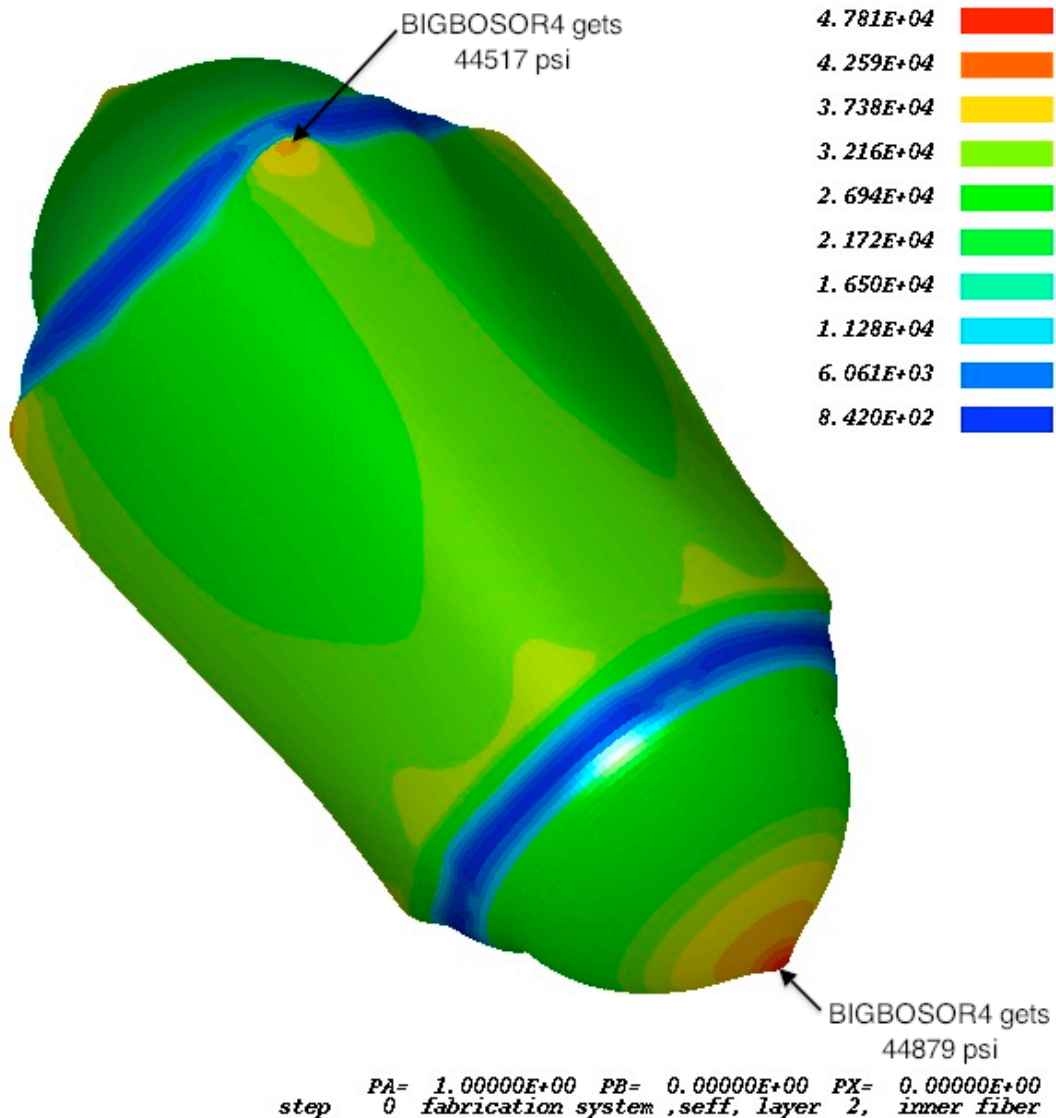


Fig. 26a Load Case 1 (10g axial acceleration + 25 psi internal pressure + 200-degree tank cool-down): **Outer fiber effective stress, “seff” (psi), in the skin of the optimized long propellant tank with aft and forward sets of struts, 4 pairs of struts at each axial location** (the specific case called “test”; struts not shown in this view). (NOTE: The caption above automatically produced by STAGS contains the string, “inner fiber”. In this particular application of STAGS the normal vectors to the shell reference surface all point toward the interior of the tank. Therefore, what STAGS calls “inner fiber” corresponds to the external surface of the tank.) In the STAGS analysis that produced this figure all the loading is in Load Set A: 10g axial acceleration, 25 psi internal pressure, and 200 degrees tank cool-down. There is no Load Set B. In STAGS jargon the load factor for Load Set A is called “PA” and the load factor for Load Set B is called “PB”. Compare with the GENOPT/BIGBOSOR4 prediction shown in Fig. 21a(A). What are external tapered doublers with maximum thickness = 0.886 inch in the GENOPT/BIGBOSOR4 model are replaced by external doublers of constant average thickness = 0.443 inch in this STAGS model. The predictions from BIGBOSOR4 are given in Fig. 21a(A), indicated there as Critical Point Nos. 1 and 3.

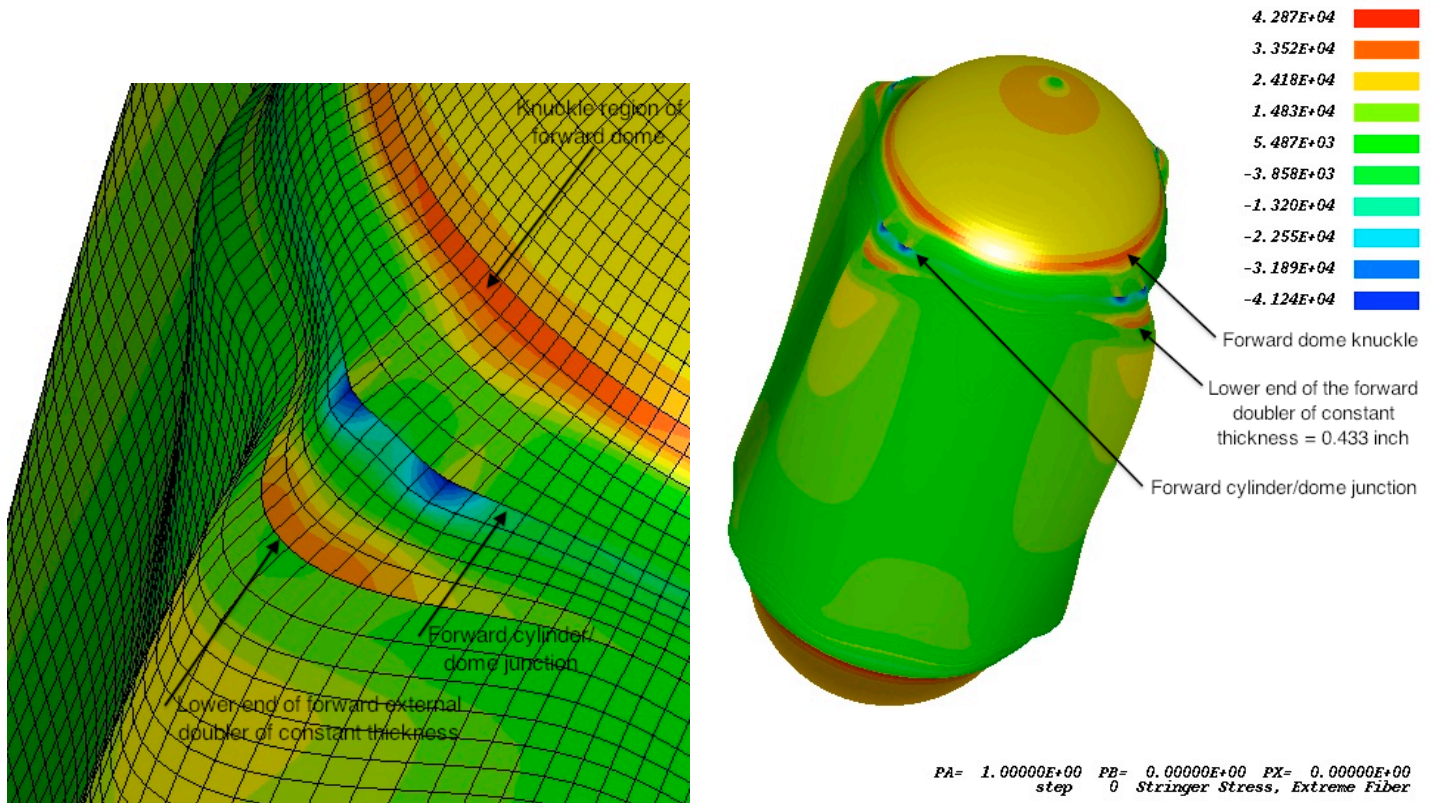


Fig. 26b Load Case 1 (10g axial acceleration + 25 psi internal pressure + 200-degree tank cool-down): Stress (psi) at the tips of the internal orthogrid stringers of the optimized long propellant tank with aft and forward sets of struts, 4 pairs of struts at each axial location. Compare with the GENOPT/BIGBOSOR4 prediction shown in Fig. 21a(A). In the STAGS model the internal orthogrid is modeled as an orthotropic layer of the propellant tank shell wall with “effective” meridional and circumferential stiffnesses equal to the actual material modulus reduced by the ratio of stringer thickness divided by stringer spacing and ring thickness divided by ring spacing, respectively. Note that the GENOPT/BIGBOSOR4 model with tapered external doublers [Fig.21a(A)] predicts significantly higher maximum **tensile** stress at the tips of the internal orthogrid stringers (Critical point no. 2 = 50000 psi) than does this STAGS model (maximum **tensile** stringer stress in the knuckle of the ellipsoidal dome = 42870 psi). In this STAGS model the external doublers have constant thickness = 0.443 inch. Figure 21c(B) shows predictions from a BIGBOSOR4 model with similar constant thickness doublers that yields dramatically higher maximum **compressive** stress at the tips of the internal orthogrid stringers (-119000 psi), indicating that the STAGS prediction of maximum compressive stress at the tips of the internal orthogrid stringers (-41240 psi) displayed here is not converged with respect to finite element mesh density. The **tensile** stress concentration at the tips of the orthogrid stringers that occurs at the lower edge of the forward external **constant thickness doubler** does not appear in the BIGBOSOR4 model with the external **tapered doubler**. Compare the maximum tensile and compressive stresses at the stringer tips shown here with those displayed in the much more refined STAGS 45-degree model displayed in Figs. 26c and 26e.

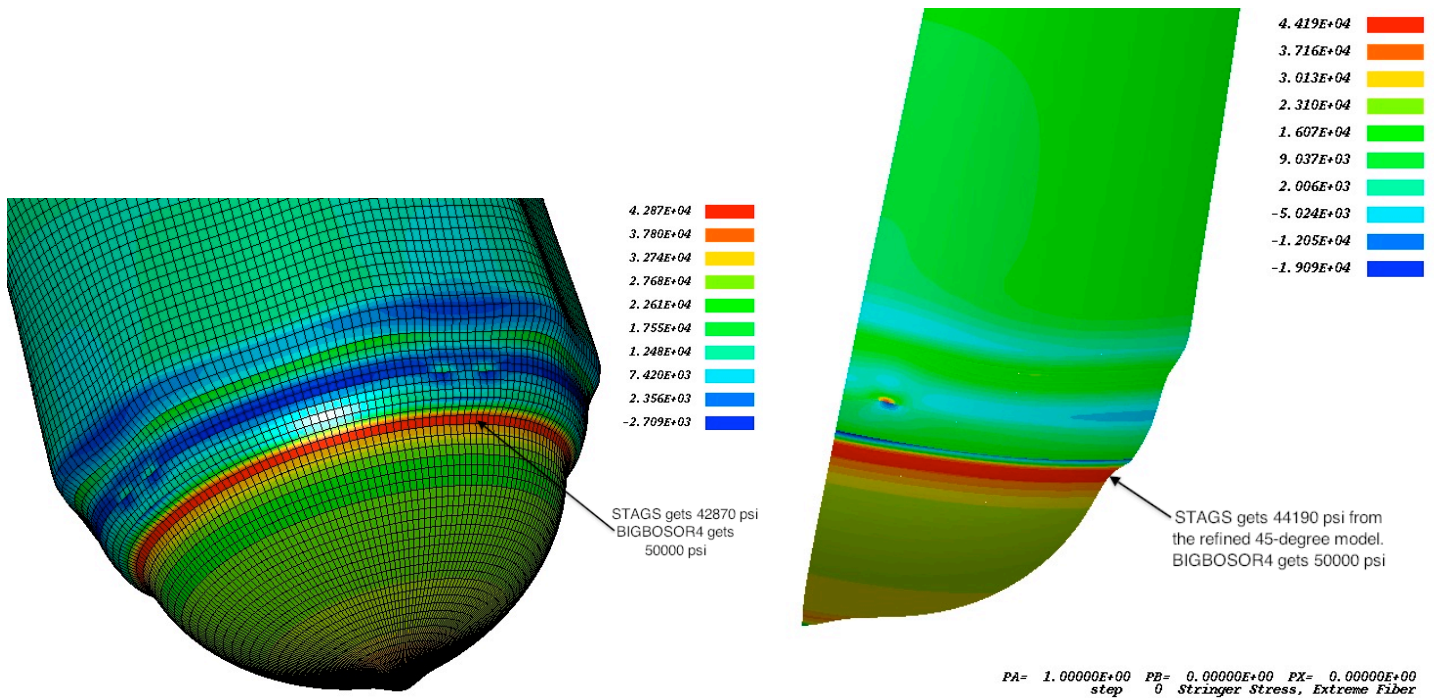


Fig. 26c Load Case 1 (10g axial acceleration + 25 psi internal pressure + 200 degrees tank cool-down): Stress (psi) at the tips of the internal orthogrid stringers from the STAGS 360-degree model and from the refined STAGS 45-degree model of the optimized long propellant tank with aft and forward sets of struts, 4 pairs of struts at each axial location. (The struts are not shown in this view.) This figure shows the aft end of the same STAGS model as that displayed in the previous figure. The maximum **tensile stress at the tips of the orthogrid stringers (narrow red band) occurs in the knuckle region of the aft ellipsoidal dome and is essentially axisymmetric. It is generated almost entirely by the uniform internal pressure, 25 psi, plus the linearly varying normal pressure head applied by the propellant to the shell wall as a result of the 10 g axial acceleration. Compare with the GENOPT/BIGBOSOR4 prediction of 50000 psi at Critical Point No. 2 as shown in Fig. 21a(A). Both the STAGS prediction shown here and the BIGBOSOR4 prediction shown in Fig. 21a(A) are generated from linear stress analyses.**

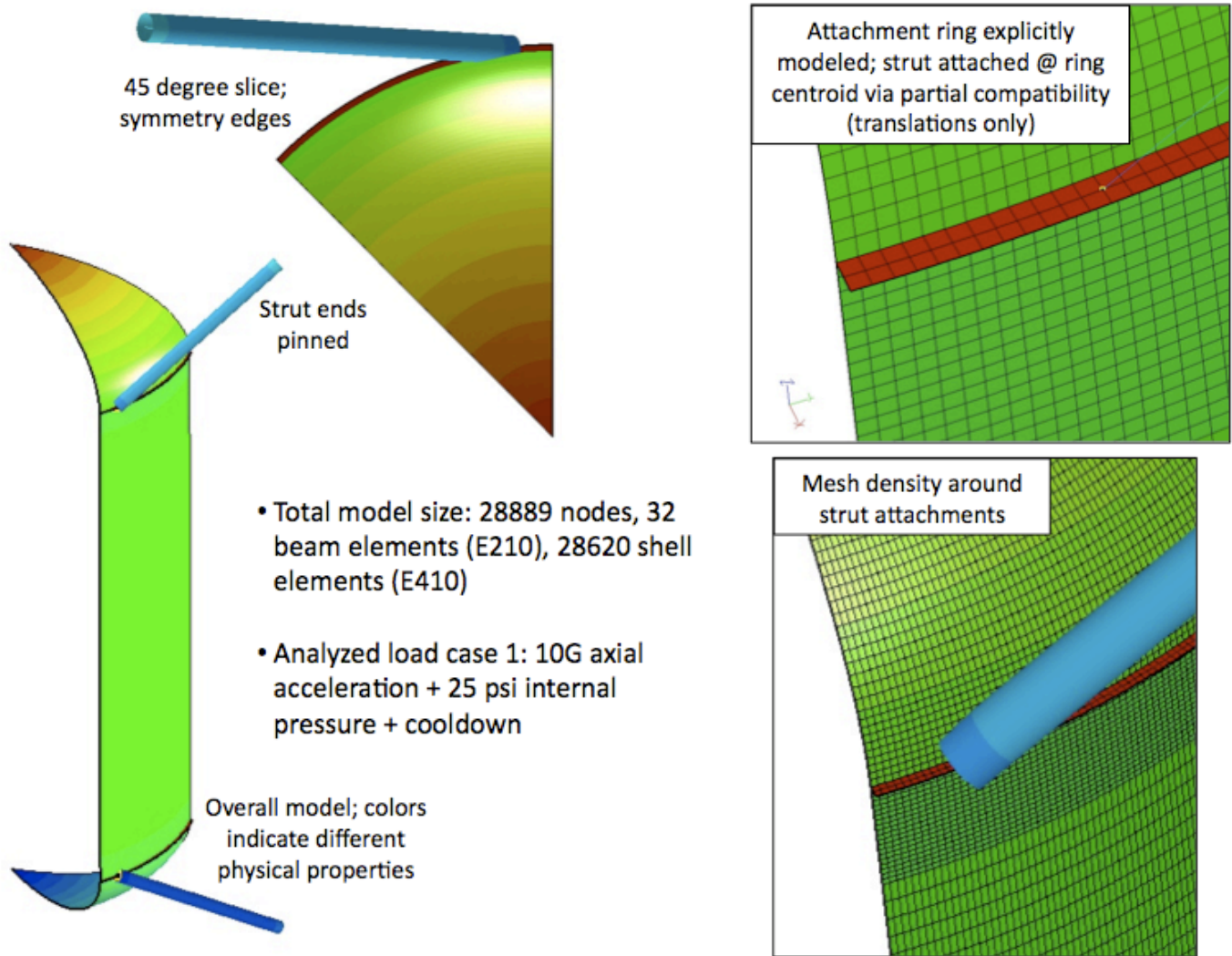


Fig. 26d A very refined STAGS model of the tank/strut system for the prediction of stresses at the tips of the internal orthogrid stringers under Load Case 1 (10 g axial acceleration + 25 psi internal pressure + 200 degrees tank cool-down). Compare this model with the STAGS 360-degree model of the tank/strut system shown in Fig. 24.

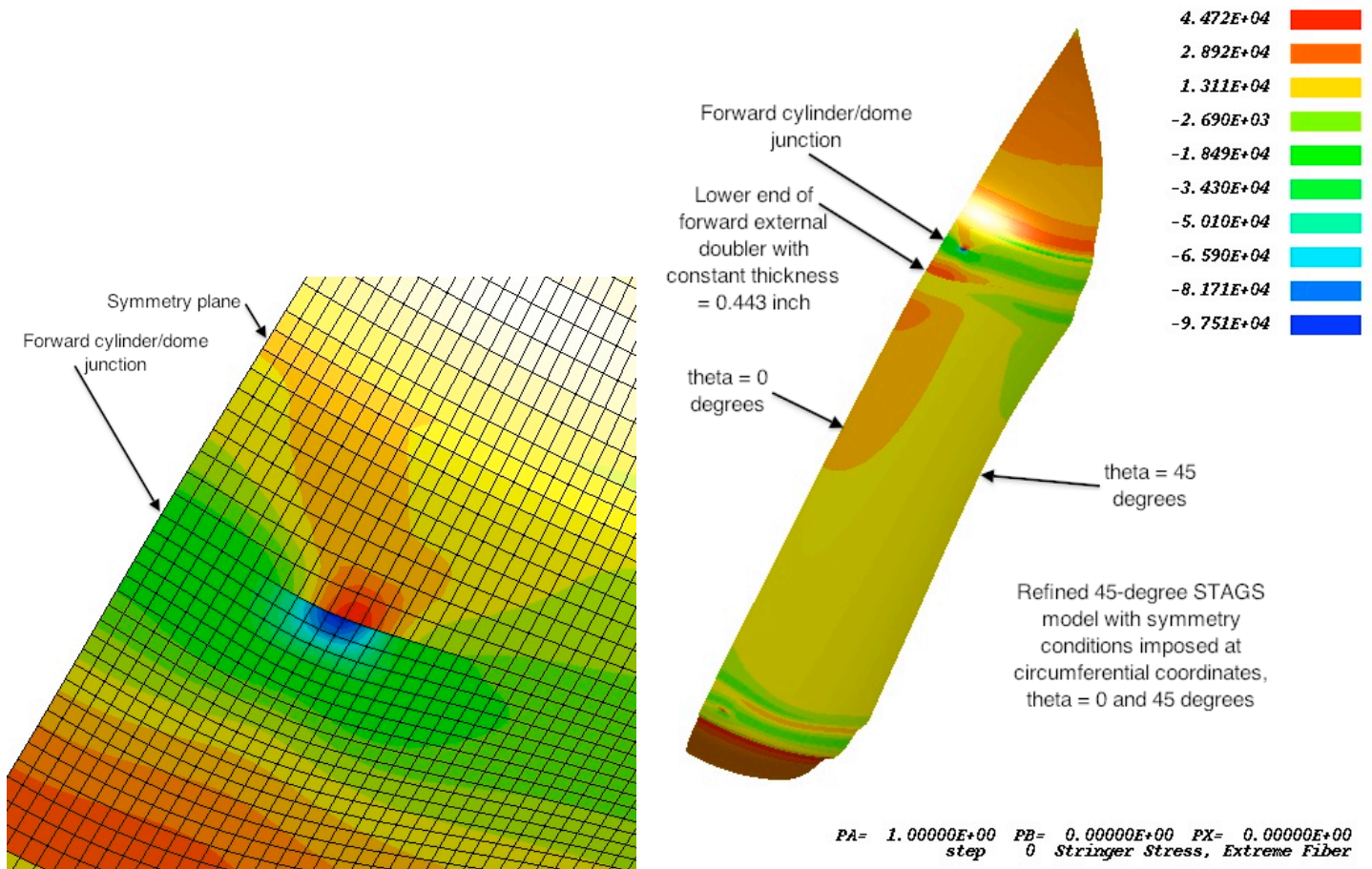


Fig. 26e Load Case 1 (10g axial acceleration + 25 psi internal pressure + 200-degree tank cool-down): Stress (psi) at the tips of the internal orthogrid stringers predicted from the refined STAGS 45-degree model shown in the previous figure. Compare with the orthogrid stringer tip stresses displayed in Fig. 26b. The maximum stresses at the tips of the stringers in the internal orthogrid “layer” of the shell wall at the forward cylinder/dome junction is much greater in this refined STAGS model than in the BIGBOSOR4 model with tapered external doublers, that is, the configuration that was optimized by GENOPT/TANK/BIGBOSOR4. However, it agrees fairly well with the predictions from the BIGBOSOR4 model with the constant thickness doublers, that is, the BIGBOSOR4 model that simulates the STAGS model. [See Fig. 21c(B).]

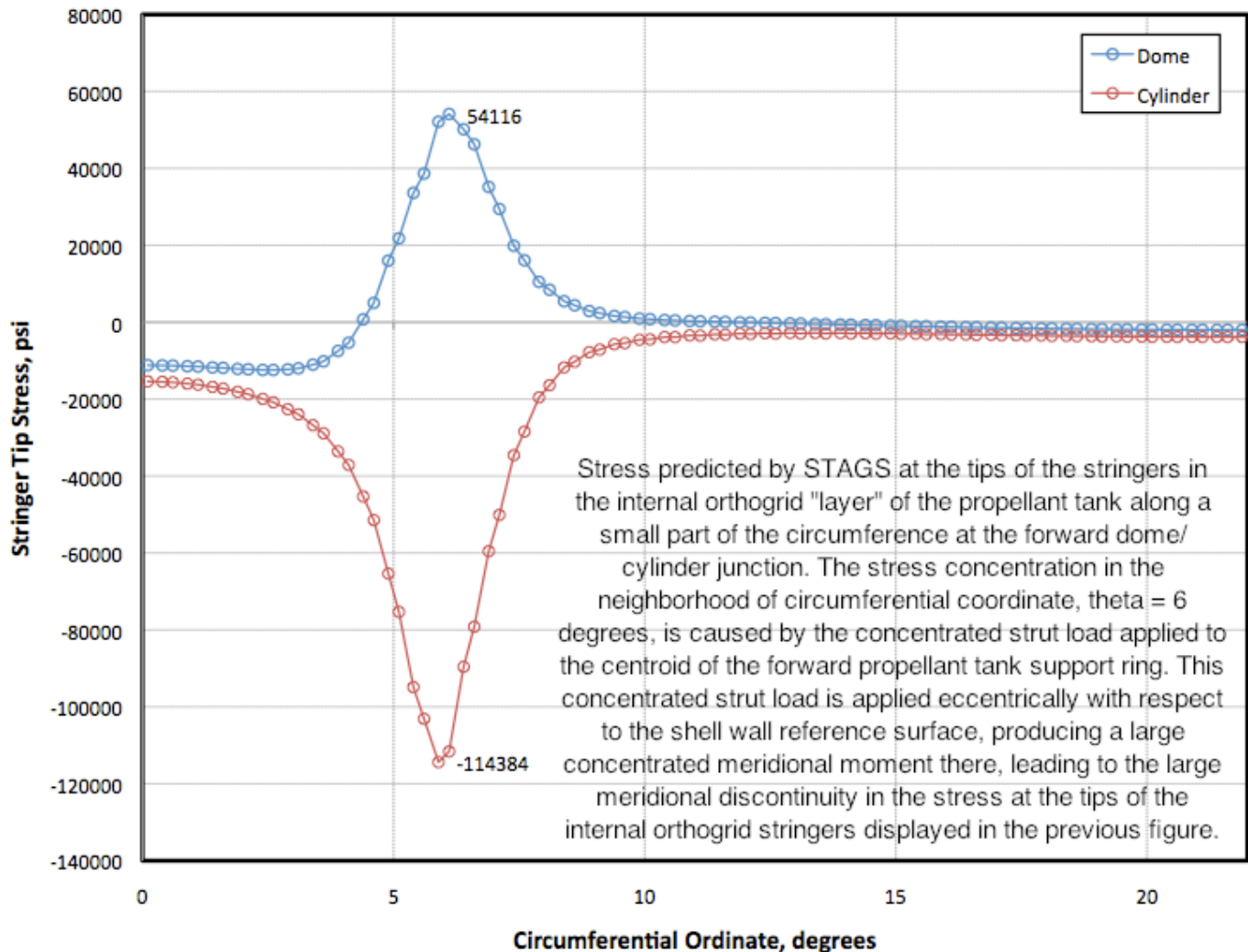


Fig. 26f The specific case, “test”, propellant tank under **Load Case 1** (10 g axial acceleration, 25 psi internal pressure and 200 degree tank cool-down). **Plots of the stress at the tips of the internal orthogrid stringers from the refined STAGS 45-degree model** shown in Figs. 26d and 26e. **Compare with the stresses predicted by the BIGBOSOR4 model with constant thickness doublers (the BIGBOSOR4 model that simulates the STAGS model).** These “BIGBOSOR4” stresses are plotted at the same location and are shown in Fig. 21d.

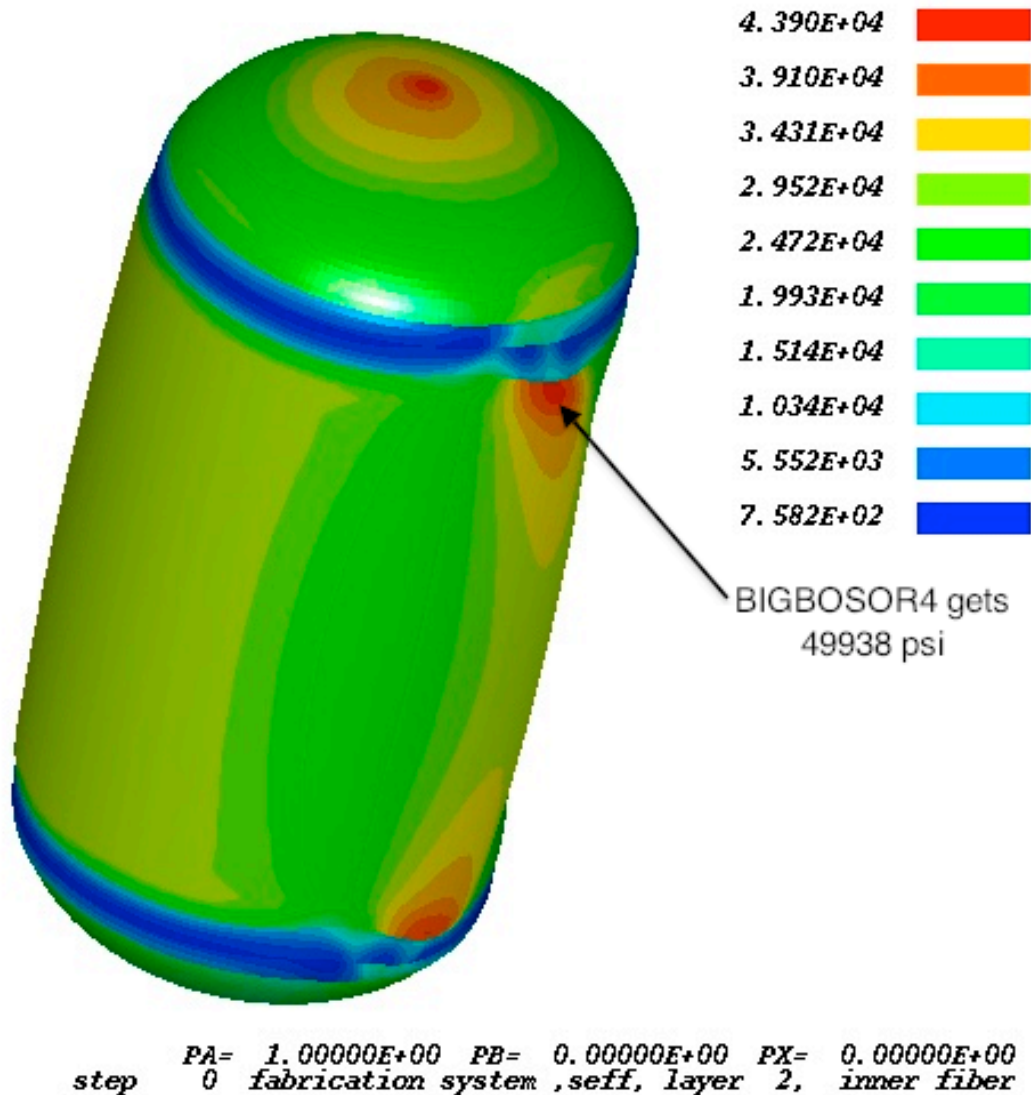


Fig. 27a STAGS model under Load Case 2 (lateral acceleration + 25 psi internal pressure + 200-degree tank cool-down): Outer fiber effective stress, “seff” (psi), in the skin of the optimized long propellant tank with aft and forward sets of struts, 4 pairs of struts at each axial location. (NOTE: The caption above automatically produced by STAGS contains the string, “inner fiber”. In this particular application of STAGS the normal vectors to the shell reference surface all point toward the interior of the tank. Therefore, what STAGS calls “inner fiber” corresponds to the external surface of the tank.) In the STAGS analysis that produced this figure all the loading is in Load Set A: 10g lateral acceleration, 25 psi internal pressure, and 200 degrees tank cool-down. There is no Load Set B. In STAGS jargon the load factor for Load Set A is called “PA” and the load factor for Load Set B is called “PB”. **Compare with the GENOPT/TANK/BIGBOSOR4 prediction shown in Fig. 21a(B).** The prediction of maximum effective stress in the skin from BIGBOSOR4 is indicated in Fig. 21a(B) as Critical Point No. 1: maximum effective stress = 49938 psi. In the BIGBOSOR4 model the external doublers are tapered with maximum thickness = 0.886 inch, whereas in this STAGS model the external doublers are of average constant thickness = 0.443 inch. No BIGBOSOR4 model with constant thickness doublers was constructed for analysis under Load Case 2.

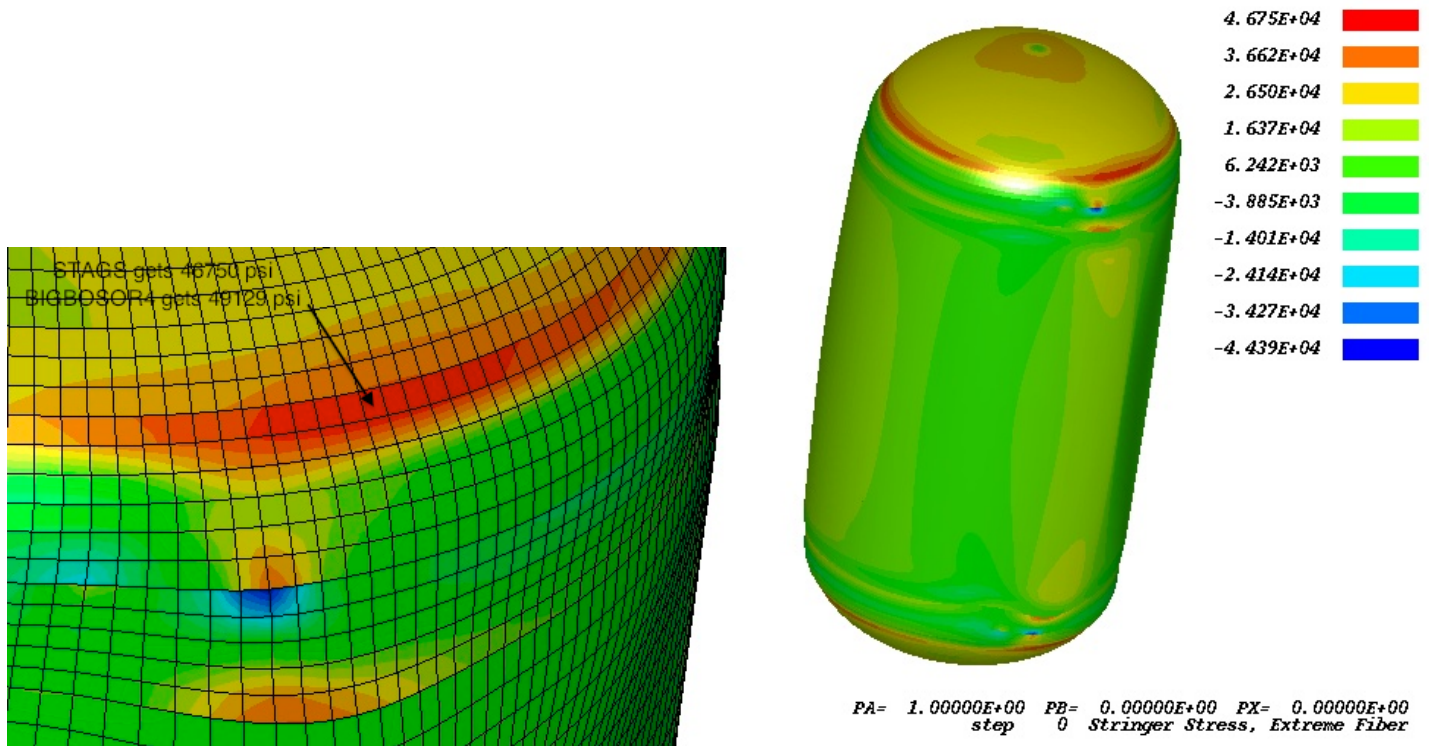
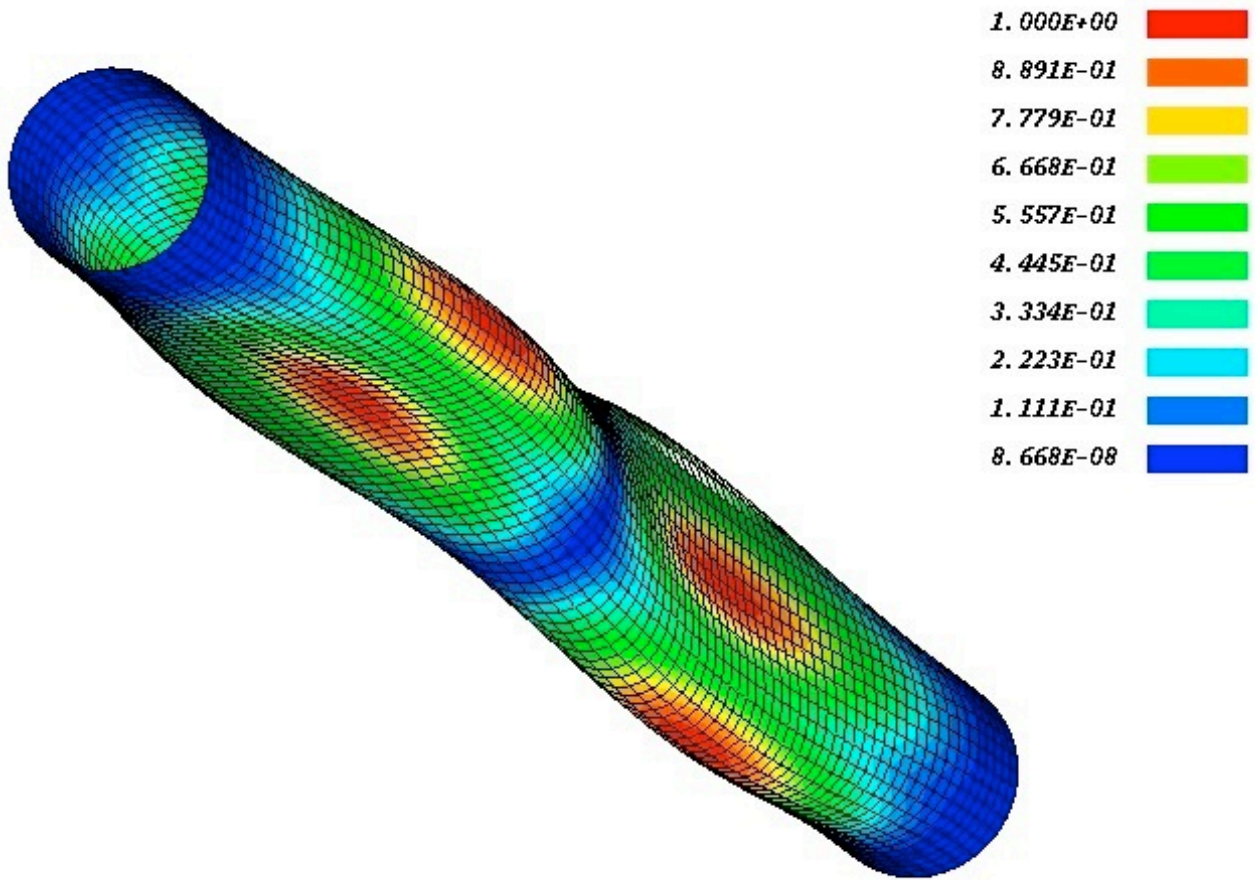
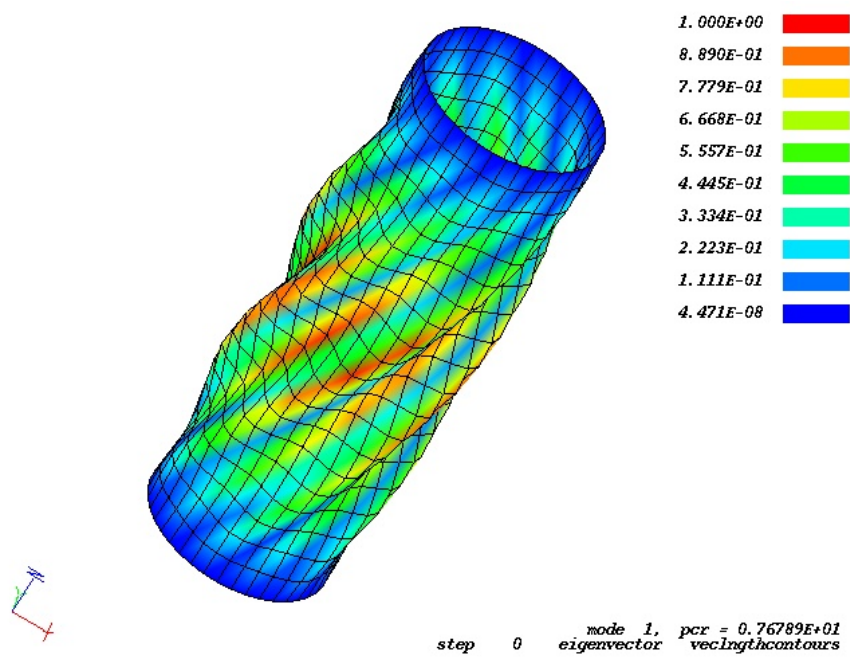


Fig. 27b STAGS model under Load Case 2 (10g lateral acceleration + 25 psi internal pressure + 200-degree tank cool-down): Stress (psi) at the tips of the internal orthogrid stringers of the optimized long propellant tank with aft and forward sets of struts, 4 pairs of struts at each axial location. Compare with the GENOPT/BIGBOSOR4 prediction shown in Fig. 21a(B), in particular Critical Point No. 2 indicated there, for which BIGBOSOR4 yields a prediction of 49129 psi. In the STAGS model the internal orthogrid is modeled as an orthotropic layer of the propellant tank shell wall with “effective” meridional and circumferential stiffnesses equal to the actual material modulus reduced by the ratio of stringer thickness divided by stringer spacing and ring thickness divided by ring spacing, respectively.

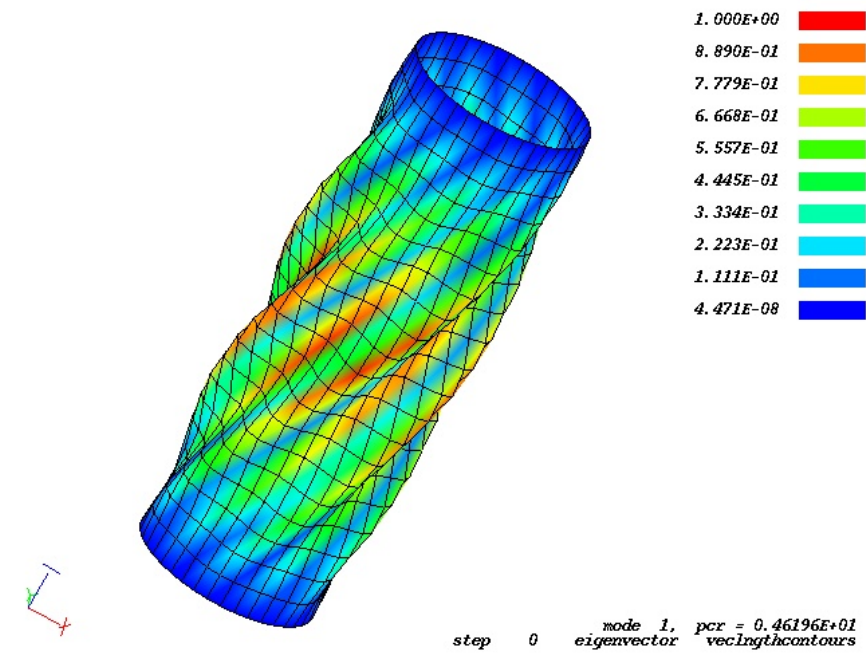


~~XXX~~ 473
 step 0 mode 3, pcr = 4.62267E+01
 eigenvector vecLengthcontours

Fig. 28 Load Case 1: STAGS prediction of the critical shell buckling mode and load factor, $pcr = 4.73$, for the entire length of an aft strut for the optimized long propellant tank/strut system with two sets of struts, aft and forward, 4 pairs of struts in each set. The applied compressive load from the STAGS model is 24841 lbs. and the buckling load factor corresponding to this strut shell buckling mode is 4.73, which corresponds to the third eigenvalue (mode). The first two modes correspond to buckling of the strut as a column. **Compare with the strut shell buckling mode from BIGBOSOR4 shown in Fig. 20(A).** The difference in the BIGBOSOR4 and STAGS prediction for the buckling load factors here and in Fig. 20(A) is primarily due to the different prediction from GENOPT/TANK/BIGBOSOR4 and STAGS of maximum compressive load in an aft strut in Load Case 1 (axial acceleration): -22693 lbs according to GENOPT/TANK and -24841 lbs according to STAGS. [See Table 7(b, e).]



(A) Short segment of the aft strut, Load Case 1. Buckling load factor = 7.679 [See Fig. 20(C)]



(B) Short segment of the aft strut, Load Case 2. Buckling load factor = 4.620 [See Fig. 20(D)]

Fig. 29 STAGS predictions of shell buckling of a short segment of the aft strut in Load Cases 1 and 2

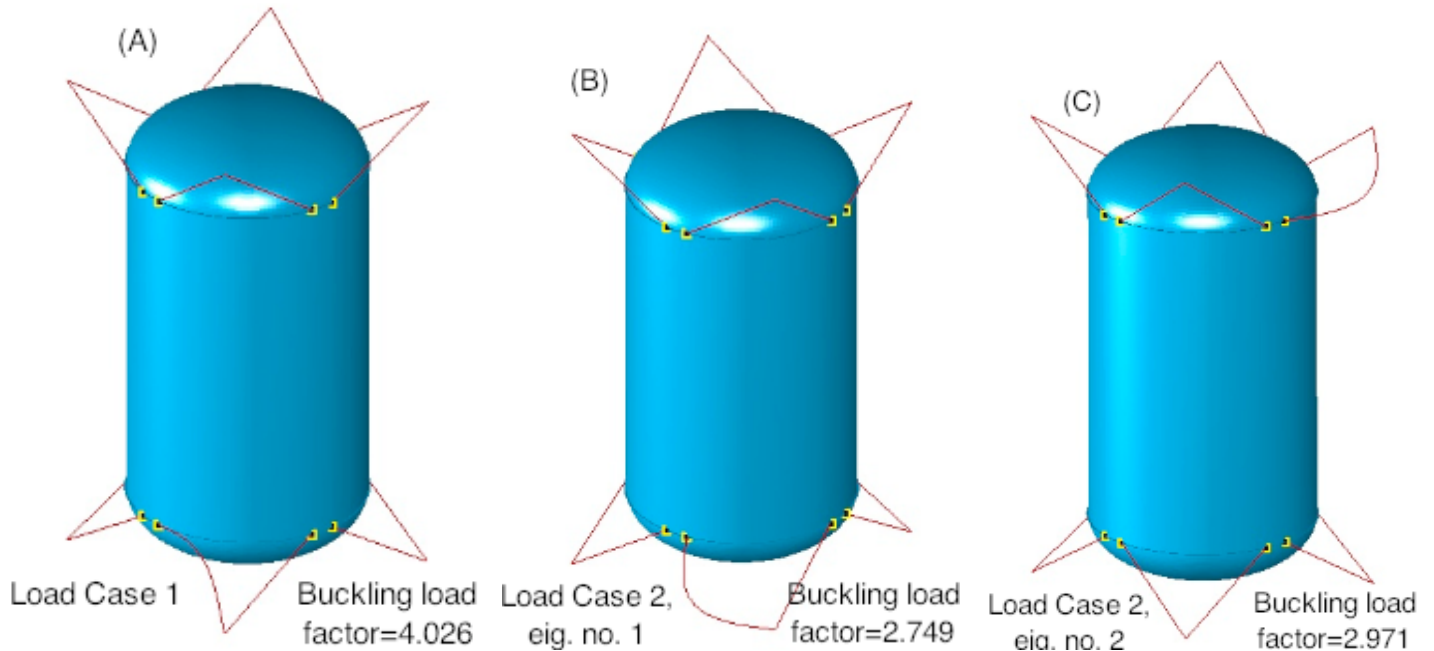


Fig. 30 STAGS prediction of linear buckling of the tank/strut system. In each of the three frames the lowest buckling load factor corresponds to buckling of only one strut as a column. All of the three loading components, 10g acceleration with associated spatially linearly varying normal pressure head, 25 psi uniform internal pressure, and 200-degree tank cool-down, are included in Load Set A (“eigenvalue” loads) in these particular buckling analyses. There is no Load Set B.

(A) Buckling of one of the aft struts under 10g upward **axial acceleration** plus 25 psi internal pressure plus 200-degree tank cool-down (eigenvalue no. 1 for Load Case 1).

(B) Buckling of one of the aft struts under 10g **lateral acceleration** plus 25 psi internal pressure plus 200-degree tank cool-down (eigenvalue no. 1 for Load Case 2).

(C) Buckling of one of the forward struts under 10g **lateral acceleration** plus 25 psi internal pressure plus 200-degree tank cool-down (eigenvalue no. 2 for Load Case 2).

Note that **Table 7(d)** also includes STAGS predictions for buckling of the struts as columns. The STAGS predictions listed in Table 7(d) are obtained from models in which only one pinned strut is included in each STAGS model; the propellant tank is absent. Therefore, any possible influence of the flexibility of the propellant tank on the STAGS buckling load factors listed in Table 7(d) is neglected. Notice that the strut buckling load factors computed from the STAGS model of the tank/strut system depicted here are almost exactly the same as those listed in Table 7(d): 4.026 here versus 3.99 in Table 7(d), 2.749 here versus 2.74 in Table 7(d), and 2.971 here versus 3.00 in Table 7(d). Therefore, according to predictions from STAGS, the flexibility of the propellant tank, included in the tank/strut system here, has virtually no influence on the buckling load factors predicted by STAGS.

The predictions from STAGS shown here are reasonably close to those predicted by GENOPT/TANK and listed in Table 7(d): 4.026 from STAGS versus 4.163 from GENOPT/TANK, 2.749 from STAGS versus 2.398 from GENOPT/TANK, 2.971 from STAGS versus 2.645 from GENOPT/TANK.

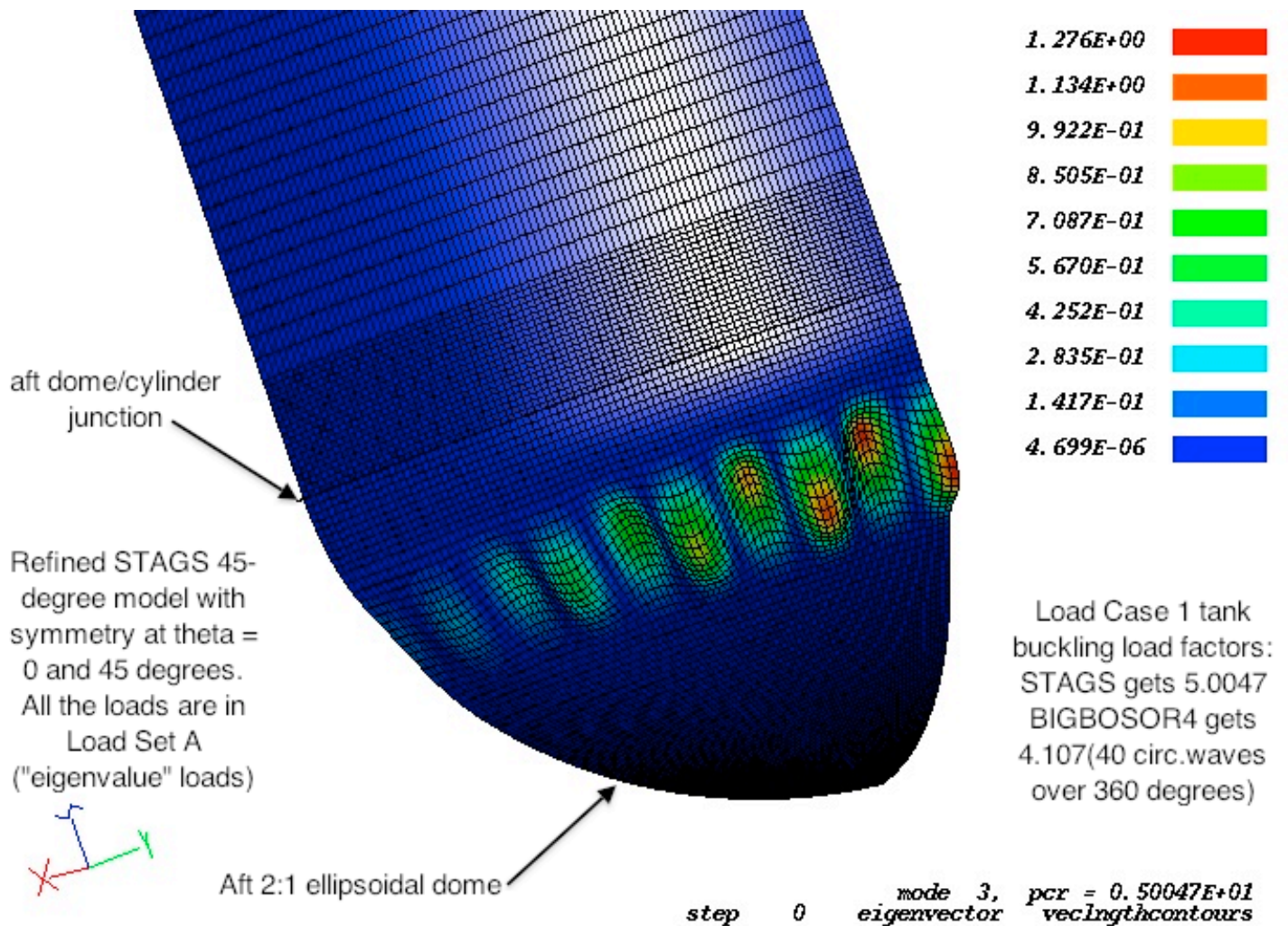


Fig. 31 **STAGS model of buckling of the propellant tank under Load Case 1** (10g axial acceleration plus 25 psi internal ullage pressure plus 200-degree tank cool-down). This is the same refined 45-degree STAGS model as that displayed in Fig. 26d except that this is a linear buckling model. In this STAGS model **all the load components are in Load Set A ("eigenvalue" loads). There is no Load Set B.** (For this problem it is very difficult to obtain with STAGS non-spurious buckling modes when there exist non-trivial loads in both Load Set A and Load Set B.) The struts shown in Fig. 26d are not shown in this view. In this STAGS model the fundamental (lowest) buckling load factor corresponding to buckling of the propellant tank is Buckling Mode No. 3. (The first two buckling modes involve buckling of the aft strut shown in Fig. 26d.) With all load components in Load Set A, BIGBOSOR4 obtains a buckling load factor of 4.107, which is somewhat lower than that predicted by this STAGS model (5.0047). The difference in predictions from BIGBOSOR4 and STAGS is caused primarily by the different widths of the external doublers in the two models. The critical buckling mode according to BIGBOSOR4 is the same as that shown in Fig. 22. Note that this STAGS model predicts 5 full circumferential waves over 45 degrees of circumference, which is the same as the 40 circumferential waves that BIGBOSOR4 predicts over 360 degrees of circumference. As shown in Fig. 22, with only the loads associated with the 10g axial acceleration in Load Set A and the 25 psi ullage pressure plus 200-degrees tank cool-down in Load Set B, BIGBOSOR4 predicts a much higher buckling load factor: 10.999.

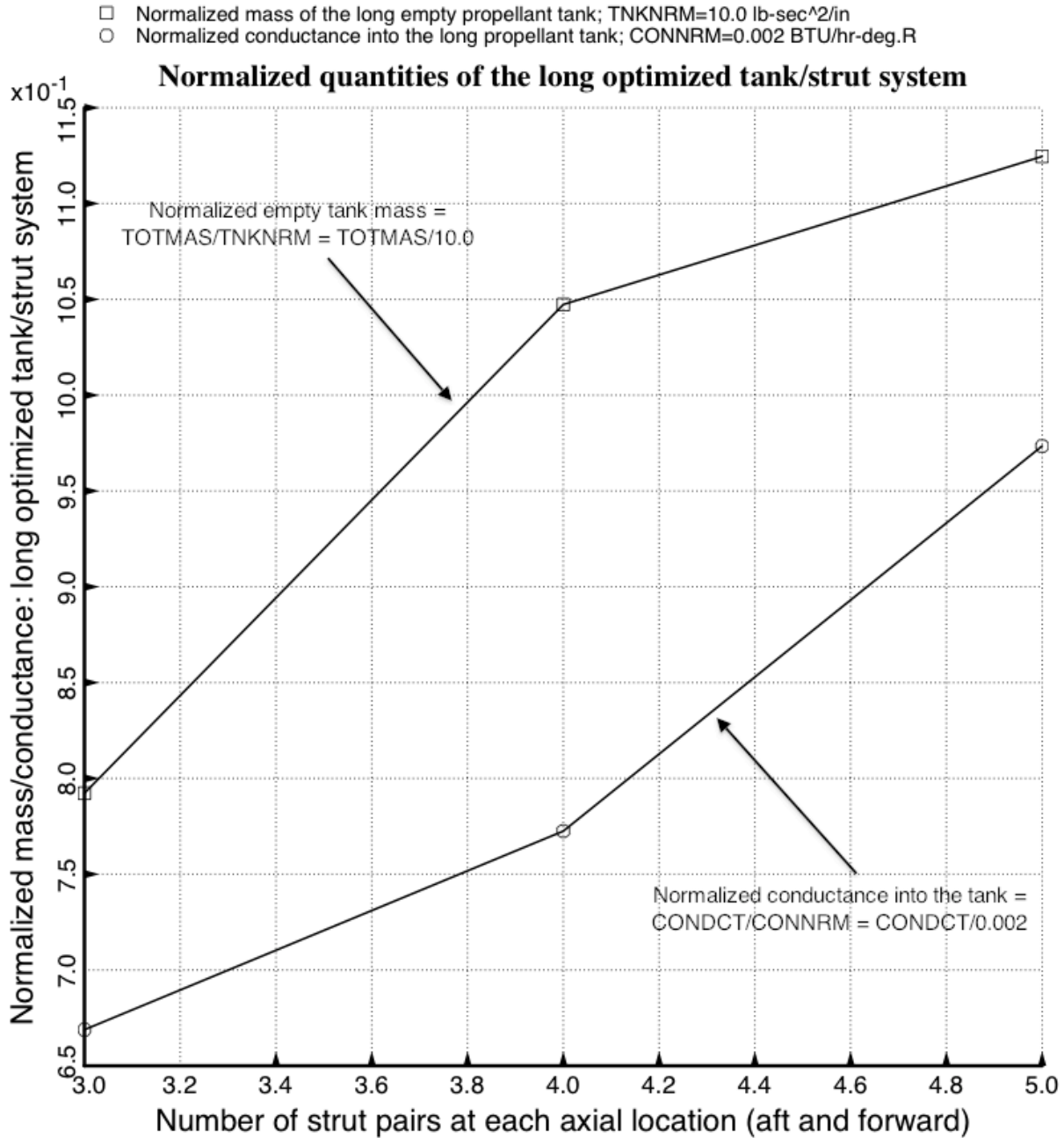


Fig.32 Results from the specific cases called “test”, test3, etc: Optimized **long propellant tank with two sets of struts, aft and forward**. Shown here are the optimized empty tank mass and total conductance into the propellant tank as functions of the number of strut pairs at each axial location. Although the best design appears from this figure to have 3 pairs of struts at each axial location, note from Fig. 12 that in the “3-pair” optimized configuration the struts penetrate the wall of the propellant tank somewhat. Therefore, the configuration displayed in Figs. 5 and 6 (4 strut pairs at each axial location) is probably a better design even though the “4-pair” optimized objective, $WGT \times (TOTMAS/TNKNRM) + (1 - WGT) \times (CONDCT/CONNRM)$, is somewhat higher than the optimized objective for the “3-pair” design.

- Normalized mass of the short empty propellant tank; TNKNRM=3.0 lb-sec²/in
- Normalized conductance into the short propellant tank; CONNRM=0.0006 BTU/hr-deg.R

Normalized quantities of the short optimized tank/strut system

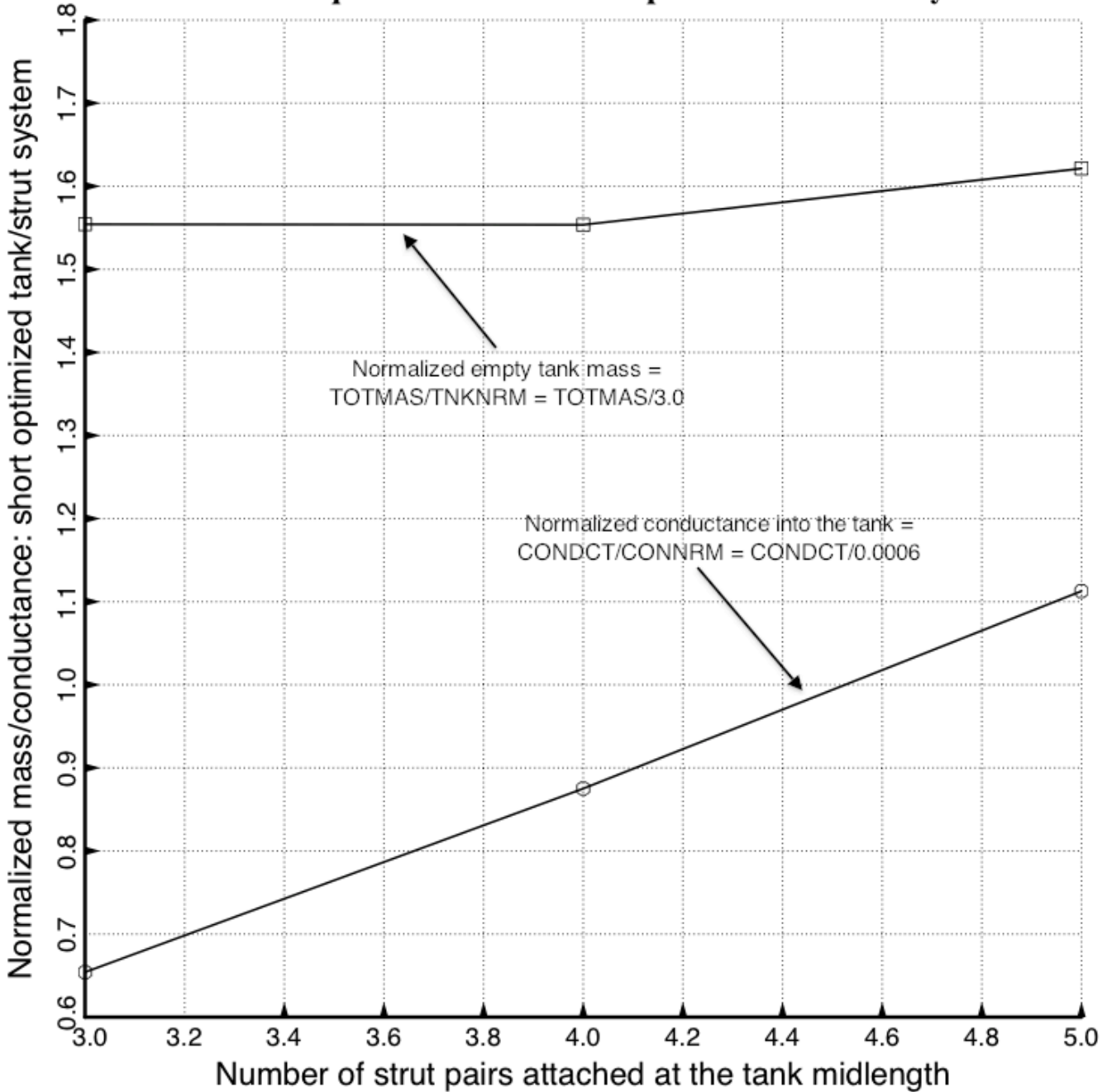


Fig.33 Results from the specific cases called “test2”: Optimized **short propellant tank with one set of struts** attached at the midlength of the tank. Shown here are the optimized empty tank mass and total conductance into the short propellant tank as functions of the number of strut pairs.